

Some pages of this thesis may have been removed for copyright restrictions.

If you have discovered material in Aston Research Explorer which is unlawful e.g. breaches copyright, (either yours or that of a third party) or any other law, including but not limited to those relating to patent, trademark, confidentiality, data protection, obscenity, defamation, libel, then please read our [Takedown policy](#) and contact the service immediately (openaccess@aston.ac.uk)

REMOBILISATION OF URANIUM AND THORIUM BY ORE-FORMING FLUIDS:
A MINERALOGICAL STUDY

VOL. I

CHRISTOPHER MICHAEL POINTER

Doctor of Philosophy

THE UNIVERSITY OF ASTON IN BIRMINGHAM

May 1987

This copy of the thesis has been supplied on condition that anyone who consults it is understood to recognise that its copyright rests with its author and that no quotation from the thesis and no information derived from it may be published without the author's prior, written consent.

The University of Aston in Birmingham

Remobilisation of Uranium and Thorium by Ore-forming Fluids:
a Mineralogical Study

Christopher Michael Pointer

Submitted for the degree of
Doctor of Philosophy
1987

Summary

Mineralogical investigations have determined the sites of U and Th associated with two radioelement-enriched granites from different geological settings. In the Ririwai ring complex, Nigeria, the U- and Th-bearing accessories have been greatly affected by post-magmatic alteration of the biotite granite. Primary thorite, zircon and monazite were altered to Zr(+Y)-rich thorite, partially metamict zircon (enriched in Th, U, Y, P, Fe, Mn, Ca) and an unidentified LREE-phase respectively, by pervasive fluids which later precipitated Zr-rich coffinite.

More intense, localised alteration and albitisation completely remobilised primary accessories and gave rise to a distinctive generation of haematite- and uranothorite-enriched zircon with clear, Hf-enriched rims and xenotime overgrowths. In the Ririwai lode, microclinisation and later greisenisation locally remobilised or altered zircon and deposited Y-rich coffinite and Y(+Zr)-rich thorite which was overgrown by traces of xenotime and LREE-phase(s) of complex and variable composition.

Compositions indicating extensive solid-solution among thorite, coffinite, xenotime and altered zircon are probably metastable and formed at low temperatures. The widespread occurrence of REE-rich fluorite suggests that F-complexing aided the mobility of REE, Y, U, Th and Zr during late-magmatic to post-magmatic alteration, while uranyl-carbonate complexing may have occurred during albitisation.

The Caledonian, Helmsdale granite in northern Scotland has undergone pervasive and localised hydrothermal alteration associated with U enrichment. Zircon xenocrysts, primary sphene and apatite contain a small proportion of this U which is largely adsorbed on to secondary iron-oxide, TiO₂ and phyllosilicates. Additional sites for U in the overlying, Lower Devonian Ousdale arkose include coffinite, secondary uranyl phosphates, hydrocarbon and traces of xenotime and unidentified LREE-phases. U may have been leached from the granite and deposited in the arkose, along channelways associated with the Helmsdale fault, by convecting, hydrothermal fluids.

Key Words: uranium, thorium, mineralogy, remobilisation, alteration

Acknowledgements

I am indebted to Dr John Ashworth and Dr Rob Ixer for their constant encouragement and invaluable advice. I am also grateful to Peter Simpson of the British Geological Survey for useful discussions and for arranging the irradiation of samples for fission-track work and to Jane Hurdley for supplying polished sections of my samples. Dr Peter Bowden and Dr Judith Kinnaird of the Department of Geology, St. Andrews University kindly provided the samples from Ririwai and Niger. My thanks to Gus Mackenzie of the Scottish Universities Research and Reactor Centre, East Kilbride, for organising the irradiation of samples for fission-track work and to Ian Sinclair and Dr Susan Parry for their help during my visits to the Imperial College Reactor Centre at Silwood Park, Ascot. My efforts with the electron microprobe benefited from the endless patience of Roger Howell. Last, but not least, I thank Aileen for persevering with the typing. This study was made possible by an award from the Natural Environment Research Council.

List of Contents (Volume I)

	Page
Summary	2
Acknowledgements	3
Key to Abbreviations	30
Chapter 1 Introduction	31
Chapter 2 The Geochemistry and Mineralogy of Uranium and Thorium	
1. Geochemistry	33
a) Late-magmatic/post-magmatic transport	33
b) Hydrothermal and groundwater transport	34
c) Deposition	36
2. Mineralogy	38
a) U ⁴⁺ and Th minerals	38
i) Uraninite	38
ii) Thorianite	40
iii) Coffinite	40
iv) Thorite, uranothorite, huttonite and thorogummite	45
v) Brannerite-thorutite and complex uranotitanates	50
Analysis of U-Ti phases in the Witwatersrand conglomerate.	54
vi) Multiple oxides of Nb and Ta	55
b) Accessory minerals with minor U ⁴⁺ and Th	56
i) Zircon	56
ii) Monazite	60
iii) Xenotime	62
iv) Allanite	63
v) Apatite	64
vi) Sphene	66
c) U ⁶⁺ minerals	67
d) Rock-forming minerals	68

	Page
e) Other sites for U and Th	69
i) TiO ₂	69
ii) Fe- and Mn-oxides/hydroxides	70
iii) Phyllosilicates	71
iv) Organic matter	73
Chapter 3 The Ririwai Ring Complex	
1. Geological setting	76
2. Volcanic and subvolcanic activity	77
3. The biotite granite	78
a) Petrography	78
b) Geochemistry	80
c) Mineralisation	81
4. Metasomatism	81
a) Albitisation	81
i) Petrography	81
ii) Geochemistry	82
iii) Mineralisation	83
b) Microclinisation	84
i) Petrography	84
ii) Geochemistry	84
iii) Mineralisation	85
c) Greisenisation	86
i) Petrography	86
ii) Geochemistry	87
iii) Mineralisation	87
d) Quartz-sphalerite-cassiterite veining	88
5. Summary	88
6. Comparisons with other areas	89

	Page
Chapter 4 Uranium- and Thorium-bearing Accessory Minerals in the Ririwai Biotite Granite and its Altered Lithologies	
1. Introduction	90
2. The biotite granite	91
a) Surface Sample N75	91
i) Zircon	91
ii) Thorite	92
iii) Fluorite	93
b) Surface Sample N94	93
i) Zircon	93
ii) Thorite	93
iii) Fluorite	94
c) Borehole samples	94
i) Zircon	94
ii) Thorite	98
iii) Monazite	102
iv) Fluorite	103
v) LREE-phase	104
vi) Coffinite	105
vii) Pyrochlore	106
3. Albitised granite	107
i) Zircon	107
ii) Thorite	111
iii) Monazite	113
iv) Fluorite	114
v) LREE-phase	114
vi) Xenotime	115
4. Albitite	116
i) Zircon	116

	Page
ii) Thorite	117
iii) Monazite	118
iv) Fluorite	118
v) LREE-phase	119
vi) Xenotime	119
vii) ?Pyrochlore	120
5. Ririwai lode	120
a) Microcline	120
i) Zircon	120
ii) Thorite and U-Th-Si phases	121
iii) Coffinite	123
iv) ?Pyrochlore	124
v) Monazite	124
vi) LREE-phases	124
b) Greisenised wallrock	125
i) Zircon	125
ii) Thorite	127
iii) Th-Pb-P-phase	128
iv) U-Th-Y-Si-phase	129
v) Monazite	130
vi) LREE-phases	130
vii) Xenotime	131
c) Greisen	131
i) Zircon	131
ii) Thorite	131
iii) Monazite	132
iv) LREE-phases	133
v) Xenotime	133
6. Summary	134

	Page
Chapter 5 Conclusions and Discussion on the Ririwai Material	
1. Mineral composition in relation to rock-type	137
2. Paragenetic sequence	138
a) General remarks	138
b) Biotite granite	139
c) Albitised rocks	146
d) Microcline and greisenised rocks	149
3. Mineral Chemistry	157
a) Zircon	157
i) Possible exsolution in zircon	163
b) Thorite	165
c) Coffinite	167
d) Solid-solution ranges in the Th-U-Zr-Y system	168
e) Monazite and other LREE-phases	174
4. Suggestions about melt and fluid chemistry	175
5. Trace element geochemistry and its relation to the accessory mineralogy	184
a) U and Th	184
b) Other elements	188
6. Comparisons of Ririwai with other areas	190
a) Late-magmatic/post-magmatic processes	191
i) Nigeria-Niger Younger Granite Province	191
ii) Other areas	193
b) Albitisation	195
i) Nigeria	195
ii) Canada	196
iii) Sweden	198
iv) Other areas	200
c) Greisenisation and sericitisation	203
d) Summary and conclusions	205

	Page
Chapter 6 The Helmsdale Area	
1. Introduction	207
2. Geological setting	207
3. The Helmsdale granite	209
a) Petrography	209
b) Alteration and U mineralisation	210
4. Ousdale arkose	214
a) Petrography	214
b) U mineralisation	215
5. Genesis of U mineralisation	217
Chapter 7 Distribution of Uranium in the Helmsdale Granite and Ousdale arkose	
1. Introduction	221
2. Ousdale arkose	221
a) Primary magmatic sites	221
i) Zircon	221
ii) Sphene	222
iii) Apatite	223
b) U minerals	223
i) Coffinite	223
ii) ?Uraninite	226
iii) Uranyl minerals	227
c) Other sites for U	228
i) Fe-oxide	228
ii) TiO ₂	229
iii) Hydrocarbon	230
iv) Xenotime	232
v) LREE-phase(s)	232
vi) Unidentified sites	233

	Page
3. Helmsdale granite	
a) Primary magmatic sites	234
i) Zircon	234
ii) Sphene	234
iii) Apatite	234
b) Other sites	234
i) Fe-oxide	234
ii) TiO ₂	236
iii) Phyllosilicates	236
iv) Hydrocarbon	237
4. Summary of U distribution	237
Chapter 8 Discussion and Conclusions on the Helmsdale Material	
1. Introduction	239
2. Crystallisation of the granite	240
3. Alteration of the granite	241
4. Mineralisation of the arkose	244
5. Paragenesis of U-sites in the granite and arkose	250
Chapter 9 Summary and Discussion	
1. Introduction	252
2. Ririwai	252
3. Helmsdale	255
a) Comparison of Ousdale with other areas	257
4. Suggestions for future work	258
a) Techniques	258
b) Bulk geochemistry	260
c) Sample selection	261
d) Solid solution	262
Chapter 10 Synthesis and Final Remarks	
1. Ririwai area	263
2. Helmsdale area	268

	Page
Appendix 1 Petrographic and Mineralogical Techniques	
1. Light microscopy	269
2. Alpha-particle autoradiography	269
3. Fission-track radiography	270
4. Electron probe microanalysis	272
5. Scanning electron microscopy with energy dispersive microanalysis	280
6. Transmission electron microscopy	281
7. X-ray diffraction	281
Appendix 2 Instrumental Neutron Activation Analysis for the Measurement of U and Th	
1. Introduction	283
2. Sample preparation	283
3. Irradiation	283
4. Counting	284
5. Interferences	284
6. Short irradiation for the analysis of U	285
7. Assessment of results	285
Appendix 3 Field Radiometry	286
Appendix 4 Calculation of Hypothetical wt. % H₂O in Coffinite, Thorite and Zircon	287
Appendix 5 Calculation of Hypothetical Initial Composition of Type 2 Zircon from the Albitised Granite	288
Appendix 6 Samples Collected in the Helmsdale Area	289
Appendix 7 Approximate Modal Analysis of Coffinite in the Ousdale Arkose	291
References	292

List of Tables (Volume II)

	Page
1 Uranium and thorium contents of common rocks and water.	21
2 Ionic charges and radii for U, Th and elements for which they commonly substitute.	21
3 List of uranyl and uranous complexes known to form with various anions.	22
4 Typical enrichment factor values for natural materials.	24
5 Literature analyses of coffinite and "coffinite-like" phases.	26
6 Literature analyses of thorite/thorogummite.	29
7 Elements which have been reported as occurring in thorite, huttonite and coffinite.	32
8 EPMA of uraniferous inclusions in phyllosilicates and porous pyrite clasts from conglomerate, Wwatersrand basin, S. Africa.	34
9 The pyrochlore group.	34
10 Radiation effects detected in zircon with increasing metamictisation.	38
11 Ionic radii of elements substituting for 8-coordinated Zr and 4-coordinated Si.	38
12 HfO ₂ contents of zircon.	38
13 U and Th contents of zircon.	42
14 U and Th contents of monazite.	44
15 U and Th contents of xenotime.	45
16 U and Th contents of allanite and epidote.	46
17 U and Th contents of apatite.	47
18 U and Th contents of sphene.	48
19 Some of the more important uranyl minerals.	49
20 U content of igneous rock-forming minerals.	49
21 U and Th contents of TiO ₂ .	50
22 U and Th contents of Fe-oxide.	50

	Page
23 U and Th contents of phyllosilicates.	51
24 U and Th contents of organic matter.	51
25 Size and abundance of radioactive accessories and fluorite in borehole and surface samples of granite.	65
26 Probe analyses of zircon from surface and borehole samples of biotite granite.	75
27 Partial analyses of zircon 11 from 155 m depth in the granite.	76
28 Correlation coefficients for elements in Table 27.	76
29 Probe analyses of zircon from the borehole samples of biotite granite.	78
30 Comparative analyses of low and high reflectance areas in zircon from various samples.	79
31 Probe analyses of thorite from surface samples of the biotite granite	81
32 Probe analyses of thorite from borehole sample of greisenised biotite granite.	83
33 Probe analyses of thorite from the borehole samples of biotite granite.	85
34 Probe analyses of monazite from the biotite granite and greisenised wallrock.	93
35 Semi-quantitative, partial analyses of the monazite grains in Fig. 27 and Plate 78.	94
36 Probe analyses of LREE-phase(s) from the biotite and albitised granites and Ririwai lode.	98
37 Probe analyses of coffinite and U-Th-Y-Si-phases from the biotite granite and Ririwai lode.	100
38 Probe analyses of pyrochlore and related phases from the arfvedsonite and biotite granites, albitite and Ririwai lode.	102
39 Probe analyses of zircon from the biotite and albitised granites.	106

	Page
40 Probe analyses of thorite from the biotite and albitised granites.	108
41 Probe analyses of zircon from the albitised granite and albitite.	113
42 Probe analyses of thorite from the albitised granite and albitite	117
43 Probe analyses of xenotime and an unidentified Th-Pb-P-phase.	123
44 Size and abundance of radioactive accessory minerals and fluorite from the Ririwai lode.	124
45 Probe analyses of zircon from the Ririwai lode.	126
46 Probe analyses of U-Si-phase and thorite from the microcline and greisenised wallrock, Ririwai lode.	130
47 Probe analyses of thorite from the greisenised wallrock, Ririwai lode.	136
48 Probe analyses of thorite from the greisen, Ririwai lode.	140
49 Summary of alteration sequence and paragenesis of radioelement-bearing accessory minerals in the Ririwai biotite granite.	152
50 EPMA results and calculation of mean atomic number and back-scattered electron coefficient in zircon with dark patches.	156
51 Correlation coefficients for elements in thorite from Sample 94.	160
52 Correlation coefficients for elements in thorite from 305m depth.	160
53 Correlation coefficients for elements in thorite from 390m depth.	160
54 Correlation coefficients for elements in thorite from R1/42-3.	160
55 Hypothetical wt. % H ₂ O calculated for coffinite analyses.	161
56 Compositions of co-existing xenotime-zircon-thorite in albitite.	161
57 Bulk rock analyses for U and Th of rocks from Ririwai.	165
58 Bulk rock analyses for selected elements of surface and borehole granite samples from Ririwai.	166
59 A comparison of selected accessory minerals from the Taghouaji and Ririwai complexes.	167

	Page
60 Summary of mineralogical and geochemical changes during subsolidus alteration of granitoids from S. E. Massif Central.	169
61 Compilation of bulk U and Th data for the Helmsdale granite and common world granites.	175
62 Bulk rock U and Th data for the Helmsdale granite and Ousdale arkose.	176
63 Probe analyses of zircon from borehole and surface samples of the Ousdale arkose.	190
64 Probe analyses of sphene from borehole 1 in the Ousdale arkose.	193
65 XRD data of selected minerals from the Helmsdale area.	194
66 Probe analyses of coffinite from Borehole 2 in the arkose.	201
67 Probe analyses of metatorbernite and apatite from Surface Anomaly 5 in the Ousdale arkose.	208
68 Comparison of the Ousdale U and Olympic Dam Cu-U-Au deposits.	220
69 EPMA detection limits for various elements and minerals.	224
70 Conditions and standards used during EPMA for different elements.	226
71 Composition of U glass standard UG2.	229
72 Checking different standards for U by electron microprobe.	229
73 Comparison of INAA for U using the long and short irradiation methods.	231

List of Figures (Volume II)

	Page
1 Distribution of uranyl complexes at 200°C.	22
2 Distribution of uranyl complexes at 300°C.	22
3 Distribution of uranyl complexes at 100°C.	23
4 Distribution of uranous complexes at 25°C.	23
5 Log f_{O_2} -pH diagram showing distribution of uranyl and uranous complexes and solubility of uranium oxide at 200°C.	23
6 Eh-pH diagram of U-O ₂ -H ₂ O-CO ₂ system at 25°C.	23
7 Distribution of uranyl complexes for typical ligand concentrations in ground waters at 25°C.	23
8 Subsolidus phase assemblages in the system SiO ₂ -ThO ₂ -UO ₂ -ZrO ₂ .	27
9 Possible phase relations in coffinite-bearing assemblages.	27
10 Possible equilibrium conditions involving dissolved silica, amorphous silica, coffinite and uraninite.	27
11 Compositions of natural thorites in the system SiO ₂ -H ₂ O-ThO ₂ .	27
12 EPMA data of brannerite expressed as molecular %.	33
13 Compositons of natural zircons in the system SiO ₂ -H ₂ O-ZrO ₂ .	37
14 Nomenclature for the monazite-structure silicate and phosphate minerals.	37
15 Coffinite, thorite, xenotime and zircon compositions from the literature, plotted as mole %.	40
16 The Mesozoic ring complexes of Nigeria.	52
17 Simplified geological sketch map of the Ririwai complex.	53
18 Summary of main post-magmatic transformations in Ririwai granite.	54
19 Schematic diagram showing relation of mine levels, drill-core L13 and surface sample locations in the Ririwai granite.	62
20 Sections across the Ririwai lode.	62
21 Size and abundance of zircons from the Ririwai granite.	66
22 Concentration profiles of thorite grains from Sample N94.	67

	Page
23	Variation of analytical oxide totals for thorite from Ririwai. 86
24	Variation of wt. % UO_2 in thorite from Ririwai. 87
25	Variation of wt. % Y_2O_3 in thorite from Ririwai. 88
26	Variation of wt. % ZrO_2 in thorite from Ririwai. 89
27	Cluster of anhedral monazite grains from 390 m depth. 94
28	Concentration profiles for Th, U and Hf across a zoned zircon. 111
	<u>Energy dispersive spectra of accessory phases from Ririwai</u>
29	Low reflectance patches in zircon. 142
30	As Fig. 29. 142
31	Low reflectance patches in zircon close to thorite. 142
32	Pyrochlore associated with columbite. 142
33	Pb-pyrochlore intergrown with columbite. 142
34	?Microlite intergrown with pyrite, columbite and U-Si-phase. 142
35	25 μ m diameter pyrochlore inclusion in zircon. 142
36	Columbite. 142
37	Monazite in quartz. 144
38	Monazite in biotite. 144
39	Thorite grains in biotite. 144
40	Thorite in Li-mica. 144
41	Uranothorite inclusion in Type 2 zircon. 144
42	Zr-rich thorite. 144
43	Lozenge-shaped thorite grain with suppressed Si peak. 144
44	Th-Pb-P-phase intergrown with thorite and monazite. 144
45	Xenotime overgrowth on zircon. 146
46	As Fig. 45. 146
47	Cluster of U-Th-Y-Si phase grains. 146
48	U-Th-Y-Si phase intergrown with pyrite and ?microlite. 146
49	Coffinite. 146
50	Coffinite. 146

	Page
51 ?Coffinite intergrown with TiO_2 .	146
52 Complex LREE-phase overgrowing thorite.	148
53 Complex LREE-phase in fluorite.	148
54 Complex LREE-phase overgrowing thorite.	148
55 Complex LREE-phase overgrowing zircon.	148
56 Complex LREE-phase included in Li-mica.	148
57 Complex LREE-phase intergrown with coffinite.	148
58 Complex LREE-phase in fluorite.	148
59 Simple LREE-phase.	148
60 Complex LREE-phase in fluorite.	150
61 Complex LREE-phase overgrowing zircon.	150
62 Complex LREE-phase in fluorite.	150
63 As Fig. 62.	150
64 Complex LREE-phase with minor Th and Pb.	150
65 Complex Th-Pb-LREE phase.	150
66 Simple LREE-phase replacing monazite.	150
67 Simple LREE-phase in fluorite.	150
68 Wt. % Y_2O_3 vs wt. % ZrO_2 for thorite from the biotite and albitised granite.	151
69 Wt. % Y_2O_3 vs wt. % ZrO_2 for thorite from the greisenised granite and Ririwai lode.	151
70 Wt. % Y_2O_3 vs wt. % ZrO_2 for coffinite from the biotite granite and Ririwai lode.	151
71 Possible explanation of the zircon morphology in Plate 70.	153
72 Possible explanation for the intergrowth of monazite, simple LREE-phase and complex Pb-Th-LREE-phase in the Ririwai lode.	154
73 Wt. % Y_2O_3 vs wt. % P_2O_5 for all zircons.	155
74 Wt. % ThO_2 vs wt. % SiO_2 for all monazites.	155

	Page
75 Variation of hypothetical wt. % H ₂ O in thorite from Ririwai.	158
76 Wt. % Y ₂ O ₃ , vs wt. % P ₂ O ₅ , for all thorite.	159
77 Wt. % Y ₂ O ₃ , vs wt. % P ₂ O ₅ , for thorite from samples N75 and N94.	159
78 Wt. % ZrO ₂ vs wt. % SiO ₂ for all thorites.	159
79 Mole % Zr+Hf, Y and Th+U for zircon from Ririwai.	162
80 Mole % Th+U, Y and Zr+Hf for thorite and coffinite from Ririwai.	163
81 Mole % U/(U+Th) for thorite, coffinite and zircon from Ririwai.	164
82 Sample localities and geology of the Helmsdale area.	170
83 Location of samples in the Helmsdale granite.	171
84 As Fig. 83.	172
85 Location of samples in the Helmsdale granite and Ousdale arkose.	173
86 Minor faulting in the disaggregated, porphyritic granite.	180
87 General geology and location of radioactive anomalies in the Ousdale area.	181
88 Diamond drill holes 1 and 2 in Anomaly 2, Ousdale Burn.	182
89 Geology, radiometry and uranium content of uranium mineralisation in weathered Ousdale arkose at Anomaly 5.	183
90 Possible mechanism for migration and emplacement of metals and hydrocarbon found in the Helmsdale granite and Ousdale arkose.	184
91 Location of full analyses in zircon 1, Sample 802.	186
92 Location of partial analyses in zircon from Sample 777.	186
93 As Fig. 92.	186
<u>Energy dispersive spectra of accessories from the Ousdale arkose</u>	
94 Small zircon in altered pyrite.	188
95 Outer, U-enriched zone of a zircon.	188
96 As Fig. 95.	188
97 Core of the zircon in Fig. 96.	188
98 Coffinite replacing TiO ₂ needles.	188
99 Coffinite inclusion in TiO ₂ .	188

	Page
100 Coffinite/uraninite?	188
101 Coffinite/Cu-sulphide admixture.	188
102 Coffinite intergrown with TiO_2 .	200
103 Coffinite.	200
104 P-Th-coffinite associated with TiO_2 .	200
105 Zr-coffinite.	200
106 Zr-coffinite, intergrown with TiO_2 .	200
107 LREE-phase.	200
108 LREE-phase and ?uraninite.	200
109 As Fig. 108.	200
110 LREE-phase and coffinite with ?uraninite.	207
111 Metatorbernite with limonite staining.	207
112 Fracture in K-feldspar.	207
113 Pyrite altering to goethite associated with DFT.	207
114 TiO_2 pseudomorph after sphene, associated with DFT.	207
115 Hydrocarbon associated with DFT.	207
116 As Fig. 115.	207
117 Xenotime inclusions in hydrocarbon.	207
118 Xenotime overgrowing zircon.	212
119 LREE-phase.	212
120 LREE-phase and coffinite admixture.	212
121 Ca-LREE-phase.	212
122 TiO_2 and Fe-oxide staining.	212
123 Hydrocarbon from alteration zone in Helmsdale granite.	212
124 Proposed stability relations in the system UO_2 - TiO_2 - SiO_2 .	217
125 Section through coffinite mineralisation in the Ousdale arkose, lower Ousdale Burn, showing proposed path of mineralising fluids.	218
126 Paragenesis of uranium sites and other accessories in the Helmsdale granite and Ousdale arkose.	219

	Page
127 Cartoon showing the effect of metasomatism on the U- and Th-bearing accessories of the Ririwai biotite granite.	221
128 Wavelength dispersive spectra for monazite.	227
129A Wt. % ZrO_2 measured in zircon using Zr metal and zircon standards.	228
129B Wt. % ZrO_2 measured in thorite using Zr metal and zircon standards.	228
130 The effect of increasing wt. % ThO_2 content on UM_α/UM_β for different counter flow mixtures.	228

List of Plates (Volume II)

		Page
	<u>Conglomerate from the Witwatersrand basin, South Africa.</u>	
1	Porous pyrite concretion.	36
2	Lexan of same concretionary pyrite.	36
3	Granule of phyllosilicates.	36
4	Lexan of the same granule.	36
5	U-Ti phase inclusion in porous pyrite concretion.	36
6	X-ray map for U of the inclusion in Plate 5.	36
7	X-ray map for Ti of the inclusion in Plate 5.	36
8	X-ray map for Pb of the inclusion in Plate 5.	36
	<u>Ririwai biotite granite and altered facies</u>	
9	Albite replacing K-feldspar in biotite granite.	55
10	Twinned albite in the albitised granite.	55
11	Fine-grained texture in the biotite granite.	55
12	Haematite laths lying parallel to the cleavage in biotite.	56
13	Feldspar replacing biotite along cleavage.	56
14	Fluorite with biotite inclusion in a larger biotite.	56
15	Calcite included in biotite.	56
16	Core samples of albitite and albitised and biotite granite.	58
17	Interstitial calcite with haematite inclusions in albitite.	58
18	High magnification of haematite inclusions in calcite.	58
19	Polished slab of microcline - greisen - quartz vein contact in Ririwai lode.	58
20	Zoned Li-mica crystal in greisenised granite.	59
21	White mica replacing chloritised biotite in the Ririwai lode.	59
22	White mica replacing microcline in the Ririwai lode.	60
23	Li-mica in the greisen.	60

	Page
<u>Ignimbrite from the Goundai volcanic centre, Air, Niger.</u>	
24	Zircon in TiO_2 . 61
25	Lexan of the same area, showing densest fission tracks associated with the TiO_2 and lower density tracks associated with zircon. 61
26	Uraniferous zircons with low reflectance patches associated with very dense fission tracks. 61
27	Lexan superimposed on the ignimbrite, showing low concentrations of U associated with the matrix. 61
<u>Surface samples of Ririwai biotite granite</u>	
28	Haematite-rich zircon with thorite overgrowth. 64
29	Haematite-rich thorites in biotite. 64
<u>Borehole samples of Ririwai biotite granite</u>	
30	Fluorite, zircon and columbite/ TiO_2 . 64
31	Corroded zircon with thorite overgrowths. 64
32	Zircon with thorite overgrowth. 64
33	Euhedral zircon with thorite inclusion in overgrowth. 64
34	The same zircon with the thorite inclusion more evident 64
35	Zircon containing large inclusions of thorite and haematite. 64
36	Zircon containing abundant thorite and haematite inclusions. 69
37	Zircon embayed by white mica. 69
38	Residual rim of corroded zircon. Greisenised granite. 69
39	Haematite-rich zircon with finely-banded outer zone. 69
40	Haematite- and thorite-rich zircon with clear rims. 69
41	Zircon with low reflectance, trace-element enriched patches. 71
42	BSEI of part of the same zircon. 71
43	BSEI high magnification of dark patches. 71
44	Incipient development of the dark patch along zoning. 71

	Page
45 Zircon with concentric, dark, trace-element enriched patches.	71
46 Zircon with dark patches along outer growth-zone.	73
47 Similar zircon to Plate 46.	73
48 Similar zircon to Plate 46.	73
49 Zircon with outer, haematite-rich zone and dark patches.	73
50 Zircon with positions of analyses marked.	73
51 Haematite-rich thorite grains in altered biotite.	73
52 Two thorite grains, with haematite rims, in K-feldspar.	73
53 Thorite with fluorite in biotite.	73
54 Zoned thorite with thick haematite rim.	91
55 Thorite replacing and overgrowing zircon.	91
56 Zircon partially in cassiterite, enclosing/replaced by thorite.	91
57 1 mm long monazite interstitial to quartz and feldspar.	91
58 Irregular monazite, interstitial to quartz and feldspar.	91
59 Monazite showing alteration to a LREE-phase.	96
60 LREE-phase included in fluorite in biotite.	96
61 Interstitial coffinite in biotite.	96
62 Coffinite enclosing molybdenite and admixed with sphalerite.	96
63 Pyrochlore intergrown with columbite.	96
<u>Ririwai albitised granite</u>	
64 Concentric zoning of Types 1, 2 and 3 zircon in a large grain.	104
65 The same zircon, partly included in biotite and overgrown by bladed haematite.	104
66 Hf-enriched, outer Type 1 zone of zircon in Plates 69 and 70.	104
67 Zircon showing embayment by feldspar.	104
68 Banding in Type 3 zircon.	104
69 Concentric zoning of Types 1, 2 and 3 zircon in a large grain.	110
70 BSEI of the same zircon, emphasising the thorite inclusions.	110

	Page
71 Zoning of Types 1, 2 and 3 zircon in a smaller grain.	115
72 High magnification of the analysis 2 area in Plate 70.	115
73 Thorite, monazite and fluorite associated with columbite.	115
74 Interstitial thorite with indistinct banding structure.	115
75 Thorite replacing the outer zone of zircon.	115
76 Thorite overgrowing/replacing zircon.	115
77 Interstitial thorite surrounded by rim of Fe-oxide.	115
78 Corroded remains of large monazite included in feldspar.	115
79 Monazite enclosed by a rim of Fe-oxide.	119
80 Clear monazite showing replacement by a turbid LREE-phase.	119
81 LREE-phase inclusions in fluorite replacing zircon.	119
82 Inclusions of LREE-phase showing alignment in fluorite.	119
83 High magnification of LREE-phase inclusions in zircon.	119
84 Embayed zircon, overgrown by fluorite and xenotime.	119
<u>Ririwai albitite</u>	
85 Embayed zircon with 40 μ m diameter thorite inclusion.	121
86 The same grain, showing isotropic domains of Type 3 zircon.	121
87 Subhedral zircon showing truncation of concentric zoning.	121
88 Zircon with large thorite overgrowth and inclusion.	121
89 Irregular, interstitial monazite associated with sphalerite.	121
90 Zircon with xenotime overgrowths and LREE-phase inclusion.	121
91 Complex Ta-Nb-Pb-etc. silicate with surrounding pyrite rim.	121
<u>Microclinite, Ririwai lode</u>	
92 Zircons included in quartz along fractures.	128
93 Zircon intergrown with thorite/U-Si-phase and pyrite.	128
94 ?REE-microlite, pyrite, columbite and a U-Th-Y-Si phase.	128
95 Interstitial, poorly crystallised coffinite.	128
96 Coffinite/LREE-phase intergrowth and X-ray maps for U and LREE.	128

	Page
<u>Greisenised wallrock, Ririwai lode</u>	
97	Euhedral monazite included in Li-mica with pleochroic halo. 132
98	Zircon with dark patches enriched in Th, U, Fe, Ca, Mn, Y & P. 132
	Part of the zircon is highly enriched in Hf.
	It is partly enclosed by a 250 μ m long thorite.
99	Zircon with dark patches, highly enriched in Th and Fe. 132
100	Complex intergrowth of zircon, thorite, xenotime and monazite. 132
101	Complex intergrowth of zircon, thorite, xenotime & LREE-phase. 132
102	X-ray map for Zr, Th and Y (for Plate 100). 132
103	X-ray map for Zr, Y, Th and LREE (for Plate 101). 132
104	Complex intergrowth of thorite, zircon, columbite, fluorite, 132
	cassiterite and pyrite.
105	Thorite overgrowing zircon, included in quartz. 134
106	Cluster of tiny thorites included in Li-mica. 134
107	Pale yellow thorites associated with pyrite in K-feldspar. 134
108	Thorite lozenge overgrown by cassiterite. 134
109	Intergrowth of Zr-rich thorite and altered zircon. 134
110	Intergrowth of Th-Pb-P phase with Zr-thorite and monazite. 134
111	Cluster of U-Th-Y-Si phase grains. 134
112	Monazite intergrown with LREE-phases. 134
<u>Greisen, Ririwai lode</u>	
113	"Welded clump" of zircons with low reflectance patches. 138
114	Lexan fission-tracks associated with trail of thorites 138
115	Typical thorite with core enriched in haematite inclusions. 138
116	Interstitial thorite with abundant haematite and pyrite. 138
117	Monazite aggregate showing alteration to a LREE-phase. 138
118	Complex Th-Y-LREE phase included in Li-mica. 138
119	Complex Th-LREE phase overgrowing zircon. 138

	Page
<u>The Helmsdale area</u>	
120	Photomicrograph of Helmsdale granite (plane polarised light). 174
121	Same area as Plate 120 (crossed polarised light). 174
122	Alteration zone of sericitised and haematised granite. 177
123	Alteration with U enrichment along a minor fault in granite. 177
124	Fractured and reddened, radioactive granite. 178
125	Impregnated slab of reddened, porphyritic granite. 178
126	Photomicrograph of an alteration zone in granite. 179
127	Radioactive, clay-filled alteration zone in granite. 179
128	Purple fluorite and clusters of apatite crystals in arkose. 180
129	Interstitial calcite in the arkose. 180
130	Interstitial baryte in the arkose. 180
131	Interstitial, purple fluorite in the arkose. 180
132	Site of Borehole 1 in the Ousdale arkose. 181
133	Site of excavation at Anomaly 5 in the Ousdale arkose. 183
134	Joint coating of secondary uranyl minerals in the arkose. 184
<u>Ousdale Arkose</u>	
135	Zircon with complex zoning which is cut by the grain edge. 186
136	Zircon with a second nucleus of zoning. 186
137	Concentrically-zoned zircon with larger, outer zone/overgrowth. 186
138	Zoned zircon included in hydrocarbon. 186
139	Zoned zircon. 186
140	X-ray map of the same zircon showing distribution of U. 186
141	Euhedral sphene included in quartz. 192
142	Pleochroic sphene included in quartz. 192
143	Apatite and small zircon, included in K-feldspar. 192
144	Lexan of the area in Plate 143. 192
145	Electron diffraction pattern of coffinite from Borehole 2. 192

	Page
146	Electron image of the same coffinite. 192
147	Interstitial coffinite infilling feldspar cleavage. 192
148	Interstitial coffinite. 192
149	Coffinite replacing pyrite. 196
150	Large intergrowth of coffinite with pyrite. 196
151	The same intergrowth in transmitted light. 196
152	Intergrowth of coffinite with TiO_2 . 196
153	Similar intergrowth to Plate 152. 196
154	Selective enlargement of Plate 153. 196
155	Coffinite overgrowing zircon. 196
156	Coffinite replacing and overgrowing hydrocarbon. 196
157	U-Zr-Si phase, possibly Zr-rich coffinite. 198
158	BSEI of the same grain. 198
159	U-Th-Zr-Si phase, possibly Zr-coffinite, associated with TiO_2 . 198
160	Coffinite intergrown with part of a TiO_2 pseudomorph. 198
161	Coffinite associated with TiO_2 . 198
162	Metatorbernite veinlet. 203
163	Metatorbernite replacing euhedral apatite. 203
164	X-ray map for U of grain in Plate 163. 203
165	X-ray map for P of grain in Plate 163. 203
166	Metatorbernite partially replacing apatite with zircon. 203
167	Metatorbernite pseudomorph after apatite. 205
168	Metatorbernite pseudomorph after a 2 mm long, tabular apatite. 205
169	Lexan of the pseudomorph in Plate 168. 205
170	Metatorbernite intergrown with white mica. 205
171	Typical, subhedral anatase. 205
172	Disseminated leucoxene along quartz and feldspar boundaries. 205
173	Trellis pattern of TiO_2 . 205
174	TiO_2 pseudomorph after sphene with a core of calcite. 205

	Page	
175	TiO ₂ pseudomorph after sphene with a small zircon inclusion.	210
176	Pyrite-marcasite intergrowths overgrowing hydrocarbon.	210
177	Irregular strands of TiO ₂ in hydrocarbon.	210
178	Inclusion of xenotime in hydrocarbon.	210
179	Xenotime overgrowing zircon.	210
180	LREE-phase overgrown by pyrite.	210
181	LREE-phase intergrown with coffinite.	210
182	LREE-phase intergrown with ?uraninite.	210
183	Low magnification of mineralised arkose.	214
184	Lexan of the area in Plate 183.	214
185	Lexan showing fission tracks with small fractures in quartz.	214
186	Lexan showing fission tracks with calcite & quartz veinlets.	214
187	Lexan showing fission tracks with marcasite veins.	214
	<u>Helmsdale granite</u>	
188	Sphene included in quartz.	214
189	Lexan of the same sphene.	214
190	Euhedral martite with superimposed Lexan.	214
191	Part of a 2 mm diameter pyrite crystal in a quartz vein.	216
192	Lexan of the area in Plate 191.	216
193	TiO ₂ and haematite pseudomorph in deformed biotite.	216
194	Anatase and leucoxene in a pseudomorph after sphene.	216
195	Lexan of the area in Plate 194.	216
196	Sericite-clay patches in an alteration zone.	216
197	Lexan of the area in Plate 196.	216
	<u>Appendices</u>	
198	Cellulose nitrate alpha particle detectors.	223
199	Lexan fission track detectors.	223
200	Cambridge Microscan V electron microprobe.	225
201	Wire-grid wound around a polished thin-section.	230
202	Cambridge S150 scanning electron microscope.	230

Key to Abbreviations

LREE	Light rare earth elements.
HREE	Heavy rare earth elements.
HFS	High field strength (elements).
ED	Energy dispersive (spectrometry/spectra).
WDS	Wave-length dispersive " .
SEM	Scanning electron microscopy/microscope.
TEM	Transmission electron microscopy/microscope.
EPMA	Electron probe microanalysis.
BSEI	Back-scattered electron image.
ZAF	Atomic number (Z), absorption (A), fluorescence (F) correction.
XRD	X-ray diffraction.
cps	counts per second.
FT	Fission tracks.
NFT	No fission tracks visible.
FFT	Fine FT i.e. Very sparse. The tracks can be counted.
MFT	Medium FT i.e. Too many tracks to count but there are spaces between individual tracks.
DFT	Dense FT i.e. No spaces occur between tracks which render the Lexan opaque.
BFT	Burned-out FT i.e. Light brown discoloration with no FT visible, due to the U content exceeding the recording capacity of the Lexan. Usually surrounded by DFT. (see Appendix 1, Section 3.)

Chapter 1 Introduction

1. General aims of the study

This thesis aims to clarify the behaviour of U and Th in the natural environment, through a detailed study of their mineralogy. Emphasis is placed on the remobilisation of U and Th in primary accessory minerals at low to medium temperatures, during the post-magmatic alteration of granite. The two granites concerned in this study are the Helmsdale granite, northern Scotland and the Ririwai granite, northern Nigeria. In both intrusions, earlier studies had revealed enriched concentrations of radioelements but their mineralogical sites had not been fully characterised.

2. Approach

A selective review of the geochemistry and mineralogy of U and Th in Chapter 2 provides a framework and basis for comparisons with new data from the Ririwai and Helmsdale areas. Chapters 3 and 6 introduce the two areas and review petrographic, geochemical and mineralogical work, together with genetic models. Details of the U- and Th-bearing minerals in Chapters 4 and 7 are based on the data from laboratory techniques which are briefly outlined in Appendix 1. In Chapters 5 and 8 the results are discussed, in the light of published literature, and genetic models and parageneses are constructed. Chapters 5 and 8 are summarised in Chapter 9 which suggests ideas for future work. All tables, figures and plates are included in Volume II.

3. Applications

New data on the mineralogy of U and Th are likely to find direct applications in several fields of the earth sciences:-

- a) Mineral exploration - Knowledge of the mineralogy of U and Th and their behaviour in fluids will help formulate models of mineralisation which may be used in the exploration for new ore deposits.
- b) Radioactive waste disposal - The chemical behaviour of the actinide elements Pu, Np and Am, the most abundant actinides in nuclear fuel waste (Boulton, 1978), is similar to the geochemical behaviour of U (Bagnall, 1972), while Th is a good analog for Pu⁴⁺ (Krauskopf, 1986). Thus, new data concerning the mobility of U and Th and the stability of their mineralogical sites may be relevant to the design and location of repositories for radioactive waste. Similar applications could be made to the stabilisation of radionuclides in U mine tailings.
- c) Geochronology - The stability of U- and Th-bearing minerals during post-magmatic alteration may have direct implications for the U-Pb, Th-Pb and Pb-Pb dating of accessory minerals such as zircon, which is widely regarded as being resistant to leaching.
- d) Geothermal energy - U, Th and K are the main heat-producing elements in the Earth's crust, in which localised areas of high heat-flow can be harnessed for the production of geothermal energy or may drive natural, hydrothermal convection systems, responsible for mineralisation. Mass balance calculations, based on a knowledge of the mineralogical sites of U, Th and K, can help determine the controls of radioelement distributions in granitic rocks.

Chapter 2 The Geochemistry and Mineralogy of Uranium and Thorium

1. Geochemistry

Brief introductions to the chemistry and geochemistry of U are given in Rich et al. (1977), Rogers and Adams (1969), Dongarra (1984) and Nash et al. (1981). U is an oxyphile and lithophile element which is enriched in the upper crust, where it is more abundant than 22 other naturally occurring elements and has an average abundance of 2 ppm (range of 1-4 ppm). The abundance of U and Th in various rock-types is shown in Table 1.

In nature, the valence states 4+, 5+ and 6+ occur, but the 4+ (uranous) and 6+ (uranyl) states are most important geochemically. Due to their identical ionic charge and close ionic radii, U^{4+} and Th^{4+} are geochemically very similar and tend to occur together in the same minerals, where they substitute for other elements of similar ionic charges or radii (Table 2). The large ionic radii and high valencies of U and Th prevent them from entering the crystal lattices of the major rock-forming minerals, except in trace amounts (Table 20). For this reason, U^{4+} and Th^{4+} tend to be concentrated in accessory minerals, as well as forming a few minerals containing essential U^{4+} and/or Th.

a) Late-magmatic/post-magmatic transport

The incompatible natures of U and Th are reflected by their abundances in igneous rocks. Table 1 shows them to be enriched in the late-stage members of igneous differentiation suites and there is a general tendency for U and Th to increase with increasing silica and/or alkali contents. At the surface, U^{4+} is readily oxidised to U^{6+} , which

forms UO_2^{4+} (uranyl ion), the chemical properties of which differ significantly from those of Th and the other elements in Table 2. The much greater solubility of uranyl accounts for the variation in Th/U ratios in surface material and the lack of Th etc. in secondary minerals (Table 19). For example, Ragland et al. (1967) found a negative correlation between the U content and degree of fractionation of granite in the Enchanted Rock batholith, Texas, U.S.A.. They attributed this to a loss of U as a result of increasingly effective oxidative processes during crystallisation of the magma. U^{4+} was oxidised to UO_2^{2+} which is more soluble in the volatile igneous phases. Ragland et al. (op. cit.) concluded that autometasomatism was an important mechanism of chemical fractionation during crystallisation.

Further examples of U mobility at magmatic temperatures, due to autometasomatism are reviewed in Section 6, Chapter 5. These demonstrate the importance of F in complexing with U as UF_6 which is retained in the melt or partitioned into fluid phases and removed (e.g. Bohse et al., 1974). The abundance of fluorite and other F-containing gangue minerals in areas of U mineralisation indicates the importance of uranyl fluoride complexes, which predominate in acid to neutral solutions below 300°C (Fig. 1, after Romberger, 1984). As temperatures increase, fluoride complexes are superseded by hydroxide complexes (Fig. 2) which may be the only soluble U species at temperatures of 300°C and above (Romberger, op. cit.).

b) Hydrothermal and groundwater transport

The hydrothermal transport and deposition of U can occur at high temperatures but the geochemistry of U is better characterised at low temperatures (Kimberley, 1978). Fluid inclusion data indicate that

temperatures of U transport reach 340-350°C (Poty et al., 1974) or even 500°C (Sassano et al., 1972). In pure water, at near-neutral pH, the concentration of U in solutions equilibrated with uraninite passes through a maximum near 260°C (Lemoine, 1975). In natural waters, the transport of U may be aided by a large variety of complexes (Table 3) and the relative importance of these depends on temperature and the composition of the aqueous solution (Romberger, 1984). For example, in near neutral solutions, phosphate complexing may be important at very low levels of phosphate while, in alkaline solutions at low temperatures, carbonate complexes predominate (Fig. 3). Fig. 5 is a log fO_2 - pH diagram, showing the distribution of uranyl and uranous complexes and the solubility of U oxides at 200°C in solutions containing 100 ppm F, 1000 ppm S and 1M NaCl at pCO_2 of 10 atm. (after Romberger, 1984).

The geochemistry of U at much lower temperatures was studied by Langmuir (1978) who concluded that U is usually complexed in natural waters at 25°C. With typical concentrations of ligands under anoxic conditions, various fluoride complexes predominate below pH 3-4 and uranous hydroxyl complexes at high pH's (Fig. 4). In oxidised waters, uranyl fluoride complexes and UO_2^{2+} predominate below pH 5, while $UO_2(HPO_4)_2^{2-}$ predominates from about 4 to 7.5 and uranyl di- and tricarboxylate complexes predominate at higher pH's (Fig. 7). Complexes in the system U-O₂-H₂O-CO₂ at 25°C and 1 atm. for U=10⁻⁶ m and pCO_2 = 10⁻² atm. are shown in an Eh-pH diagram (Fig. 6, modified by Dongarra, 1984 after Langmuir, 1978), in which the stability field for crystalline uraninite is shaded.

Langmuir and Herman (1980) found complexing to increase the mobility of dissolved U by many orders of magnitude below pH 8 in

natural water at low temperatures. The important inorganic complexes of Th with increasing pH are $\text{Th}(\text{SO}_4)_2^0$, ThF_2^{2+} , $\text{Th}(\text{HPO}_4)_2^0$, $\text{Th}(\text{HPO}_4)_3^{2-}$ and $\text{Th}(\text{OH})_4^0$, but organic complexes, such as citrate and oxalate, predominate in organic-rich waters, including soil-water.

c) Deposition

Romberger (1984) and Rich et al. (1977) discussed the various mechanisms of U deposition. Where uranyl carbonate complexes predominate, loss of CO_2 due to boiling or reaction with the wallrock may be an important mechanism of U deposition (e.g. Poty et al., 1974; Tugarinov, 1975; Cathelineau and Leroy, 1981). According to Hostetler and Garrels (1962), uranyl-carbonate complexes break down at temperatures above 120°C , resulting in uraninite precipitation. However, the potential precipitation of substantial amounts of U due to loss of CO_2 has been questioned by Rich et al. (1977). Dilution of the hydrothermal solutions and precipitation of gangue minerals that contain the appropriate anions (e.g. fluorite, calcite) are further mechanisms mentioned by Romberger (op. cit.).

Fig. 5 demonstrates that U oxide precipitates during reduction and increasing pH, and the relative importance of these two processes depends on the initial conditions and the composition of the transporting solution. Increases in pH may be caused by reactions of the transporting solutions with the wallrock or boiling. Reduction can be accomplished by Fe, S and organic compounds. Rich et al. (1977) commented on the common association of haematite with pitchblende and suggested the role of Fe^{2+} as a reductant for U^{6+} . Nash et al. (1981) found the evidence of a direct role of Fe^{2+} in the precipitation of U inconclusive and believed that such reduction could only be effective

at high temperatures. Romberger (1984) suggested that ferric oxides may have resulted from U deposition, rather than oxidation of Fe being the cause of U precipitation.

Nash et al. (op. cit.) discussed the association of U with organic materials which tend to contain oxygen-bearing moieties. The coordinate positions of the U or uranyl ions are typically bonded to oxygen atoms in the various ligands. Often H₂S is responsible for the reduction of uranyl species and it is not always clear whether organic matter plays a direct role. It seems more likely that organic matter fixes the uranyl ion and reduction follows more slowly.

Sorption can play an important role in the concentration of uranyl, prior to its reduction to U⁴⁺ in uraninite or coffinite. Langmuir (1978) found the pH range of minimum solubility of the uranyl minerals to coincide with the pH range of maximal uranyl sorption on organic matter, Fe-, Mn- and Ti-oxyhydroxides, zeolites and clays. Langmuir (op. cit.) quoted the enrichment factors (weight of sorbed U per weight of sorbent plus U, divided by the weight of dissolved U per weight of solution) for various materials (Table 4) and concluded that clays are relatively unimportant as concentrators of U.

Langmuir and Herman (1980) concluded that the adsorption of dissolved Th increases markedly with pH above a pH of 2, reaching 95-100% adsorption on to clays, oxyhydroxides and organic matter at a pH above 5.5-6.5. They found adsorption to be more complete on to humic organic solids than on to clays and to be inhibited by organic ligands, which form strong Th complexes.

2. Mineralogy

Frondel (1958) has given the most comprehensive description of U and Th minerals. A brief introduction to U mineralogy was given by Steacy and Kaiman (1978) who, together with Morton (1978), compiled a list of U-bearing minerals. Smith (1984) provided a more detailed treatment of U mineralogy and classified the minerals into a "reduced" family, with U^{4+} as the dominant valence state and an "oxidised" family, in which all or most of the U exists as U^{6+} , usually in the form of the uranyl ion (UO_2^{2+}). This classification is preferred to the old one of "primary" and "secondary" minerals, since some species, e.g. coffinite, can have either primary or secondary origins. The classification of Smith (op. cit.) is used here and only the more important U- and/or Th-bearing minerals are included, with more emphasis placed on those found in the Helmsdale or Ririwai areas.

a) U^{4+} and Th minerals

i) Uraninite (UO_{2+x})

Uraninite is, by far, the most common U^{4+} mineral, the only significant oxide of U and comprises the main ore mineral in the majority of U deposits. The term "pitchblende" has been extensively used for the massive, microcrystalline variety of uraninite which is free of Th and REE and typically occurs in low-temperature, hydrothermal vein deposits, but Smith (1984) recommends that use of the term be discontinued.

Uraninite always shows some oxidation of stoichiometric UO_2 and is probably restricted to the range $UO_{2.07}$ - $UO_{2.15}$ in nature. The cell parameters of uraninite tend to decrease linearly with increasing oxidation and decreasing temperature of formation, and this has been

utilised by many workers (e.g. Von Pecharmann and Bianconi, 1982) to determine its origin :

Pegmatite	:	5.465	Å
Vein	:	5.439	Å
Sediment	:	5.410	Å

Cell parameters should be used with caution, since they can be modified by oxidation due to weathering or the radioactive decay of U and are dependent on the substitution of trace elements. Oxidised, low temperature uraninite also gives a more diffuse XRD pattern.

Experimental syntheses have shown that uraninite may precipitate in a particularly oxidised state, while Voultzidis and Classen (1978) reported the occurrence, in the Key Lake deposit, Saskatchewan, of tetragonal α - U_3O_7 , which was probably metastable. These higher oxides of U have a strong affinity for water and form a brightly coloured mixture of hydrated, secondary uranyl minerals (Section c) around weathered uraninite.

Uraninite has a fluorite-type structure and is isostructural with cerianite (CeO_2) and thorianite (ThO_2) with which it forms complete solid solutions, thus accounting for the high REE and Th content of many pegmatitic uraninites. Uraninite may also contain significant quantities of Y, Ca and Zr which substitute for U, together with radiogenic Pb which may remain dispersed throughout the structure or nucleate into Pb- or galena-rich areas (Bowles, 1978). Experimental studies by Mumpton and Roy (1959) confirmed the complete solid solution between ThO_2 and UO_2 at 1300°C and extensive defect fluorite solid solutions between ThO_2 and U_3O_8 . A large solid solution gap lies between ZrO_2 and UO_2 , with up to 8 mole % ZrO_2 dissolving in UO_2 and less than 4 mole % UO_2 in ZrO_2 at temperatures up to 1300°C. Ludwig

and Grauch (1980) reported up to 7 wt % SiO_2 substituting in uraninite but Marlow (1981) was unsure whether Si, Ti, K, Fe and Al were substituting in the uraninite lattice or were present as microinclusions.

ii) Thorianite (ThO_2)

Thorianite is much less common than uraninite and closely resembles the latter in its physical and optical properties. U is always present in considerable amounts but material containing equal amounts of Th and U is rare. Below 400°C , under hydrothermal conditions, Mumpton and Roy (1959) prepared a continuous, although metastable series of solid solutions with the fluorite structure, with compositions varying from ThO_2 to nearly pure ZrO_2 . Barretto and Fujimori (1986) reported Zr-rich thorianite in a phonolite from Brazil.

iii) Coffinite ($\text{U}(\text{SiO}_4)_{1-x}(\text{OH})_{4x}$)

Coffinite was first described from sandstones of the Colorado Plateau U deposits by Stieff et al. (1956) who proposed the above formula. Chemical, infra-red, X-ray and differential thermal analysis (DTA) studies of Belova et al. (1969), Abdel-Gawad and Kerr (1961) and Ludwig and Grauch (1980) indicated that natural coffinites lacked an essential OH component but contained adsorbed water, while Fuchs and Gebert (1958) and Fuchs and Hoekstra (1959) found no evidence of essential OH in coffinite synthesised hydrothermally. Mumpton and Roy (1961) concluded that the system UO_2 - SiO_2 contains no compounds after they and Frondel and Collette (1957) consistently failed in attempts to synthesise " USiO_4 ".

Published analyses of coffinite (Table 5) usually have low oxide

totals, while the U:Si ratio deviates from unity and these effects may be due to the fine-grained, poorly crystallised nature of the mineral as well as to voids and adsorbed water related to metamictisation (see Chapter 5, Section 3.c.). Admixed organic matter, together with organometallic complexes of U (Smith, 1984) or small uraninite inclusions (see below), may also be to blame. Ludwig and Grauch (1980) suggested their low totals could be due to unmeasured V, lattice hydroxyl, U^{6+} and the presence of submicron voids due to shrinkage during crystallisation.

Coffinite is isostructural with zircon, hafnon, thorite and xenotime and may show significant solid solution with each of these tetragonal minerals (Smith, 1984). The few experimental studies in the U-Th-Zr-Y system are discussed more fully in Chapter 5 (Section 3.d.), while the subsolidus assemblages in the system SiO_2 - ThO_2 - UO_2 - ZrO_2 , based on the experimental work of Mumpton and Roy (1961), are summarised in Fig. 8 (after Speer, 1982). In a limited number of published coffinite analyses (Table 5 and Fig. 15A), Zr is unreported. Marlow (1981) reported up to 2.1 wt % ZrO_2 in an unidentified U-silicate which showed pressure solution contacts with intergrown zircon. Th can occur in substantial amounts in coffinite (up to 17.3 wt % ThO_2 in Table 5; up to 20 mol % $ThSiO_4$, Robinson and Spooner, 1984), while the analyses of Marlow (1981) suggest that there is complete solid solution between thorite/thorogummite and an unidentified U-Si phase which replaced uraninite during a deuteric phase of alteration.

Y reaches a maximum of 12.9 wt % Y_2O_3 (Premoli, 1982; Table 5) but is generally much lower or unreported. A value of 8.96 wt % Y_2O_3 (Harrison et al., 1983) was recalculated from a very poor analysis of

finely disseminated coffinite with hydrocarbon, in which the oxide total of 19.56 wt % was normalised to 100%, with the omission of Al, K, S and Ca, which were assumed to be contaminants. Speer (1982) noted that coffinite can contain trace amounts of Y, while qualitative ED spectra of Gocht and Pluhar (1981) revealed significant Y and HREE in coffinite associated with organic matter and silica. Silver et al. (1980) concluded, from correlated Y and P, that these elements were present as a xenotime component in coffinite.

Ca invariably substitutes for U in minor amounts, but it can reach significant concentrations of up to 5.9 wt % CaO in coffinite and 8.3 wt % CaO in the U-silicate of Marlow (1981). Radiogenic Pb is generally much lower than in uraninite, partly because the coffinite structure does not accept Pb as an isomorphic replacement so that it is continuously diffused out of the structure (Cuney, 1978). Speer (1982) noted that the oldest coffinites are frequently dusted with galena because metamict coffinite (and thorite) loses Pb more easily than uraninite. A variety of other elements are reported in coffinite in minor and trace amounts (Fe, Al, Mg, V, K, Ti, S) in Table 5, but many of these could be present as admixed contaminants. Silver et al. (1980) found coffinite to be irregularly zoned in U, Th, Fe, Ca, Y, P and REE, with highest Fe in the core and highest U in the outer zones, while Silver et al. (1984) noted an inverse correlation between the U content and Fe and Th contents.

Often, coffinite occurs in intimate association with uraninite (e.g. Ludwig and Grauch, 1980; Ludwig et al., 1981), while some workers (e.g. Abdel-Gawad and Kerr, 1961; Gocht and Pluhar, 1981; Moench, 1962) have attributed variable U: Si ratios of coffinite, or uraninite lines in XRD traces of coffinite, to sub-microscopic, admixed uraninite

grains. This was confirmed by Nord (1977) who, using a TEM, was able to resolve 5-15 nm sized particles of uraninite ($a = 5.45 \text{ \AA}$) which, together with amorphous silica, he attributed to breakdown of coffinite as a result of oxidation. In most cases, it has been demonstrated that coffinite replaces uraninite (e.g. Wallis et al., 1984; Halenius and Smellie, 1983; Darnley et al., 1965; Morton, 1974) during decreasing temperatures (Leroy, 1978) or increasing temperatures (Cuney, 1978) but sometimes uraninite replaces coffinite (e.g. Bayushkin et al., 1968). Ludwig and Grauch (1980) believed there to be no marked time break between the formation of co-existing coffinite and uraninite.

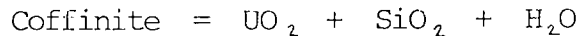
Speer (1982) and Langmuir (1978) discussed the possible controls on the stabilities of coffinite and uraninite. Brookins (1975) estimated $\Delta G^\circ_f = -456 \pm 2.6 \text{ kcal/gfw}$ for USiO_4 . This free energy value indicates that the reaction;



is at equilibrium when dissolved silica is $10^{-6.9} \text{ mol/l}$ or 8 ppb SiO_2 . Langmuir (1978) argued that this would make coffinite stable relative to uraninite at low temperatures in all natural waters (which contain an average of 17 ppm SiO_2). In order to explain the common occurrence of quartz and uraninite, Langmuir (op. cit.) proposed that coffinite becomes stable relative to uraninite at intermediate dissolved silica levels, above those in average groundwaters (i.e. >60 ppm SiO_2) but below saturation with amorphous silica.

Speer (1982) pointed out that the co-existence of pure coffinite and stoichiometric uraninite with quartz is a metastable condition but the three-phase assemblage may be stable if the uraninite is oxidised (Fig. 9). Langmuir (1978) constructed diagrams (Fig. 10) showing possible equilibrium relations between uraninite, coffinite, amorphous

silica and dissolved silica concentrations as a function of the oxidation state of the uraninite. The upper oxidation limit of uraninite able to co-exist with coffinite ($\text{UO}_{2.03}$) was calculated from the uraninite cell edge of Nord (1977, see above). Hostetler and Garrels (1962) concluded, from their proposed reaction;



that equilibrium between the solid phases was a function of the activity of water and aqueous silica. In high temperature, hydrothermal veins and pegmatites the reaction is driven to the right.

Coffinite is stable under low temperature and pressure, reducing environments, as shown by its widespread occurrence in the unoxidised portions of the Colorado Plateau-type deposits (Speer, 1982), although it is also found in vein-type (e.g. Arribas, 1966) and various other deposits. The upper temperature limit of coffinite formation usually lies in the range 200-360°C (e.g. Abdel-Gawad and Kerr, 1961; Speer et al., 1981; Wallis et al., 1984). The deposition of coffinite is favoured by acidic, reducing conditions (Langmuir, 1978) but Abdel-Gawad and Kerr (op. cit.) believe an alkaline-reducing environment to be essential.

Reduction is accomplished by metastable S species of intermediate oxidation state (Ludwig et al., 1981) or organic matter. Numerous examples of coffinite intimately associated with organic matter exist (e.g. Dubinchuk et al., 1977; Harrison, 1975; Harrison et al., 1983; Moench, 1962 etc.). Preconcentration of U prior to coffinite deposition may also be accomplished by silica gel, to give a coffinite-opal mixture (e.g. Gocht and Pluhar, 1981; Bomber et al., 1986; Mueller and Halbach, 1983) or by zeolites (e.g. Katayama et al., 1974; Mueller and Halbach, op. cit.) or by TiO_2 .

Basham and Rice (1974) described thin bands of authigenic coffinite around Ti-bearing grains, while Wallis et al. (1984) identified coffinite which was intergrown with and replacing authigenic rutile. Reynolds and Goldhaber (1978) and Reynolds et al. (1977) studied the association of U with TiO_2 , formed by the action of sulphidising fluids on Fe-Ti oxides in roll-front deposits. They interpreted U-Si correlations in TiO_2 as possible coffinite. Ruhlmann (1980) similarly noted the localised deposition of coffinite against anatase and proposed a hypothetical solid solution between $U(TiO_4)_{1-x}(OH)_{4x}$ and $U(SiO_4)_{1-x}(OH)_{4x}$, although experimental work is needed to confirm this. Ruzicka and Littlejohn (1982) described intergrowths of anatase, coffinite and U-Ti aggregates from the Beaverlodge area, Saskatchewan and concluded that both Ti and U were mobile together in the ore-fluids.

iv) Thorite, uranothorite, huttonite ((Th,U)SiO₄)
and thorogummite ((Th,U)(SiO₄)_{1-x}(OH)_{4x})

Monoclinic huttonite is the only stable polymorph of $ThSiO_4$, according to Mumpton and Roy (1961), who synthesised it at 1100°C and above, whereas metastable thorite (tetragonal) was only formed at 1175°C and below. Other studies have shown that thorite is stable between 110°C (Openshaw, 1979) and $1225 \pm 10^\circ C$ (Finch et al., 1964). Frondel and Collette (1957) hydrothermally synthesised what they believed to be hydroxyl thorite (thorogummite) at temperatures of 400-150°C. They based their conclusion on expanded cell dimensions, diffuse XRD patterns and a strong (OH) absorption indicated in infra-red studies. Mumpton and Roy (1961) similarly prepared poorly crystallised thorite below 250°C but concluded that water was present as adsorbed H_2O ,

rather than as hydroxyl. They plotted published analyses on a $\text{SiO}_2\text{-H}_2\text{O}$ - ThO_2 ternary diagram (Fig. 11) and found them to lie along the $\text{ThSiO}_4\text{-H}_2\text{O}$ join, instead of the $\text{ThSiO}_4\text{-Th(OH)}_4$ join, thus arguing against the formula $\text{Th(SiO}_4)_{1-x}\text{(OH)}_{4x}$ for hydrous thorite. Many of the thorite analyses in Table 6 have low oxide totals, suggesting the presence of water, although other factors, such as metamictisation, may be partly responsible (see Chapter 5, Section 3.b.).

Despite the findings of Mumpton and Roy (op. cit.), many workers have used the term "thorogummite", which Frondel (1953) defined as a hydroxylated, secondary alteration product of thorite, typically occurring as a non-metamict, fine-crystalline aggregate. Semenov and Kazakova (1961) noted that "hydrothorite" characteristically had a low U content, while Barritt (1983), Perez (1985), Maurice (1982), Smellie (1982b), Basham et al. (1982d) and Staatz et al. (1976) found that selective leaching of U was associated with the hydration and oxidation of thorite. Silver et al. (1984) attributed variable compositions in thorite to leaching and the addition of different elements during its alteration to thorogummite. Phair and Shimamoto (1952) described the alteration of green uranothorite to a yellow-brown hydrothorite containing 4.2 wt % U, while Rimsaite (1981a, 1982b) described the replacement of uranothorite by Fe-rich thorogummite. Marlow (1981) was uncertain whether to explain the very variable internal composition (U, Th, Si, Ca and Fe) of thorogummite as primary variations in the original thorite or as hydration associated with its secondary alteration or a combination of both. Pagel (1982) attributed the spread in $\text{ThSiO}_4\text{-USiO}_4$ compositions of thorite to metamictisation, which encourages the hydration of thorites and leaching of U.

Cameron-Schimann (1978) applied the name thorogummite to a late, interstitial material that was bright yellow, amorphous and rapidly deteriorated under the probe beam. Ballantyne and Littlejohn (1982) noted a significant decrease in UO_2 (from 23.4 to 3.0 wt %) and SiO_2 (from 22.9 to 10 wt %) associated with the hydration of euhedral, cubic uranothorite to a mottled, low relief phase. In contrast to the above observations, Khvostova (1969) identified a hydrous, U-rich thorite, although the exact U content was not specified.

Virtually all of the thorite analyses in Table 6 show some U, although there is considerable variation from less than 1 wt % to 35 wt % UO_2 . This upper limit of U in thorite is similar to that synthesised metastably and found in a literature search by Mumpton and Roy (1961), who concluded that there was little justification in calling some U-bearing thorites "uranothorite". However, analyses of naturally occurring and synthesised thorites suggest a continuous solid solution between USiO_4 and ThSiO_4 (Chapter 5, Section 3.d).

Other minor and trace elements that have been reported in thorite are listed in Table 7 (after Speer, 1982). Table 6 shows that Zr is frequently unreported or attains just a few wt % ZrO_2 in thorite; exceptionally it reaches about 9 wt % ZrO_2 (Perez, 1985; Marlow, 1981). Reported amounts of Hf and Zr could represent solid solutions with zircon (and hafnon; Speer, 1982), which is often intimately associated with thorite as epitaxial overgrowths or inclusions (e.g. Silver *et al.*, 1980 and 1984; Perez, 1985; Marlow, 1981; Rimsaite, 1986). Silver *et al.* (1980) reported a maximum of 10% zircon component in thorite, which is the maximum value quoted by Mumpton and Roy (1961) from 90 analyses of thorite in the literature.

Although REE in thorite are generally limited to between 0.5 and 7

wt % (Speer, 1982), higher amounts of Y and REE are found in the literature (e.g. Staatz et al., 1976 in Table 6) for thorites which contain dominantly LREE or HREE. Henderson (1984) found LREE were usually dominant in thorite. Earlier suggestions of a continuous ThSiO_4 - CeSiO_4 solid solution series are not supported by the data of Andersen and Neumann (1985). Vlasov (1966) reported that substantial Y (typically 3 wt % Y_2O_3) and HREE contents were found in thorite formed in hydrothermal rocks, in which HREE minerals normally have a Dy maximum (e.g. 25% of REE in thorite). From their data and from an appraisal of a limited number of thorite analyses in the literature, Staatz et al. (1976) concluded that thorite does not selectively accommodate one group of REE over another, but rather incorporates whatever is available.

Like zircon, xenotime frequently forms epitaxial overgrowths on or inclusions in thorite and probably represents a solid solution component in thorite in some cases. Silver et al. (1980) reported a 10-15% xenotime component in thorite but Silver et al. (1984) found insufficient P to balance the Y. Speer (1982) pointed out that the amounts of P^{5+} and As^{5+} substituting for Si^{4+} are much less than those needed to compensate for the amounts of Ca, Fe, Y and REE reported in thorites, and this is confirmed by most of the analyses in Table 6. P_2O_5 is usually less than 3 wt % but, exceptionally, ranges from 4 up to almost 14 wt %. Frondel (1958) described a highly P-rich variety of thorite/thorogummite called "auerlite", with $(\text{PO}_4) : (\text{SiO}_4) = 0.8 : 1$.

Like coffinite, thorite invariably contains Ca, which probably substitutes for Th (Speer, 1982) and is normally present in concentrations of 1 - 5 wt % CaO (Table 6), although up to 10 wt % CaO (Cameron-Schimann, 1978) has been reported. Similarly, Fe is

usually reported and Speer (1982) regards it as a major substituent in thorite, since it is present in amounts up to 12 wt % Fe_2O_3 . George (1951) inferred that anhydrous, blue-green thorite contained U and Fe in the lower oxidation state, whereas yellow and orange thorite had undergone oxidation and hydration. Staatz et al. (1976) reported a metamict thorite with 5 wt % Fe_2O_3 , containing small inclusions of goethite, while Robinson and Abbey (1957) reported pyrite and magnetite as contaminants in an Fe-bearing thorite. It is possible that some of the higher FeO values quoted in Table 6 are also due to contamination, since iron-oxide and -sulphides are often closely associated with thorite (e.g. Yeliseyeva, 1977; Perez, 1985; Rimsaite, 1983). Other elements which Speer (1982) regards as contaminants include C, present as inclusions of carbonate minerals or as microscopic films of hydrocarbon (Robinson and Abbey, 1957), Mn, Cl and F. Pb is probably of radiogenic origin but, as in coffinite, it is only present in small amounts.

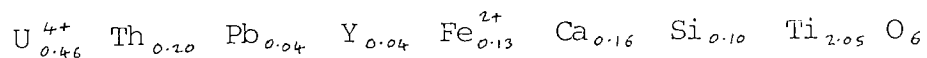
Thorite is a relatively rare though widespread mineral which usually occurs in pegmatites associated with granites or syenites and in placer concentrates derived from them (Speer, 1982). Thorite is increasingly being discovered in igneous and metamorphic rocks with normal Th concentrations, in which the bulk Th/U ratio is positively correlated with the Th/U ratio of the thorite (e.g. Barritt, 1983; Perez, 1985). Speer et al. (1981) found that, where the Th/U ratio of a granite was 3.5-10, U could be entirely incorporated into uranoan thorite, which contained up to 10 mole % USiO_4 . Where the Th/U ratio ranged from 1.2-3.0, the amount of U exceeded the limit of ThSiO_4 - USiO_4 solid solutions, giving rise to uraninite, which co-existed with uranoan thorite containing 15 mole % USiO_4 . In some cases (e.g. Pagel,

1982; Cuney, 1978) early crystallisation of thorite in a granite leads to depletion of Th and enrichment of U in the residual melt. Thorite has been less commonly described from hydrothermal deposits (Phair and Shimamoto, 1952).

v) Brannerite-thorutite ((U,Th)Ti₂O₆) and complex uranotitanates

Brannerite (UTi₂O₆) is monoclinic and isostructural with thorutite (ThTi₂O₆, Ruh and Wadsley, 1966), but an orthorhombic variety with the proposed formula U⁴⁺U⁶⁺(Ti, Fe)₄O₁₂(OH)₂ has been reported by the Peking Institute of Uranium Geology (1978). The identification and structural determination of brannerite are difficult, due to its altered and metamict nature. Heating usually restores an X-ray pattern but Jenkins (1974) warns that chemical changes may occur.

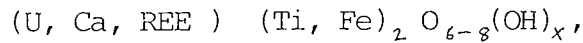
Theoretically, there is complete solid solution between UTi₂O₆ and ThTi₂O₆ but, so far, natural specimens have shown a gap between Th_{0.21} and Th_{0.87} (Ferris and Ruud, 1971). Thorian brannerite, corresponding to the lower limit of this gap, has been found in sodic granitoids and felsic gneisses at Crocker's Well, South Australia (see Chapter 5, Section 6 for genesis of thorian brannerite). Jenkins (1974) plotted EPMA data of the brannerite as mole % on a TiO₂ + Fe₂O₃, UO₂ + 0.5 (CaO + PbO), ThO₂ + 0.5 (CaO + PbO) ternary diagram (Fig. 12A). Ashley (1984) distinguished two varieties of brannerite, both with the approximate composition:



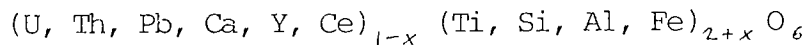
A dark brown, opaque brannerite containing inclusions of TiO₂ and radiogenic galena, with 2% H₂O, weathered to a greenish translucent, inclusion-free variety, containing 11% H₂O.

In brannerite, U may be partially oxidised and replaced by Ca and

REE, while Fe may replace some of the Ti and partial hydration can occur. A more realistic formula may be;

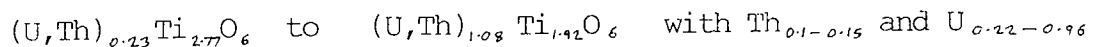


where the variable O content reflects the oxidation of U which is not compensated by the substitution of Ca and REE (Smith, 1984). Szymanski and Scott (1982) noted that brannerite is commonly deficient in U but contains excess Ti and they proposed the formula;



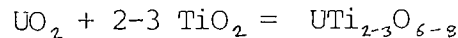
where $x = 0.3-0.75$. With increasing leaching of U, brannerite acquires a yellowish rim of anatase and is ultimately replaced by TiO_2 . Silver et al. (1980; 1984) described four different zones in brannerite which had undergone varying degrees of post-magmatic alteration. EPMA of the different zones indicated the inner two to be of branneritic composition, whereas the outer two consisted of a Pb-, U- and Th-bearing aggregate of anatase and other phases. Silver et al. (1984) concluded that recrystallisation of the brannerite had been accompanied by expulsion of Pb and Th from the central zone.

From the EPMA of various world occurrences of brannerite (Fig. 12B), Ferris and Ruud (1971) concluded that the composition ranged from;



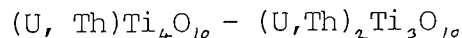
They noted that compositions in the Blind River ores, from Ontario, Canada, ranged from uraniferous leucoxene to brannerite and these were often associated with TiO_2 and pyrite from the breakdown of detrital ilmenite. Ferris and Ruud (op. cit.) concluded that the grains did not have a detrital origin, but rather formed by the adsorption of U on titanogels, which are very effective concentrators of uranyl (Section 2. e.i.) and which later crystallised as "brannerite" or "protobrannerite"

(Schindlmayr and Beerbaum, 1986). Korolev and Rumyantseva (1976) coprecipitated U and Ti hydroxide gels from HCl solutions of U and Ti in the proportions 1 : 2. XRD of the heated precipitates gave a brannerite pattern. Ramdohr (1957) named this in situ formation of brannerite the Pronto Reaction;



and it may involve either Ti-bearing solutions migrating to and reacting with uraninite or U-bearing solutions migrating to TiO_2 .

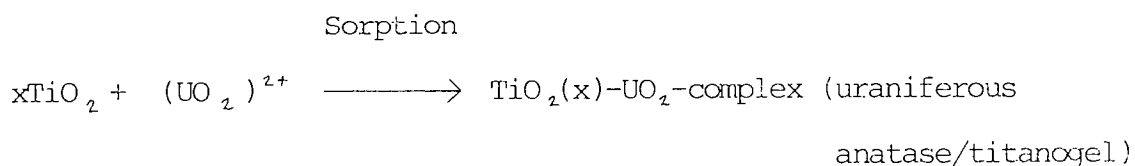
Jenkins (1974) also proposed an authigenic origin to the Blind River brannerite, after plotting EPMA data on the ternary diagrams already described (Fig. 12B). These demonstrate that the Blind River material does not have a true branneritic composition but instead varies from U-bearing rutile to Ti-deficient brannerite. Since "brannerite" implies a mineral of specific composition, Jenkins (1974) preferred the term "brannerite series," including:



A similar, authigenic origin of brannerite has been accepted by many other workers for the Proterozoic quartz-pebble conglomerates from the Elliot Lake - Blind River area (e.g. Clemmey 1981; Robinson and Spooner, 1984; Saager and Stupp, 1983) and from the Witwatersrand and Pongola Basins, South Africa (e.g. Schidlowski, 1981; Feather, 1981; Thiel et al., 1979; Saager et al., 1981; Clemmey, 1981). In the Witwatersrand, migrating Ti-bearing solutions were responsible for the brannerite pseudomorphs after uraninite "ghosts", while U-bearing solutions reacted with altered Fe-Ti oxides to give uraniferous leucoxene aggregates. Andreoli et al. (1985) believed that uraniferous leucoxene and/or "rutile-like phases" in hydrothermally altered granite of the pre-Witwatersrand basement, could be detrital precursors to the brannerite-uraniferous leucoxene of the Witwatersrand reef

horizons.

An authigenic origin has also been attributed to brannerite from the Karpinka Lake U Prospect in Saskatchewan, Canada, which is believed to represent a metamorphosed, epigenetic sandstone-type U deposit (Williams-Jones and Sawiuk, 1985). Sulphidising fluids caused replacement of detrital Fe-Ti oxides by spongy Ti-rich cores rimmed by pyrite, together with alteration of feldspar and pyroclastic fragments to kaolinite. U was adsorbed on to the titania and kaolinite which, after metamorphism, recrystallised to brannerite and uraninite-sillimanite associations, respectively. Brannerite formation has also been attributed to adsorption of U on TiO_2 from another sandstone-type U deposit, in the Great Slave region of North Western Territory (Morton, 1974):



In Sweden, reactions between uraninite and Ti-bearing solutions, sphene and altered Fe-Ti oxides gave rise to uranotitanates of a highly variable composition in altered granites of the Arjeplog-Arvidsjaur-Sorsele U province (Adamek and Wilson, 1979; Halenius and Smellie, 1983; Halenius et al., 1986; Smellie and Laurikko, 1984; see Chapter 5, Section 6.b.iii.), at Duobblon (Lindroos and Smellie, 1979; Smellie, 1982a) and in Precambrian rocks of the Olden Window (Smellie, 1982b; Troëng, 1982). A detrital origin has been proposed for brannerite, irregularly disseminated in graphite schists (formerly black shales) from the Mauji-Reshian area, Azad Kashmir, Pakistan (Rahman, 1979). The brannerite shows peripheral replacement by graphite but there is no evidence for the Pronto Reaction (e.g. uraninite inclusions).

Analysis of U-Ti phases in the Witwatersrand conglomerate

Simpson and Bowles (1977) investigated the association of U with lenticular to rounded granules of quartz, kaolinite and pyrophyllite from the Witwatersrand basket-type ores. U is disseminated throughout the granules but fission-tracks revealed point-sources, which Simpson and Bowles (op. cit.) were unable to correlate with a specific mineral.

Schidlowski (1981) noted ubiquitous, small brannerite specks interspersed in the Witwatersrand conglomerate matrix and believed these to have formed in situ from the random encounter of U- and Ti-bearing, mineralising fluids. Clemmey (1981) noted an association of U with Ti in phyllic minerals and envisaged the precipitation of U and Ti in micro-reducing environments, around specks of carbon.

Plates 1-4 show the association of fission-tracks with phyllic granules and partial replacements of pyrite concretions in a sample (1022) of conglomerate from the Orange Free State. Probe analyses in this study have subsequently shown at least some of the point-sources to be associated with small, U- and Ti-bearing grains of a highly variable composition (Table 8). The grains range from less than 10 μm up to 20 μm across and are frequently associated with pyrite (Plates 5-8). In Table 8, high values for Si, Al and Fe probably reflect contamination from the host phyllosilicates, while high Fe and S are likely to be from the pyrite. S concentrations are sufficiently high for the Pb to be present as galena which could be of radiogenic origin. In all the analyses, U and Th are positively correlated, suggesting they belong to the same mineral. In Grain 4, there is also a correlation of U and Ti, but in the other two grains there is little correlation and U tends to greatly exceed Ti. These compositional variations might reflect different stages in the progressive reaction

of U-bearing solutions with TiO_2 to form a range of U-Ti phases. An association of the U-Ti phases with pyrite is consistent with the TiO_2 resulting from the alteration of Fe-Ti oxides by sulphidising fluids.

vi) Multiple oxides of Nb and Ta

Compositions of these minerals vary greatly because of complex substitutions but they may be expressed by the general formula

$A_x B_y O_z$ where:

A = REE, U, Ca, Th, Fe^{2+} , Na

B = Nb, Ta, Ti, Fe^{3+}

O = O, OH, F

U can reach 24% but is generally below 10% in these minerals which comprise approximately 25 species, half of which belong to the pyrochlore group, the euxenite-polycrase, fergusonite-formanite and other isomorphous series (Steacy and Kaiman, 1978).

The pyrochlore group has been revised by Hogarth (1977) who identified a number of synonyms, doubtful species and discredited names and outlined a classification based on the relative proportions of Ti, Nb and Ta in the B-site and on the identity of the dominant A-site atoms (Table 9). Defects to the pyrochlore structure, resulting from charge balance effects and coupled substitutions, contribute to the deviations from ideal stoichiometry shown by many pyrochlores (Smith, 1984).

Pyrochlores, together with other complex oxides such as euxenite, polycrase and samarskite which have a columbite-type structure, are often metamict and contain U which has been oxidised to U^{6+} . Despite this, they are refractory minerals which can occur in placer deposits. More usually, they are found as accessory minerals in granitic and syenitic rocks, their pegmatite facies or in carbonatites.

b) Accessory minerals with minor U⁺⁺ and Th

Tables 13-18 show the range of U and Th contents in various accessory minerals. Apatite, epidote and sphene generally contain low concentrations of U and Th, allanite and monazite are dominated by Th, while zircon and xenotime may contain high Th and/or high U.

i) Zircon (Zr, Hf)SiO₄

Zircon is typically enclosed by the major minerals and crystallises early from the melt at high temperatures (Deer et al., 1966). Pupin (1980) suggested that zircon crystallises early in water-poor magma, but crystallisation is more prolonged in hydrous magmas, culminating in the late development of trace element-enriched hydrozircon. Infra-red studies showed that zircon, synthesised hydrothermally at 150°C by Frondel and Collette (1957), contained (OH)₄ in substitution for (SiO₄), while Caruba et al. (1985) concluded that F was essential for the stability of hydroxylated zircon synthesised at temperatures down to 400°C. Mumpton and Roy (1961) pointed out that, if natural zircons are ZrSiO₄-Zr(OH)₄ solid solutions, they should lie along this join in a SiO₂-ZrO₂-H₂O plot. Fig. 13 shows that zircon analyses lie along the ZrSiO₄-H₂O join, indicating that water of natural zircons is present largely as molecular water, not hydroxyl. From a review of studies of water in zircon, Speer (1982) concluded that the substitution of (OH)⁻ for SiO₄ in natural zircons is minor and most water is adsorbed by metamict material as either H₂O or (OH)⁻. Vlasov (1966b) described "gelzircon" (ZrSiO₄.nH₂O) containing up to 20% H₂O.

Although zircon is fairly resistant to normal chemical attack (Deer et al., 1966), the crystal structure can undergo progressive

breakdown as a result of the radioactive decay of constituent U and Th atoms. The mechanism of this metamictisation is discussed more fully in Chapter 5 (Section 3.a.) and it results in a systematic decrease in density, birefringence and refractive index of the zircon (Table 10). Experimental studies of Tole (1985) indicate that, whereas crystalline zircon is thermodynamically stable in aqueous solutions of pH 0 - 9 at 25 - 80°C, amorphous (metamict) zircon exhibits limited dissolution at a pH of 5. Dissolution is further increased by the presence of F and alkali ions, which form stable complexes with Zr (Chyi, 1986; Vlasov, 1966a; Henderson, 1984).

Over 50 elements have been reported in zircon analyses and, of these, the best documented are listed, with their atomic radii, in Table 11 (after Speer, 1982). Hf is the main substituent for Zr and ranges from 0.59-5.13 wt % HfO₂ in Table 12. In a compilation of 463 zircons by Ahrens and Erlank (1969), Hf contents ranged from 0.6 to 7.0 wt %, with a mean of 1.71 % but were generally less than 3 %. Much higher Hf contents occur in pegmatite zircons from the Pyrenees (<26 wt % HfO₂; Fontan et al., 1980), South West Africa (<31 wt % HfO₂; von Knorring and Hornung, 1961) and Norway (22-24 wt % HfO₂). Correia Neves et al. (1974) suggested the following classification for natural (Zr, Hf)SiO₄ solid solutions :

mol % HfSiO ₄ :	0-10	10-50	50-90	90-100
	Zircon	Hafnian	Zirconian	Hafnon
		Zircon	Hafnon	

Complete solid solution between zircon and hafnon was demonstrated by Ramakrishnan et al. (1969) who synthesised intermediate compositions in the ZrSiO₄- HfSiO₄ system.

Speer (1982) concluded, from the similar average Zr : Hf ratios in

zircon (40 : 1) and the earth's crust, that geochemical separation of these elements must be inefficient in most geological situations. Igneous zircons with Hf-enriched rims (e.g. Ono, 1975) and the uncommon enrichment of Hf in zircon with differentiation of the host rock (Ahrens and Erlank, 1969; Ehmann et al., 1979; Deer et al., 1982) demonstrate that infrequent enrichment of Hf does occur. Metasomatic processes (e.g. albitisation, Chapter 5, Section 4) may also be responsible for Hf enrichment.

Y is generally unreported in zircon or ranges from 1 to 4 wt % Y_2O_3 and, exceptionally, attains approximately 10 wt % Y_2O_3 . The analyses of Barritt (1983) demonstrate a solid solution series between zircon and xenotime (Fig. 15A). Medenbach (1976) reported up to 25 wt% (Y + REE₄O₃) in zircon while Speer (1982) concluded, from a review of zircon, that Y can attain 16.5 wt % Y_2O_3 , with the highest Y and P corresponding to about 25 mol % xenotime (analyses of Romans et al., 1975). HREE generally predominate, since the size of Zr⁴⁺ is closer to the HREE than to the LREE (Table 11). This is supported by partition coefficients obtained from natural (Nagasawa, 1970) and experimental (Watson, 1980) systems, although Krasnobayev et al. (1976) concluded, from a study of 62 zircons, that the mineral will incorporate whatever REE are available. Y and P are incorporated in zircon overgrowths or late zircon during falling magmatic temperatures at the end of crystallisation (Veniale et al., 1968; Kohler, 1970; Pupin and Turco, 1975). Hoffman and Long (1984) noted domains of Y enrichment with Zr and Hf depletion and domains of Y depletion with Hf enrichment in Lewisian zircons showing sector zoning. In a compilation of U and Th concentrations in zircon (Table 13), values are predominantly below 1 wt % but can reach 7 wt % U and 10 wt % Th. Enriched radioelement

contents are typically associated with low oxide totals which are sometimes below 90% and are probably due to voids, with or without adsorbed water, resulting from radiation damage to the zircon lattice.

Ahrens (1965) and Ahrens et al. (1967) found that the Th/U ratio in zircons was less than one, in contrast to the general value of 3.5-4 for igneous rocks. This could either reflect the preferential inclusion of U^{4+} in zircon because it is closer to Zr in ionic radius than Th (Table 11) or co-crystallisation with a Th-enriched phase, such as monazite or thorite, or both (Speer, 1982). Ahrens (1965) found the Th/U ratio to increase with increasing U and Th contents of zircon and remarked on the previously observed tendency for zircon Th/U ratios to increase with differentiation in basic and granitic rocks. In contrast to the above observations, the enrichment of U with differentiation of granites is indicated by the common occurrence of zircon with rims containing higher U than the cores (e.g. Chovan and Kral, 1979; Grauert and Seitz, 1973; Silver et al., 1980; Silver and Deutsch, 1963; Yeliseyeva, 1977; Troëng, 1982; Berzina et al., 1974; Clark et al., 1979). Conversely, Silver et al. (1984) and Stuckless and Van Trump (1982) described zircon with cores enriched in U relative to the rims. High U cores are often due to inherited or xenocrystic zircons. Stuckless and Van Trump (1982) attributed zoning and other non-uniform distributions of U within and among zircons from a single sample to variations in partitioning coefficients for U between melt and zircon. For example, the oxygen fugacity of the magma will control the level of U^{4+} , which is preferentially incorporated into the zircon structure, relative to U^{6+} . Other variables which can affect the distribution of U in zircon are coupled substitutions, lattice defects and diffusion rates relative to crystallisation rates (Stuckless and Van Trump,

op. cit.). Yeliseyeva et al. (1975) believed U enriched rims to reflect a uniform distribution of U and Zr throughout the melt as a result of diffusion, allowing the build-up of a U concentration gradient around the zircon. With periods of intensive stirring of the melt, this diffusion zone was destroyed, leading to repeated alternations of U-poor and U-rich zones in the zircon.

ii) Monazite (LREE, Th)PO₄

Monazite is monoclinic and isostructural with huttonite (Th(SiO₄)), brabantite (Ca, Th(PO₄)₂) and cheralite (LREE, Th, Ca, U(P, Si)O₄). Solid solution in the ternary system ThSiO₄-REEPO₄-CaTh(PO₄)₂ is represented in Fig. 14 (after Speer, 1982). Table 14 shows Th values generally fall within the range 2-12 wt % Th, although 24.78 wt % Th is quoted by Vlasov (1966b). This exceptionally high Th content is accompanied by high Si (6.09 wt % SiO₂) and indicates the coupled substitution $Si^{4+} \rightleftharpoons P^{5+}$. Henderson (1984) reported that Th is usually present in monazite in substitution for REE up to 13 wt% ThO₂, with charge balance maintained through the simultaneous substitution of Si. This charge balance mechanism appears to be operative in other analyses and probably represents solid solution between monazite and huttonite. Price et al. (1982) were able to express compositional variations in monazite in terms of two solutions between four end members; monazite to xenotime and huttonite to an unnamed Pr, Nd compound. Other coupled substitutions suggested by Gramaccioli and Segalstad (1978) include $Ca^{2+} \rightleftharpoons REE^{3+}$ (equivalent to solid solution with cheralite) and $K^{+} \rightleftharpoons REE^{3+}$. Jefferies (1985a) suggested the first of these controlled entry of Th into monazite from the Carnmenellis granite, Cornwall, on the basis of a strong 1:1 correlation of Th and Ca. The slight decrease in unit

cell dimensions of monazite, resulting from this substitution, lead to the preferential incorporation of the smaller Y atom and hence a positive correlation between Ca, Th and Y. According to Mannucci et al. (1986), the similar unit cell volumes of the various end member components indicate an ideal-solution behaviour in monazite, so that the solubility of Th, Ca and U should be independent of temperature or other components in solid solution. Thus, element correlations reflect processes of fractionation before the monazite crystallised.

Price et al. (1982) found the variation of Th and U among 10 monazites to be greater than that between 20 spots in one grain. Th variation within some grains was more substantial (Table 14) and an X-ray map of one example showed a Th-enriched core, although U-rich domains were not evident in a monazite with enhanced U. Similarly, Chovan and Kral (1979) found U to be homogeneously dispersed in monazite, although it differed between grains (Table 14). Chovan and Kral (op. cit.) and Silver et al. (1980) noted that Th concentrations were higher in the margins of zoned grains.

U concentrations rarely exceed 0.5 wt % in monazite (Overstreet, 1967) and generally remain below 2.5 wt % U in Table 14. U is probably present as U⁴⁺ and so it can share in the same coupled substitutions associated with Th (Mannucci et al., 1986). Factor analysis studies by Price et al. (1982) showed that U behaves like the smaller trivalent REE.

U and Th may also be present as inclusions of other minerals. Monazite (and xenotime) from the Alston Block orefield in the north Pennines (Groverake and Redburn mines) contains tiny (1 µm) inclusions of uraninite (Flowers, per. comm.). Chovan and Kral (1979) noted 3 µm-sized inclusions of a U-Si phase which they suggested was coffinite,

while Robinson and Spooner (1984) and Silver et al. (1980) found thorite inclusions. Apatite, thorite and cheralite inclusions were believed by Silver et al. (1984) to have exsolved from the host monazite. Yeliseyeva (1977) noted microscopic Si-Y-Zr-rich grains in monazite and these could have been xenotime and zircon inclusions.

Monazite is a rare accessory in granitic rocks and syenitic and granitic pegmatites (Deer et al., 1966). Overstreet (1967) observed a correlation between the Th content of monazite and the geologic environment in which it crystallised. Vlasov (1966b) found monazite from granites to contain 3 - 6 wt % ThO₂, whereas those from granite pegmatites had increased Th contents and those in hydrothermal-greisen deposits were characterised by low Th (0 - 5% ThO₂), although this increased in higher temperature greisens.

iii) Xenotime (Y, HREE)PO₄

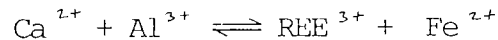
Xenotime contains up to approximately 4 wt % U and 6 wt % Th, with either element predominating in a particular analysis (Table 15). Zr is usually unreported but sometimes reaches 5 wt % ZrO₂, while exceptionally high values are reported in xenotime from the Cairngorm granite (Webb and Brown, 1984a; Barritt, 1983; in Fig. 15A).

Silver et al. (1980) described xenotime with tiny inclusions of thorite, zircon and other phases, while Rimsaite (1984) observed the reaction of uranothorite and uraninite inclusions with their xenotime hosts to produce an Y-P-U phase. Xenotime may alter to secondary, radioactive bastnaesite group minerals (Rimsaite, 1983) or to churchite (YPO₄.2H₂O ; e.g. Cameron-Schimann, 1978; Table 15). Simpson and Bowles (1977) identified churchite from its lower proportions of Dy, Er and Yb, relative to Gd compared with xenotime.

Xenotime is generally associated with granites and occurs in pegmatites, where it is characterised by a high U content or is found in hydrothermal rocks (e.g. Brodin et al., 1976) when it contains lower U and Th (Vlasov, 1966b). Lyakhovich (1962) found a Dy maximum in granitic xenotime and an Yb maximum in pegmatitic xenotime, but this is not universally applicable (Henderson, 1984). As well as the occurrences listed in Table 15, uraniferous xenotime has been described as small inclusions in hydrocarbon cores to sandstone reduction spots (Parnell, 1985).

iv) Allanite (Ca, Ce)₂(Fe⁺², Fe⁺³) Al₂O .OH (Si₂O₇) (SiO₄)

Allanite is the only member of the epidote group in which Fe²⁺ is an essential component (Deer et al., 1966). The coupled substitution;



is accompanied by an increase in refractive index. Ce usually comprises over half of the REE present and is two or three times more abundant than La (Fronzel, 1964). Compared with other epidote-group minerals, allanite has a higher Th content (0.1 - 3.5 wt%; Table 16) which usually exceeds U (<1 wt %), although higher contents of U may occur in altered allanite (e.g. Rimsaite, 1982b). Smellie (1982b) described primary igneous allanite with U-enriched margins. Allanite sometimes contains inclusions of uraninite, uranothorite, zircon and other minerals (Rimsaite, 1981b, 1982a).

Metamictisation is common and may be accompanied by hydration, with expansion of the mineral, giving rise to surrounding, anastomising cracks. Allanite is resistant to alteration, except in higher temperature, hydrothermal regimes but, when metamict, it becomes susceptible to leaching during weathering (Basham et al., 1982a). In

the outer Starav granite, from the Etive Complex in the south west Grampian Highlands, U was leached from the outer zones of metamict allanite, and redeposited along surrounding, radiating cracks (Barritt, 1983). Similar leaching and redeposition of U occurred in allanite from uraniferous granites at Baffin Island, North West Territory, Canada (Maurice, 1982) and from the Strath Halladale Complex and Criffel-Dalbeattie granites, Scotland (Basham *et al.*, 1982b). Cameron-Schimann (1978) described U-free, H₂O-bearing allanite with Th, Fe and Mg concentrated in a metamict, dark green rim, while Ca and REE were enriched in the centre.

The deuteric replacement of allanite by bastnaesite ((LREE)FCO₃) is a common feature in Canada, the US and USSR (Littlejohn, 1981). Bastnaesite overgrowths and replacements of allanite have been described from the Grenville Structural Province of Canada by Littlejohn (*op. cit.*) and Rimsaite (1981b), while Yeliseyeva (1977) noted an enrichment of U associated with the marginal replacement of allanite by bast naesite in the USSR.

Allanite is characteristically found in granites, granodiorites, monzonites, syenites and particularly pegmatities (Deer *et al.*, 1966) and, in some cases, crystallises from REE-rich residual fluids during the late-stage consolidation of granite (Exley, 1980). Allanite can also be a secondary mineral, formed during metamorphism (Smellie, 1982b) or meteoric-hydrothermal alteration (Exley, 1980; Fowler, 1981).

v) Apatite Ca₅(PO₄)₃(OH, F, Cl)

Apatite is a common accessory found in all igneous rock types, as well as metamorphic and sedimentary rocks. Fluorapatite is the most abundant end-member of an isomorphous series which also includes

chlorapatite, hydroxy-apatite and carbonate-apatite (Deer et al., 1966). Cryptocrystalline phosphates, in which the apatite phases cannot be resolved, are termed collophane and can contain significant quantities of U (e.g. <639 ppm U; Miller, 1983).

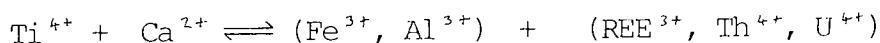
U and Th concentrations in apatite rarely exceed 1 wt % and are usually present in concentrations of 10's - 100's ppm (Table 17). U can reach significant levels in fluorapatite associated with bone phosphate in fossil vertebrates, due to absorption from circulating groundwaters (e.g. 0.27 wt % U, Bowie and Atkin, 1956; 0.29 wt % U, Udas and Mahadevan, 1974). The tail bones of a dinosaur named Seismosaurus, recently discovered in the Jemez Mountains of New Mexico, contain concentrations of U 400 times that of the surrounding rock (Anderson, 1987). U can be introduced or leached from apatite as a secondary process (Altschuler et al., 1954). Chovan and Kral (1979) noted domains of secondary U infiltration in apatite from Czechoslovakia, while Fowler (1981) attributed low U rims of apatite to scavenging of U by an intergranular fluid phase in the Glendessary syenite, Scotland. U may be leached from dislocation sites in the lattices of apatite and monazite (Rose and Bornhorst, 1981).

U (together with Th) may be present in the 4+ valence state as a substitution for Ca^{2+} in the apatite lattice (Altschuler et al., 1954), or as UO_2^{2+} , which displaces Ca^{2+} and combines with two adjacent phosphate groups at the surface of apatite crystals (Bowie and Atkin, 1956). The latter mechanism explains why Th^{4+} may be absent from apatite and why U in groundwater does not substitute for Ca in other accessory minerals (Bowie and Atkin, op. cit.), but the former mechanism is suggested by the presence of significant proportions of U^{4+} in igneous and marine apatites (Clarke and Altschuler, 1958).

U and Th contents in apatite may also be attributed to inclusions of uraninite (e.g. Krishna Rao and Rao, 1983) or zircon (e.g. Chovan and Kral, 1979) or to intergrowths with thorite, monazite and Y-Th-fluorocarbonates (Silver et al., 1984). Yeliseyeva (1977) suggested uneven distributions of U in apatite might be due to radioactive inclusions, U concentrations along cracks, late U-enriched margins and U-bearing gas-liquid inclusions.

vi) Sphene $\text{CaTi}(\text{SiO}_4)(\text{O}, \text{OH}, \text{F})$

The orthosilicate sphene is a widespread accessory in igneous rocks and is also found in metamorphic rocks and as detrital or authigenic grains in sedimentary rocks (Deer et al., 1966). Like apatite, U and Th contents in sphene are almost invariably below 1 wt%, with either element predominating (Table 18). The coupled substitution;



contributes to charge balancing during the substitution of REE, Th and U for Ca.

Often, the crystallisation of later generations of more uraniferous sphene is accompanied by the growth of U-enriched rims, reflecting an accumulation of U in the melt (e.g. Barritt, 1983; Fowler, 1981; Sawka and Chappell, 1985). Fowler (op. cit.) and Sawka and Chappell (op. cit.) described the enrichment of U in secondary generations of sphene, which can result from the reaction between quartz or feldspar and Fe-Ti oxides (e.g. Silver et al., 1984). In the Eye-Dashwa Lakes pluton, north west Ontario, fracture fillings of sphene scavenged up to 600 ppm U (Kamineneni, 1986). U concentrations may be increased by several orders of magnitude after the replacement of sphene by TiO_2 , Fe-Ti oxides, quartz and calcite (Section 2.e.i.).

c) U⁶⁺ minerals

More than 133 minerals are known in which U is an essential constituent (listed in Steacy and Kaiman, 1978; Morton, 1978) and, of these, the great majority contain U⁶⁺ as uranyl and are of secondary origin. They may be deposited in the oxidised zone associated with a primary U deposit or the U may be transported in solution a considerable distance from its source area before precipitation. A variety of bright colours characterise secondary uranyl minerals which either replace the original U phases directly or comprise stains and patches, often containing a mixture of different species. Frondel (1956) collectively termed these mixtures "gummite" and, together with Rimsaite (1977), noted a zonation of minerals from earlier Pb-uranyl species nearest uraninite to Pb-free uranyl silicates etc. further away. Vochten et al. (1979) noted a sequence from uraninite, through hydrated U-oxides, -silicates, -carbonates to -phosphates, during the weathering of a U deposit. The greatest migration of UO_2^{2+} from the ore occurs during the uranyl-phosphate stage.

Dall'aglio et al. (1974) found that, in certain environments, geochemical processes favour the precipitation of secondary uranyl minerals, even where there is no primary U mineralisation. Examples discussed included the deposition of autunite under humid climatic conditions on the Sila Plateau, Italy and the deposition of carnotite under arid conditions in the calcrete area of Western Australia.

Most uranyl minerals are relatively rare and only the more important ones are listed in Table 19, which includes the few of economic importance; carnotite, tyuyamunite and uranophane. The only uranyl minerals described in this study belong to the autunite and



meta-autunite groups which are, by far, the largest and best studied groups of uranyl phosphates and arsenates. Their relative abundance reflects the ease of forming UO_2-PO_4 or UO_2-AsO_4 complexes in solution (Langmuir, 1978). The two groups are closely related compositionally (Table 19) and both structures comprise infinite sheets, but they differ primarily in the degree of hydration and stacking arrangement of the sheets, according to Smith (1984), who warned that autunites can easily dehydrate to meta-autunites after sampling.

d) Rock-forming minerals

Due to their incompatible natures (Section 1), U and Th tend to occur in very low concentrations in quartz, feldspar, mica and the mafic minerals (Table 20). It is unclear how U and Th are present in these major rock-forming minerals but Rogers and Adams (1969) suggested the following possible sites:

1. Isomorphous substitution in the lattice.
2. Concentration in lattice defects.
3. Adsorption along crystal imperfections and grain borders.
4. Inclusion as microcrystals of U and Th minerals.

Rankin et al. (1982) detected an average of 200-300 ppm U (range of <1 to >1000 ppm U) in fluid inclusions in quartz and concluded that fluid inclusions may contribute much of the 10 ppm U reported for quartz (Table 20).

e) Other sites for U and Th

i) TiO₂

There are a number of examples in which U is spatially and genetically associated with TiO₂. In some cases, U and Ti have reacted to give uranotitanates of a highly variable composition (i.e. "brannerite", Section 2.a.v.), in others the U appears to be adsorbed on to TiO₂, while elsewhere it is present as a U-phase (e.g. coffinite; Section 2.a.iii.) which is intimately intergrown with the TiO₂.

Whereas the U content of uranotitanates ranges up to about 60 wt % UO₂, TiO₂ generally contains <1 wt % adsorbed U and Th (Table 21). Crystalline TiO₂, such as anatase, does not have a strong affinity for U, according to Ruhlmann (1980) who suggested that U was first reduced to U⁴⁺, before being fixed in chains of Ti(OH₄)_n colloids, which later crystallised as TiO₂. Goldhaber et al. (1983) believed that U⁶⁺ was adsorbed in TiO₂ phases and later reduced by aqueous sulphide. Davies et al. (1964) demonstrated the high sorptive capacity of artificial titanogels, which contained up to 268 ppm U, extracted from sea-water.

Saager et al. (1981) noted high concentrations of U with leucoxene aggregates (Table 21) and concluded that Ti-hydroxides are more efficient U concentrators than Fe hydroxides (Table 22). In most cases, the TiO₂ is authigenic, resulting from the alteration of Fe-Ti oxides, biotite etc. A widely documented phenomenon is the enrichment of U associated with the alteration of sphene to aggregates of TiO₂, quartz and calcite (e.g. Berzina et al., 1974; Webb and Brown, 1984b; Yeliseyeva, 1977; Tieh and Ledger, 1981; Guthrie and Kleeman, 1986; Speer et al., 1981). The U is usually adsorbed on to the TiO₂, but Kamineni (1986) identified thorogummite rims around hydrous, Fe-Ti oxide pseudomorphs after sphene.

ii) Fe- and Mn-oxides/hydroxides

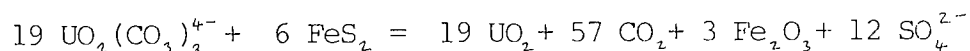
Table 22 shows that concentrations of U in Fe oxide range from 10's to 100's ppm, whereas Th is either unreported or attains just a few 10's ppm at the most. The higher affinity of Fe oxide for U, compared to Th, is probably related to the greater mobility of U⁶⁺ in the oxidising environments associated with Fe oxide deposition, although the precise role of Fe oxide in the precipitation of U is not fully resolved (Section 1.c.).

Nash (1977) found most of the U in a two-mica porphyritic granite to be associated with magnetite, while Robb and Schoch (1985) detected relatively high concentrations of U in late deuteric magnetite overgrowing primary magnetite with lower U. Higher concentrations of U tend to occur in magnetite which has altered to martite (e.g. Smellie, 1982a). The U is usually adsorbed on to this secondary haematite or goethite which formed during the weathering or hydrothermal alteration of granitoids (e.g. Basham and Rice, 1974; Berzina et al., 1974; Caruso et al., 1982; Kamineni, 1986; Webb and Brown, 1984a and b) or volcanic rocks (e.g. Stuart et al., 1983; Henry and Deux, 1981; Zielinski, 1982; Bowden et al., 1981) or conglomerates (e.g. Thiel et al., 1979). Barretto and Fujimori (1986) noted enhanced concentrations of Th present as amorphous complexes adsorbed in Fe- and Al-oxides/hydroxides in a weathered phonolite from Brazil.

In many cases the U is present in the Fe oxide as admixed, fine uraninite (e.g. Halenius and Smellie, 1983; Kamineni et al., 1986; Morton, 1974) or brannerite (Brodin et al., 1976) grains. Krishna Rao and Rao (1983) found that the redox-controlled precipitation of Fe and U gave rise to uraniferous Fe oxide at supergene temperatures but

uraninite and haematite at higher temperatures in uraniferous apatite-magnetite veins from India. A close association of U and Th deposits with limonite in the western states of the U.S.A. reflects the presence of uranyl and ferric sulphates in acid waters (Lovering, 1955). When neutralised, the ferric sulphate hydrolyses to a colloidal ferric oxide hydrate which adsorbs uranyl and eventually crystallises to goethite and secondary U minerals (Lovering, op. cit.).

Guthrie and Kleeman (1986) found secondary Mn oxide inclusions in biotite to have a higher sorptive/ion exchange capacity for U compared with Fe oxide in an incipiently weathered granite, although this capacity was greatly reduced in both the Fe and Mn oxides with more intense weathering of the granite. Pyrite has an even greater capacity for fixing U and, per mole, can reduce six times more U than can Fe^{2+} (Speer et al., 1981);



iii) Phyllosilicates

In Table 23, the U content of phyllosilicates does not exceed 1 wt. % and is mainly in the range 10's to 100's ppm, while Th is rarely reported. The U content of biotite increases with increasing alteration and 100's ppm U may be adsorbed along cleavage planes (Berzina et al., 1974) or microfractures (Maurice, 1982) in the mica. In autoradiograph studies, Baranov et al. (1962) found the α track density to increase with the intensity of chloritisation of biotite and sericitisation of feldspar. Chlorite readily adsorbs U from solutions (Thiel et al., 1979) and is commonly associated with diffuse radioactivity (e.g. Lindroos and Smellie, 1979; Robb and Schoch, 1985; Rimsaite, 1978). Low levels of disseminated U are also commonly adsorbed on to sericite

replacing feldspar (e.g. Basham et al., 1982c; Maurice, 1982; Smellie, 1982a). Cameron (1982) found U enrichment to be associated with sericitisation of a granite on a large scale, although investigations on a smaller scale showed it to be associated with Fe oxide, rather than the sericite itself.

Clay minerals, such as montmorillonite, can readily adsorb U (e.g. Zielinski, 1982), mainly at alkaline pH's (El Shazly et al., 1974) and in the Precambrian conglomerates of South Africa, for example, they can hold 100's ppm U (e.g. Simpson and Bowles, 1977; Thiel et al., 1979). Guthrie and Kleeman (1986) studied the distribution of U in hydrothermally altered and incipiently weathered feldspar, chloritised biotite and secondary illite. With more intense weathering, there was a nett loss of U from the rock, due to the breakdown of illite to more stable kaolinite and gibbsite, which have a lower adsorption potential for U.

U may also enter the structure of clay minerals, such as illite (Kaminen et al., 1986) and concentrations in the interlayer positions may be high enough to cause metamictisation of the host phyllosilicate (Rimsaite, 1978). Leaching studies of Shirvington (1983) showed there to be extensive isomorphic substitution of U into the lattices of clay minerals, with UO_2^{2+} replacing K^+ in the interlayer positions of the illite and montmorillonite series.

Clay minerals can also be important sites for Th, particularly in altered rocks, although examples are less widely documented than for U. In a study of a Pennsylvanian weathering profile, Pliler and Adams (1962) found up to 34 ppm Th in kaolinised rock, with much of this attached to the clay. Barretto and Fujimori (1986) studied a sericitised and kaolinised phonolite from Brazil and suggested that

very fine Th-bearing particles could be amorphous oxides or hydroxides of Th adsorbed on to clay particles. Adams and Richardson (1960) measured over 50 ppm Th in bauxite and part of this was held in Al hydroxide minerals and was adsorbed on to residual clays.

Zeolites are able to adsorb higher concentrations of U than biotite (e.g. Speer et al., 1981) at a wider range of pH's than clay minerals (El Shazly et al., 1974). Katayama et al. (1974) described the concentration of U in zeolites due to repeated leaching and adsorption with fluctuating pH, controlled by the oxidation of pyrite to H_2SO_4 . Where the U concentration exceeded the adsorption capacity of the zeolite, coffinite crystallised.

iv) Organic matter

Radioactive organic matter commonly contains 100's ppm up to 10's wt % U, whereas Th is less frequently reported but sometimes attains 1000's ppm or several wt % (Table 24). The higher values of U are usually present as fine, admixed uraninite (e.g. Kochenov et al., 1981) or coffinite (Section 2.a.iii.) in a black, coaly material, first termed "thucolite" by Ellsworth (1928) who referred to the main elements present (Th, U, C, H, O). Despite the name, Th is often below detection or, if present, is usually in the form of finely divided uraninite or thorianite (Steacy and Kaiman, 1978), but Bowie and Atkin (1956) believed 0.51% ThO_2 to be present as an organic complex in the hydrocarbon of a fossil fish.

U can also be present as an organometallic complex, or it can be adsorbed. Using X-ray maps for U, C, Si and O with an electron microprobe, Haji-Vassiliou (1980) was able to determine whether U in organic matter, from various localities, was present as disseminated

uraninite, coffinite or urano-organic compounds. Other U-bearing compounds which have been found in organic matter include monazite (Parnell, 1984), xenotime and brannerite (Rahman, 1979; Parnell, 1985). Although uraninite is commonly dispersed as fine grains within the organic matter, it can also comprise much larger crystals which are mantled by hydrocarbon (e.g. Jefferies, 1985b; Basham et al., 1982d).

However the U is present, the organic matter usually plays a role in fixing it by adsorption and/or complexing. Ishak and Dunlop (1985) found U to be adsorbed on to vegetal debris and charcoal which had been washed from forests into stream sediments. Decomposing plant material gives rise to humic acids which readily adsorb UO_2^{2+} by H^+ exchange, giving rise to insoluble uranyl humates (Borovec et al., 1979). In the humic acid, functional groups (e.g. carboxyl, hydroxyl) form ion-exchange and/or chelate sites for soluble U species (Jennings and Leventhal, 1977). In time, or with heating, the U is reduced by the organic material and separates out as independent minerals, such as uraninite or coffinite (Martin Calvo, 1974; Kornichuk and Burtik, 1974; Nakashima et al., 1984).

In some cases, radiation from the U causes dehydrogenation (or demethanation or carbonisation) as a result of polymerisation-condensation reactions within the organic matter, which may acquire a graphite- or diamond-type structure (e.g. Dubinchuk et al., 1977), with a higher reflectance (Breger, 1974). Parnell (1984) interpreted this process from decreasing H:C ratios with increasing U contents in coaly nodules from the upper Cambrian, Kolm. Kornichuk and Burtik (1974) found that polymerisation was accompanied by oxidation of the organic matter, leading to an increased sorptive capacity, due to the formation of COOH groups. Pen'kov (1976) also noted a decrease in the

C/(O+N) atomic ratio with increasing U in uraninite-bearing bitumens. Bowie (1955) and Haji-Vassiliou and Kerr (1972) believed that irradiation was responsible for the polymerisation and hardening of fluid hydrocarbons which reduced U although, in some cases, the high temperatures of the hydrothermal fluids are the dominant cause of polymerisation (Abdel-Gawad and Kerr, 1961).

Chapter 3 The Ririwai Ring Complex

1. Geological setting

The oval-shaped Ririwai ring complex, which measures 17 x 16 km, is located in the south corner of the Kano province of north Nigeria (Fig. 16). It is one of over 80 such anorogenic centres which show a southerly age trend from north Niger (Ordovician) to south central Nigeria (Jurassic), as confirmed by Rb-Sr dating (Rahaman et al., 1984). The centres represent the eroded roots of volcanoes, with the magmatism migrating at an average rate of $0.37 \text{ cm}^{-1} \text{ year}^{-1}$ (Bowden and Kinnaird, 1984a), along a series of en-echelon, ENE-WSW and N-S lineaments of incipient-rifting in the Precambrian basement. The migration was episodic, with three consecutive 50 to 60 Ma periods of ENE-trending magmatism corresponding to times of quasi-static plate migration, as shown by palaeomagnetic data (Bowden et al., 1976). Age patterns suggest that contemporaneous magmatism may have been locally derived from several, simultaneous, high-level magma chambers connected to a common, deeper source (Rahaman et al., op. cit.).

Instead of a simple model of movement of the African plate over a fixed mantle hot-spot during the Palaeozoic and Mesozoic, the regional age migration rates indicate relative movement between the lithosphere and a sub-lithospheric hot spot, located in a lithosphere-asthenosphere decoupling zone (Bowden and Kinnaird, op. cit.). Alternatively, the thermal anomaly might have been due to successive diapiric intrusions of peridotite along propagating fractures in the lithosphere (Rahaman et al., op. cit.).

2. Volcanic and subvolcanic activity

The structural evolution of a complex, such as Ririwai (Fig. 17), began with violent eruptions dominated by pyroclastic deposits which gave rise to a central shield volcano, built on updomed terrain (Kinnaird et al., 1985b). According to Kinnaird et al. (op. cit.), a fluidised granite magma erupted through a master cone fracture, which emptied the magma chamber. This resulted in collapse of the volcanic pile, with the extrusion of intracaldera ignimbrites through feeders, which later crystallised as quartz fayalite porphyry in ring fractures. The fracture-controlled displacement of the quartz porphyry by granite porphyry, which corresponds to the gas-poor magma, marks the transition to the subvolcanic phase of activity.

The Younger Granites were emplaced by means of piecemeal stoping through the collapsed central block of basement to high levels in the volcanic pile. Although ring complexes show some evidence for fractionation of basalt, the overwhelming proportion of acid rocks fractionated independently from magma of syenitic to granitic compositions (Bowden, 1982). The granitoids which, in Nigeria, comprise over 95% of the intrusives, have been divided, on the basis of their A/CNK ratios (Martin and Bowden, 1981), into three distinct types which, at Ririwai, include peralkaline and biotite granites.

Peralkaline granites are restricted to the south-east of the complex (Fig. 17) and include the arfvedsonite aegirine and arfvedsonite albite granites. With the exception of one sample of arfvedsonite granite (N81; which was examined for pyrochlore), the accessory mineralogy of the peralkaline granites was not studied here and no further petrographic or geochemical details are given.

Post-magmatic alteration processes, which affected the biotite

granite, can be recognised by structural variations in alkali feldspar, the growth of new micas, local textural variations and the changing compositions of opaque and accessory assemblages (Kinnaird et al., 1985b). The earliest, highest temperature process which affected both biotite and peralkaline granites was albitisation. Subsequent processes of microclinisation, followed by greisenisation with quartz veining affected only the biotite granite. A Q-Ab-Or plot (Fig. 18, after Martin and Bowden, 1981) summarises the main post-magmatic transformations which affected just the fresh granite or were superimposed on previously altered assemblages.

3. The biotite granite

a) Petrography

The petrography, geochemistry and mineralisation of the Ririwai biotite granite are described by Kinnaird et al. (1985b) and Martin and Bowden (1981). It forms a central stock which covers an area of about 30 km² and has low angled, outward dipping contacts. Although the granite has been divided into medium and coarse-grained varieties by Jacobson and MacLeod (1977), there exist a range of biotite-bearing, medium to coarse-grained granites that possess subtle porphyritic to equigranular textures.

Surface sample N94 is the most pristine specimen of biotite granite and represents a chilled facies of granite magma in the roof (Kinnaird et al., 1985b). It has phenocrysts, up to 8 mm across, of euhedral perthite containing orthoclase and albite in a groundmass of iron-stained quartz, perthite and interstitial, micropoikilitic biotite. Rapid cooling prevented the efficient ordering of Si and Al in the K-feldspar phenocrysts, which contain the most disordered

feldspar observed in the granite. The groundmass feldspar, which contains a large proportion of Na-rich domains, has become more ordered due to Na-for-K exchange in response to subsolidus rock-fluid interaction (Martin and Bowden, 1981).

Borehole L13 is located close to the Ririwai lode (Fig. 17) and penetrates the intrusion to a depth of approximately 450m. Between 365 m and 385m, it enters albitised rocks (Section 4.a.). Coarse to medium-grained granites higher up the borehole consist mainly of perthitic K-feldspar, quartz, lesser albite and accessory biotite. The groundmass and phenocrysts of perthite are heavily dusted with haematite and frequently show peripheral replacement by clearer albite (Plate 9). In many samples, larger feldspars show an overall development of poorly defined, narrow, discontinuous albite twinning which, in some grains, grades outwards into more well-defined twinning (Plate 10). The degree of albitisation varies between samples and appears to increase with depth until, at 256 m, large (up to 7 mm long), interstitial albite with poorly defined twinning is found replacing smaller grains of K-feldspar.

Samples from between 305 m and 365 m contain less albite but the sample from 365 m is distinctive, in that it is much finer-grained than any of the others (Plate 11). It may be from one of the microgranitic bands, described by Martin and Bowden (op. cit.), which occur repeatedly down the borehole and which reflect major recrystallisation associated with the introduction of disseminated columbite. Ordered microcline in these bands may result from protracted hydrothermal activity, suggesting that they represent channelways developed along horizontal joints.

Isolated flakes (up to 2 mm in diameter) or clumps (up to 5 mm in

diameter) of biotite are mainly fresh but locally show alteration to chlorite or limonite, sometimes with haematite laths lying parallel to the cleavage (Plate 12). In places, the biotite appears to have been replaced by a fine mosaic of feldspar or by fluorite (Plates 13 and 14), which is usually demonstrably secondary (Martin and Bowden, op. cit.). In addition to the fluorite inclusions, which are described in Chapter 4, some biotite contains inclusions of calcite (Plate 15).

b) Geochemistry

According to the geochemistry of the Nigerian granites, they belong to the group designated "A-type" by Loiselle and Wones (1979) and they contain lower MgO, CaO, TiO₂ and P₂O₅ but higher K₂O and Na₂O compared to I-type granitoids of similar SiO₂ content (Kinnaird et al., 1985a).

Although, mineralogically, the Ririwai biotite granite is an oversaturated, alkaline rock, geochemically, it is mildly peraluminous as a result of fluid reactions which have increased normative corundum, quartz and haematite but have decreased anorthite. CaO never exceeds 1 wt %, with much of this present in fluorite, while most samples of biotite granite contain more Al and SiO₂ compared to samples of the granite- and quartz-porphyrries which, compositionally, are closely representative of the original, unmodified magma near the top of the reservoir (Martin and Bowden, op. cit.). The excess Al is incorporated in trioctahedral micas of compositions in the range annite-siderophyllite-zinnwaldite (Bowden, 1982). Relatively neutral and dilute liquids may have been responsible for the postmagmatic enrichment in quartz and/or dissolution of feldspar (Martin and Bowden, op. cit.).

Trace elements also indicate that subsolidus crystal-fluid

reactions have been substantial in surface samples of biotite granite at Ririwai (Kinnaird et al., 1985b). The mineralized roof zone contains high Zn, Sr, W, Nb, U, Li, Rb, Th, Y and F but lower Sr and Ba relative to barren rocks of similar composition and lower REE compared with the peralkaline granites.

c) Mineralisation

The mineralogy of accessory and ore minerals associated with late-stage, possibly magmatic, processes within the biotite granite is described by Ixer et al. (in press). Zr, U, Pb, Nb, Ta and Ti have been precipitated as complex intergrowths of columbite, U-bearing pyrochlore, ilmenite, TiO₂ minerals and zircon. Secondary haematite is ubiquitous and is accompanied by various sulphides and minor to trace amounts of monazite, uranothorite and cassiterite.

4. Metasomatism

a) Albitisation

i) Petrography

Borehole samples between 385 m and 408 m contain dominant albite, which replaces K-feldspar in a similar fashion to the subsidiary albite described in higher samples from L13. The fine- to medium-grained, equigranular rocks also contain quartz and biotite, much of which has been replaced by a fine-grained chlorite aggregate and is locally stained brown from iron-oxide. The albitite encountered at depth is thought, perhaps, to represent the roof facies of a later granite (Kinnaird et al., 1985b).

A sample from 385 m contains more albite than deeper samples of the albitised granite and is probably from one of a number of bands of

albitised granite described by Martin and Bowden (op. cit.), who interpret them as horizontal cooling joints, along which Na-rich fluids circulated. According to Martin and Bowden (op. cit.), the complete replacement of K by Na at such depths may indicate; 1) slightly higher temperatures, 2) the longer duration of water interaction along the channelways, or 3) the increased alkalinity of the latest fluids to percolate along the joints. However, most albitisation was disseminated throughout the roof zone of the granite cupola, prior to jointing or faulting.

The core samples in Plate 16 illustrate the distinct change in petrography from biotite and albitised granite (right and centre respectively) to albitite (left). At 411m, virtually all of the feldspar has been replaced by an interlocking, equigranular mosaic of albite, while quartz and perthite have disappeared, although quartz reappears between 440 and 445 m. Samples between 416 m and 450 m contain only sparse biotite, which rarely exceeds 1 mm in size and is largely replaced by chlorite, often as radiating aggregates, locally associated with bladed haematite. Between 423 m and 445 m, interstitial calcite forms 120 to 4000 μm sized compound, rhombic grains which locally enclose abundant, radiating laths of haematite (Plates 17 and 18).

ii) Geochemistry

Albitisation may have resulted from a decrease in confining pressure (Kinnaird et al., 1985a). Normative calculations show a substantial increase in albite (from 32 to 69%) with a decrease in quartz (from 34 to 7%) and orthoclase (from 29 to 14%) from the biotite granite to the albitite. The early exsolved fluid responsible

for the alteration was hot (260-460°C), according to fluid inclusion data, and introduced Na and Fe, together with U, Th, Zr, Nb and HREE.

Bowden and Kinnaird (1984a) discuss the probable origin of this peralkaline fluid-phase on the basis of experimental work by Roedder and Coombs (1967) and others. It may have initially been derived from the residual silicate melt as a dense brine, which underwent vapour phase separation to form a low density, aqueous fluid. The mobility of incompatible elements was enhanced by the presence of F and Cl, which form stable complexes with them. Bowden and Kinnaird (op. cit.) envisage the partitioning of LREE towards the fluid and of HREE towards the rock at high temperatures, during albitisation. Eu depletion in the mineralised granites probably resulted from rock-fluid interaction, as well as from crystal fractionation, since experimental work by Flynn and Burnham (1978) has shown that Eu is preferentially incorporated into an aqueous chloride fluid phase from the granitic melt.

iii) Mineralisation

The mineralisation associated with albitisation has been described by Kinnaird et al. (1985b) and Ixer et al. (in press) and consists of major, dispersed columbite and haematite, with minor cassiterite, ilmenite, magnetite, TiO₂ minerals and sulphides. According to Kinnaird et al. (op. cit.), loss of CO₂ was important for the deposition of U in the lattice of minerals such as monazite, pyrochlore, thorite and zircon which, together with coffinite, xenotime and an unidentified LREE-phase, are described in more detail in Chapter 4. Kinnaird (1985) describes the enrichment of U together with REE associated with the albitisation of alkali granites in other complexes, such as Jos Bukuru and Jarawa, and these elements have been

concentrated in thorite, xenotime, monazite and zircon (analysis of thorite in Table 6; Kinnaird, 1985).

b) Microclinisation

i) Petrography

This is a localised alteration which is most apparent in the wall-rock of the Ririwai lode. Replacement of Na by K in feldspar, with concomitant expulsion of 1-2 μm long haematite laths from the feldspar lattice has resulted in a distinctive, reddened microcline, which grades into the grey-green greisen (Plate 19). Both the microcline and the greisen have been studied in samples from the Ririwai tin mine (Fig. 20) as well as in surface samples from the lode.

In thin-section, the microcline feldspar generated during this metasomatism is without the characteristic cross-hatch twinning, but XRD studies have confirmed its identity and that it is more fully ordered compared with feldspar from the host biotite granite (Martin and Bowden, 1981). Much of the biotite observed in the microcline shows various degrees of replacement by chlorite, but Kinnaird et al. (1985a) link feldspar alteration to a growth of new mica in the composition range annite to ferrous siderophyllite.

ii) Geochemistry

Kinnaird et al. (1985a) cite Rose and Burt (1979) in suggesting that the change from albitisation to microclinisation was caused by the boiling of fluids, resulting in the selective removal of CO_2 , with a concomitant increase in pH and the K^+/H^+ ratio. This process shifted the fluid out of the stability field of albite and may have been assisted by the percolation of F-rich hydrothermal fluids (Manning and

Pichevant, 1984) and by pressure release (Fournier, 1976).

The introduction of saline, 360 to 460°C fluids resulted in an increase in K, Rb, Li, Zn, Sn and a loss of Na during microclinisation. A depletion in most trace element populations and the REE was accompanied by an increase in the Th : U ratio which, in two samples (Table 57; Chapter 5, Section 5), is significantly higher than that of the unaltered biotite granite and albitite. MacKenzie et al. (1984) undertook a combined neutron activation and particle track analysis of element distributions in the wallrock and vein material from the Ririwai lode and concluded that U was concentrated in the microcline relative to the greisen.

iii) Mineralisation

Mineralisation in the Ririwai lode has been described by Kinnaird et al. (1985b) with particular reference to the sulphide phases and by Ixer et al. (in press) who concentrated on the oxide and accessory phases. Both microclinisation and subsequent greisenisation produced cassiterite as the main oxide phase, accompanied by sphalerite, galena, molybdenite, chalcopyrite, pyrite and marcasite. Columbite, wolframite, TiO₂ minerals and yttrifluorite are also present, as are trace amounts of ilmenite.

Mackenzie et al. (op. cit.) suggested that U in the Ririwai lode was held in Hf-rich zircon, xenotime, allanite and the Li-micas while, for other complexes, Kinnaird et al. (1985a) described the occurrence of U in monazite, columbite (up to 0.5 wt% U), thorite and rare uraninite. Zircon, thorite, coffinite, pyrochlore, monazite and an unidentified LREE-phase, which are all found in microcline from the Ririwai lode, are described in more detail in Chapter 4.

c) Greisenisation

i) Petrography

Incipient greisenisation is evident at 125 m in borehole L13, but the alteration is best developed along the Ririwai lode, where it usually occurs between the microcline and the ore-bearing quartz veins. Greisenisation is characterised by the destabilisation of the granitic minerals, giving a new mineral assemblage, the nature of which depends on the intensity of earlier alteration processes. At 125 m depth in the borehole, much of the feldspar and virtually all of the biotite has been replaced by a hexagonal-shaped, colourless to pale brown or green, zoned mica, whose optical properties are consistent with those of zinnwaldite (Plate 20). Rarely, flakes of this mica overgrow biotite in samples down to 185 m. Kinnaird *et al.* (1985b) described mica in the composition range siderophyllite-protolithionite-zinnwaldite, which rims the annitic biotite and replaces perthite or microcline feldspar. It may be accompanied by sericite, micaceous aggregates, chlorite, clay minerals, fluorite, cryolite or topaz.

In the Ririwai lode, the gradation from microcline to greisen is reflected by the increasing replacement of chlorite by white mica, which is also scattered throughout the microcline (Plates 21 and 22). Ultimately, the rock is transformed into an assemblage of white to pale-coloured mica (?zinnwaldite) and quartz, with no or little chlorite (Plate 23). Samples RS6(2) and RS6(3) differ, in that they show substantial replacement of K-feldspar and lesser plagioclase by a fine-grained intergrowth of chlorite and sericite, with no evidence of the white mica. Although these samples contain quartz veining, they do

not show the fully developed greisen assemblage and have been categorised as "greisenised wall-rock" in Chapter 4.

ii) Geochemistry

The change from microclinisation to greisenisation probably resulted from the changing K^+ / H^+ ratio in the fluid (Rose and Burt, 1979) and was enhanced by pressure release. Greisen veins developed when boiling and phase segregation occurred (e.g. the Ririwai lode), whereas pervasive greisenisation resulted when boiling was retarded.

Kinnaird et al. (1985b) believe that low salinity, acidic, 360 to 380°C, hydrothermal fluids altered the bulk rock geochemistry by removing Al, K and Zr and by increasing the contents of Li, Fe, Si, Sn, W, Pb, Zn, Cu, LREE and Y. Th, together with Ce and the HREE, were enriched during greisenisation (Mackenzie et al., 1984), whereas U was selectively removed. Kinnaird et al. (op. cit.) warn that trace element patterns in the greisens vary according to the earlier processes of alteration, although they conclude from REE patterns that LREE were partitioned into the greisen, whereas HREE were partitioned slightly into the fluid.

iii) Mineralisation

According to Mackenzie et al. (op. cit.), Th, Ce and the HREE were held in thorite, Th-rich monazite, zircon and cassiterite. Kinnaird et al. (op. cit.) give values of wt% Th in zircon (up to 2%), xenotime (up to 5%) and monazite (up to 8%) and these minerals, together with thorite, coffinite and various unidentified U-, Th- and REE-phases, are described in more detail in Chapter 4.

d) Quartz-sphalerite-cassiterite veining

Although minor silicification occurs throughout the granite outcrop, the process is best developed as quartz veining along the Ririwai lode (Kinnaird et al., 1985b). Cassiterite and a sulphide assemblage of ore minerals, dominated by sphalerite, were introduced with the quartz veins, which are steeply dipping, parallel to braided and reach up to 75 cm in width.

5. Summary

The Ririwai complex represents the eroded roots of an alkaline volcano developed as part of a sequential chain of anorogenic centres during the lower Jurassic. The central biotite granite, which was emplaced into a caldera-collapsed volcanic pile, has undergone a sequence of metasomatic alterations. The earliest of these was pervasive albitisation, which was concentrated at the top of the granite cupolas and introduced hot fluids, rich in Na, Fe, U, Th, Zn, Nb and HREE. This ultimately led to the replacement of K-feldspar, quartz and chloritised biotite by albite and was accompanied by a disseminated mineralisation, dominated by columbite. The various U/Th-bearing accessories found in the biotite granite and albitite are described in Chapter 4.

More localised microclinisation followed and this introduced K, Rb, Li, Zn, Sn and U in exchange for Na, resulting in the replacement of feldspar by reddened microcline and the chloritisation of biotite. Succeeding the microclinisation along the Ririwai lode and at 125m depth in the biotite granite was greisenisation, which removed Al, K and U but introduced Li, Fe, Si, Sn, W, Pb, Zn, Cu, LREE, Y and Th leading to the replacement of feldspar and mica by Li-mica, chlorite,

sericite and quartz veining. Along the Ririwai lode, alteration was accompanied by cassiterite and sulphide mineralisation, together with the crystallisation of various U/Th-bearing accessories which are described in Chapter 4.

6. Comparisons with other areas

In a comparison of the Nigerian Younger Granites with other tin provinces, Kinnaird et al. (1985a) conclude that there are similarities in the style of hydrothermal alteration, fluid evolution and related mineralisation, but that there exist important differences in the sequence of these processes.

Bowden et al. (1981) studied the distribution of U in alkaline ignimbrites preserved in two Palaeozoic anorogenic centres in Air, central Niger. They showed that U is concentrated in the matrix and on secondary iron-oxide coatings surrounding lithic and crystal fragments. A very brief study of samples from the Bilete and Goundaï volcanic centres has confirmed this distribution of U but also shows that significant amounts are associated with zircon and TiO_2 (Plates 24-27).

From their results, Bowden et al. (op. cit.) concluded that the original ignimbrite field was enriched in U, but that a considerable proportion was leached during the weathering of the pile and may have contributed to U mineralisation in lower Carboniferous and Jurassic sediments to the west. Similar sedimentological and tectonic controls favourable to U concentration do not appear to have operated in Nigeria during the erosion of the Mesozoic volcanic centres, but Bowden et al. (op. cit.) postulate the existence of local vein deposits of uraninite and dispersed U in some recent sedimentary horizons.

Chapter 4 Uranium- and Thorium-bearing Accessory Minerals in the
Ririwai Biotite Granite and its Altered Lithologies

1. Introduction

Samples of relatively fresh and more altered granite were collected from the central part of the Ririwai ring complex by members of the Department of Geology at St. Andrews University. Samples were collected from the biotite granite, microgranite and the arfvedsonite albite and aegirine granites (Fig.17). Samples of the biotite granite and its albitised varieties were also obtained from Borehole L13, near the Ririwai lode (Fig. 19). Samples of greisen, quartz vein and wallrock (microcline) were collected from mine levels running E-W along the Ririwai lode (Fig. 20).

Two surface samples of biotite granite and twenty three borehole samples of biotite granite and albitite, together with seven samples from the Ririwai lode were studied. The available borehole samples originate from between 100 and 450 m depth and are separated by intervals of between 3 and 50 m, with the shortest intervals lying in the albitised granite and albitite (Table 25).

The samples from the Ririwai lode originate from the surface (samples RS....) and from No.1 Level of the tin mine, (approximately 30 m depth, samples R1....). Individual samples were often collected across boundaries of reddened wallrock (microcline), greisenised wallrock, greisen and quartz vein (Plate 19), and sections from these positions are differentiated by the last digits in the sample numbers in Table 44.

The U- and Th-bearing and associated accessory minerals in polished thin-sections and araldite blocks of the samples were studied

using the techniques described in Appendix 1. Samples in the following descriptions are classified according to their geographical locations i.e. surface, borehole or Ririwai lode, and according to their main rock-type, i.e. biotite granite, albitite, greisen and wallrock (microcline). This classification of accessory minerals according to host rock-type was felt necessary, in view of the important influence of the alteration fluids on the nature of the accessory mineral assemblage, as shown by the mineralogical study of Ixer et al. (in press).

The discrimination of incipiently altered rock (i.e. albitised granite and greisenised wallrock) in the classification recognises the progressive effect of the alteration processes on the accessory minerals as demonstrated, for example, by the co-existence of relict phases with new ones. Within the rock-types, each mineral is described in terms of its size and abundance, mode of occurrence (with any mutual associations, such as inclusions or overgrowths), morphology (including zoning), optical properties and chemistry. ED spectra of various phases encountered are shown near the end of the chapter (Figs. 29-67).

2. The biotite granite

a) Surface Sample N75

i) Zircon

Common, 10 to 40 μm diameter, clear to pale brown, anhedral zircons are found, enclosed in pleochroic haloes, as inclusions in biotite. Larger zircons (70 to 500 μm in diameter) are interstitial to or included in quartz or K-feldspar but are only rarely included in the biotite. They resemble zircons from Borehole Sample L13-365 in having abundant, fine-grained haematite inclusions, which tend to be

concentrated in zircon cores, rendering them opaque (Plate 28). Outer zones or discontinuous, 5 to 10 μm wide rims are clear but often surrounded by thick rims of limonite or haematite.

The outer, clear zones contain higher Hf (about 7 wt% HfO_2) relative to the iron-rich cores (2.5 wt% HfO_2). U contents (0.5 to 0.7 wt% UO_2) normally exceed those of Th (0.1 wt% ThO_2), although locally higher Th contents (4.5 wt% ThO_2) probably represent thorite inclusions.

ii) Thorite

The zircons also resemble those from sample L13-365 in their high content of thorite inclusions which tend to be confined to more iron-oxide rich areas of zircon, with none occurring in the clear rims. The inclusions are typically 5 μm or less in diameter, but uncommonly reach 20 μm in diameter and are irregular in shape, colourless and are either isotropic or display low birefringence, in which case they are in optical continuity with the host zircon.

Thorite also forms a rare, 50 μm diameter, subhedral overgrowth to zircon and this is colourless but with some orange iron-staining (Plate 28). It is in optical continuity with the zircon although it gives first order interference colours and a diffuse biaxial interference figure, indicating its metamict state. Y, Zr and U analyses of the thorite overgrowth and of an inclusion in a different zircon are represented in Figs. 24-26 which show similar element concentrations for both occurrences. The U content is typical of many thorites found in the borehole granite samples and Y is quite high (about 3 wt% Y_2O_3), while Zr is very enriched (about 17 to 21 wt% ZrO_2). Although there may have been contamination from the host zircon during analyses of the

thorite inclusion, such contamination could not have contributed to the high Zr values obtained for the overgrowth.

iii) Fluorite

Fluorite is rare and forms 80 μm diameter inclusions in quartz.

b) Surface Sample N94

i) Zircon

Zircons are very common as 5 to 250 μm diameter inclusions in quartz, feldspar and biotite. Although sometimes rich in iron-oxide, many grains are clear or contain just a few relatively large inclusions of haematite in their cores. The zircons also differ from those in sample N75 in being generally smaller and free from thorite inclusions.

Hf reaches 11.8 wt% HfO_2 in some grains, but tends to be very low in others (1.4 wt% HfO_2). Although both are below 1 wt% oxide, U concentrations (0.6 wt% UO_2) tend to exceed those of Th (0.1 wt% ThO_2).

ii) Thorite

Only four grains of thorite, measuring 120 to 180 μm in diameter, were found in a section of sample N94. The ovoid-shaped grains have distinct cores rich in iron-oxide, surrounded by clear, colourless, outer zones of low birefringence which are, in turn, enclosed by thick iron-oxide coatings. The grains lie adjacent to, or are partly enclosed in biotite associated with a 7mm wide band of disseminated iron-oxide staining. They are surrounded by or partly enclose zircons (Plate 29).

Fig. 22 represents the Th, U, Zr, Y and P contents derived from 10 analyses on the rims and cores of all four grains. The plot

demonstrates that all five elements show considerable spatial variation in concentration, both within and between grains. Although there is little consistent correlation of the elements between grain core and rim, the Y content is directly matched by the P content. There is a suggestion, from grains 17b and 16a, that P, Y and Zr are enriched in the grain rims relative to the cores, with U and Th showing a reverse trend.

iii) Fluorite

Fluorite is common as 30 to 250 μm diameter inclusions enclosed by dark haloes in biotite and as grains interstitial to quartz and feldspar.

c) Borehole samples

i) Zircon

Zircon is an abundant accessory, ranging from 30 to over 100 grains per section. Grains tend to average 100 to 160 μm in diameter and rarely exceed 300 μm . The sample at 365 m is anomalous, in that its zircons range up to 500 μm with an average size of 200 μm (Table 25, Fig. 21).

Zircons are typically included in or grown around biotite which contains distinctive, dark haloes resulting from radioactive damage to the mica structure due to the decay of U and Th in the zircon. In some biotites, zircons lie adjacent to or are partly enclosed within fluorite inclusions (Plate 30) and may be associated with opaques such as ilmenite, columbite, TiO_2 , cassiterite etc.. Locally, they are overgrown by thorite (Plates 31 and 32) or contain inclusions of it (Plates 33, 34, 35 and 36). Zircons are also interstitial to quartz or

included in it, where they are often found along optical boundaries and fractures. Although inclusions typically occur in small clusters or "welded aggregates", isolated crystals are common.

Single zircons are equant to slightly elongate and euhedral prismatic to subhedral, when they show minor embayment against biotite or feldspar. Sometimes, anhedral grains show significant embayment against the fluorite inclusions in biotite (Plate 41). At 365 m, single, subhedral zircons often contain embayments filled with white mica (Plate 37) or feldspar. At 125 m, where the granite has undergone greisenisation, zircons included in the Li-mica have suffered varying degrees of corrosion (Plate 31), ultimately with complete replacement of their cores by the mica, leaving just a residual rim (Plate 38). Rarely, euhedral zircon cores are partly enclosed by anhedral zircon overgrowths (Plates 33 and 34).

Optically, three types of zoning can be recognised in zircon:

(i) Fine, concentric, geometric features apparent in transmitted light are interpreted as having formed during growth of the crystal (Plate 39). This type of zoning is widespread throughout zircons from the biotite granite, albitised granite and albitite.

(ii) Zoning is also apparent as inclusion-rich and inclusion-poor domains of zircon. In the albitised granite and albitite (Sections 3.i and 4.i), distinct bands of haematite- and thorite-rich zircon contrast with clearer zircon which sometimes displays type i) zoning. In many of the biotite granite samples, clear, outer areas of type i) zoning enclose cores rich in inclusions of haematite and, less commonly, pyrite (Plate 39). Zircons from 365m and from surface sample N75, carry abundant, very fine inclusions of iron-oxide which obscure the zircons' anisotropy or even render them opaque. Thorite inclusions, reaching up

to 10 μm in diameter, are confined to the areas of zircon containing the most inclusions of iron-oxide (Plate 36). Often, there is a discontinuous, 10-20 μm wide, outer, clear rim of zircon displaying type i) zoning (Plate 40).

(iii) Subtle, low reflectance patches occur in zircons from between 100 m and 315 m depth. The outer margins of these patches typically pick out the concentric type i) zoning in the zircon, while the inner margins tend to extend towards the zircon core as embayments (Plates 32, 41-49). More irregular patches are independent of any zoning, while others appear to follow cracks, implying that the patches formed after the zircons crystallised and are of secondary origin (Plate 43).

Chemistry

The ubiquitous occurrence of dark haloes around zircon inclusions in biotite implies some radioelement content. Tables 26 and 29 show that UO_2 and ThO_2 both tend to be present in concentrations less than 1 wt. %. In a few zircons, slightly higher values for U and Th with higher U:Th ratios were found in the cores relative to the margins, although many exceptions to this pattern were found. A 180 μm long, clear zircon from 155 m (Plate 50) was analysed in detail for U, Th, Y and P in order to investigate the spatial variations of these elements and the results are shown in Table 27. There is no evidence of compositional zoning i.e. systematic variation from core to rim. Correlation coefficients of the four elements (Table 28) indicate that Y and P are positively correlated but there is no or little correlation among other elements. U remains fairly constant and exceeds or equals Th which varies randomly. Hf tends to be evenly distributed in zircons, although there are examples (Table 26, Sample 100; Table 39, Sample

365A, Grain 9) which show subtle enrichment at the margins.

Anomalous concentrations of Th, U, and Y in zircon from 125m are interpreted as contamination of analyses by tiny, Y-rich thorite inclusions which, if they cannot be resolved in BSEI, can be recognised by great fluctuations in count rates with very small displacements of the probe beam. An overgrowth of zircon from 315 m, bearing an 18 μm long thorite inclusion (Plates 33 and 34), contains enriched Hf, U, Th, Y, Fe and P relative to the core zircon, with U remaining higher than Th (Table 29). This enhanced concentration of radioelements is insufficient to cause complete metamictisation since the overgrowth has a moderate birefringence and has a reflectance equal to that of the core zircon.

Despite their high content of thorite inclusions, the haematite-rich zircons from 365 m do not contain particularly high concentrations of radioelements and U is consistently higher than Th (Table 39). The outer, clear rims do not differ significantly in composition from the inclusion-rich areas.

An exception to the general observation of higher U than Th substituting in zircon is found in the low reflectance, secondary patches, described above, for zircons from between 100 m and 315 m depth. Table 30 shows that Th reaches up to 8 wt% ThO_2 whereas U reaches up to 4 wt% UO_2 . The patches are also enriched in Fe, Y, Ca and Mn at the expense of Zr and in P at the expense of Si relative to the zircon of higher reflectance (Figs. 29 and 30). Analytical totals are low and zircon formulae show high $(\text{Zr} + \text{Hf} + \text{etc.}) : (\text{Si} + \text{P})$ ratios (Tables 26 and 29).

BSEI photographs of up to $\times 10$ k magnification of a zircon from 100 m (Plates 42 to 44) show the low reflectance, secondary patches as

relatively darker areas. These results are discussed in Chapter 5 (Section 3.a.). The photographs do not reveal the presence of inclusions (e.g. thorite), so that the concentrations of trace and minor elements are probably present as substitutions in the zircon lattice. However, analyses of low reflectance patches in zircons from other samples have revealed point sources of high Th which are interpreted as minute thorite inclusions.

ii) Thorite

This is a relatively common accessory phase, although it is of low abundance. There are four modes of occurrence:-

1. Discrete grains measure 60 to 260 μm in diameter. These were found in most of the thorite-bearing sections, where they are generally interstitial to or included in quartz, feldspar or in highly altered and iron-stained biotite (Plates 51-54). One thorite is associated with fluorite which is included in the biotite (Plate 53). Anhedral, tabular to oval grains are invariably coated by goethite or haematite, which also tend to be concentrated as inclusions near the grain centres, rendering the grains opaque. At 125 m, thorites are coated by pyrite which also occurs as very fine inclusions (Plate 31). The clearer grains are colourless to pale yellow or brown, rarely with zoning (Plate 54), have a medium to high refractive index, a lower reflectance than zircon (although slightly higher than the major silicate minerals) and either display first order interference colours or are isotropic. The low birefringence and often diffuse biaxial or non-existent interference figures are evidence of metamictisation.

2. Overgrowths on zircon measure 20 to 100 μm in diameter and are mainly found at 125 m as inclusions in the Li-mica (Plate 31). The

overgrowths, with similar optical properties to the discrete grains, typically have curved boundaries, although more angular, subhedral grains are found and they infill the outer irregular margins of zircon. Grains invariably contain iron-oxide or pyrite inclusions.

3. Replacements of zircon measure 60 to 80 μm across and are very rare, having only been recognised in two grains. At 365 m, the outer margins of a thorite are continuous with those of zircon but it extends inwards with irregular and embayed margins against the zircon (Plate 55). Nearby, the zircon contains tiny, isolated blebs of thorite as well as pyrite inclusions. The clear and colourless thorite is optically very similar to zircon but can be distinguished by its lower reflectance and birefringence. At 125 m a thorite is almost completely enclosed by a 130 μm diameter rim of zircon (Plate 56). The contact between the minerals is very irregular, with projections and small isolated patches of thorite occurring in the zircon. This texture suggests there has been replacement of the zircon by thorite, although the passive infilling of an embayed zircon is possible.

4. Inclusions in zircon occur in about two thirds of the thorite-bearing sections but are most evident at 365 m, where the majority of large, haematite-rich zircons contain abundant thorite inclusions (Plates 36, 37 and 40). Clusters of inclusions tend to be denser in more haematite-rich areas of zircon but are always absent from the thin, outer, clear rims. Some inclusions are surrounded by or intergrown with haematite inclusions. Colourless to pale yellow thorites average 5 μm in diameter and rarely exceed 15 μm . Inclusions are anhedral and usually ovoid but may be very irregular in shape. Anisotropic thorites in optical continuity with zircon are difficult to distinguish in transmitted light but, in reflected light, they show a very subtle, lower reflectance (Plate 36).

Thorite inclusions in other samples of biotite granite are much less common but still tend to be confined to more haematite-rich areas of zircon. Often, minute inclusions of thorite are revealed in BSEI or during analyses of zircon when anomalously high concentrations of Th are detected. Large thorite inclusions are rare but examples are found at 315 m, where an 18 μm long grain occurs in an outer zircon overgrowth (Plates 33 and 34) and at 350 m, where four irregular inclusions range up to 30 μm in diameter (Plate 35).

Chemistry

Tables 32, 33 and 40 give analyses of thorite in all four modes of occurrence. Oxide totals range from 87 to 100%, with the lower totals probably due to metamictisation and/or the presence of water (see Chapter 5, Section 3.b.). Oxide totals are significantly higher than those obtained in analyses of thorite from the Ririwai lode (Fig. 23).

Concentrations of U, Zr and Y in thorite can reach extremely high values (up to 20 wt% UO_2 , 27 wt% ZrO_2 and 7.5 wt% Y_2O_3). Presumably, these elements are present as substitutions in the thorite lattice, since no inclusions of uraninite, zircon or xenotime can be detected, although a very fine-grained admixture, beyond the resolution of the probe beam (1 μm) is possible. Where thorite occurs as inclusions in zircon, the high Zr may result from contamination of the analysis by the host zircon, but the highest Zr concentration is found in a discrete thorite which is not associated with zircon (Fig. 39).

Figs. 24-26 show variations in average U, Y and Zr contents for thorites down borehole L13. Although these plots serve to show very general trends in average thorite compositions, only a limited number of individual grains were measured per sample, and variations between

and within grains in a sample (shown by the range bars in Figs. 24-26) can be considerable.

Between 125 and 365 m there is considerable variation in mean U content, which ranges from less than 1 up to 12.5 wt% UO_2 (Fig. 24). Variation between thorites within any sample can be just as great as variations between samples and so no general conclusions can be drawn regarding the trends with depth. The spatial variation of U within a grain can also be considerable, although there is little evidence of concentric zoning, with respect to U. However, the haematite-rich core of a 150 μm diameter thorite from 305 m (Plate 51) contains higher U (10.87 wt. % UO_2 , Analysis 3) compared to the rim (1.5 wt. % UO_2 , Analysis 1a). Three thorite inclusions within the same zircon (Plate 35; Table 33) show relatively small differences in U (17-21 wt% UO_2), Zr, Y and P contents. Two thorites in another zircon (Table 32, Sample 125, Grain P.1c) are also similar in composition but, in Sample 185, the U contents of two inclusions within the same host (Table 33, Grain B.3) are very different (3 and 14 wt% UO_2).

Fig. 25 shows there is also a significant variation in Y content of thorites within samples, although the range is smaller than for U and a rough trend of decreasing Y content with depth is evident. Thorites from the incipiently greisenised sample from 125 m depth have anomalously high Y and Zr compositions (up to 7.5 wt% Y_2O_3 and 25 wt% ZrO_2 respectively). Table 32 shows Y and Zr are relatively constant for thorite inclusions, overgrowths and replacements (based on 12 analyses of 7 grains). Slightly higher values for Zr in thorite inclusions (up to 29 wt% ZrO_2) probably result from contamination of the analyses by the host zircon. High Y contents are generally accompanied by enhanced P contents (up to 1.3 wt% P_2O_5), whereas concentrations of Zr are

matched by those of Hf (up to 1.8 wt% HfO_2).

Fig. 26 shows Zr to have the greatest variation of all, both within and between samples and grains. Thorites from 350 and 305 m (Plates 51 and 53) are compositionally zoned with cores relatively depleted in Zr compared to the rims (Table 33).

iii) Monazite

Although it was found in about two thirds of the samples analysed, monazite is a relatively rare accessory in the biotite granite and an average of one or two grains were identified per section. Grains range from 15 to 800 μm in length and typically form colourless to pale yellow, clear, euhedral prismatic crystals interstitial to or included in quartz, feldspar or biotite (Plate 57). Subhedral to anhedral examples were also found and, at 365 m, grains of very irregular monazite occupy the grain boundaries between quartz and feldspar (Plate 58). One of these grains is intergrown with fluorite while, at 315 m, a monazite containing iron-oxide inclusions is intergrown with and appears to be partly replaced by an unidentified LREE-phase (Plate 59).

Chemistry

Table 34 shows Th to range from about 3 up to 12 wt% ThO_2 but it is typically 7 to 8 wt% ThO_2 , while U ranges from below the detection limit (0.1 wt% U) up to about 0.3 wt% UO_2 . There is no evidence of compositional zoning but Th contents may vary within a grain, as at 145 m, for example, where it ranges from 7.3 to 10.4 wt% ThO_2 . In another sample (350 m), the Th content in a monazite is much lower but shows little variation (2.7-3.0 wt% ThO_2).

LREE generally remain constant and in the range typical for

published monazite analyses but the grain at 315 m, which is intergrown with the LREE-phase (Plate 59), contains abnormally high La (26.3 wt% La_2O_3) and low Nd (4.9 wt% Nd_2O_3) in one area (Fig. 38) but more normal concentrations of Ce and La just a few micrometres away.

iv) Fluorite

Fluorite is a relatively common accessory mineral in most samples of the biotite granite but shows a sudden modal and size decrease at 365 m (Table 25). By far the majority of grains occur as ovoid or very irregular, colourless inclusions measuring 20 to 600 μm in diameter, surrounded by dark haloes in biotite. The surrounding haloes are less intense than those around zircon and may be quite unevenly distributed, sometimes corresponding to peripheral inclusions of a Th-bearing LREE-phase in the fluorite (Plate 60).

Fluorite inclusions may be associated with other accessory minerals, such as ilmenite, columbite, haematite or thorite, but especially with zircons, which appear to cluster around fluorites included in biotite (Plate 30). Where zircons are enclosed by fluorite, they often show corroded and embayed margins. Small inclusions of the host biotite are sometimes found in the fluorite (Plate 14).

Less commonly, fluorite occurs as anhedral inclusions in quartz or feldspar or as irregular, interstitial grains of "late" appearance. At 315 m, in quartz, a fluorite shows an embayed margin against an adjacent 120 μm diameter, subhedral thorite. Qualitative chemical analyses reveal significant amounts of Y in fluorite from the biotite granite.

v) LREE-phase

An unidentified LREE-phase occurs as inclusions in some fluorites or as an alteration of monazite. Although it is fairly common in the biotite granite, the LREE-phase is less abundant than in the albitised granite and albitite.

Crystals range from 5 to 60 μm in length and typically form subhedral to euhedral prisms randomly oriented in the host fluorite, from which they are easily distinguished by their higher reflectance (slightly lower than zircon) and anisotropy (Plate 60). The phase can be clear or contain fine, dusty inclusions, ranges from colourless to pale yellow, has a high refractive index and extreme birefringence, a straight extinction and larger grains give a positive, uniaxial interference figure.

The 160 μm diameter LREE-phase which replaces monazite (Plate 59) is easily distinguished by its lower reflectance and nearly isotropic nature, and it gives a very diffuse, biaxial interference figure. It also differs in being completely clear with a lower refractive index and by having a tendency to form dark-brown spots during analysis by the probe, in contrast to monazite which is stable under the beam. Residual patches of monazite occur in the LREE-phase.

Chemistry

Table 36 and Fig. 66 show the LREE-phase consists chiefly of Ce, La and Nd with traces of Th, Ca, U, Si and Y which vary in concentration between grains. The low oxide totals (approximately 75 wt%) probably result from unmeasured CO_2 and/or F. Likely candidates for this phase include bastnaesite and fluocerite. Analyses for F are required to discriminate between these two possibilities, although F

cannot be quantitatively measured on the instrument used in this study.

The LREE-phase replacement of monazite from 315 m also contains high Ce, La and Nd but with variable Ce : La ratios (Table 36). This variation corresponds to that found in the host monazite, and suggests there may be partitioning of different LREE during alteration of the monazite. The LREE-phase contains significant Th and U and has a relatively high oxide total of 93.67 wt%. This high value probably results from a combination of loss of volatiles under the beam and the presence of high F, which will lead to an overestimation of O in the analysis.

vi) Coffinite

The only coffinite found in the L13 borehole occurs at 100 m, where the mineral forms several 250 μm diameter networks of veinlets and interstitial fillings to cleavages and grain boundaries in biotite (Plate 61). The coffinite is opaque to dark brown, isotropic and has a reflectance only slightly greater than that of the major rock-forming silicates. Intimately intergrown with and surrounded by the coffinite are molybdenite and sphalerite (Plate 62).

Chemistry

Table 37 and Fig. 49 show the coffinite contains unusually high but variable concentrations of Zr (up to 11.7 wt% ZrO_2) compared with published analyses (Table 5), with significant Th (up to 5 wt% ThO_2) and relatively low Y and P compared with coffinite found in the microcline (Section 5.a.iii.). High magnification SEM images do not reveal the presence of inclusions of zircon so that the high Zr may be present as a substitution in the coffinite lattice.

As with analyses of thorite, the oxide totals for coffinite are low (average about 90 wt%) and recalculation of the results to 4 oxygens shows the formula to be depleted in Si, whereas some analyses show an excess of cations in the U site. Possible explanations for the low totals and poor stoichiometry of probe analyses for coffinite are discussed in Chapter 5 (Section 3.c.).

vii) Pyrochlore

Pyrochlore is a rare accessory in the biotite granite and only two occurrences have been found; at 305m and at 350m depth. Ixer et al. (in press) describe a complex columbite-ilmenite-TiO₂-zircon-pyrochlore-fluorite intergrowth from 305m in which U-rich plumbopyrochlore (Fig. 33) occurs as poorly polished grains 40 μm in diameter (Plate 63). Further study of the intergrowth has revealed another pyrochlore variety with much lower Pb and U and much higher Nb (Fig. 32). The plumbopyrochlore is dark brown to opaque, has a high refractive index but low reflectance (approximately equal to that of TiO₂) and gives abundant, diffuse, white internal reflections.

At 350m, a 25 μm diameter, brown, metamict ?pyrochlore is included in zircon. Table 38 shows that, compared with the grain from 305m, this ?pyrochlore contains significantly higher Nb, Th, REE, Ca and Si but lower Pb, Ta, U and Ti (Fig. 35). According to the classification of Hogarth (1977; see Chapter 2, Table 9) it is either a uranopyrochlore, if the Si is present as an impurity, or it is not a member of the pyrochlore group, if the Si is a constituent of the mineral lattice.

Pyrochlore from the albitised, peralkaline granite was analysed so that a comparison could be made with pyrochlore from the biotite granite. Table 38 shows that, compositionally, a pyrochlore from the

arfvedsonite granite resembles pyrochlore from 305m, but has significantly higher Nb, Ti, REE and Si and lower Ta, U and Fe. In a BSEI, a brighter rim and crack is apparent and this is depleted in U, Si and Ta but is enhanced in Pb, Nb, Th, Ti and REE relative to the grain core.

3. Albitised Granite

i) Zircon

There is a marked decrease in the number of zircons, from between 30 and 100 or more in the biotite granite to between 5 and 12 grains per section in the albitised granite (Table 25, Fig. 21). No samples are available between 365 and 385 m, so it is not known whether this modal decrease is sudden or gradual, or whether it coincides with the onset of albitisation.

The mean sizes of zircons are greater in samples below 385 m than in samples above 365 m. This change corresponds to an increase in the maximum sizes of zircons and in the number of "large" (arbitrarily taken as greater or equal to 300 μm diameter) zircons (Table 25, Fig. 21).

At 385 m, all zircons are included in feldspar. Other samples contain zircons occurring interstitially or as inclusions in or grown around altered biotite, with associated pleochroic haloes. At 395 m, zircons are commonly enclosed in iron-oxide or overgrown by euhedral, bladed haematite which, itself, may be included in biotite (Plate 65). At 411 m, in addition to haematite, zircon is overgrown by pyrite and by columbite.

The character of zircons in samples from 385 and 390 m differs from that of zircons in deeper samples. Zircons from 385 and 390 m

tend to be clear or have few, relatively large, iron-oxide inclusions, often restricted to the core. Grains generally range from euhedral to subhedral, but anhedral examples show various degrees of corrosion or embayment against feldspar and truncation of the fine-scale, concentric zoning (Plate 67). Locally, irregular, clear, fracture-free patches occur in the centres of zircons. These patches are isotropic and give diffuse or no interference figures which implies that they are metamict, and they probably represent the Type 3 zircon variety, discussed below.

Zircons between 395 and 411 m tend to contain more abundant inclusions of iron-oxide than those described above. Grains often comprise complex composites of three main zircon varieties which are illustrated in a 750 μm diameter, euhedral example from 395 m (Plates 64 and 65). This zircon has a number of significant features:

1. An outer, 20 to 80 μm wide, clear, anisotropic rim displays fine-scale zoning and is discontinuous in subhedral grains. BSEI photographs emphasise the fine, rhythmic zoning (Plate 66).
2. An intermediate, 40 to 80 μm wide, inclusion-rich, zone is anisotropic and contains approximately 30 sporadically distributed inclusions (Plate 64) which are rich in Th and Si. Analyses (Table 40) indicate these inclusions to be thorite.
3. An inner, clear, isotropic, fracture-free area gives a very diffuse biaxial or no interference figure, suggesting that it is metamict. It contains two, approximately 200 μm diameter, irregular patches of Type 2 zircon which include between 10 and 30 thorite grains of smaller size than those found in the intermediate zone.

Most zircons deviate from the above case in that they do not display the different zircon varieties in such distinct, concentric

zones. Type 3 zircon may be absent and Type 1 may be unzoned, incomplete, or absent.

As well as occurring in the zircon core, irregular patches of Type 3 zircon may be scattered in marginal areas of a grain and, rarely, it forms anhedral overgrowths on euhedral zircons. Usually, the boundaries of Type 3 zircon coincide with zoning in the grain. Type 3 zircon is not always completely isotropic, and rhythmic zones of weak anisotropy may occur (Plate 68).

Thorite inclusions are not found in Types 1 and 3 zircon, whereas Type 2 zircon contains inclusions which range from sporadic and rare at 395 m, to highly abundant at 411 m. A large, concentrically zoned example from 411 m (Plates 69 and 70) is partly enclosed by chlorite. It contains the three zircon varieties in euhedral zones similar to those described above in the zircon from 395 m. Although the Type 1 zircon core is weakly anisotropic, it is impossible to determine whether the intermediate zone of Type 2 zircon is metamict, since any anisotropy would be obscured by the high density of haematite inclusions present. Chemical analyses (see below) do not support the possibility that metamictisation has resulted from radiation damage induced by the thorite inclusions, which are far more abundant than in Type 2 zircon from the 395m example. The zircon from 411m also differs from the 395m example principally in its subhedral form, which is manifested as embayments of the grain and truncation of the concentric zones by plagioclase and fluorite; a common feature of zircons from 411m and below (Plates 69 and 87).

Plate 70 illustrates the high density of thorite inclusions in the Type 2 intermediate zone of the zircon from 411 m. Individual thorite inclusions are anhedral, ranging from 1 to 10 μm in diameter and are

clearly illustrated in Plate 72 which is a selectively enlarged photograph of a BSEI at x1000 magnification. Appendix 5 describes how this photograph was used to calculate a hypothetical, initial concentration of thorite in solid solution with the zircon. This assumes that the inclusions were produced by subsequent exsolution of the thorite from the zircon lattice.

Accompanying iron-oxide in the thorite-rich zone are inclusions of marcasite and pyrite, which also infill short cracks that project radially from the intermediate zone into the core and infill more irregular fractures in the outer zone (Plate 69).

Chemistry

Table 39 shows zircon at 390 m to be enriched in Hf (10.53 wt% HfO_2), with higher concentrations of U (0.22 wt% UO_2) than Th (0.06 wt% ThO_2) but with low Y and P (both 0.09 wt% oxide). Fig. 28 shows that the concentrically zoned zircon from 411 m (Plates 69 and 70) has a distinct chemical zoning, related to the three zircon varieties.

U in the inner core of Type 3 zircon is enriched (1.35 to 6.1 wt% UO_2) relative to Th (0.51 to 1.02 wt% ThO_2). Hf is average for zircon and fairly constant at about 3 wt% HfO_2 , Y slightly exceeds P (0.37 wt% Y_2O_3 and 0.17 wt% P_2O_5 , respectively) and there are only trace amounts of Fe present. The low oxide totals of 96 to 98% may be a consequence of metamictisation caused by the relatively high concentration of U present in the zircon lattice.

In the intermediate zone of Type 2 zircon there is a substantial increase in Hf (6 wt% HfO_2) which is present in variable amounts. The concentration of U exceeds that of Th but is significantly lower than in the Type 3 zircon. A high oxide total (Table 41, 411 m, Grain 2,

Analysis 2) suggests that the zircon has not undergone metamictisation. Higher Fe values probably represent contamination of analyses by haematite inclusions. Care was taken to avoid contamination of analyses from thorite inclusions by referring to high magnification BSEI photos (i.e. Plate 72) when positioning the electron beam during EPMA. The 395m example shows a similar compositional pattern but the inner, Type 1 zircon contains higher Hf (approximately 6.5 wt% HfO_2) and the Type 2 zircon gives a lower oxide total (although there is no optical evidence of metamictisation).

Plates 64, 66 and 70 show the outer zones of Type 1 zircon in the 395 m and 411 m examples to be very distinctly and rhythmically zoned within broader light and dark grey bands in the BSEI. Table 41 reveals this banding to be an expression of variable concentrations of minor elements in the zircon lattice. Higher Hf (up to approximately 13 wt% HfO_2) U, Th, Y and P occur in the brighter bands compared to the inner, darkest band (5.33 wt% HfO_2). Highest Hf compositions correspond to hafnian zircon (Correia Neves et al., 1974; see Chapter 2, Section 2.b.i.).

Another grain from 395 m has irregular, zoned patches of Type 3 zircon near the margins. Table 39 shows these patches to contain enriched and approximately equal concentrations of U and Th (approximately 1 wt% oxide), with high Y and P.

ii) Thorite

Table 25 shows that thorite inclusions in zircon become more abundant with depth from 385 m to 411 m. At 385 m, the only thorite identified was a 20 μm diameter, ovoid, clear inclusion in columbite (Plate 73; Fig. 36). Optical properties of the thorite are similar to

those described for equivalent inclusions in the biotite granite.

Discrete grains of thorite are less common but remain constant in number with depth. They range from 20 to 500 μm but are most commonly 250 μm in diameter and occur interstitially or as inclusions in quartz, feldspar or highly altered biotite. Iron-oxide or pyrite invariably enclose thorite grains as thick rims. The grains are generally ovoid, but sometimes quite irregular and range from colourless to irregularly stained with yellow, brown or orange patches. The thorite is either isotropic with no interference figure apparent or gives first order interference colours with a very diffuse, uniaxial interference figure. An interstitial, anisotropic thorite from 408 m exhibits parallel isotropic banding in crossed-polars (Plate 74).

Plate 75 shows a 100 by 20 μm sized patch of thorite which occurs in the outer margin of a zircon at 411 m. The outer edge of this thorite is euhedral and continuous with the zircon margin, whereas the inner contact is irregular. The presence of anhedral, residual blebs of zircon up to 10 μm in diameter in the thorite suggests that the thorite has partially replaced the zircon. In the same sample, a 50 by 30 μm sized thorite overgrowth has an irregular, embayed margin with zircon, which itself contains much smaller thorite inclusions nearby (Plate 76).

Chemistry

Fig. 24 shows that thorites in the albitised granite tend to be very U-rich (e.g. Fig. 41), with averages of analyses lying between 10 and 15 wt% UO_2 , which is an increase over thorites from the biotite granite. The variation in U content can be quite considerable and 11 analyses of thorite in the sample from 411 m give values in the range

1.5 to 29 wt% UO_2 .

The mean concentration of about 3 wt% Y_2O_3 for thorite is fairly constant between samples and generally exceeds corresponding mean values in the biotite granite (Fig. 25). The range of concentration of Y, like that of U, is quite considerable and maximum values in the albitised granite greatly exceed most of those in the unaltered biotite granite.

Variations of U and Y concentration can be just as great within grains as between them. In a 500 μ m diameter grain from 390 m (Plate 77), UO_2 varies by up to 10 wt% and is inversely correlated with Y_2O_3 , which varies by up to 8 wt% (Table 40). This spatial variation is quite irregular and does not appear to result from concentric zoning. As in the biotite granite thorites, Y concentration is directly correlated with P concentration.

Average Zr contents for thorite show more variation between samples than do U and Y contents (Fig. 26). There is some uncertainty about high Zr values for small thorite inclusions in zircons from 395m, due to the possibility of contamination from the host zircon, since large discrete thorites from 390m contain negligible Zr. However, there is a great variation in Zr content within the large, peripheral replacement of zircon at 411 m (Plate 75, Table 42). Oxide totals for analyses tend to exceed those for thorites from the biotite granite and frequently reach 100%, but always exceed 95% (Fig. 23).

iii) Monazite

Monazite is a comparatively uncommon accessory mineral between 385 and 395 m. At 385 m, three 5 to 20 μ m diameter anhedral crystals are found around columbite, fluorite and a LREE-phase which are all included in biotite (Plate 73). At 390 m, a cluster of anhedral and

subhedral grains of monazite are all that remains of a 1 mm long, euhedral, prismatic crystal which appears to have undergone severe corrosion and replacement by K-feldspar (Plate 78). Table 35 and Fig. 27 show that the largest grain contains about 7 wt% ThO₂ but this substantially decreases to a few wt% or less in the more corroded fragments and is correlated with U which ranges from 0.15 to 0.36 wt% UO₂.

At 395 m, feldspar contains three 60 to 120 µm diameter monazite inclusions which are enclosed by thick rims of iron-oxide (Plate 79), and in which Th concentrations vary between grains. In this sample, a 400 µm diameter, anhedral monazite, which is interstitial to quartz, shows substantial replacement by a LREE-phase (Plate 80).

iv) Fluorite

Between 1 and 12 grains of fluorite were found per section in all samples of the albitised granite (Table 25). The fluorite occurs as inclusions, surrounded by dark haloes, in biotite and, less commonly, as interstitial, irregular grains of late appearance. At 400 m, fluorite embays zircon and is found as inclusions in it. At 411 m, zircons frequently show substantial replacement by fluorite which forms 100 to 200 µm diameter lobes, surrounded by thin, residual rims of zircon (Plate 81). Although mainly colourless, the fluorite rarely displays a purple tinge where it is in contact with LREE-phase inclusions (described below).

v) LREE-phase

The unidentified LREE-phase (bastnaesite/fluocerite?) described for the biotite granite (Section c.v.) is found in all samples of the albitised granite but is relatively rare between 385 and 395 m, where it occurs as inclusions in biotite or fluorite and replaces monazite.

An anhedral replacement of monazite at 395 m is virtually opaque but gives abundant white internal reflections (Plate 80).

Below 395 m, the LREE-phase inclusions become more abundant in fluorite grains included in biotite and embaying zircon (Plate 81). Frequently, elongate inclusions in a particular fluorite are oriented parallel to one another with all the crystals displaying simultaneous extinction (Plate 82). Some LREE-phase crystals contain dusty inclusions and exhibit orange internal reflections, indicating the presence of iron-oxide. Although LREE-phase inclusions frequently overgrow zircon which has been embayed by fluorite, only one example was found of a 20 μm long grain included in zircon without associated fluorite (Plate 83).

Chemistry

Table 36 shows that, chemically, the LREE-phase in the albitised granite is similar to equivalent grains in the biotite granite, although no examples of La-enriched varieties were found. Minor elements include Y and Th with traces of U and Ca (Fig. 67), although high values for Ca and Y and for Zr in inclusions in fluorite and zircon respectively, probably result from contamination by the host minerals.

vi) Xenotime

Xenotime was only found at 411 m, where it forms rare, anhedral to euhedral, prismatic overgrowths, up to 15 μm in diameter on the corroded and embayed margins of zircon. Optically, the xenotime is very similar to zircon, although it has a slightly lower reflectance and appears brighter in a BSEI (Plates 70 and 84).

Chemistry

Table 43 shows the xenotime in Plate 84 to contain significant HREE (13% HREE₂O₃) with minor Th and Si but no U. The low analytical total of 93% may result from unmeasured REE or may be due to the difficulty in measuring such small grains.

c) Albitite

i) Zircon

Zircons are of similar abundance and size to grains in the albitised granite, numbering between 4 and 20 per section and averaging between 200 and 300 μm in diameter, with a range of 20 to 1000 μm (Table 25, Fig. 21). The number of "large" zircons per slide is also similar. Grains are usually interstitial to plagioclase or included within it, whereas some are associated with, but rarely included within, chloritised biotite. Locally, zircons are associated with fluorite or calcite.

Morphologically, zircons resemble those in the albitised granite. Larger, subhedral and embayed grains show truncation of zoning (Plate 87), that impinges against fluorite or plagioclase, which occasionally form inclusions. On closer inspection, some large grains are seen to comprise aggregates of smaller zircons. The distinct, concentric zoning is similar to that in grains from the albitised granite with, at 416 m, abundant, minute (up to 5 μm diameter) thorite inclusions spatially restricted to near-opaque zones, rich in iron-oxide. The iron-oxide comprises abundant, coarse to dusty inclusions together with coatings around zircon and, less commonly, is accompanied by pyrite inclusions and veinlets. Below 416 m, thorite inclusions are less common, with individual zircons frequently barren of inclusions or containing a few, often relatively large, thorites which are spatially unrelated to

zoning in the host zircon. All 3 zircon types, described in the albitised granite, are found as zones in zircon but, in some grains (e.g. from 450 m), Types 2 and 3 zircon form complex intergrowths (Plates 85 and 86).

Chemistry

Zircons from the albitite exhibit a similar range in composition to those from the albitised granite (Table 41). Type 2 zircon contains low to medium U (0.1 to 0.6 wt% UO_2) which consistently exceeds Th, although the latter locally reaches much higher values, corresponding to minute thorite inclusions. U in Type 3 zircon reaches a maximum concentration of 1.5 wt% UO_2 , along with enhanced concentrations of Th, Y and P. Localised, very high values for Y and P in a zircon from 450 m correspond to common xenotime inclusions up to 30 μm in diameter. Outer zones of slightly higher reflectance, up to 40 μm wide, contain higher Hf but lower U and Th, compared with the inner cores.

ii) Thorite

As in the albitised granite, thorite in the albitite is closely associated with zircon and comprises inclusions, replacements and overgrowths as well as occasional discrete grains. Plate 88 illustrates a zircon bearing a particularly large inclusion (40 μm in diameter) and anhedral overgrowth (70 μm in diameter) of thorite, which is spatially associated with pyrite. Locally, cracks which radiate from a thorite inclusion in zircon are infilled with pyrite. Only one discrete occurrence of thorite was found in the albitite (at 423 m). The grain is included in plagioclase, measures 40 μm in diameter and is coated with a rim of iron-oxide.

Chemistry

Fig. 24 shows the rising trend of average U content in thorite to continue with depth through the albitite. Average and maximum U contents remain significantly higher than those in the unaltered biotite granite, although variable concentrations between grains give rise to large ranges in composition within samples. Figs. 25 and 26 reveal a marked decrease in average Y and Zr content for the albitite thorites, compared to albitised granite and biotite granite thorites.

iii) Monazite

Few grains of monazite are found in the albitite, and most show substantial replacement by the LREE phase. Grains, which range from 80 to 800 μm in length, are included in plagioclase or, at 445 m, form highly irregular, interstitial fillings to plagioclase and sphalerite (Plate 89).

iv) Fluorite

Colourless fluorite is a common accessory and ranges from 60 to 4000 μm in diameter. It sometimes forms inclusions in chloritised biotite which, itself, may occur as flakes within the fluorite and at 450 m a biotite, measuring 4 mm in diameter, is extensively replaced by fluorite. More commonly, fluorite overgrows, includes or replaces zircon, while larger, subhedral, cubic fluorite is interstitial to the plagioclase. All fluorite contains significant Y (about 5% Y_2O_3) with traces of Si.

v) LREE-Phase

The LREE-phase in the albitite has a similar abundance, optical properties and mode of occurrence to equivalent grains in the albitised granite. Inclusions of the phase tend to occur in fluorite associated with biotite or zircon, rather than in the large, interstitial fluorite grains although, at 445 m, a 25 μm diameter grain is included in plagioclase. As in the albitised granite, several elongate LREE-phase inclusions in a particular fluorite show parallel alignment and extinction. The LREE-phase which replaces monazite at 445 m, is brown and very turbid with an obscured anisotropy compared to the clear, second-order greens of the monazite.

Chemistry

The minor Th content (1.5 to 5 wt% ThO_2) of the LREE-phase is probably responsible for pleochroic haloes in adjacent, altered biotite, and trace amounts of U are sometimes detected, along with variable, trace amounts of Ca, Y and Si.

vi) Xenotime

Xenotime is more common in the albitite, compared to the albitised granite (Table 25), but it is still a relatively rare accessory which is nearly always associated with zircon, although an isolated grain, 25 μm in diameter, was found at 445 m. At 440 m and 445 m, xenotime forms euhedral, prismatic to anhedral overgrowths 15 to 70 μm long and also infills embayments and cracks in zircon (Plate 90). At 450 m, a zircon contains a dozen or more inclusions of xenotime, mainly 5 μm or less in diameter, although a euhedral, prismatic grain reaches 30 μm in diameter. Different grains associated with the same zircon may show variable amounts of Th, with or without U and Si.

vii) ?Pyrochlore

The only occurrence of ?pyrochlore found in the albitite is at 445 m, where a 60 μm diameter, rounded grain, enclosed by pyrite, is included in plagioclase. It is pale yellow and isotropic, with a refractive index and reflectance similar to those of zircon. The analysis in Table 38 reveals a dominant Ta content, with significant Nb, U, Pb, and Si and minor Ti, Ca, Fe, Ce, La and Th. If the Si is present as an impurity, then the phase belongs to the plumbomicrolite species of pyrochlore (Hogarth, 1977). More likely, the phase is not a member of the pyrochlore group but is a complex Ta-Nb-Pb etc. silicate mineral, since SiO_2 values are consistent for three analysis spots which do not contain obvious inclusions in high-magnification, transmitted and reflected light photomicrographs (Plate 91).

5. Ririwai lode

a) Microcline

i) Zircon

Zircon shows a variable abundance, with very few occurring in sample R1/13, but up to about 20 per section in sample R1/23, although this is still a much lower frequency, when compared with the unaltered biotite granite (Table 44). Grains range from 10 to 120 μm in diameter and tend to average about 60 μm , which is smaller than most zircons from the biotite granite or albitite.

Zircon is typically found as isolated grains or clusters of grains which are included in or interstitial to the quartz and feldspar. Less commonly, clusters of smaller grains, surrounded by dark haloes, are included in chlorite or white mica which is intergrown with the chlorite. Often, several euhedral zircons have merged together to form

an irregular, welded clump of grains. Grains included in quartz or clear K-feldspar are commonly located on junctions of cracks or optical boundaries (Plate 92).

Equant crystals range from euhedral, square or polygonal to subhedral in shape but, less commonly, are anhedral. One grain shows a corroded margin, where it is in contact with fluorite. Concentric, fine-scale zoning is common, and clear, outer zones typically enclose cores rich in haematite inclusions, although many crystals are clear or contain only a few haematite inclusions, up to 40 μm in diameter. Low reflectance patches, which tend to follow the outer zones of crystals, are rare compared with those in zircons from the biotite granite.

ii) Thorite and U-Th-Si phase(s)

Thorite is a widespread accessory in the Ririwai Lode, having been identified in 80% of the sections of wallrock and greisen examined, but its abundance in the microclinite is low, averaging two grains per section. Grains range from 30 to 400 μm in diameter and are usually included in quartz, are interstitial to quartz and feldspar or are included in Li-mica but not in chlorite. Ovoid to subhedral, tabular crystals are colourless to pale yellow, usually with orange-stained cores and range from isotropic to weakly anisotropic, with first order interference colours. Pyrite typically encloses grains or occurs as inclusions and veinlets while abundant haematite gives rise to strong yellow and orange internal reflections. Thorite grains sometimes partly enclose zircon while, in a Li-mica, small thorite overgrowths occur on zircon and thorite is intergrown with monazite.

Chemistry

Thorites from the microcline contain high, but variable, U and Y and low Zr contents (Figs. 24-26). Occasionally, ED spectra of thorites show very high Th:Si ratios (Fig. 43). Since the grains are translucent, thorianite (ThO_2) is not suspected and so there may have been a suppression of counts for Si relative to Th, although the reason for this is unclear.

Table 46 shows that a thorite from Sample R1/23 displays a large and continuous spatial variation in U concentration which attains 52 wt% UO_2 at the grain periphery; a concentration which exceeds that found in some coffinites. Despite its composition, the presence of coffinite could not be confirmed optically in this part of the grain which is indistinguishable from the more Th-rich part in reflected light (Plate 93). Y is also very high and shows a spatial variation which is less extreme than, and is unrelated to, that of U. Correlated with Y are the HREE, which reach a total concentration of 6 wt% HREE_2O_3 and P, which reaches nearly 3 wt% P_2O_5 , where Y is at a maximum of 14 wt% Y_2O_3 at the grain periphery. Although Zr concentration only reaches a significant value of 5.3 wt% ZrO_2 at the grain periphery near a zircon, this is not thought to represent contamination of the analysis by the zircon, since the wt% SiO_2 is not enhanced. Thus, U, Y, P, HREE and Zr show a maximum concentration at the grain periphery, while Th is at a maximum in the grain core, although further analyses (or an X-ray map) should confirm whether this chemical variation is in the form of concentric zoning.

Qualitative analyses of a 150 μm long lath of TiO_2 revealed significant U and Si with minor Y associated with a 10 μm diameter, bright inclusion, observed under the SEM (Fig. 51). A 25 μm diameter,

very poorly polished grain associated with pyrite, pyrochlore, columbite and cassiterite contains high U, Y, Th and Si with minor Zr and P (Fig. 48; Plate 94). Although their compositions suggest that these two grains are coffinite, identification could not be established optically.

iii) Coffinite

Coffinite has been positively identified in only one sample from the Ririwai lode. Three grains, ranging in diameter from 30 to 150 μm , were found as inclusions in K-feldspar and quartz and interstitially between these two minerals (Plate 95).

Optically, the coffinite closely resembles limonite and has a very irregular, poorly crystallised habit, although it may be distinguished by its isotropic nature, with or without faint, brown internal reflections, and by its reflectance, which slightly exceeds that of quartz. The phase invariably contains tiny (less than 5 μm in diameter) inclusions of pyrite and, in one example, is intimately intergrown with a LREE-phase (Plate 96).

Chemistry

Fig. 50 and Table 37 show that the coffinite has high but variable Y (up to 16 wt% Y_2O_3) and P (up to 5 wt % P_2O_5) in place of the high Zr and Si which are found in coffinite from the biotite granite, although the Th contents are quite similar (about 3 wt% ThO_2). The stoichiometry of the recalculated formulae is poor, while the oxide totals tend to be equal to or lower than totals for the biotite granite coffinites (Table 37).

iv) ?Pyrochlore

In Sample R1/13-3, a 20 by 10 μm sized ovoid grain enclosed by pyrite is associated with columbite, cassiterite and ?coffinite (Plate 94). The grain is colourless, with high relief, is isotropic, has a reflectance similar to that of zircon and optically resembles a type of pyrochlore, rather than tantalite.

Chemistry

The phase could be a REE-microlite (Hogarth, 1977), since it contains very high Ta (about 45 wt% Ta_2O_5), lower Nb (about 9 wt% Nb_2O_5), significant LREE (about 7 wt% LREE_2O_3) and Th (1.75 wt% ThO_2) but low U (0.48 wt % UO_2 ; see Table 38 and Fig. 34). However, the oxide total of the analysis is very low and there are insufficient elements to occupy the A-site of pyrochlore (see Chapter 2, Section 2.a.vi.).

v) Monazite

Like thorite, monazite is a widespread, though not abundant accessory which ranges from 10 to 250 μm in length. Subhedral to euhedral elongate or diamond-shaped crystals are interstitial to quartz and feldspar, or included in chlorite or Li-mica where they are surrounded by pleochroic haloes (Plate 97), and associated with zircon clusters. Some grains are enclosed by haematite while one is intergrown with thorite and pyrite.

vi) LREE-phases

The LREE-phases are widespread but rare accessories which occur, along with zircon, as inclusions in chlorite or fluorite or, rarely, are intergrown with coffinite (Plate 96) or overgrown on thorite. The

phases are usually poorly polished and difficult to identify optically, but are generally colourless or pale yellow to brown and resemble zircon in refractive index, birefringence and reflectance, while prismatic crystals show straight extinction.

Chemistry

Compositionally, the phases can be divided into two varieties; one that contains mainly LREE with perhaps traces of Th or Si (Fig. 59) and one that contains significant and variable amounts of Ca, Th, Y, Si and Pb, in addition to the LREE (Figs. 52-58, 60-65). When associated with monazite, the LREE-phase is of the simple variety, while other occurrences tend to be of the complex variety. The LREE-phase intergrown with coffinite contains enriched La (Fig. 57).

b) Greisenised wallrock

i) Zircon

Zircon shows a variable abundance, but tends to be more common than in the microcline (Table 44). It shows a similar size range and mode of occurrence to zircons in the microcline, although zircon-bearing Li-mica is much more common in the greisenised wallrock. The chlorite-sericite intergrowth found in two samples (RS6(2) and RS6(3)) tends not to contain many zircons. Zircon clusters may be associated with chlorite, monazite, cassiterite, sphalerite, columbite or fluorite.

Zoning is common and, in sample R1/13-4, a thin pyrite veinlet runs parallel to the inner margin of an incomplete, outer zone (Plate 98). Areas of lower reflectance, which partly follow outer zones or form irregular patches, are more widespread than in the microcline

and are particularly common and well-developed in sample RS10(3) (Plate 99). Rarely, zircon is overgrown by minor xenotime or thorite (Plates 100-103) or is enclosed by larger thorite grains included in quartz, Li-mica or the chlorite-sericite intergrowth (Plates 104 and 105).

Chemistry

As with zircons from the biotite granite and albitite, unaltered zircons from the Ririwai lode tend to contain higher U than Th, with both concentrations lying below 1 wt% oxide, although, in zircons from sample RS14(1), U ranges from about 1 to 2 wt% UO_2 .

Hf typically ranges from 2 to 3 wt% HfO_2 in zircon cores but, in several cases, rises to between 5 and 7.5 wt% HfO_2 at the margins. Part of a zircon from R1/13-4 (Plate 98), contains very high Hf (up to 17.3 wt% HfO_2) compared with adjacent areas which contain 3.6 wt% HfO_2 . The equivalent composition of 16.2 mole % $HfSiO_4$ corresponds to hafnian zircon (Chapter 2, Section 2.b.i.). Although the zircon has low reflectance patches, these only surround the boundary of the high Hf area (30 x 70 μm in size) and do not extend into it.

The low reflectance patches appear to be spatially related to the zircon margin, where it is partially enclosed by a thorite. The patches are enriched in Th, U, Y, Ca, Fe, Mn and P and have lower oxide totals compared with higher reflectance areas in the zircon (Tables 30 and 45). In some cases, the patches are enriched predominantly in U, Ca, Fe and Mn, with relatively low contents of Th, Y and P. The low reflectance patches in zircons from Sample RS10(3) (Plate 99) show even higher concentrations of Th and Fe only but lower Hf relative to the higher reflectance areas (Fig. 31). These zircons are also in close proximity to thorite grains.

ii) Thorite

Thorite tends to be more abundant in the greisenised wallrock, compared to the microcline (Table 44). Grains range from approximately 20 to 250 μm in diameter and are mainly found as inclusions in the Li-mica or the chlorite-sericite intergrowth (in samples RS6(2) and RS6(3)) although thorite is also included in clear K-feldspar or quartz and is found interstitially.

Inclusions in the Li-mica have prominent, brown haloes and exhibit similar optical properties and modes of occurrence to thorites in the microcline. Although mainly isotropic, weak patches of anisotropy are associated with orange staining in a 250 μm long thorite from Sample R1/13-4 (Plate 104). A cluster of submicron to 3 μm diameter thorites is included in Li-mica in Sample RS14 (Plate 106). As well as being closely associated with limonite, haematite and pyrite, thorite occurs with zircon clusters, columbite, fluorite and cassiterite (Plate 104) and, in one example, contains an inclusion of molybdenite. Pale yellow thorites included in clear K-feldspar lie along cracks which appear to have controlled their growth (Plate 107). A 100 μm diameter, pale yellow, anhedral thorite found in quartz partially encloses a euhedral zircon (Plate 105).

Inclusions in the chlorite-sericite intergrowth are enclosed by colourless haloes with dark green rims. Up to 30 thorites occur in dense clusters and typically appear as colourless, anhedral lozenge-shaped crystals which may be enclosed by cassiterite (Plate 108) or pyrite.

Chemistry

Figs. 24-26 and Table 47 show that thorite from the greisenised wallrock contains very variable amounts of Y, Zr and U, although Y is invariably present in concentrations above 3.5 wt% Y_2O_3 . Zr ranges from 0 to 15 wt% ZrO_2 , the upper value corresponding to interstitial thorite, closely associated with zircon in Sample RS10(3). As well as including grains of zircon, the thorite forms complex intergrowths with this mineral and appears to replace it (Plate 109). Zircon, which lies adjacent to the Zr-rich thorite, invariably exhibits the low reflectance patches which contain high but variable concentrations of Th. The 40 to 120 μm diameter, anhedral thorites are rich in haematite, which is reflected in the analysis for Fe (5.1 wt% Fe_2O_3), and also contain high amounts of Y (about 8 wt% Y_2O_3), HREE (about 4 wt% $HREE_2O_3$) and P (about 4 wt% P_2O_5). Qualitative analyses have confirmed that this thorite chemistry is broadly consistent for all five grains found in the section (Fig. 42).

Maximum values for U (24 wt% UO_2) occur in thorite overgrowths on zircons included in chlorite-sericite (Plates 100 and 101), although considerable variation occurs within the overgrowths (down to 18 wt% UO_2) and within a thorite in quartz (4.5-15.5 wt% UO_2) from the same sample (RS6(2), Plate 105).

iii) Th-Pb-P phase

An unidentified, anhedral phase, found in Sample RS10(3) (Plate 110) measures 40 to 120 μm across and, in reflected light, closely resembles associated Zr-rich thorite. The phase is also associated with monazite, while abundant, admixed haematite gives rise to strong, yellow and orange internal reflections.

Chemistry

The phase contains high Th, Pb and P along with traces of LREE, Y, Ca, Si and U (Table 43). A number of qualitative and quantitative analyses for three grains have confirmed a broadly consistent composition for the Th-Pb-P phase (Fig. 44). This consistent chemistry, together with its homogeneity in high-magnification, reflected light and BSEI photographs, suggest it is a single mineral, rather than a fine admixture of more than one mineral. High values for Fe (up to 13.7 wt% FeO) probably reflect contamination from the admixed haematite.

During analysis, the probe beam left an isotropic spot, free of internal reflections and measuring 20 μm across, compared to a similar spot measuring under 10 μm in diameter produced in the Zr-rich thorite (during the same period of analysis). This apparent lower stability of the Th-Pb-P phase compared to the Zr-rich thorite under the beam could be a consequence of differing amounts or types of unmeasured volatiles present (e.g. F, H₂O, CO₂) between the two phases.

The phase could be a phosphate of Th and Pb, but the amount of (P + Si) recalculated to four oxygens is very depleted (Table 43), especially when recalculated to a cation total of one. Possibly, the unmeasured volatiles substitute for some of the PO₄³⁻, although charge balancing problems would then arise. The phase could represent a new, Pb-rich member of the huttonite-monazite-brabantite series (Chapter 2, Section 2.b.ii.).

iv) U-Th-Y-Si phase

An unidentified phase containing high U, Th and Y and significant P (Table 37, Fig. 47) was observed under the SEM as a cluster of tiny

(less than 10 μm in diameter), bright grains included in chlorite-sericite (Plate 111). Although a dark halo was apparent in the host chlorite, the grains could not be resolved in transmitted light.

v) Monazite

Monazite was identified in 60% of the greisenised wallrock samples, with two samples containing 8 to 9 grains each. The monazite ranges in length from 10 to 500 μm and elongate, corroded to prismatic crystals are included in Li-mica (Plate 97), chlorite-sericite, quartz and clear K-feldspar, sometimes with zircon clusters. In Sample R1/23-2A, monazite occurs as an aggregate of bladed crystals while, in sample RS6(2), it forms part of an overgrowth to thorite, which itself encloses zircon (Plate 100). Rarely, monazite is enclosed by iron-oxide. The monazite displays normal ratios of LREE but with variable concentrations of Th, U and Si (Table 34).

vi) LREE-phases

Unidentified LREE-phases are less widespread than in the microcline and discrete grains (10 to 60 μm diameter) or "welded clumps", containing variable amounts of Th, U, Y, Si and Ca (Figs. 60-63 and Table 36) occur as inclusions in clear or purple-tinged fluorite which, itself, is included in Li-mica or chlorite-sericite. In Sample RS10(3), a LREE-phase of simple composition is intergrown with monazite and a complex Pb-Th-rich LREE-phase (Figs. 64 and 65) and is also included in the Zr-rich thorite (Plate 112).

vii) Xenotime

Xenotime is a very rare accessory and is found in only two samples of greisenised wallrock. It occurs as 20 to 80 μm long overgrowths on zircon or replacements of thorite which are included in chlorite-sericite (Plates 100 and 101). The colourless xenotime is in optical continuity with the zircon but can be distinguished by its lower reflectance, refractive index and extreme birefringence. A prismatic part to an overgrowth appears to show concentric zoning (Plate 100).

The accessory contains significant Th (1.4 wt% ThO_2) but lower U (up to 0.4 wt% UO_2) along with a high content of HREE (up to 17 wt% HREE_2O_3 ; see Figs. 45, 46 and Table 43).

c) Greisen

i) Zircon

Zircon is similar in its abundance, size range and mode of occurrence to zircons from the greisenised wall-rock although low reflectance, trace-element enriched patches are uncommon and less widespread (Plate 113; Table 44). Rarely, overgrowths of isotropic or weakly anisotropic zircon, thorite or xenotime are found on zircon grains. The U concentration often shows a spatial variation, but this is inconsistent between grains and, in one zircon, it is slightly enriched in the core while, in another, the edges contain higher U, although Th tends to remain constant.

ii) Thorite

Thorite is particularly abundant in Sample R1/14-2 where grains form a trail over 35 mm long in quartz and clear K-feldspar, (Plate 114) in which they commonly lie along fractures. The colourless,

amoeboid- or lozenge-shaped grains typically have orange-stained cores (Plate 115) with weak anisotropy and exhibit parallel extinction. In other samples, thorite is mainly included in the Li-mica, where it is frequently closely associated with zircon clusters and welded clumps (Plate 113).

Chemistry

Figs. 24-26 show that greisen thorites continue to exhibit a large range in U, Y and Zr content. In a 300 μm diameter thorite from Sample R1/14-2, there is a higher concentration of Zr near the grain periphery (up to 3 wt% ZrO_2) compared to the core (0.1 wt% ZrO_2). In another sample (R1/14-1), ED spectra (Fig. 40) demonstrate significantly higher concentrations of U, Y and HREE to be present around the outer area of a 100 μm diameter thorite compared to its core. A different thorite from the same sample shows this relative enrichment in U, Y and HREE in only part of the outer margin. Thorites associated with a welded clump of zircons (Plate 113) display a wide range of Zr concentration whereas, in another sample, an anhedral thorite (Plate 116) shows apparently random spatial variations in U, Y and P concentration while Zr remains below detection (Table 48).

iii) Monazite

This accessory is similar in abundance, size, range and mode of occurrence to monazite from the greisenised wallrock (Table 44). Interstitial prisms or bladed aggregates sometimes show corroded outlines, with thin residual margins and fragments, while a 600 μm long grain contains an irregular, 100 μm diameter patch of a LREE phase (Plate 117). This grain shows a variable La : Ce ratio which reaches a

maximum, close to the LREE-phase patch. Th is high, but shows a small variation in concentration, both within and between monazite grains (Fig. 37).

iv) LREE-phases

The LREE-phase patch in monazite is of simple composition, containing very low Th and Si, but it also shows an increased La : Ce ratio. Optically, it can be distinguished from the clear monazite by its brown colour, lower reflectance and abundant white internal reflections.

LREE-phases of more complex composition comprise rare, 20-30 μm diameter inclusions in Li-mica (Plate 118) and overgrowths on thorite and zircon (Plate 119). Anhedral to subhedral, prismatic crystals range from colourless to pale brown or opaque, display first to third order birefringence colours with a reflectance and refractive index similar to those of zircon. Qualitative analyses (Figs. 54-56) reveal significant but variable concentrations of Th and Y with traces of P, Si, Pb and Ca although, within grains, the composition is broadly homogeneous. A 20 μm diameter overgrowth on zircon (Plate 119) contains 23 wt% ThO_2 , 7.3 wt% P_2O_5 , and significant Si, Zr, Ca and Y (Table 36, Sample R1/14-2).

v) Xenotime

The only occurrence of xenotime found in the greisen is as 6 μm diameter overgrowths on a zircon included in quartz.

6. Summary

Zircons in the biotite granite are typically included in quartz, feldspar or biotite, in association with other accessory minerals, whereas those in Samples N75 and L13-365 of the biotite granite and in the albitised granite and albitite are mainly interstitial to quartz and feldspar and are often enclosed by iron-oxide. Biotite granite zircons are more abundant, smaller and contain fewer iron-oxide and thorite inclusions compared with those from N75, L13-365, the albitised granite and albitite, where grains contain distinct zones, rich in iron-oxide and thorite. Such zircons often have clear, outer zones which, in the albitised granite, show banding related to changes in HF concentrations. Euhedral grains sometimes show minor embayment by fluorite in the biotite granite, but subhedral to anhedral grains in the albitised granite and albitite show truncation of zoning and embayment by surrounding fluorite and plagioclase. U is enriched in clear, metamict zircon in the albitised granite and albitite, whereas Th, U, Fe, Mn, Y and P are enriched in secondary, metamict patches in zircon from the biotite granite. Otherwise, both U and Th lie below 1 wt % oxide, with U tending to exceed Th concentrations.

Thorite overgrows and replaces zircon and occurs as small inclusions that tend to be most abundant in zircon between 400 and 416 m depth. Discrete grains of metamict thorite are rare but widespread in the biotite and albitised granites, where they occur in altered biotite, quartz or feldspar and invariably show a close association with iron-oxide and pyrite. The thorite is compositionally very impure, with high but erratic concentrations of Zr, Y and U which only rarely show enrichment at margins, relative to cores. There is a general trend of increasing mean U content of thorites with depth, with

highest values occurring in the albitite thorites, whereas highest Zr values are found in thorites from the biotite granite.

Monazite is a rare, though widespread, accessory found in most samples of the biotite granite but it is very scarce below 395 m. Grains are euhedral, prismatic or highly irregular, interstitial and show alteration to a LREE-phase in the biotite granite and albitite, with effects of dissolution apparent in the albitised granite. Rarely, where the LREE-phase replaces monazite, both phases show abnormally high La : Ce ratios. More commonly, the LREE-phase is found as inclusions in fluorite in the biotite granite, but mainly in the albitised granite and albitite. Unlike monazite, which contains high but variable Th, the LREE-phase contains only traces of Th along with Y, Si, Ca and U.

Other rare accessories in the borehole samples include xenotime, found exclusively in the albitised rocks, usually overgrowing zircon; pyrochlore, found in the biotite granite and albitite; and Zr-rich coffinite, found only at 100 m in the biotite granite.

Zircons from the incipiently greisenised granite at 125 m show substantial replacement of their cores by Li-mica and are overgrown by thorite, which is highly enriched in Y and Zr. In the Ririwai lode, zircons, which are found in quartz, feldspar or mica in association with other accessories, tend to be smaller, less abundant and contain no thorite and fewer haematite inclusions, compared with zircons in the granite and albitite. Secondary, low reflectance patches are enriched in Th, U and other elements, whereas higher reflectance zircon contains low U, which normally exceeds Th. Outer zones contain enriched Hf, which reaches very high concentrations in a zircon from the greisenised wall-rock.

Thorite from the Ririwai lode is compositionally impure, and generally contains higher Y and lower Zr, compared with biotite granite thorites. There is limited evidence of thorite cores showing relative depletion in Zr, Y or U but the spatial variations of these elements in other grains appear to be random. Highest U is found in thorites from the microcline, which also contains most of the unidentified U-Th-Y-Si-phases, Zr-rich coffinite and ?pyrochlore. Associated with Zr-rich thorite and monazite in one sample of greisenised wall-rock is an unidentified Th-Pb-P-phase while, in the same sample, an unidentified Pb-Th-rich, LREE-phase is intergrown with a LREE-phase of simpler composition. This purer LREE-phase also replaces monazite in the greisen, while compositionally more complex LREE-phases, containing variable amounts of Th, Y, Ca and Pb overgrow zircon, thorite or coffinite or are included in fluorite or mica. Rarely, xenotime overgrows zircon and replaces thorite which are included in the chlorite-sericite intergrowth and quartz.

Chapter 5 Conclusions and Discussion on the Ririwai Material

1. Mineral composition in relation to rock-type

The accessory mineral showing the greatest variation in composition in the biotite granite and its altered facies is thorite, which usually contains significant amounts of U, Zr and Y. In all rock-types, some thorites are nearly pure end-member, but the range of substitutions is characteristic of the rock-type (Figs. 68-70 and 80).

- i) Biotite granite - thorite (and coffinite) ranges to Zr-rich compositions. The highest Zr content (27 wt % ZrO_2 , Table 33) greatly exceeds that of any thorite found in a literature search (Chapter 2, Table 6). The highest Zr content of coffinite (11.7 wt % ZrO_2 , Table 37) appears to be similarly unique.
- ii) Ririwai lode (microclinite and greisenised rocks) - thorite (and coffinite) ranges to Y-rich compositions. The highest Y content (10 wt % Y_2O_3 , Table 31) exceeds that of the majority of thorite analyses in Table 6. Highest Y contents (up to 16 wt % Y_2O_3) are found in coffinite and unidentified U silicates from the microclinite and greatly exceed those of published coffinite analyses in Table 5 (Chapter 2), with the exception of Premoli (1982).
- iii) Albitised rocks - Neither Zr nor Y reach the maximum levels found in the biotite granite and Ririwai lode thorites but U tends to be higher (up to 29 wt. % UO_2).

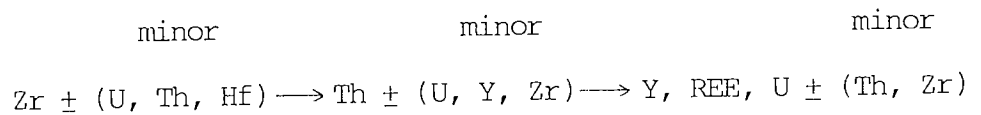
In a few samples of biotite and greisenised granite, both the Y and Zr contents of thorite are high. The composition of zircon is much less variable than that of thorite but shows some of the same trends. In the albitised rocks, the radioelement-rich zircons contain more U

than Th, while Y tends to be higher in secondary patches in the greisenised rocks, compared to the biotite granite. Unidentified LREE-rich phases of complex composition may contain high concentrations of Y, Th, Pb and Ca in the lode samples but are relatively pure in composition in other rock-types.

2. Paragenetic sequence

a) General remarks

A consistent paragenetic sequence can generally be worked out within one rock-type and some correlation between rock-types is also attempted (Table 49). Thorite tends to be later than zircon, while xenotime, LREE-phases and coffinite are later still, implying the following general sequence of element deposition (cf. Ixer et al., in press):



This sequence is expressed by the mineral parageneses within each alteration process, as well as by the changing mineral chemistries from biotite granite, through the albitised samples to the microcline and greisenised rocks. For example, in the biotite granite, Y and P enrichments are found in thorite peripheries, while the relatively late deposition of Y during albitisation is reflected by the lower Y range of earlier thorite and by the xenotime overgrowths on zircon. In the greisen, zircon is overgrown by thorite which, itself, is replaced by xenotime. At the same time, a progressive increase in Y deposition is noted from the biotite granite, which contains yttrifluorite, through the albitised samples, which additionally contain xenotime, to the greisenised and microclinised samples, which contain Y-thorite and

Y-coffinite, as well as yttrifluorite and xenotime.

In the biotite granite, most of the zircon, thorite and monazite are assumed to be magmatic but the origin of these and other accessories in the altered rocks is not always clear. Several criteria can be employed when comparing magmatic accessories in the biotite granite with counterparts in the altered rocks. As discussed above, compositional variations have been particularly useful in distinguishing different generations of thorite. Size, morphology and the presence or absence of metamictization or inclusions are further attributes which have helped distinguish different generations of zircon. The inclusion of accessories in biotite and chloritised biotite or their interstitial occurrence in quartz and feldspar have been used to distinguish primary and secondary generations respectively. Accessories which are included in secondary major minerals, such as Li-mica, are not necessarily secondary themselves and could have been inherited from the biotite granite.

b) Biotite granite

Zircon usually occurs as small, early-formed crystals which form at high temperatures and so are liable to be enclosed in later minerals (Deer et al., 1966). In the biotite granite, zircon is found as inclusions in biotite and quartz, implying that it crystallised before or with these essential minerals. Within quartz it also frequently occurs at the triple junctions of optical or grain boundaries and so may be interstitial and of later origin. Thorite inclusions are found in quartz, feldspar and biotite and are assumed to have formed contemporaneously with these minerals, in which case they are also of primary magmatic origin. The small thorite inclusions in zircon

probably also formed contemporaneously with their host, which is thought to be of primary magmatic origin in most of the biotite granite, but in samples L13-365 and N75 a metasomatic origin has been postulated for both zircon and thorite, (see below).

Zircons are either clear or have iron-oxide inclusions concentrated in their cores. One interpretation is that initial zircon crystallisation was accompanied by haematite crystallisation from an Fe-rich melt, but that precipitation of Fe temporarily ceased, while zircons continued to grow. It is conceivable that the Fe was precipitated initially in solid solution in the zircon, and later exsolved as haematite. Precipitation of Fe later resumed during the crystallisation of biotite and iron-oxide coatings on zircon. The sharp cut-off between the inner, haematite-rich core and the outer, clear zone of the zircon in Plate 39 suggests that zircon growth was interrupted, rather than continuous. The outer, fine-scale zoning of haematite-free zircon is similar to the 3 mm thick banding in zircons described by Sahama (1981), who attributed this to rhythmic fluctuations in the rate of crystallisation. This resulted from irregular, convective flow in the crystallizing medium, giving rise to strain between the adjoining fine bands.

Another interpretation is that the haematite inclusions are much later than zircon and represent void infillings or pseudomorphs after pyrite or marcasite, which themselves formed late. However, this does not explain the confinement of many inclusions to the zircon cores and there is normally an absence of haematite-filled cracks/veinlets allowing Fe into the grain centres. The only other method of introducing the Fe into zircon, subsequent to its crystallisation, is by diffusion through the crystal lattice, which might be expected to

give rise to haematite-rich, outer zones and clear cores.

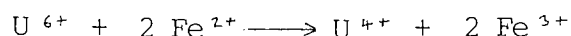
Interrupted zircon growth is further demonstrated by an anhedral overgrowth of zircon (Plates 33 and 34) which contains a thorite inclusion, together with enhanced concentrations of U, Th, Hf, Fe, Y and P (Table 29) relative to the host zircon. This suggests that there was a slight accumulation of trace elements in the melt, or conditions became more favourable for their precipitation, during a temporary cessation of zircon growth. Enhanced concentrations of Th in the melt are reflected by the presence of thorite inclusions in some zircons but these inclusions attain greater importance in samples N75 and L13-365.

The lack of thorite inclusions in most zircons and the occurrence of an inclusion only in the overgrowth of a zircon, suggest that thorite precipitation did not occur throughout the crystallisation history of zircon, but was initiated during later zircon growth, possibly when Th levels in the melt had sufficiently accumulated. Overgrowths of thorite on zircon (Plates 28 and 29) and the apparent replacement of zircon by thorite (Plate 55) demonstrate that thorite continued to nucleate after at least some zircon had finished growing.

Rare, compositional zoning in thorite always shows some enrichment of minor elements, such as Zr, Y, and P, at the peripheries of grains. The peripheral enrichment of trace elements could reflect growth-zoning but passive-zoning (Speer, 1982), in which trace element-rich fluids interact with and partially replace the outer margins of pre-existing thorite, is also possible. Thus, although the thorites themselves crystallised magmatically, their localised Zr-rich compositions may reflect post-magmatic, sub-solidus alteration.

The enrichment of U in haematite-bearing thorite cores relative to the rims, observed in a few grains (e.g. Plate 51), together with

positive correlations between U and Fe in these grains (Table 52), suggest a genetic link between the precipitation of Fe³⁺ and U⁴⁺ :



Alternatively, hydration may have been accompanied by the oxidation of U⁴⁺ to U⁶⁺ which was preferentially leached from the thorite grain peripheries by oxidising, post-magmatic fluids, leading to relatively high concentrations of U in the cores. A number of examples of this phenomenon exist in the literature (Chapter 2, Section 2.a.iv).

The low reflectance, trace-element enriched patches in zircon (Chapter 4, Section 2.c.i.) appear to have formed after the crystallisation of zircon, as their spatial distribution has been partly influenced by pre-existing zoning and fractures. This suggests that they formed by post- or late-magmatic alteration, during which fluids, rich in trace elements, selectively replaced the primary zircon along lines of weakness in the structure. U, Th, Y, Fe, Mn and Ca replaced part of the Zr and Hf while P and possibly (OH) replaced part of the Si in the zircon lattice.

If the alteration were late magmatic, it may have coincided with thorite crystallisation, in which case the same Th-rich fluids responsible for thorite precipitation may also have altered zircon. If the alteration were post-magmatic, it may have resulted from an interaction between the granite and disseminated fluids, rich in Th and other trace elements, which were derived from the residual melt and then trapped within the largely crystallised granite. The alteration patches have only been found in zircons from samples above 350 m (Table 25), suggesting that this alteration was a localised event in the pluton. However, due to the limited number of sections examined, it is

quite possible that examples which do occur below 350 m have been missed.

An interaction of thorite with oxidising, Fe-rich fluids is indicated by the ubiquitous occurrence of goethite and haematite-bearing rims around grains. Rimsaite (1982a), Robinson and Abbey (1957) and Marlow (1981) described uranothorite with prominent rims of iron-oxide and/or pyrite, while Yeliseyeva (1977) reported thorite with U-enriched rims and cores of Fe-oxide. It is not certain, in the case of the biotite granite, whether the Fe-oxide rims contain enhanced U. Fission-track studies are required to determine the relationship of U with iron-oxide in the granite, since concentrations of adsorbed U in iron-oxide are generally below the detection limit of the microprobe. In the biotite granite, thorite is invariably associated with iron-oxide while, in the greisenised and microclinised samples, it is also associated with pyrite.

The embayed, anhedral appearance of many zircons implies some dissolution of this phase and Deer et al. (1966) note that some rounding of zircon can take place by magmatic resorption. Zircons included in biotite are frequently associated with fluorite which sometimes embays and appears to replace zircon, which is consistent with the suggestion already made (Chapter 3, Section 3.a.) that the fluorite is later and may be of secondary origin. The replacement of zircon may be aided by the formation of stable Zr-F complexes which are easily mobilised (Vlasov, 1966a).

Zircons from samples N75 and L13-365 differ in character from those in other samples of biotite granite. They tend to be larger, with abundant haematite and thorite inclusions but with clear rims and are found interstitially in quartz and feldspar, rather than as

inclusions in biotite. They might represent a later generation of zircon in the residual melt of the cupola roof. This later zircon grew after the biotite crystallised, whereas an earlier generation of zircon was preserved as the smaller, clearer inclusions in biotite, found in sample N75.

This explanation is inconsistent with the presence of late zircon in sample L13-365, which crystallised well below the cupola roof, where it is less likely that a residual melt, enriched in trace elements, would accumulate. Here, the zircons may have formed metasomatically in a similar way to Types 1 and 2 zircon in the albitised rocks (Section 2.c.). The secondary growth of zircon may have been associated with protracted hydrothermal activity along horizontal joints, which was envisaged to explain the microcrystalline nature of sample L13-365 (Chapter 3, Section 3.a.). An association of thorite inclusions with more haematite-rich areas of zircon might result from the same processes of exsolution or redox co-precipitation suggested to explain similar features in Type 2 zircon from the albitised samples (see Section 3.a.).

Rare pyrochlore in the biotite granite is believed to be primary magmatic (Iyer et al., in press), in contrast to the peralkaline granites, where pyrochlore crystallisation was associated with a phase of albitisation (Kinnaird et al., 1985b). In the biotite granite, the inclusion of pyrochlore in zircon is consistent with a primary magmatic origin.

The occurrence of monazite as euhedral, prismatic crystals included in the major minerals suggests it is of primary magmatic origin. Minor embayments in some euhedral grains suggest limited magmatic resorption. A particularly anhedral, interstitial occurrence

of monazite at 365 m (Plate 58) may have undergone more extensive remobilisation, along with zircon and thorite, during the metasomatism which has been postulated for this sample (see above).

Locally, monazite has been replaced by a LREE-phase, possibly bastnaesite, during post-magmatic alteration of the granite. Associated with this replacement is the fractionation of La, resulting in varying La:Ce ratios, both in the LREE-phase and the nearby monazite. The hydrothermal replacement of monazite by members of the hydroxyl-bastnaesite group has been described by Rimsaite (1982a, 1983, 1984, 1986) who noted that such replacements contained similar proportions of REE to the monazite, whereas overgrowths were enriched in La and contained La:Ce ratios greater than one. According to Kamineni and Bonardi (1983), the replacement of monazite by bastnaesite is a supergene process.

The interstitial nature of coffinite, which occurs between quartz, feldspar and biotite grains and along cleavage planes in biotite (Plate 61), indicates that it formed post-magmatically. This is consistent with the intimate intergrowths of coffinite with sphalerite and molybdenite (Plate 62), which are believed to have formed during hydrothermal alteration and mineralisation of the granite (Iyer *et al.*, in press). An association of coffinite with Mo mineralisation has also been noted by Bayushkin (1970), Goldhaber *et al.* (1983) and Mueller and Halbach (1983) for hydrothermal U deposits in a variety of rock-types. Coffinite mineralisation appears to have been a localised phenomenon in the biotite granite, since it has only been found at 100 m, although samples above this depth have not been examined. Consequently, coffinite probably contributes an insignificant amount to the overall, bulk U content of the granite, compared with uranothorite and zircon.

c) Albitised rocks

The importance of small inclusions in zircon as a site for thorite increases with depth, from 385 m, with increasing albitisation of the granite. There is a concomitant decrease in the number of discrete thorite grains, and only one was found in the albitite (Table 25). As with zircon, fewer grains of thorite are included in biotite and most are interstitial to feldspar ± quartz. This changing mode of occurrence of thorite is consistent with the hypothesis, based upon zircon populations (Section 4), that albitisation plays an important role in the crystallisation of U- and Th-bearing accessory minerals.

The decreasing association of thorite with biotite is an inevitable consequence of the alteration and eventual dissolution of biotite. Primary magmatic thorite, which may have been present as inclusions in the mica, would have dissolved and possibly reprecipitated in interstitial sites in the quartz and feldspar of the albitised granite and albitite.

Zircons from the albitised granite and albitite tend to be larger, fewer in number and more haematite- and thorite-rich compared with those from the biotite granite and Ririwai lode. This change in the size, abundance and character of zircon may be associated with the onset of albitisation, observed between 385 and 411 m depth, and/or may be related to the position of the zircons in the roof facies of a hypothetical, later granite at depth (Chapter 3, Section 4.a.i.).

Domains of Type 3 zircon tend to occupy the cores of grains which are concentrically zoned with respect to the three different zircon types (e.g. Plate 64), suggesting that they crystallised before Types 1 and 2 zircon. Locally, intergrowths of Types 2 and 3 zircon suggest the co-precipitation of these two zircon types, perhaps as immiscible

phases or, more likely, the replacement of Type 3 by Type 2 zircon (Plates 85 and 86).

Zones of Types 1 and 2 zircon are commonly incomplete and impinge against plagioclase or chloritised biotite in the albitised granite. Either these zircon types originally grew as complete, concentric zones which were later partially replaced by the surrounding minerals, or they grew interstitially after the feldspar and mica had crystallised.

In the case of a zircon from 411m (Plates 69 and 70), it seems that the second hypothesis is more likely. The outer, rhythmically banded zone of Type 1 zircon is truncated along a straight line which is parallel to the grain boundary and cleavage of an adjacent plagioclase crystal. Fig. 71 is one interpretation of this texture, in which Types 2 and 3 zircon nucleated against a chloritised biotite grain. The crystallisation of new plagioclase adjacent to the zircon left only limited space for the growth of a later, incomplete zone of Type 1 zircon. It is unlikely that the plagioclase was younger than and selectively replaced part of the Type 1 zircon, since the zone of Type 2 zircon projects into the newer plagioclase and shows no evidence of replacement. Similarly, truncation of the concentric zoning in a grain from 445 m (Plate 87) could be interpreted as impingement of late-crystallising zircon against a plagioclase crystal. Corrosion and replacement of a pre-existing zircon would be expected to give a more irregular, embayed margin rather than the sharp, straight edge observed.

Although at least some zircon grew after the crystallisation of feldspar, it is difficult to demonstrate whether or not the feldspar had already been albitised at this time, i.e. whether Types 1 and 2 zircon crystallised late-magmatically or post-magmatically.

An argument against the crystallisation of zircon under hydrous, low temperature magmatic or metasomatic conditions in the albitised samples (or in samples N75 and L13-365 of the biotite granite) arises from the results of experimental studies of zircon synthesis (Chapter 2, Section 2.b.i.). These suggest that zircon, formed at low temperatures, tends to be hydrous. The presence of water in zircon will result in low analytical totals, while the formulae of hydroxylated zircons will also show deficient Si. Although Tables 26, 29, 39 and 41 show that some zircons have low oxide totals and deficient Si, these probably result from secondary processes of metamictisation and hydration due to the high levels of U and Th present. Many other unaltered zircons, including those from N75 and L13-365, have oxide totals closely approximating 100% and Si closely approximating one in the formulae, implying the absence of water. This suggests their formation under relatively high temperature, magmatic conditions, rather than under low temperature, hydrous conditions. On the other hand, if magmatic, the zircon is remarkably pristine compared with the patchily altered ones in other metasomatised rocks (e.g. the greisenised samples).

Whether the zircon is late-magmatic or post-magmatic, it managed to acquire the mineral-chemical characteristics of the albitised environment. These include the high U/Th ratio of Type 3 zircon which is not particularly enriched in Y, features which are shared by the late thorite overgrowths and replacements. Subsequent events included the partial replacement of some zircon by yttrifluorite and the overgrowth of zircon by sulphides and haematite.

The absence of xenotime from the biotite granite and its overgrowth on the corroded edges of zircon, which it sometimes embays,

in the albitised rocks are consistent with crystallisation of this accessory during the later stages of albitisation. A decrease in the abundance of monazite from the biotite granite to the albitite suggests dissolution of this phase during albitisation. Remobilisation of monazite is also suggested by the corroded or irregular, interstitial character of this phase in the albitised granite and albitite. Preferential leaching of Th may have occurred in smaller, residual fragments of corroded monazite (see Fig. 27, Table 35).

d) Microcline and greisenised rocks

At 125 m in the borehole, where the granite has been partially greisenised, zircons have been substantially replaced by Li-mica. The selective removal of zircon cores may reflect original inhomogeneities in zircon composition and the predisposition of certain areas to leaching (Section 4).

No zircons from the Ririwai lode show substantial replacement of their cores by Li-mica. Grains tend to be smaller and clearer than those in the biotite granite and at 125 m, and this either reflects primary variations in zircon crystallisation in the magma or is related to subsequent processes of alteration. There is no evidence of recrystallisation of a new population of zircons during greisenisation, since zircons from the greisen and microcline are similar in size and character and there are no obvious relict zircons in the greisenised wallrock, as there are at 125 m. Thus, the scarcity of zircons in the chlorite-sericite intergrowths in the greisenised samples probably reflects the reduced crystallisation of zircon locally in the intrusion, rather than the dissolution of zircon during greisenisation. It is possible, however, that a new generation of zircons

recrystallised when biotite was chloritised during microclinisation but, again, there are no relict zircons. Alderton et al. (1980) found that zircon remains stable during K-silicate, sericitic and chloritic alterations, but Cuney (1978) found zircon, monazite and xenotime to be corroded, during the chloritisation of biotite.

The association of zircon clusters with accessory minerals which are known to have formed during greisenisation e.g. cassiterite, sphalerite and columbite, suggests that a new generation of zircons might have crystallised during greisenisation although this evidence is purely circumstantial. If zircon did crystallise during greisenisation, then it must have done so before thorite, xenotime or the REE-phases, which are sometimes found as overgrowths on zircon. It is possible that zircons included in quartz recrystallised during silicification and quartz veining in the lode, although they could equally have been inherited.

Thus, although zircon was clearly destabilised during greisenisation at 125 m, the evidence for recrystallisation of zircon associated with alteration in the Ririwai lode is equivocal. The occurrence of Hf-enriched rims and local extreme variations in Hf concentrations between closely associated zircons is a similar feature to that found in zircons from the biotite granite (e.g. Sample N94, Chapter 4, Section 2.b.i.). The greisen zircons probably preserve a record of increasing Hf concentration and acute, chemical disequilibria in the original melt.

Low reflectance, U-, Th- etc.-enriched patches sometimes occur with zircon which is intergrown with thorite (e.g. Plate 98). The patches are analagous to those in the biotite granite zircons (Section 2.b.) but, if their formation is related to local thorite, they must

be later in origin and are not inherited from the granite, since thorite in the lode is thought to have crystallised during microclinisation and greisenisation (see below). The alteration patches either resulted from an interaction between zircon and the fluids responsible for thorite crystallisation, or subsequent dissolution of thorite released U, Th etc. which then interacted with the zircon. In sample RS10 (3), replacement of zircon by Th-, Fe-rich zircon reached greater extremes and the simultaneous mobility of Th and Zr is demonstrated by the enclosure of Th-, Fe-enriched zircon by Zr-rich thorite (Plate 109). The Zr-rich thorite probably does not represent former zircon which has been converted to thorite, since the thorite does not pseudomorph zircon.

Thorites in the greisenised granite at 125 m overgrow the corroded edges of zircon and therefore post-date or are contemporaneous with zircon dissolution. This is consistent with their high contents of Zr, part of which could have been remobilised from the corroded zircons. Since the zircons are replaced by Li-mica, which was formed as part of the greisenisation process, it follows that thorite crystallisation may also have occurred during this hydrothermal alteration.

Further evidence of the hydrothermal origin of thorite is its common occurrence as inclusions in the Li-mica, both at 125 m and in the Ririwai lode, whereas relict chlorite in the partially greisenised wall-rock and in the microcline does not contain thorite. The absence of thorite inclusions from chlorite suggests that the alteration of biotite to chlorite, during microclinisation, resulted in the dissolution of primary magmatic thorite, assuming this were present. This is analogous to the dissolution of thorite inclusions during chloritisation in the albitised granite and albitite

(Section 2.c.).

In parts of the Ririwai lode, abundant thorite crystallised, together with cassiterite, sphalerite, pyrite, molybdenite etc., during the replacement of feldspar by a fine-grained chlorite-sericite intergrowth, as a result of greisenisation. The occurrence of thorite grains in trails in the greisen (Plate 114) is further evidence of its hydrothermal origin. The occurrence of less abundant, interstitial thorite in the reddened wallrock, which shows no or little evidence of greisenisation, indicates a period of more limited thorite growth associated with the earlier process of microclinisation.

Thorite overgrowths and discrete grains associated with greisenisation are characterised by high Y. If thorite inclusions in the zircons at 125 m crystallised contemporaneously with their host from the melt, as has been assumed for most other granite samples, it follows that the compositions of these inclusions should reflect the composition of the melt, rather than fluids associated with any subsequent alteration. Indeed, one thorite inclusion from near the centre of a zircon at 125 m contains low Y (0.88 wt % Y_2O_3). On the other hand, two thorite inclusions in another zircon from this sample contain Y and Zr concentrations very similar to other thorites in the sample. It is possible that their primary magmatic compositions have been modified by subsequent greisenising fluids, since the inclusions are very close to the zircon periphery.

As with the biotite granite thorites, spatial variations of minor elements sometimes occur within thorites from the Ririwai lode. Although the enrichment of U, Y and HREE at grain peripheries might reflect growth zoning, the chemical modification of pre-existing thorite is suggested by the discontinuous nature of this outer

enrichment in one grain and by the total lack of any pattern to chemical variation in another.

Although thorites from the Ririwai lode and 125 m both contain high concentrations of Y, those from the Ririwai lode are much poorer in Zr, with the exception of three samples, in which thorites contain significant amounts of Zr (Fig. 26). The rare enrichment of Zr at thorite grain peripheries is a similar feature to some thorites from the biotite granite and suggests increasing levels of Zr in the fluids during later thorite growth, or perhaps the chemical modification of thorite which has already crystallised. This minor zoning of Zr in thorite and the occurrence of high Zr thorites in some samples and lower Zr thorites in others suggest that at least localised mobilisation of Zr took place in the Ririwai lode.

Zr mobilisation was more substantial in sample RS10 (3), where Zr-rich (up to 15 wt % ZrO_2) thorite co-exists with zircon containing Th-rich alteration patches. In sample R1/14, thorite containing up to 7.5 wt % ZrO_2 is intimately associated with zircon, but Zr compositions are variable and can be only 1 wt % ZrO_2 . Samples RS14, RS14(1) and RS14(2) contain Zr-rich (up to 9 wt % ZrO_2) thorite which is included in Li-mica and sometimes associated with zircon clusters. In samples R1/14 and RS14 etc., zircon contains low reflectance patches related to crystallographic zoning, although it has not been ascertained whether these patches are trace-element enriched.

It is not clear why samples R1/14, RS10(3) and RS14 etc. should contain thorite with high Zr concentrations, in addition to Y, whereas, in remaining samples of the lode, thorite contains high Y concentrations which are accompanied by no more than 3 wt % ZrO_2 . The intimate association of high-Zr thorite with zircon is probably significant,

especially when the zircon has evidently undergone partial alteration and replacement by Th. Zr^{4+} , released from the alteration of zircon, may have been incorporated in the thorite during its growth, although Zr was not detected in one thorite enclosing altered zircon (Plate 104).

Another common feature of Zr-rich thorite is its intimate association with iron-oxide, in the form of admixed haematite or thick rims of goethite while, in other samples of the lode and at 125 m, thorite is usually associated with pyrite, together with lesser iron-oxide. Relatively oxidising, greisenizing fluids appear to have been associated with haematite- and Zr-rich thorite in some parts of the lode, whereas more reducing fluids gave rise to pyrite-rich, Zr-poor thorites in others. This pattern is consistent with the occurrence of high Zr contents in many biotite granite thorites, which are invariably associated with iron-oxide, rather than pyrite, although it is inconsistent with the occurrence of high Zr thorite associated with pyrite at 125 m.

Euhedral crystals of monazite are included in chlorite of the microcline and Li-mica of the greisen and occur interstitially in both rocks. Most crystals show little evidence of dissolution associated with either of the hydrothermal processes and, along with zircon, monazite could have been inherited from the biotite granite. The crystallisation of at least some new monazite during greisenisation is suggested by the greater abundance of this accessory in certain of the greisenised samples (e.g. R1/13-5, RS6(2) in Table 44) compared with the microcline and biotite granite samples.

Some dissolution of monazite is evident in two, very embayed crystals included in quartz in the greisen. One of these is partially replaced by a LREE-phase with associated fractionation of La, which is

a phenomenon very similar to that found in some monazites from the biotite granite and albitised granite. Either these partially replaced monazites were inherited from the granite or similar alteration processes to those in the biotite granite operated on monazite during greisenisation. Vlasov (1966b) notes that monazite is a common accessory in hydrothermal-greisen deposits where it is often replaced by fluocerite or members of the bastnaesite group. In sample RS6(3), a monazite shows substantial corrosion and replacement by a chlorite-sericite intergrowth. Basham et al. (1982c) recorded the partial mobilisation of monazite by sericitisation, while Jefferies (1985a) noted the marginal dissolution of monazite included in partially chloritised biotite.

The occurrence of LREE-phases containing significant but variable quantities of Ca, Th, Y, Si and Pb in the Ririwai lode, but not in the biotite granite or albitite, suggests that crystallisation of these complex REE-phases occurred during microclinisation and greisenisation. Their late crystallisation, associated with hydrothermal alteration, is supported by their overgrowing other accessories, namely zircon, thorite and coffinite. The overgrowth of LREE-phases on Y-thorite and their inclusion in Li-mica, both of which are demonstrated to have crystallised during greisenisation, lends further support to the origin of these complex LREE-phases during greisenisation.

The complex LREE-phase overgrowths probably crystallised late from the greisenising fluids. In sample RS10(3) there is evidence that such phases may also have formed by the alteration of a pre-existing LREE-phase of simple composition. Fig. 72 illustrates the textural relationship between monazite, a LREE-phase of simple composition and a

LREE-phase containing significant concentrations of Pb and Th (Fig. 65). It is proposed that the monazite was initially replaced by the simple LREE-phase. Subsequently, there was precipitation of Th and Pb, which crystallised locally as galena and Zr-rich thorite and which also reacted with the LREE-phase, giving rise to the complex Pb-Th-LREE phase. The progressive nature of this alteration is demonstrated by a zone of intermediate composition between the simple and complex LREE-phases (Fig. 64).

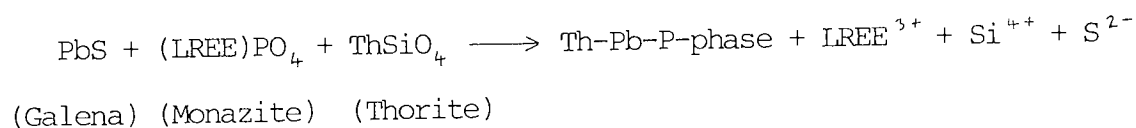
Mobilisation of Y during microclinisation and greisenisation is indicated by the presence of Y-rich thorite, coffinite and yttrifluorite. Further evidence for the mobilisation of Y is provided by the presence of rare xenotime as epitaxial overgrowths on zircon and thorite, in greisenised samples only. Plate 100 illustrates the irregular, poorly defined boundary between thorite and an overgrowth of xenotime, which either suggests that thorite and xenotime crystallisation occurred closely in time or that thorite was partially replaced by xenotime. In the former case, xenotime crystallisation could have been initiated by a sudden decrease in Th precipitation after the crystallisation of Y-rich thorite.

The poorly crystallised, interstitial nature of coffinite from the microcline resembles that of the biotite granite coffinite and similarly suggests its post-magmatic crystallisation under relatively low temperature, hydrothermal conditions. The presence of high Y and P in place of the high Zr and Si found in the biotite granite coffinite, is consistent with the different origins of the two coffinite occurrences and, instead, suggests a genetic link with Y-rich thorite in the Ririwai lode.

The inclusion in TiO_2 of a U-rich phase, whose ED spectrum closely

resembles that of coffinite (Fig. 51), is reminiscent of similar U-Ti associations in the literature (Chapter 2, Section 2.e.i.) and in the Ousdale arkose of Scotland (Chapter 7), in which coffinite appears to replace the TiO_2 . During microclinisation, at least some of the U precipitated during the crystallisation of columbite and Ta-rich pyrochlore, which are intergrown with a U-Th-Y-Si-phase in the microcline (Plate 94).

The intimate occurrence of the unidentified Th-Pb-P-phase with monazite and thorite and the presence of galena in the sample suggest that the Th-Pb-P-phase is a metastable product arising from the remobilisation of these accessory minerals during greisenisation. The following generalised reaction can be envisaged:



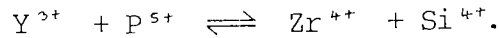
The mobilisation of Pb^{2+} , Th^{4+} and PO_4^{3-} during greisenisation has already been implied for a model suggesting the mode of formation of a Pb-Th-LREE phase in the same sample (Fig. 72), while the mobilisation of Th^{4+} together with Zr^{4+} has been suggested for the formation of Zr-rich thorite and Th-rich alteration patches in zircon (Section 2.b.).

3. Mineral chemistry

a) Zircon

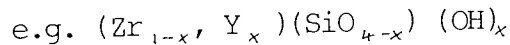
Where nearly pure (Zr, Hf) silicate, zircon gives totals near 100% and a recalculated (Zr + Hf + etc.) : (Si + P) ratio near one, which implies that the analytical technique is sound. The low reflectance patches, enriched in the Th, Y, U, Ca etc., give low totals and the above ratio is consistently greater than one. A positive correlation

between Y and P concentrations (Table 28) suggests that the following coupled substitution is operative:

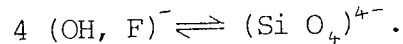


Where the (atomic % Y) : (atomic % P) ratio approximates one, these elements may be regarded as a xenotime component in solid solution with the zircon. Webb and Brown (1984a) drew similar conclusions from zircon containing up to 2.7 wt % Y_2O_3 , and 3.2 wt % P_2O_5 from the Eastern Highland granites, Scotland, while Silver et al. (1980) found the outer zone of a zircon to contain a 3.6 wt % xenotime component.

Where, more usually, Y : P exceeds one (or in Fig. 73, where wt% Y_2O_3 : P_2O_5 exceeds the ratio for xenotime), other charge balancing mechanisms could apply;



(Caruba et al., 1985; Medenbach, 1976; Robinson, 1978). Substitutions of small quantities of Ca, Fe, Al or S could also contribute to charge balancing (Romans et al., 1975). (Zr + Hf + etc.) : (Si + P) greater than one indicates additionally:



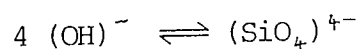
Even a combination of the above two substitutions would not generally indicate enough H_2O to account for the low oxide totals. This suggests that molecular H_2O and/or submicroscopic voids are present.

Using an SEM, with a BSE detector (Appendix 1, Section 5), the low-reflectance, trace element-enriched patches were studied in more detail. The dark appearance of the patches, relative to the remaining zircon (Plates 42-44) implies that they have a lower backscattered electron coefficient ($\bar{\eta}$) suggesting a lower average atomic number (\bar{Z}), despite their enrichment in heavy elements (Table 26). This

effect must be related to the low totals in the analyses of the secondary patches. The low totals are attributed to a combination of H₂O content (which cannot be analysed) and submicroscopic voids, both of which are commonly found in metamict zircon (Speer, 1982). Caruba et al. (1985) propose that hydrothermal zircons may incorporate OH (and F) during growth, predisposing them to metamictisation. However, in the present study there is little indication of OH or F in U-, Th-poor zircons (Section 2.c.), so probably the low totals are a result of metamictisation.

To examine whether H₂O alone (without void space) could account for the BSEI contrast, \bar{Z} and $\bar{\eta}$ were calculated by the method of Hall and Lloyd (1981) for a zircon with secondary, low-reflectance patches from 100 m depth (Plate 41). Table 50A shows the results for high-reflectance areas with normal totals for the probe analyses. For the low-reflectance areas in Table 50B, the weight % of oxygen is estimated as the difference between 100% and the total for the other elements. This assumes that all the difference between the tabulated sum of the oxides and 100% is water and neglects the fact that a small weight of this is hydrogen (which has negligible effect on \bar{Z} and $\bar{\eta}$ because H is extremely light).

According to Caruba et al. (1985), Frondel and Collette (1957) and Chyi (1986) water may be incorporated into zircon by means of the following substitution:-



Calculations (described in Appendix 4) indicate that the maximum % of H₂O which may be incorporated into the zircon by the above substitution ranges from approximately 2 to 3 for the three analyses (Table 50B). Since the total assumed H₂O per analysis ranges from 7 to 13%, it

appears that most, if not all, of the H_2O must be present in molecular form, rather than as the above substitution. This is consistent with the findings of Mumpton and Roy (1961), who demonstrated that hydrous-metamict zircons most probably contain strongly adsorbed H_2O , rather than hydroxyl in substitution for silica (Chapter 2, Section 2.b.i.).

The calculated values of \bar{Z} and $\bar{\eta}$ do not vary consistently between zircon and its secondary patches (Tables 50A and B), implying that the observed difference in contrast is not explained by the presence of water. If the low totals are partly due to other unanalysed oxides e.g. of REE, then the problem is exacerbated (because these are heavier than water). Thus, the observed contrast must be partly due to submicroscopic voids which have resulted from the expansion of the zircon lattice during metamictisation, as a result of radiation damage induced by the high concentrations of U and Th present.

Table 50C shows the results of calculating effective \bar{Z} and $\bar{\eta}$ for secondary patches from probe analyses, assuming that the low totals are due entirely to void space (to which zero Z and η are assigned). Oxygen is thus calculated by stoichiometry from the other elements, on the assumption of no unmeasured oxides such as H_2O . For consistency, this approach was used during the ZAF corrections, resulting in slightly lower corrected concentrations for elements other than oxygen, relative to Table 50B (Appendix 1, Section 4.h.ii.).

Although \bar{Z} does not differ significantly between light and dark patches, $\bar{\eta}$ is consistently, although only marginally, lower in the dark patches. This discrepancy between \bar{Z} and $\bar{\eta}$ is due to the non-linear relation between them (Hall and Lloyd, 1981) and emphasises the importance of calculating $\bar{\eta}$ and not just \bar{Z} .

The comparison chart (Table 50D) shows that predicted % contrast from Table 50C (measured as a % of the total BSE signal) tends, on the whole, to be greater between light and dark zones than within them, although two anomalous values are marked, in which % contrast within the dark zones is greater. These anomalies may be due to the presence of unmeasured heavy elements.

The assumptions inherent in Table 50C are more consistent with the observed BSE contrast than those inherent in Table 50B, thus indicating the presence of void space in the darker, secondary patches, while not ruling out the presence of some H₂O. The void space is probably related to radiation damage, arising from the high concentrations of U and Th present.

High resolution, TEM studies (including those of Yada et al., 1981; Headley et al., 1981; Bursill and McLaren, 1966 ; Sommerauer, 1977) have revealed the detailed nature and cause of metamictisation in zircon. Structural breakdown of the lattice is accomplished mainly by the formation of fission tracks in the paths of α particles emitted from the decay of U and Th. A less significant contribution to the breakdown arises from the displacement of lattice atoms by recoil nuclei. The degree of metamictisation is proportional to the density of fission tracks. Intermediate zircon comprises amorphous domains and 50-100 Å sized, slightly misoriented, regular lattice domains. Eventually, in metamict zircon, these domains are reduced to a glass-like state which is amorphous to within about 10 Å.

Headley et al. (1981) proposed that the microcrystalline domains, which contain trace amounts of Ca, grew within the amorphous matrix as a result of recrystallisation, associated with hydrothermal alteration. Sahama (1981) noted the partial re-ordering of metamict zircon, in the

form of small patches of birefringent zircon, and attributed this to fluctuations in temperature during or after late crystal growth. Sahama (op. cit.) also noted the presence of coarse banding caused by variations in radioactive damage, related to changes in U concentration. This banding may be similar in origin to the alternating, slightly anisotropic and isotropic banding in Type 3 zircon from Ririwai (Plate 68), although associated changes in U concentration have yet to be confirmed.

Type 3 zircon is most probably metamict or nearly metamict as a result of its higher concentration of U (1-6 wt % UO_2) relative to Types 1 and 2 zircon. Hoffman and Long (1984) found the metamictisation in zircon to be most severe when the U content exceeded 1%. Despite the high content of thorite inclusions in Type 2 zircon in some grains, its anisotropy, high analytical oxide totals and higher $\bar{\eta}$ relative to Type 3 zircon, imply that Type 2 zircon is non metamict, although partial metamictisation is sometimes indicated by a diffuse biaxial interference figure. This suggests that the process of metamictisation is most effective when the decaying atoms of U and Th are dispersed throughout the zircon lattice, rather than concentrated as inclusions, although even the zircon directly in contact with thorite inclusions does not appear damaged.

Koppel and Sommerauer (1974) believed the susceptibility of zircon to metamictisation to be a function of the rate of cooling of the rock. With a prolonged cooling history, the U, Y, P, Ca and other trace elements in zircon had time to arrange themselves into separate phosphate phases. With more rapid cooling, trace elements remained in solid solution, causing distortion of the zircon lattice, which was rendered more susceptible to radiation damage and metamictisation.

i) Possible Exsolution in Zircon

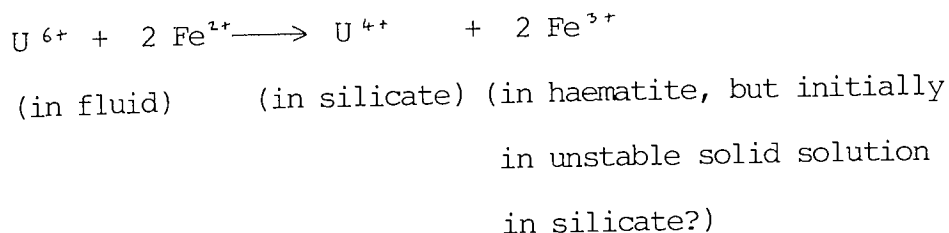
Type 2 zircon from the albitised rocks and zircons from samples N75 and L13-365 of the biotite granite are characterised by a close association between haematite inclusions and abundant, small thorite inclusions. This effect is particularly apparent in one example (Plate 70), where it is confined to a sharply defined, geometrically shaped zone of Type 2 zircon. The sharp crystallographic boundary makes a hypothesis of replacement of zircon by thorite very implausible. Alternatively, the thorite co-precipitated with the zircon, but this hypothesis does not account for the small grain-size of thorite, which is able to attain a much greater size elsewhere in the rock. Also, co-precipitation of thorite and zircon might be expected to give more solid solution in each mineral, but Table 41 (Grain 2, Analysis 2) shows the zircon to be nearly pure $(Zr,Hf)SiO_4$, while Table 42 (Grain 2, Analysis 9) shows the thorite to be nearly pure $(Th,U)SiO_4$, since the analysis total is very close to 100%.

Both conditions of small grain size and pure composition can be accommodated by a third hypothesis involving the exsolution of thorite from an originally unstable Th-, U-rich composition of zircon, with cooling. Assuming that all the thorite inclusions were exsolved, the hypothetical original composition of a small area (Plate 72) of the Type 2 zircon zone in Plate 70 was reconstructed from the analyses and volume proportions of thorite and zircon, using the method outlined in Appendix 5. The results indicate that the original zircon would have contained approximately 4.0 mole% (U + Th), which is probably above the stable limit in zircon at low temperatures (see Section d. below).

However, this raises the question of why zircons containing much higher contents of (U + Th) in the Ririwai samples did not exsolve. In

the same grain, unexsolved Type 3 zircon (Analysis 7) contains less (U + Th) than the reconstituted Type 2 composition, but Type 3 zircon in another grain from the same rock (Grain 1, Analysis 9 in Table 41) contains higher (U + Th). There is also higher (U + Th) in some altered, low-reflectance patches in the biotite granites and greisenised rocks. One possibility is that exsolution was catalysed by the haematite particles, around which the thorite nucleated. Exsolution in Type 3 zircon and the low reflectance patches may have been inhibited through their lack of haematite inclusions. The haematite particles themselves either exsolved from a non-stoichiometric zircon or co-precipitated with the zircon. The former seems more likely on grain-size grounds, since there are independent large haematite grains in the albitised rocks (Iyer *et al.*, in press).

Co-precipitation is likely for thorite inclusions where these are less abundant in zircon. These thorite-poor zircons would have contained a much lower original solid solution component of thorite, which may well have been insufficient for subsequent exsolution of the inclusions. In this case, the $USiO_4$ component of thorite might have co-precipitated with the haematite by means of the following redox reaction:



The above reaction could equally account for the presence of enhanced U in the haematite-rich cores of some thorites.

Rimsaite (1986) described zircon with inclusions of thorite, while the exsolution of thorite from monazite has been described in the

Lawler Peak granite, south-western USA by Silver et al. (1984). The monazite originally crystallised with widely varying contents of Th (up to 13 wt % ThO_2), Ca and Si. With cooling, the monazite grains with the highest contents of non-LREE substituents recrystallised and exsolved apatite and thorite or cheralite, depending on how much Si was substituting for P. Exsolution gave rise to complex intergrowths of apatite, thorite or cheralite, together with clear, unrecrystallised monazite, which represents the original Ca-, Th- and Si-rich monazite that was at least metastable during recrystallisation.

At Ririwai, it is possible that Type 3 zircon represents unexsolved Type 2 zircon and is thus analagous to the clear monazite of the Lawler Peak granite, where these two zircon types are intergrown (e.g. Plates 85 and 86). However, this seems unlikely, in view of the low Th/U ratio of Type 3 zircon.

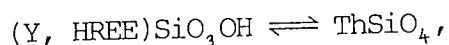
b) Thorite

Analytical oxide totals for thorite are generally low, while the (Th + etc.) : (Si + P) ratio invariably exceeds one. The latter effect is particularly apparent where Fe is high, suggesting that most of the Fe is present as inclusions of iron-oxide. Unanalysed HREE might account for a few wt % of the low totals in Y-rich thorite but this would exacerbate the (Th + etc.) : (Si + P) problem. The deficient Si and P suggest that some substitution of OH for SiO_4 may have occurred, in which case the phase is more properly termed thorogummite $(\text{Th}(\text{SiO}_4)_{1-x}(\text{OH})_{4x})$, following Frondel (1953).

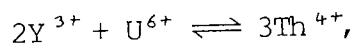
Fig. 23 shows that mean oxide totals of thorite analyses in the Ririwai lode are significantly lower than those of thorite analyses in the biotite granite and albitite. This may be due to a greater degree

of metamictisation of the greisen thorites, resulting in a larger void space and hence lower totals and/or to a larger proportion of water in the Ririwai lode thorites. Increased water present in the Ririwai lode thorites is consistent with their hydrothermal origin during greisenisation at temperatures of 360-380°C (according to fluid inclusion data of Kinnaird et al., 1985b). Thorites formed during albitisation (460°C; Kinnaird et al., op. cit.) and crystallisation of the biotite granite may contain less water, due to the less hydrous, higher temperature conditions of their formation. However, there is controversy about the nature of water in thorite, which may be present as (OH) substituting for (SiO₄) and/or adsorbed OH/H₂O (Chapter 2, Section 2.a.iv). The hypothetical wt % H₂O present as (OH) substituting for (SiO₄) was calculated for thorite using the method outlined in Appendix 4. Fig. 75 shows the marked variation in hypothetical wt% H₂O among different thorite analyses but there is no clear difference between thorite populations from the borehole and Ririwai lode samples. Thus, if the lower oxide totals of the Ririwai lode thorites are due to increased water present, this water is likely to be adsorbed rather than substituting as (OH) for (SiO₄).

Additional OH could arise from the substitution;

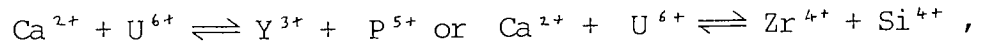


which is required to account for the greater amounts of Y relative to P in most thorites (Fig. 76), although there appears to be straightforward xenotime substitution in thorite from sample N94 (Fig. 77). Other charge balancing substitutions could involve U⁶⁺;



or small quantities of Ca, Fe, Al or S (Speer, 1982). The correlation coefficients of heterogeneously distributed elements within single

thorite grains (Tables 51-54) show a positive correlation among U, Th and Ca and among Y, P and Zr but a negative correlation between these two element groups. This implies a role of Ca^{2+} in charge balancing, possibly as;

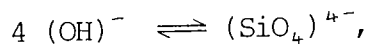


although the contribution must be relatively insignificant, bearing in mind the low concentrations of Ca present.

Thus, due to the presence of unmeasured REE and the uncertainty about the presence of adsorbed molecular H_2O , hydroxyl substitution for SiO_4 and submicroscopic voids (Chapter 2, Section 2.a.iv.), any recalculation for thorite is much less certain than for zircon.

c) Coffinite

Low totals in the coffinite analyses, together with depleted Si plus P in the formulae relative to ideal USiO_4 , suggest that water may be present in the form of hydroxyl, partly substituting for silica;



as suggested by Stieff et al. (1956), who gave the formula of coffinite as $\text{U}(\text{SiO}_4)_{1-x}(\text{OH})_{4x}$.

The hypothetical (OH) content of the biotite granite coffinite was estimated from the analyses in Table 37, using the above formula for coffinite, which implies that the sum of U plus the cations substituting for it should equal one. The recalculation used is illustrated for a worked example in Appendix 4. The results (Table 55) indicate that the estimated wt% H_2O hypothetically present as (OH) is far short of accounting for the poor totals of the analyses.

In Section 3.a. it was concluded that the low analytical totals of altered, U- and Th-rich zircon were largely due to void space, related

to metamictisation and expansion of the zircon lattice. A similar explanation may apply for the low analytical totals of the coffinite, although the voids may additionally contain strongly adsorbed H_2O . This is consistent with published studies of synthetic and natural coffinite which suggest that essential OH is not present in hydrothermal coffinite (Chapter 2, Section 2.a.iii.).

As in zircon and thorite, further OH is probably present as a result of Y substitution in the microcline coffinite, while unmeasured HREE could contribute significantly to the low totals, since up to 6 wt % $HREE_2O_3$ were measured in an Y-rich, unidentified U-silicate, co-existing with thorite (Table 46). Low totals also probably arise through voids associated with the poorly crystalline, fine-grained nature of the coffinite.

d) Solid-solution ranges in the Th-U-Zr-Y system

It is interesting to compare ranges of mineral compositions in the thorite-coffinite-zircon-xenotime group (Figs. 79-81) with experimental data and published analyses from other areas (reviewed in more detail in Chapter 2). In comparisons with experimental data, allowance must be made for the complex compositions of natural minerals compared to their synthetic equivalents. For example, it has been inferred that Y forms a $YSiO_3OH$ component as well as YPO_4 and that thorite and coffinite may contain significant amounts of hydroxyl in substitution for silica. Although the products in dry experimental systems are generally more simple, hydrothermal experiments have succeeded in producing (OH)-bearing forms (e.g. Frondel and Collette, 1957).

In the biotite granite and its metasomatically altered facies, the Th (and U) concentrations in the melt or fluids were evidently

sufficient to precipitate thorite with the zircon but the U and Th concentration of the zircons themselves tend to lie below or around 1 wt %. Zircons co-existing with U- and Th-silicates and oxides are assumed to have incorporated maximum amounts of U and Th (Speer, 1982) and nucleation (exsolution?) of excess Th, U, Si etc. gave rise to the thorite inclusions. That the zircon still contains relatively low concentrations of U and Th testifies to the wide miscibility gaps on the $ZrSiO_4$ - $USiO_4$, $ZrSiO_4$ - $ThSiO_4$ joins, at least under these particular conditions of crystallisation. Speer (op. cit.) quotes maximum values in zircon of 0.5 wt % U when co-existing with uraninite, 300 ppm and 10 wt % Th with thorite and thorianite and 0.07 wt % U and Th with uraninite and thorite. Silver et al. (1984) identified coffinite inclusions in a zircon core which contained lower U compared with the zircon edge. Assuming the coffinite co-existed at equilibrium with the host zircon, the saturation level for U in zircon must have been lower during crystallisation of the core than crystallisation of the edge.

In unaltered zircon, U concentrations invariably exceed those of Th, (Fig. 81) which may have been preferentially partitioned into the co-existing thorite. The preferential incorporation of U into the zircon structure may also reflect the closer ionic radius of Zr^{4+} to U^{4+} compared with Th^{4+} , in eight-fold co-ordination (Ahrens, 1965).

In the low reflectance, altered patches of zircon, ThO_2 and UO_2 attain maximum concentrations of approximately 8 wt % and 4 wt % respectively (Table 30). The equivalent mole % $ThSiO_4$ (Fig. 79) exceeds or is close to 4 ± 2 mole % which is the maximum limit of solubility of $ThSiO_4$ in $ZrSiO_4$ at $1000^\circ C$, as determined empirically by Mumpton and Roy (1961). The solubility of Th in zircon synthesised hydrothermally at $400-700^\circ C$ is very low (Fron del and Collette, 1957).

Since the low reflectance patches are thought to have formed at temperatures considerably below 1000°C, the limit of solubility of ThSiO₄ should be even lower. The patches probably represent metastable solid solutions which are able to contain as much as 35 mole % ThSiO₄ (Mumpton and Roy, 1961).

Mihalik (1968) describes similar features to the low-reflectance, trace element-enriched patches in zircons from the Dominion Reef and Witwatersrand Systems. Generally irregular-shaped but sometimes zonally-arranged, darker areas are dusted with radiogenic galena and contain U with associated Th, P, Y, Ca, Mn, Fe and Al, in addition to the Zr, Si and Hf. Although uncertain about their origin, Mihalik (op. cit.) prefers to attribute these dark areas to the formation of a new mineral phase, rather than to substitution of trace elements in the zircon lattice.

The secondary replacement of lattice Zr by U and other trace elements without new zircon growth is well documented and has been termed "passive zoning" by Speer (1982). The secondary enrichment of U in zircon, related to its alteration has been noted by Baranov and Lieh-T'ien (1961). Grauert and Seitz (1973) and Krogh and Davis (1973) attributed discordant U-Pb ages to U gain without new zircon growth which Grauert et al. (1974) interpreted as penetration of U along tiny cracks in the frosted surfaces of detrital zircons, with subsequent fixation of the U due to zircon recrystallisation. Experimental studies by Pidgeon et al. (1973) showed that metamict zircons in 2 M NaCl solutions at 1000 bar fluid pressure and 350-800°C incorporate and hold quantities of U of the order of 2000 ppm. Krasnobayev (1979) concluded, from the identification of U concentrated along cracks, in microinclusions and intergranular spaces, that zircon

had adsorbed U from a kimberlite melt. Rimsaite (1981a and 1986) described how, under hydrous-oxidising conditions, zircon lost some Zr and reacted with mobilized U, Th and Fe, giving U-rich domains (containing up to 30% UO_2) along peripheries which retained the crystal outline. Tieh and Ledger (1981) attributed U gain in the outer zones of zircon to the mobilisation of U, as a result of metamictisation. Clark et al. (1979) suggested that U gain in the outer zone of a zircon was by absorption and diffusion from an external source, perhaps associated with the recrystallisation of a pre-existing zircon.

The strong positive correlation between ZrO_2 and SiO_2 and positive correlations between ZrO_2 and HfO_2 and between HfO_2 and SiO_2 in thorite (Table 52, Fig. 78) suggest that Zr^{4+} is present as a zircon component, although Si^{4+} is depleted. Maximum concentrations of Zr (27 wt % ZrO_2 or 50 mole % $ZrSiO_4$) greatly exceed the empirical solid solution limit of $ZrSiO_4$ in thorite at 1000°C (6 ± 2 moles % $ZrSiO_4$) determined by Mumpton and Roy (1961), which implies that these thorites represent metastable phases along the $ZrSiO_4$ - $ThSiO_4$ binary join. The maximum wt % ZrO_2 found in the literature is about 9 (Chapter 2, Section 2.a.iv.). Mumpton and Roy (1961) obtained metastable solid solutions of thorite containing up to 25 mole % $ZrSiO_4$ but found that these exsolved to the stable end members at higher temperatures. This implies that the Zr-rich thorites in the biotite granite were not subjected to high temperatures, since there is no evidence of zircon exsolution in them and they may have formed at relatively low temperatures. This is consistent with their proposed formation at low temperatures by the subsolidus alteration of magmatic thorite by Zr-rich fluids (see Section 2.b.).

Y and P concentrations tend to lie below 1 wt % oxide in unaltered

zircon at Ririwai, although values up to 4.8 wt % Y_2O_3 and 3.4 wt % P_2O_5 were obtained in altered zircons from the greisen. Much higher values of Y and P are described by Silver et al. (1984), who applied the name "Zirxe" to a mineral half-way in composition between zircon and xenotime, and Barritt (1983), who presented mineral analyses demonstrating complete solid solution between xenotime and zircon (Fig. 15A). The above examples probably represent metastable phases, since there is usually a wide miscibility gap in the $ZrSiO_4$ - YPO_4 join (Speer, 1982). This gap is also shown by the very low Zr contents (below detection) of xenotime inclusions in zircon from the albitite (sample 450). Either the xenotime co-crystallised with the Type 2 zircon or exsolved from it. The host zircon contains a higher than average Y content of 1.02 wt % Y_2O_3 , while the Y content of the thorite inclusions is estimated at 5-6 wt % Y_2O_3 (Table 56). Assuming that all three phases were co-existing at equilibrium, these values of Y should represent the solid solution limits in thorite and zircon under the prevailing conditions of crystallisation, although many more analyses are required to confirm this. A limit of 5-6 wt % Y_2O_3 in thorite is consistent with Y levels measured in thorites from other xenotime-bearing albitised samples, which never exceed 6 wt % Y_2O_3 and are normally much lower.

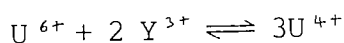
Y levels in thorite range from 0 up to 11.4 wt % Y_2O_3 in published analyses (Table 6, Chapter 2), which contain comparable levels to the Ririwai thorites, although it is uncertain whether or not these compositions are metastable. Maximum U values in the biotite granite thorites tend to lie around or below 15 wt % UO_2 , but inclusions in a zircon from 350 m contain up to 20 wt % UO_2 (equivalent to 22 moles % $USiO_4$; Fig. 81) which corresponds to the upper stability limit of

approximately 20 moles % $USiO_4$ in $ThSiO_4$ at $1000^\circ C$, suggested by the experimental data of Mumpton and Roy (1961). Up to 28 wt % UO_2 was measured in thorite from the albitised samples, while thorite with a similar concentration of U was synthesised by Mumpton and Roy (op. cit.) who regarded the composition as metastable due to its exsolution to the stable solid solution limits, upon heating. They quoted values of up to 35 moles % $USiO_4$ from the literature, although many values lay below 5 moles %. In some cases e.g. Staatz et al. (1976), high concentrations of U in thorite may be due to the presence of small uraninite inclusions, although these were never indicated in any of the U-rich thorites from Ririwai.

The highest U contents of all thorites in the Ririwai samples were obtained in the microcline for a thorite which appears to demonstrate complete solid solution between the $ThSiO_4$ and $USiO_4$ end members (sample R1/23-1B in Fig. 81), despite the solid solution limits suggested by some experimental work and analyses in the literature. The domain of enriched U comprises an irregular patch near the periphery on one side of the grain only, arguing against simple growth zoning related to changing U concentrations in the fluids. The $USiO_4$ -rich domain may have either resulted from the alteration of a pre-existing thorite grain by U-rich fluids or exsolution. Zimmer (1983) found that thorite could incorporate up to 40 mole % $USiO_4$, while Fuchs and Gebert (1958) were able to synthesise uranorthorites which demonstrated a continuous solid solution between $USiO_4$ and $ThSiO_4$. Analyses demonstrating complete solid solution between U-depleted thorite and Th-poor uranyl silicates (Marlow, 1981) are presented in Chapter 2 (Tables 5 and 6).

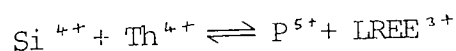
Very little experimental work concerning the solid solution of Zr

and other elements in coffinite are present in the literature and, although Fuchs and Hoekstra (1959) synthesised coffinite, Frondel and Collette (1957) and Mumpton and Roy (1961) were unable to synthesise $USiO_4$. At 1350°C in the system $ZrO_2-UO_2-SiO_2$, mixtures on the " $USiO_4$ "-zircon join gave (zircon + $SiO_2 + UO_2$), according to Mumpton and Roy (1961), who concluded that " $USiO_4$ " was a metastable compound. In a brief review of the literature, Speer (1982) listed minor amounts of Ca and P, together with traces of Ti, Y, Fe, P, Th, Ce, Zn, U and Cr as substituents in coffinite but did not mention Zr. Zr is not reported in the majority of coffinite analyses presented in Chapter 2 (Table 5), although Y reaches concentrations comparable to those of the Ririwai coffinite in the analyses of Premoli (1982). In the Ririwai lode, the higher Y levels present in coffinite and unidentified U-silicates compared with thorite, might reflect the greater amount of U^{6+} available for the coupled substitution;



e) Monazite and other LREE-phases

Th contents range from 2.7 up to 12.16 wt % ThO_2 and average approximately 7 wt % ThO_2 , which is comparable with most of the 21 analyses of monazite in granite presented by Jefferies (1985a) and with other published analyses (Table 14). A positive correlation between Th and Si (Fig. 74) suggests that the coupled substitution;



is operative (Chapter 2, Section 2.b.ii.). Despite its significant content of Th, monazite is probably not a major contributor to the bulk Th content of the granite, since it is relatively uncommon, compared to thorite. The LREE-phase contains approximately one quarter to one

tenth of the Th content of monazite, whose replacement must therefore release Th into the alteration fluids. In sample 350, a lower than average Th content of monazite is accompanied by a similarly low Th content in the LREE-phase, included in fluorite in biotite.

Th concentrations in the LREE-phase of simple composition (1.4-2.4 wt% ThO₂) are comparable with concentrations found in minerals of the bastnaesite-fluocerite series by Perez (1985). The variable compositions of the complex LREE phase grains demonstrate the substantial solid solution possible in REE-fluorides and fluorocarbonates, which can incorporate high concentrations of Th (up to 23 wt % ThO₂, Table 36) as well as significant Y, P, Ca, Si and Pb. High concentrations of Th (46.79 wt % ThO₂) have been recorded in thorbastnaesite which replaces thorite in albitites from alkali metasomatic rocks in E. Siberia (Pavlenko *et al.*, 1965). Thorbastnaesite in an altered phonolite from Brazil contains very variable Th concentrations of 1 to 40% Th (Barretto and Fujimori, 1986). Variations in the compositions of REE-phases, including F and Ca, were attributed to solid solution between the bastnaesite group and fluocerite by Perez (1985). Possibly, the compositional variations in the greisen and microcline phases represent solid solution between bastnaesite or fluocerite and xenotime and thorite/huttonite components.

4. Suggestions about melt and fluid chemistry

Zircons from the biotite granite which have been analysed in detail do not show obvious, concentric zoning of Th, U, Y or P, suggesting that concentrations of these elements in the melt did not change significantly during the growth of at least some grains. Alternatively, if any changes did occur, these were slow enough to allow equilibration of the zircons with the new melt chemistry. The

presence of a thorite inclusion, together with enhanced concentrations of U, Th, Hf, Y, P and Fe, in one zircon overgrowth indicate local increases in the precipitation of these elements during interrupted zircon growth, possibly reflecting their accumulation in the melt.

The enrichment of Hf in the outer zones of some zircons suggests that concentrations of this element increased during the later stages of zircon growth. Hf concentration in zircon tends to increase with increasing differentiation of a granite (Deer et al., 1982; Vlasov, 1966a) and a number of examples exist of zircons with Hf-enriched rims (e.g. Ono, 1975; Silver et al., 1980). However, the higher bonding energy of Hf compared with Zr should mean it is selectively stabilized in early crystallised minerals, giving rise to increasing Zr/Hf ratios with magmatic differentiation (Chyi, 1986). The occurrence of both Hf-enriched and Hf-poor zircons in sample N94 suggests that there was a severe chemical disequilibrium in the melt. Fontan et al. (1980) drew similar conclusions from zircons showing large ranges in HfO_2 over a small scale in samples of pegmatite from the Pyrenees.

The relatively large size of zircon in the albitised samples, compared with the biotite granite, may be at least partly due to more prolonged crystallisation of grains in a water-rich magma, as has been noted by Pupin (1980). The solubility of Zr increases with the alkalinity (Na + K/Al) of a melt (Bowden, 1966). Thus, the early crystallisation of zircon will be inhibited by the evolution of a melt into a more alkaline composition. This increase in the solubility of Zr in a peralkaline melt is usually due to the formation of stable Zr complexes containing F, Cl and Na (Chyi, 1986).

Above 300°C an OH-complex may be the only soluble U species (Romberger, 1984) although UF_6 may also exist at magmatic temperatures

(Kimberley, 1978), while Bohse et al. (1974) described the accumulation of U in a residual, peralkaline melt, due to complexing with Cl. Changes in pH, Eh, temperature etc. may have lead to the breakdown of these soluble Zr- and uranyl-complexes with their precipitation in U-enriched, Type 3 zircon.

However, the biotite granite at Ririwai is mildly peraluminous and the presence of albitised granite at 385 m and below has been attributed to metasomatism, rather than to an increasingly alkaline magma (Chapter 3, Section 4.a.). Furthermore, the similar bulk Zr content and the lower abundance of zircon compared with the biotite granite suggest that the growth of large zircons in the albitised granite and albitite was not accompanied by enrichment of Zr in the melt.

Alternatively, zircon growth may have at least partly accompanied albitisation. Vlasov (1966a) described the extensive precipitation and mobilisation of Zr during albitisation of granite pegmatites. Pupin (1980) reported the occurrence of large populations of late zircon with unique morphology in albitised, alkaline series granites.

The increasing mean U content of thorite with albitisation (Fig. 24), suggests that the fluids responsible for albitisation contained a higher U : Th ratio than did the melt responsible for primary crystallisation of thorite in the biotite granite. This implies that either U was introduced with the albitising fluids, or that Th was selectively lost. The greater mobility of U^{6+} , compared with Th^{4+} , suggests that the former case is more likely. Alternatively, the U : Th ratio was similar to that in the melt, but physicochemical conditions were more favourable for U precipitation during albitisation.

Similarly, the crystallisation of Type 3 zircon could have

accompanied an early, high temperature phase of albitisation, during which loss of CO₂ seems to have been important for the deposition of U in the lattices of minerals such as thorite, zircon and pyrochlore (Kinnaird et al., 1985b). This implies that U was dominantly present in the fluids as soluble uranyl-carbonate complexes and would account for the presence of late calcite in the albitite. However, geochemical data indicating bulk enrichment of U and Th in the albitised rocks relative to the least altered biotite granite are inconclusive (Table 57 and Section 5). According to Kinnaird et al. (1985b), the geochemical data indicate that the early exsolved fluid responsible for albitisation must have contained important concentrations of Fe, U, Th, Zr, Nb and HREE. At least some of the Fe may have been released during the chloritisation and subsequent dissolution of biotite and the replacement of haematite-dusted K-feldspar by plagioclase, which accompanied albitisation. Similarly, the Th and U may have been released from any primary thorite which was included in the biotite. The Fe precipitated as coarse haematite laths included in chlorite and overgrowing zircon, together with sulphides. If zircon crystallised during albitisation, then the mobile Fe, Th and U would also be available for the precipitation of the abundant haematite and thorite inclusions, which are found in Type 2 zircon. As described in Section 3.a., an association of haematite inclusions with the relatively high bulk U content of zircon-plus-thorite in Type 2 zircon could reflect a redox mechanism during co-precipitation. The peripheral replacement and overgrowth of Type 2 zircon by thorite suggest that thorite crystallisation continued during a temporary halt in zircon growth.

Outer zones of Type 1 zircon in the albitite often contain concentrations of Hf which are high compared to concentrations normally

encountered in zircon (Chapter 2, Section 2.b.i.). High Hf zircons, especially when metamict, are associated with albitites (Vlasov, 1966b) but are mostly found in pegmatites containing Ta and Nb minerals (Speer, 1982). If the Type 1 zircon crystallised during albitisation, this suggests that the fluids responsible for the alteration were enriched in Hf as well as Th, U, Zr and Fe.

The ore mineralogy of the albitite is dominated by disseminated haematite and columbite which is Ta-poor and not inherited from the biotite granite (Ixer et al., in press) implying that the fluids responsible for albitisation were also enriched in Nb and contained minor Ta. An association of high Hf (up to 26 wt % HfO_2) zircons with Nb and Ta mineralisation in pegmatites from the Pyrenees has been described by Fontan et al. (1980), while Von Knorring and Hornung (1961) described an association of high Hf (up to 31 wt % HfO_2) zircons with Ta-rich mineralization in Li-bearing pegmatites from S. W. Africa. Von Knorring and Hornung (op. cit) attributed the association of Ta with Hf to a geochemical similarity between these elements and they suggested that Nb and Zr mineralization should be associated for similar reasons. This is consistent with the presence of Zr and Nb mineralisation at Ririwai, while the occurrence of Ta-rich pyrochlore may be genetically related to the presence of high Hf in Type 1 zircon.

Concentrations of Hf are also enriched in zones of Type 2 zircon in certain grains, suggesting that the accumulation of Hf in the fluids began during the crystallisation of Type 2 zircon, when haematite and thorite were still precipitating, and increased during subsequent Type 1 zircon crystallisation. Analyses have confirmed that the brighter bands in the outer zone of Type 1 zircon in one grain at 411 m (Plate 66) are due mainly to increased concentrations of Hf (Table 41). These

rhythmic changes in Hf concentration either reflect fluctuations in the conditions controlling Hf precipitation, the introduction of Hf-rich fluids in pulses or the mixing of fluids containing different Hf concentrations. The distinct, sharp boundaries between bands of different Hf concentration suggest that these geochemical changes were abrupt during the continuous growth of zircon. Alternatively, zircon growth was periodically halted during more gradual geochemical changes, but this seems less likely, since the latest growth zones would have more time to equilibriate with the new fluid chemistry.

Vlasov (1966a) described the increase and separation of Zr and Hf during metasomatism but attributed the low ZrO_2/HfO_2 ratios found in corroded zircon relicts from weakly albitised rocks to the preferential removal of Zr, rather than to the relative accumulation of Hf. The decay of U and Th in zircon selectively weakens the Zr-O bond, rendering Zr more vulnerable to leaching (Chyi, 1986). Conversely, the much larger thermal neutron capture cross-section of Hf relative to Zr means that substitution of Hf, as well as other elements for Zr, will raise the capture cross-section of zircon and increase its susceptibility to damage (Speer, 1982). Zr is preferentially removed during alteration since, compared with Hf, it forms more stable complexes with F (Vlasov, 1966a). In more strongly albitised rocks, the Zr/Hf ratio reaches a maximum, while HfO_2 is at a minimum, due to an increase in the activity of Hf with an increase in the alkalinity of the post-magmatic solution (Vlasov, *op. cit.*). The regular zoning of high Hf zircon in the albitised granite at Ririwai, together with the low radioelement content of Type 1 zircon, suggest that concentrations of Hf were controlled by growth processes, rather than by the selective removal of Zr from zircon, related to radiation damage of the structure.

At 125 m in the borehole, where the granite has been partially greisenised, zircons have been substantially replaced by Li-mica. The selective removal of zircon cores may reflect original inhomogeneities in zircon composition. Zircons in which the cores are still present sometimes show a slight enrichment of Hf in their outer rims, suggesting that zircon containing lower concentrations of Hf has been selectively leached during greisenisation, in a manner similar to that described by Vlasov (1966a) and Chyi (1986; see above). Another possibility is that zircon cores contained higher concentrations of radioelements, leading to greater metamictization and vulnerability to leaching by hydrothermal solutions, although U- and/or Th-rich relict zircon cores were not found.

The identification of coffinite in the microcline but not in the greisen and the association of all but one of the unidentified U-rich phases with the microcline is consistent with the findings of Mackenzie et al. (1984) who concluded that U was enriched during microclinisation in the Ririwai lode.

The coffinite and two of the U-rich phases are intimately associated with pyrite, suggesting that mobile uranyl in the mineralising solutions was reduced to the less soluble U^{4+} valency, during its precipitation. The Y-rich composition of coffinite, thorite and the presence of LREE-phases and xenotime in the Ririwai lode imply that the fluids were also rich in Th, Y and REE during hydrothermal alteration.

The mobilisation of U and Zr at low temperatures in the biotite granite is indicated by the presence of interstitial, Zr-rich coffinite, which is deposited hydrothermally at temperatures of 200-360°C (Abdel-Gawad and Kerr, 1961) or below 300°C (Speer et al., 1981) in alkaline,

reducing environments. The presence of admixed sulphides confirms that deposition of the coffinite in biotite granite also took place in a reducing environment. The fluids responsible for the biotite granite coffinite may have been derived from those responsible for the subsolidus alteration of thorite to Zr-rich compositions (see Section 2.b.). During the magmatic crystallisation of this thorite, there may have been an increase in the U/Th ratio of the melt, which accumulated the more soluble U^{6+} ion. Hydrothermal fluids immediately derived from the residual melt would thus be enriched in U and these may have migrated up to cooler areas of the pluton where they deposited the coffinite. In this case, further coffinite mineralization would be expected to occur above 100 m in the borehole, or much of it may have been lost due to unroofing of the pluton.

The prominence of yttrifluorite in all rock-types suggests that F was available for complexing with elements such as U, Th, Zr, Y and REE, aiding their transport during crystallisation of the granite and its subsequent alteration. The replacement of zircon by fluorite in the albitised rocks may reflect the removal of Zr as highly stable and soluble Zr-F complexes. Henderson (1984) attributed the destabilisation of zircon by hydrothermal fluids containing F^- to the formation of ZrF_6^{-2} . Zircon may show appreciable corrosion as the result of metasomatism (Deer et al., 1966), particularly albitisation (Vlasov, 1966a) and grains frequently show replacement by plagioclase in the albitised samples. Fowler (1981) attributed embayments in zircon to corrosion, with release of U, during subsolidus fluid migration in a syenite.

LREE-phases are often included in yttrifluorite from all rock-types, implying the role of F in the transport of REE and Y during crystallisation and alteration of the granite. The presence of F^-

significantly increases the mobility of REE (Alderton et al., 1980) due to the formation of REE (Cl, F)₂⁺ for most REE and REE (Cl, F)₃ for La (Sillén and Martell, 1964).

Vlasov (1966a) believes albitisation to be the most important post-magmatic process, associated with alkali and granite complexes, for REE mineralization which involves the crystallisation of both independent HREE and LREE-minerals. According to Henderson (1984) and Mineyev (1963) REE and Y may be carried as alkali fluoride complexes.

A decrease in the Na⁺ content in the fluid during albitisation leads to the precipitation of fluorides and to the preferential crystallisation of LREE, which have the least stable complexes. This gives rise to an enrichment of the residual solutions in HREE, which eventually precipitate when the alkali content of the fluid becomes too low (Henderson, op. cit.). This sequence of LREE to HREE precipitation during albitisation (or greisenisation) could not be confirmed at Ririwai, since the order of LREE-phase and xenotime deposition is uncertain.

Chatterjee and Strong (1984) concluded that, during the cooling of batholith fluid, the transport of REE as F⁻ complexes becomes increasingly important. During albitisation, LREE are depleted due to their mobilisation dominantly by Cl-rich fluids, whereas F⁻ and CO₂-rich fluids are responsible for the deposition and enrichment of HREE. With subsequent greisenisation, LREE remain depleted, whereas HREE are variably affected and locally removed by F⁻.

In the albitite, fluid inclusion data (Kinnaird et al., 1985b) together with the presence of late calcite suggest that REE were mobilised by fluids enriched in CO₂ in addition to F⁻. During later microclinisation, the fluids were saline, suggesting that Cl was also

available for complexing with REE. REE and other high valence cations may also form polynuclear complexes with F (Giere, 1986) which would have been introduced during microclinisation. In the low salinity fluids associated with subsequent pervasive greisenisation, F was probably the dominant ligand available for REE complexing.

5. Trace element geochemistry and its relation to the accessory mineralogy

Geochemical data for U, Th and other trace elements in the Ririwai biotite granite for the L13 borehole, surface and Ririwai lode samples are presented in Kinnaird et al. (1985b). Unfortunately, these data are limited and many of the samples analysed are different from those used for mineralogical study here. This, together with the great variation in composition of a wide assortment of U- and Th-bearing phases, have prevented any meaningful mass balance calculations, while only cautious comparisons can be made between trace element geochemistry and the accessory mineralogy.

a) U and Th

The U and Th contents of four samples of biotite granite and two samples of albitised granite from the borehole, together with six surface samples of granite and three samples from the Ririwai lode are presented in Table 57 (data from Kinnaird et al., 1985b). In all borehole samples, both Th and U are highly enriched, while the Th/U ratio remains close to one. U contents vary from 30 to 81 ppm, with the highest values occurring at 115 m and 411 m and the lowest at 10 m. The higher value of U relative to Th at 10 m suggests that hydrothermal or magmatic controls were responsible for the depletion of U and Th, since surface leaching would increase the Th/U ratio. The virtually

identical values for U and Th at 115 m in the biotite granite and 411 m in the albitised granite argue against albitisation as a mechanism for bulk U and Th enrichment. Rather than enrich the rock U content, albitisation may have just redistributed U from primary magmatic sites to secondary metasomatic sites, such as uranothorite and uraniferous ?pyrochlore.

The major site for Th in the biotite granite and albitised granite is probably thorite, while lesser contributions come from zircon, monazite, LREE-phase and pyrochlore and, in the albitite, xenotime. Thorite is probably also a major contributor to bulk U, particularly in the albitite where it tends to contain more U. Uraniferous ?pyrochlore and zircon contribute lower amounts of U but the only other U-rich site found was coffinite in just one sample, at 100 m in the biotite granite. Another major site for U must exist in order to account for the Th/U ratio of one in the biotite and albitised granite samples. Further coffinite mineralisation associated with that found at 100 m, might occur at 115 m (with 80 ppm U), but this sample was not available for study. Given the limited number of sections examined per sample (between 1 and 2 in most cases), it seems feasible that a U-rich phase such as coffinite or uraninite, has been overlooked in the other borehole samples. Even though 39 sections of biotite and albitised granite have been examined in detail, it is possible that a few small coffinite or uraninite grains have escaped detection, especially since fission track work was not employed on the borehole samples.

Basham et al. (1982a) illustrated this problem with a diagrammatic representation of the U location in a U-enriched granite from Portugal, based on actual measured mineralogical and chemical parameters. Although uraninite accounted for 70% of the whole-rock

value of U, it was virtually inestimable modally, occurring at a frequency of about one grain in five sections. They estimated that grains in the range 10 to 100 μm across could be found at a frequency of one per five to twenty average rock sections, so that the examination of one or two sections for most of the borehole samples is clearly inadequate.

It is apparent, from the high Th/U ratios in Table 57, that surface samples of biotite granite have suffered leaching of their U contents. Surface weathering has not affected Th, which is about the same as or higher than borehole Th values, and this agrees with the occurrence of thorite in samples N75 and N94. Although it was inferred that discrete thorite included in biotite from sample N94 has undergone some leaching and alteration (Section 2.b.), thorite U contents are still comparable with those from the borehole samples (Fig. 24). Thorite inclusions from sample N75 are even less likely to have lost much U through leaching, due to their protection by the host zircon, and U contents do not seem significantly depleted. Therefore, much of the U content that was leached must have originated from a site other than thorite and this is consistent with the need for another site for U in order to account for the bulk U/Th ratio of one. The susceptibility of this hypothetical U site to leaching suggests that it is not a resistate phase, such as zircon or pyrochlore, but could be uraninite or coffinite, both of which commonly show marked dissolution in surface samples of granite e.g. Ball and Basham (1979).

Mine level 1 samples (R1-18 and R1-35) from the microcline are greatly depleted in U relative to borehole samples from the biotite granite, while Th values are only slightly depleted. Neither of the two samples analysed were examined for their accessory mineralogy, however,

so only a very tentative interpretation can be made. The low U values are very similar to those obtained from surface samples of biotite granite and it seems reasonable to suppose that the same leachable site of U has been dissolved during microclinisation. Late-stage mobilisation of U is evident in a surface sample of microcline (RS6(4)), which contains interstitial coffinite and this U may have been remobilised from the granite during microclinisation. Other samples from level 1 contain unidentified U-Th-Y-Si-rich phases, as well as uranothorite, suggesting that U was enriched rather than depleted during microclinisation, although bulk measurements of these samples are needed to confirm this. Mackenzie *et al.* (1984) concluded that U was enriched during microclinisation of granite obtained from level 1. The relative locations of different samples of microcline in the Ririwai lode from level 1 and on the surface need to be precisely determined in order to clarify which parts of the wallrock have suffered U enrichment and which parts U depletion.

Bulk U and Th data are available for only one sample of greisen vein, which was obtained from level 1 and which was examined in three sections (R1/14, R1/14-1, R1/14-2). Th is significantly enriched relative to the microcline and the borehole granite, suggesting the introduction of Th during greisenisation. This is supported by the abundance of thorite in sample R1/14 and is consistent with the conclusion, based on mineralogical observations, that thorite crystallised during greisenisation. Only a small amount of U could have been introduced with the greisenising fluids, since the bulk U content was increased by only 6 to 9 ppm over that of the microcline and is still substantially depleted relative to that of the borehole granite. The average U content of thorites from section R1/14-2 is 4.7 wt % UO_2 (based on 12 analyses) and this must have been largely

remobilised from accessory phases in the microcline.

Whole-rock U and Th data are not available from the greisenised granite at 125 m in the borehole and so it is not known whether the bulk U content was reduced by greisenisation, without prior microclinisation of the granite. The presence of coffinite at 100 m may be analogous to the coffinite occurrence in surface samples of the microcline, in that it represents U remobilised during hydrothermal alteration (at 125 m).

b) Other elements

In the surface samples of biotite granite, N75 is significantly enhanced in Zr, Hf, Th, Y and LREE, relative to N94 (Table 58). Enrichment of these elements may have occurred during the localised metasomatism which was proposed (Section 2.b) in order to explain the distinctive zircon population of sample N75.

Despite the alteration and dissolution of biotite during albitisation, bulk FeO and Fe₂O₃ contents at 411 and 440 m are not significantly different from those in other samples of granite. This is consistent with a closed system for Fe which was released from the biotite and precipitated locally as the abundant haematite blades and inclusions associated with chlorite and zircon respectively, although a much higher Fe₂O₃ : FeO ratio might be expected in this case. Much of the FeO probably resides in chlorite although mineralogical analyses are needed to confirm this. Y was depleted during albitisation, which is in agreement with the generally low Y content of thorite, but is unexpected, in view of the accessory xenotime found in the albitite. Y may have been remobilised from primary magmatic accessories (e.g. Y-thorite) and subsequently precipitated as xenotime or lost from the system. The crystallisation of late fluorite and calcite in the

albitite has not noticeably increased CaO or F contents of the rock.

A sample at 115 m contains anomalously high Li, which suggests that the area of greisenisation intersected at 125 m extends at least 10 m above this depth, since Li was introduced during greisenisation (Chapter 3, Section 4.c.ii). In Section 2.d., it was suggested that Zr, remobilised from zircon during greisenisation at 125 m, may have contributed to the high Zr contents of later thorite. Bulk Zr enrichment at 115 m suggests that some Zr may have been introduced during greisenisation, as well as remobilised. Despite the high Y content of thorite at 125 m, the bulk Y content at 115 m is not enhanced. If Y was introduced during greisenisation at 125 m, it appears not to have migrated up as far as 115 m, which may explain why the coffinite at 100 m is not very enriched in Y.

Trace element geochemistry of the Ririwai lode samples indicates depletion of trace element populations, including Y and REE, during microclinisation, followed by some enrichment in Ce, La and Y during greisenisation (Kinnaird et al., 1985b). Monazite is less common in the microcline than in some of the greisenised samples but there is no mineralogical evidence of its dissolution during microclinisation. Unidentified LREE-phases are of similar or greater abundance in the microcline compared to the greisen. A partitioning of HREE and Y to the greisen mineral assemblage is reflected by the occurrence of late overgrowths of xenotime and by the development of abundant yttrifluorite and Y-thorite. Although the enhancement of LREE may reflect, in part, the crystallisation of late overgrowths of LREE-phases, these accessories tend to be very small and scarce and a further site for LREE probably exists. The growth of new monazite would easily account for the increase in LREE, although mineralogical evidence indicating monazite crystallisation during greisenisation is equivocal.

6. Comparisons of Ririwai with other areas

The mobilisation of U, Th, and other incompatible elements during late- to post-magmatic alteration has been widely documented for granitic, alkali and volcanic rocks from other areas:

1. Nigeria-Niger --- Younger Granite Province
2. South Africa ---- Cape Granite Suite
Namaqualand metamorphic complex
3. Cameroon ----- Kitongo granite
4. South Greenland - Gardar igneous province
5. Arabian Shield
6. South Australia - Crocker's Well
7. Canada ----- Meguma Zone, Nova Scotia
E. Kemptville tin deposit, Nova Scotia
Gunnar U deposit, Saskatchewan
Pronto Deposit, Ontario
Otish Mountains and Mistamisk Valley, Quebec
Upper Aillik Group, Labrador
8. Sweden ----- The Arjeplog-Arvidsjaur-Sorsele U province
West Bergslagen
9. France ----- Margnac U deposit, western Massif Central
St.Chely and Les Bombes, S. E. Massif Central
10. Brazil ----- Borborema-Norte U province
Espinhaco U province
11. Alaska ----- Bokan mountain
12. Soviet Union ---- Ukraine and Central Kazakhstan
13. Britain ----- Cornubian batholith, south-west England
Cairngorm granite, Scotland
Skiddaw granite, Lake District
14. Portugal ----- Urgeiriça
15. China

An attempt has been made to classify the above examples as late-magmatic/deuteric processes, albitisation and greisenisation. Generally, albitisation and greisenisation occur during the post-magmatic stage but, in some examples, they have been attributed to the post-/late-magmatic stage. Sericitisation has been included with greisenisation, since the terms appear to be interchangeable in many examples.

a) Late-magmatic/post-magmatic processes

i) Nigeria-Niger Younger Granite Province

Bowden et al. (1981) noted, from analyses of U and Th for various ring complexes in Nigeria, that syenites, peralkaline granites and albite-granites were relatively enriched in U and Th, compared with their non-peralkaline components. The albite-rich facies contain a dispersed mineralisation of uraniferous pyrochlore, together with Th-rich monazite which Bowden and Kinnaird (1984b) believe resulted from autometasomatism, caused by rock-fluid retention.

Economic metals were retained in the peralkaline melts due to F complexing but, whereas metals such as Nb, Sn and Zn were lost as a volatile gaseous phase during eruption, U and Th were trapped in the ignimbritic, volcanic pile (Bowden, 1982). In Niger, the distribution of this U and Th in the ignimbritic piles of the Air massif was studied by Bowden et al. (1981; see Chapter 3, Section 6), whereas the distribution of U, Th and related elements in the subvolcanic rocks of the Taghouaji complex was studied by Perez (1985).

The Taghouaji complex in Niger resembles the Ririwai complex in its anorogenic setting, its association of peralkaline with biotite granites, its high concentrations of U and Th and mineralisation of U,

Th, Nb, Ta, Zr, REE, Y and F. A number of similarities exist between the two complexes regarding details of the U- and Th-bearing accessory minerals and these, together with the contrasts, are summarised in Table 59. Despite their similarities, the mineral assemblages at the two complexes had quite different origins, which were dominated by magmatic processes at Taghouaji but involved both magmatic and post-magmatic processes at Ririwai. Even the alteration of accessory minerals, for example during greisenisation, has been attributed to late-magmatic, rather than hydrothermal processes at Taghouaji.

The greisenisation appears to have had a dual effect on the bulk U and Th concentrations of the Taghouaji granite. Where the alteration occurred without cassiterite mineralisation, the original U and Th contents were largely unchanged, whereas cassiterite mineralisation was accompanied by an enhancement of U and depletion of Th. Autoradiographs showed the U to be associated with cassiterite where it was probably fixed in micro-inclusions of columbite, after having been remobilised from primary, U-bearing phases by late-/post-magmatic fluids.

In the Ririwai lode, greisenisation with cassiterite mineralisation was accompanied by the depletion of U and the enrichment of Th. Fission tracks do not reveal a direct association of U with cassiterite but cassiterite and uranothorite are spatially related. This contrasting behaviour of U and Th during greisenisation in the two complexes could reflect differences in the nature and origin of the respective mineralising fluids. More oxidising, hydrothermal fluids at Ririwai would probably have removed any U^{6+} whereas, in more reducing, late-/post-magmatic fluids at Taghouaji, the U may have been present as less mobile U^{4+} .

F played a major role in the chemistry, paragenetic evolution and

alteration of accessory minerals and was responsible for their different assemblages in the peralkaline and biotite granites of the Taghouaji complex. The alteration of U-bearing accessory minerals by F during the magmatic stage was responsible for the mobilisation of U, which was subsequently incorporated into later phases, such as thorite, zircon or cassiterite (in the greisen veins). Later post-magmatic mobilisation of U arose through the metamictisation of thorite.

In this respect, the mineralisation processes at Taghouaji resemble those at Ririwai, where the abundance of fluorite suggests that F was available for complexing with Th, U etc., both during the crystallisation of the biotite granite and its subsequent alteration. The great variation in U concentrations of thorite suggests that the metamictisation and leaching of this mineral lead to late-stage remobilisation of U at Ririwai too.

ii) Other areas

Other examples of late/post-magmatic processes also demonstrate the importance of F in the complexing of U, Th and other HFS elements in the peralkaline melt and their partitioning into subsequent aqueous phases, prior to a disseminated-type mineralisation. In the Hildebrand Complex of the Cape Granite Suite in South Africa, F complexed with Zr, leading to the late crystallisation of U-enriched zircon in which excess U crystallised as uraninite inclusions (Brynard, 1984). This process seems analogous to the exsolution of thorite inclusions during the crystallisation of Th-enriched, Type 2 zircon in the Ririwai albitite. In the leucogranite intrusions of the Namaqualand metamorphic complex in South Africa, deuteric alteration at about 500°C was responsible for the incorporation of U into secondary

chlorite, epidote, Ti- and Fe-oxides (Robb and Schoch, 1985).

"Efficient flushing of a U-charged fluid phase" and "prolonged equilibration between fluid and minerals" allowed the incorporation of significant but variable concentrations of U in the mineral structures.

In the Gardar igneous province of South Greenland, the crystallisation of complex U-, Th- etc.-rich phases, such as steenstrupine ($\text{Na}_2 \text{Ce} (\text{Mn}, \text{Nb}, \text{Fe}) \text{H}_2 ((\text{Si}, \text{P}) \text{O}_4)_3$) was favoured by the conditions in a strongly peralkaline melt which gave rise to U-enriched, highly differentiated syenites (Steenfelt and Armour-Brown, 1985). Bohse et al. (1974) state that this concentration of U in the late-stage melt was due to its oxidation and formation of complexes with halides and hydrocarbons. Cl and F were expelled into a fluid phase which extracted the U, Th etc. and resulted in a disseminated, porphyry-type U deposit, with subsequent pressure release.

A similar process of halide complexing in a late fluid-phase was described by Jackson et al. (1985) in order to explain the disseminated mineralisation of pyrochlore, columbite-tantalite, thorite, Th-rich zircon, xenotime and LREE-rich minerals in the alkali granites of the Arabian Shield. High field strength (HFS) and rare earth elements were retained in the melt due to their complexing with the high concentrations of F present (up to 4 wt % F). Finally, the elements were partitioned into an aqueous fluid phase, where they gave rise to a disseminated "porphyry-style" mineralisation of Nb, Zr, REE, U and Th.

Ashley (1984) described significant U and Th mineralisation in the form of Th-brannerite occurring in disseminated form and as veins and breccia bodies in sodic granite rocks and felsic gneisses at Crocker's Well, South Australia. U, Th and other HFS elements were partitioned

from the melt due to complexing with high concentrations of F and Cl present in saline fluids which evolved during crystallisation of the sodic granitoids. A subsequent decrease in the F activity of the fluid with cooling resulted in the breakdown of the complexes and the deposition of Th-brannerite, monazite, zircon, synchysite and fluorite. Like the workers cited above, Ashley (op. cit.) regarded the process as being analagous to that found in porphyry Cu and stockwork Mo systems.

b) Albitisation

i) Nigeria

The albitisation of biotite granite at Ririwai is a process common to other complexes in the Younger Granite Province, where it is also associated with U, Th, Nb, Zr and REE mineralisation. In the peralkaline granites it gave rise to a dispersed mineralization, including Th-rich monazite and pyrochlore containing over 5 % U₃O₈ (Kinnaird et al., 1985b). Other areas which preserve records of intense albitisation include Odegi in the Afu complex and Harwell in the Jos-Bukuru complex, where uranothorite (Table 6) is accompanied by xenotime (Fig. 15A, Analysis 11), monazite and Th- and Hf-rich zircon. In the Kaffo albitite-riebeckite granite of the Liruei ring-complex, extensive albitisation gave rise to enriched U (12 to 118 ppm) together with Th, Zr, Hf, Ta and F (Orajaka, 1986). The mineralisation included pyrochlore containing 4-5 % U (Jacobson and Macleod, 1977). Bowden and Kinnaird (1984b) attributed the mobility of U and Nb during albitisation to concomitant, high-temperature CO₂-degassing and envisaged the mobilisation of Mo, HREE, Th and Zr by a similar process.

ii) Canada

The Canadian examples emphasise the importance of CO₂ as well as halides in the transport and deposition of U during albitisation. In this respect, they resemble the Nigerian examples, where CO₂ degassing was shown to be crucial to the deposition of U (Kinmaird et al., 1985b). However, in the Meguma Zone, Nova Scotia, albitisation, along with other processes, actually depleted U and remobilised it to form deposits elsewhere. Airborne gamma ray spectrometry surveys reveal an association of high U and U/Th ratios with albitisation and greisenisation of the granite rocks of the Meguma Zone (Ford and O'Reilly, 1985). In particular, Sn, W, U and Mo mineralization is spatially and genetically associated with a "para-intrusive" suite in which hydrothermal fluids interacted with the residual magma, resulting in albitisation, greisenisation and other processes (Chatterjee and Strong, 1985). At the Millet Brook U deposit, a para-intrusive suite (the Lewis Lake pluton) lost approximately 70% of its original U content from the top 100 m, due to resurgent boiling and the evolution of hydrothermal fluids which were responsible for extensive fracturing, alteration and the U depletion. The U was redeposited as pitchblende, torbernite and autunite veins in the nearby biotite granodiorite.

In granites associated with the East Kemptville tin deposit of Nova Scotia, Chatterjee and Strong (1984) noted a depletion of LREE and enrichment of HREE with albitisation. With more intense albitisation, the LREE were virtually lost, while the HREE were also slightly decreased.

In the Gunner U deposit of Saskatchewan, albitisation was accompanied by, or followed closely in time by, the deposition of pitchblende, according to Gandhi (1983), who suggested that both

processes may have resulted from the same hydrothermal fluids or from separate phases of an evolving hydrothermal system. A drop in pressure and increase in acidity initiated the precipitation of U from carbonate-rich, low temperature, alkaline solutions. Carbonatisation accompanied the deposition of pitchblende in the strongly albitised and fractured Aphebian granite gneiss. Carbonatisation also succeeded albitisation during the remobilisation of brannerite and uraninite as part of the hydrothermal alteration of conglomeratic U ores at the Pronto Deposit in Ontario (Heinrich, 1981).

In a review of U deposits in Canada, Ruzicka and LeCheminant (1984) described a number of occurrences of epigenetic U mineralisation in veins associated with sodic metasomatism in the Otish Mountains area of Quebec. Also in Quebec, in the Mistamisk Valley of the Labrador Trough, Kish and Cuney (1981) described the formation of uraninite-albite veins from highly sodic, oxidising fluids in which CO_2 was available to form mobile uranyl-carbonate complexes. Deposition of uraninite was controlled by changes in the composition of the gas phase, which buffered the O_2 fugacity of the fluid, while the presence of hydrocarbon inclusions in the albite suggests that conditions were reducing.

White and Martin (1980) described the remobilisation of primary enrichments of alkalis, U, Th and other incompatible elements during autometamorphic reactions in tuffs of the Upper Aillik Group in Labrador. They suggested that earlier K-metasomatism was not associated with changes in the primary U/Th ratios because the temperatures were too low to selectively mobilise Th, while the pH range was too low to complex the U. In contrast, the subsequent higher temperature processes of sodic metasomatism and desilication were

associated with important U mineralisation and accumulations of Zr. Although the concentration of U showed an increase with progressive desilication and sodic metasomatism, a sharp cut off in the alteration was accompanied by a more gradual decrease in U concentration, possibly reflecting the lower mobility of U relative to Na. CO_2 , Cl and F levels also showed progressive increases with increasing desilication and White and Martin (op. cit.) concluded that CO_3^{2-} and F^- were important in the transport of U, but the role of Cl may have been insignificant. They suggested that the contrasting K- and Na-metasomatic alterations took place in different parts of convection cells set up in the tuffs. In the cooler parts ($>200^\circ\text{C}$), U was selectively dissolved and transported as a Na-uranyl carbonate or halide complex. In the hotter parts, U was precipitated, following the breakdown of the uranyl complexes and in response to a reduction of $f\text{O}_2$ or pH in the fluid medium, which reflected the crystallisation of sodic pyroxenes and amphiboles and possibly the early deposition of U as pyrochlore.

iii) Sweden

Swedish rocks also show that halide and carbonate complexes are important in the transport of U, together with Zr, Y and REE, although the process of albitisation actually preceded U mineralisation in the Arjeplog-Arvidsjaur-Sorsele U province. This U province lies immediately south of the Arctic circle and is characterised by thirty known mineralisations, the most important of which are epigenetic (Smellie and Laurikko, 1984). The association of U minerals with the products of albitisation is a ubiquitous feature of all epigenetic U mineralisations in the province (Adamek and Wilson, 1979). The alteration is associated with an addition of Na, Al, Ca and Mg together

with Zr which varies between 0.05 and 0.5 wt %. Zircon appears to have formed early during the albitisation process and it contains relatively high Hf but is virtually free of U and Th. The albitisation is associated with the formation of late calcite, and the U is thought to have been transported as uranyl carbonate/fluorine-carbonate complexes (Adamek and Wilson, op. cit.). The fluids responsible for the albitisation were probably derived from the basement during metamorphism, while the U etc. were either scavenged en route from the basement or were locally derived from U-, Zr- and Y-enriched, peralkaline rhyolites.

At Skuppesavon, in the north part of the province, the main albitisation event preceded the mineralisation of U and opened up zones for the U-, Ca- and Ti-bearing solutions which precipitated uraninite, sphene and complex uranotitanates (Smellie and Laurriko, 1984). There was no obvious enrichment of U within any of the metasomatic silicate phases characterising the mineralised zone. Uraninite is associated with the more mafic-rich parts of the albitites, implying the contribution of Fe^{2+} to local redox reactions, leading to U^{4+} precipitation. A similar pattern of alteration and mineralisation was noted by Halenius and Smellie (1983) for five other mineralised localities in the province.

In common with the Meguma Zone example in Nova Scotia, U depletion is characteristic of the albitisation at West Bergslagen in central Sweden. Baker (1985) noted that U, together with Fe, F, REE and other elements, were removed while Ti, Al, P, Y and Hf remained immobile during the albitisation of 20 m wide zones in a Proterozoic, peraluminous granite. A selective depletion of the LREE indicates that Cl^- was the dominant complexing anion in the hydrothermal fluids

(sea-water), since the LREE preferentially complex with Cl^- (Flynn and Burnham, 1978; Taylor and Fryer, 1982) whereas the HREE complex with F^- (Fryer and Edgar, 1977) and CO_3^{2-} (McLennan and Taylor, 1979; Kerrich and Fryer, 1979).

iv) Other areas

Albitisation and the related process of episyenisation are associated with the enrichment of U and other HFS elements in a diverse number of geological settings, world-wide. Element variations similar to those described in Sweden have been reported from several granites in France. Leroy (1978) noted that episyenisation of feldspar and mica was associated with U enrichment in uraninite-bearing, two-mica granites of the Margnac U deposit, western Massif Central. According to Ranchin (1971), the uraninite crystals formed by deuteric processes related to muscovitisation of the granite. Vein-type and disseminated pitchblende mineralisation succeeded the sodic alterations.

In the south-east Massif Central, primary magmatic accessories in peraluminous granites have been affected by quartz leaching ± albitisation. Cathelineau (1987) recognised three types of subsolidus alteration which are summarised in Table 60. Dissolution of uraninite, monazite, zircon, and sphene and the deposition of authigenic thorite, xenotime, zirconosilicates etc. were largely controlled by the fluid's phosphate activity, which was locally reduced by the formation of neutral alkali-phosphate complexes during albitisation. Phosphates and, to a lesser degree, halogens played an important role in the transport of U, Th, Zr and REE which form stable phosphate complexes. At St. Chely, LREE-Cl complexes were responsible for the dissolution of monazite in the albitising fluids whereas, at Les Bombes, HREE

enrichment (xenotime, thorite) was attributed to high F^- and PO_4^{3-} activity. The low CO_2 content of fluid inclusions suggests that CO_3^{2-} complexes were not involved in the mineralisation.

Sarcia (1983) commented on the widespread occurrence of albite with uraninite-pitchblende associations and concluded that U deposits in albitites occur within shearing zones and breccias connected with deep-seated lineaments but without obvious magmatism. In contrast, the episyenites of western Europe are never found outside the Hercynian leucogranites.

Barretto (1985) noted an association of U mineralisation with albitisation affecting various rock-types in the Brazilian platform. The processes were characterised by a depletion of K, Si, Fe and Cl and an addition of Na, Ca, F and LREE. MacKevett (1963) described the mainly hydrothermal U-Th deposits located in or near the Bokan Mountain peralkaline boss, south-east Alaska. Several of the deposits occur in a surrounding albitised aureole and MacKevett (*op. cit.*) suggested that the Na-rich fluids responsible for albitisation were closely related to the ore-forming fluids which deposited uraninite, uranothorite, uranian thorianite and subordinate coffinite, allanite, phosphates, niobates and brannerite.

An association of U deposits with albitisation is well documented in the Soviet Union, where the concept was first introduced (Sarcia, 1983). For example, Kasanskij *et al.* (1976) found a close relationship between sodic metasomatism, basement and source of mineralisation in the Ukraine. Zharkova and Tananaeva (1968) noted an early stage of albitisation and greisenisation, prior to vein-type, pitchblende-fluorite mineralization. From experimental work, Bayushkin and Dikov (1974) were able to predict the existence of metastable U compounds

during the formation of U-bearing albitites. As the hydrothermal solutions changed from alkaline to nearly neutral, the complex, polymerized U silicates were transformed into simpler and more stable U orthosilicates, such as coffinite. Although coffinite was not found in the albitised granite at Ririwai, the $USiO_4$ component of uranothorite may have evolved in a similar manner.

In syenites of the southern Greenland Gardar igneous province, late- to post-magmatic metasomatism caused the remobilisation and deposition of high concentrations of U (>500 ppm) as pyrochlore, along with Th, REE, Nb, Ta and Zr (Steenfelt and Armour-Brown, 1985). U^{6+} was strongly partitioned into a volatile phase in the magma and the alkaline, hydrothermal fluids gave rise to albitisation and K-metasomatism along fractures. Pitchblende was deposited at low temperatures from the CO_2 - and hydrocarbon-bearing, aqueous solutions.

In China, upper mantle-derived, Na_2CO_3 -rich solutions gave rise to enriched U (48 ppm) during the Na-metasomatism of various rock-types (Letian, 1986). The metasomatism and later fracturing created a favourable environment for ore bodies containing up to 0.39 % U as uraninite and U titanites, together with enhanced Th, Y, Ce and Zr along deep-seated faults.

In the Panafrican Kitongo granite of northern Cameroon, hydrothermal U mineralisation is genetically and spatially associated with albitisation (Oesterlen and Vetter, 1986). Like the Swedish examples, the albitisation actually preceded the U mineralisation and the U concentration is not directly correlated with the Na_2O content of the rock. Bulk U in the albitite reaches 1257 ppm, and is held in interstitial uraninite, which also hosts an enriched rock Th content. During albitisation, Ce, La and Zr were introduced and remobilised and,

together with U and Fe, they formed alkaline complexes with Na bicarbonate, carbonate, hydroxides and possibly Na phosphates and chloride. As at Ririwai, albitisation was associated with the crystallisation and remobilisation of a secondary generation of zircon.

c) Greisenisation and sericitisation

During the processes of greisenisation and sericitisation, Zr and Th are usually immobile, while concentrations of REE and U may be unaffected or depleted. This differential behaviour of REE and U probably reflects the diverse nature of the fluids during the alteration processes, as well as the different susceptibilities of various U- and REE-bearing phases to leaching. Zircon is normally stable, whereas monazite and uraninite may or may not be leached.

In south west England, Ball and Basham (1979) and Basham et al. (1982b) found the U content of granite and the distribution of uraninite, in particular, to be unaffected by the processes of greisenisation and sericitic alteration. In samples of progressively greisenised granite from the Bosworgey cusp, Ball et al. (1982) found the U content to be slightly greater in the most heavily greisenised sample but was otherwise unchanged, as were concentrations of Th, REE and Zr, reflecting the resistance of zircon and monazite to the alteration process. Alderton et al. (1980) similarly found that zircon, Th and most REE were unaffected by sericitic alteration in south-west England, although they found a depletion in Eu. Unchanged Zr concentrations in greisenised samples of the Cligga Head granite, on the north coast of Cornwall, were confirmed by Hall (1971) who concluded that this reflected the low solubility of zircon in the alteration fluids. In contrast to the above examples, Simpson et al.

(1979) observed the dissolution of uraniferous zircon in the centres of tourmaline-greisen veins from the St. Austell and Cligga Head granites. In the western lobe of the St. Austell granite, Allman-Ward (1985) found uraninite to be leached and bulk U depleted in greisenised samples, although Th was still unaffected. In the Cairngorm granite, mobilisation of U may have occurred during greisenisation and other processes of hydrothermal alteration (Webb et al., 1985) but greisenisation of mineralogically similar rocks from the Skiddaw granite in the Lake District was accompanied by little nett change in U content (Webb and Brown, 1984b).

In a sericitised granite from Portugal, zircon was unaffected but monazite showed signs of mobilisation during the alteration (Basham et al., 1982c). Uraninite was still present, but its corroded form suggested some remobilisation. Cameron (1982) found that sericitisation of a two mica, Hercynian granite from Portugal released Fe and U from biotite and leached uraninite, with the Fe and U precipitating as haematite and pitchblende fracture veins. Chatterjee and Strong (1984) noted an increasing divergence of the geochemical behaviours of F, U and Th with progressive greisenisation of granites associated with the East Kemptville tin deposit of Nova Scotia, Canada. Th and Zr were immobile in the greisen fluids relative to other elements in the granite. During greisenisation, the REE remained depleted from previous albitisation, while the HREE were variably affected. Depletion of REE was attributed to complexing with F in the hydrothermal fluids.

In the Namaqualand Metamorphic Complex of South Africa, deuteric sericitisation released U and possibly Th from primary sites such as biotite, zircon and allanite in alaskites (Brynard, 1984). A significant amount of the U and Th appears to have been readily

partitioned or fixed into the alteration products, in particular epidote, chlorite and ilmenite. Dmitriev and Leonova (1962) found U to be enriched during greisenisation of granites from Central Kazakhstan, USSR, while both U and Th concentrations were increased (9 ppm U, 18 ppm Th) in F-enriched and intensely greisenised biotite granites from the Soviet north east (Zagruzina and Smyslov, 1978).

d) Summary and conclusions

Halides, particularly F, play an important role in the transport and concentration of U and other HFS elements during late-magmatic/post-magmatic processes. Characteristically, aqueous phases derived from the peralkaline, parent magma give rise to a disseminated-type mineralisation. The examples cited are probably more relevant to the disseminated mineralisation of uraniferous pyrochlore in the peralkaline and albite-granites at Ririwai, rather than to the peraluminous biotite granite. However, the abundance of fluorite in the biotite granite suggests that F was available for complexing with Th, U etc. during the disseminated mineralisation of uranothorite, pyrochlore, monazite and other Th-bearing, LREE-phases, together with the secondary enrichment of U, Th etc. in zircon.

The remobilisation of U and other HFS elements during or shortly after albitisation appears to be dependent on the formation of carbonate, as well as halide complexes. In some cases, the metasomatism is associated with an enrichment of U, whereas in others, it is associated with a depletion of U, which is remobilised to give a deposit elsewhere. Although albitisation was certainly associated with the remobilisation of U at Ririwai it is uncertain whether or not a bulk enrichment of U occurred (Section 5.a).

During greisenisation and sericitisation, bulk concentrations of U, Th and REE are variably affected, reflecting inconsistencies in the stabilities of accessories such as uraninite and monazite. Although greisenisation led to the replacement of zircon by tourmaline in the St. Austell and Cligga Head granites, further evidence from south west England and other areas suggests that zircon is stable during greisenisation and sericitisation. At Ririwai, considerable mobility of U, Th and REE is also apparent during greisenisation, but this is accompanied by the mobilisation of Y and Zr. Bulk enrichments of Th reflect the crystallisation of thorite, while the mobility of Zr is at least partly due to the destabilisation of zircon and its replacement by Li-mica.

The conflicting evidence of element mobilities at Ririwai and the other areas is probably a consequence of the limited number of examples reviewed, from a diverse group of geological settings. The terms "greisenisation" and "sericitisation" probably encompass a variety of different alteration processes whose effects on U, Th etc. mobility depend on factors such as the nature of the fluids and of the host minerals.

Chapter 6 The Helmsdale Area

1. Introduction

Helmsdale (grid reference ND 025 155) is located in the north of Scotland in Sutherland, near the border with Caithness (Fig. 82). Samples were collected from the Helmsdale granite and Ousdale arkose, where exposure is limited to stream beds and the occasional cutting or excavation (Figs. 83-85). A portable gamma scintillometer was used to measure the radioactivity of exposures (Appendix 3) and samples were mainly taken from the more radioactive sites, although some were collected from sites showing background radiation for comparison (see Appendix 6 for description of samples and radioactivity of collection sites). Enough material was collected from each site for the preparation of several thin sections and for the bulk measurement of U and Th by instrumental neutron activation analysis (see Appendix 2).

A reconnaissance by the British Geological Survey (BGS) between 1965 and 1971 had made available borehole and surface samples of arkose, together with field and laboratory data concerning U mineralisation in the granite and arkose (Gallagher et al., 1971; Bowie et al., 1973). Borehole material, recovered from the fine-grained granite at Creag Thoraraidh (grid ref. 041 186, Fig. 84) and now housed in the BGS rock-store, was also available for study.

2. Geological setting

The Helmsdale granite was emplaced during the Caledonian orogeny and belongs to the "newer, forceful intrusions", as defined by Read (1961). It is an adamellite, intruded at a high structural level into

Moine schists and comprises an outer, porphyritic granite, grading into an inner, fine-grained granite. External contacts are sharp and angular and are associated with zones of brittle fracturing with little contact metamorphism (Read, 1931; Read et al., 1925). The granite is truncated by the transcurrent Helmsdale fault, which is a south-west north-east trending off-shoot of the Great Glen fault that was active during Lower Old Red Sandstone times, with a later, post-Jurassic, normal movement.

During uplift and erosion of the Caledonian orogen in the Devonian, a molasse facies sequence was deposited in the Orcadian basin to the north and east. Around the margins of this basin, a restricted development of the Lower Old Red Sandstone is exposed, consisting of sandstones and conglomerates which were deposited in fault-bounded, intramontane basins contemporaneously with the initiation of the Great Glen and Helmsdale fault systems. The lower part of the Lower Old Red Sandstone, Ousdale arkose was formed by the weathering and disaggregation of the Helmsdale granite, with subsequent lithification of the granite debris. Other deposits represent fossilised talus and scree formed on the slopes of the early Devonian hills, while finer arkoses and mudstones were deposited in the valleys. The Lower Old Red Sandstone is unconformably overlain by the Middle Old Red Sandstone which is the dominant group in the Orcadian basin and consists of marginal red bed sedimentation with a central, thick development of grey, calcareous siltstones known as the Caithness Flags. These are overlain by the Upper Old Red Sandstone red beds which are developed across the whole basin.

3. The Helmsdale granite

a) Petrography

A detailed petrographic description of the Helmsdale granite was given by Read et al. (1925) and also by Gallagher et al. (1971), Bowie et al. (1973) and Tweedie (1981). The pink, porphyritic adamellite comprises equal proportions of quartz, plagioclase and K-feldspar, with up to 5% biotite (Plates 120 and 121). The quartz is interstitial or forms aggregates and contains intricate trails of fluid inclusions. The plagioclase, which is variably sericitised, has an approximate composition $Ab_{90} An_{10}$ and ranges from albite to oligoclase (Read et al., 1925). It forms subhedral clusters or euhedral inclusions which lie parallel to the cleavage in K-feldspar. The K-feldspar is mainly orthoclase with some microcline and forms tabular phenocrysts up to 25 mm in length, with coarse perthitic banding or irregular patches of plagioclase. Biotite forms ragged laths showing Fe-staining with alteration to chlorite, haematite and TiO_2 or is often bleached. Rare hornblende is pseudomorphed by chlorite and calcite. The fine-grained granite contains essentially the same mineralogy but the orthoclase usually measures 1-2 mm across, the plagioclase is slightly more calcic and the biotite is generally less abundant (up to 2%).

Apatite, zircon and sphene are the main primary accessory minerals and are described in Chapter 7, along with the secondary minerals haematite (martite), goethite, TiO_2 and sericite. Very minor amounts of other accessories have been reported from panned concentrates or drill sludges (Gallagher et al., 1971). These include thorite, monazite, baryte, bismutite, pyromorphite and tourmaline. Locally, there are veins of fluorite, calcite, galena, sphalerite, pyrite, chalcopyrite

and molybdenite. Minor occurrences of secondary uranyl minerals in the granite include kasolite, autunite, meta-autunite, torbernite and meta-torbernite in loose boulders and in situ at Caen Burn and Gartymore Burn (Gallagher et al., 1971).

b) Alteration and U mineralisation

Surface radioactivity from the Helmsdale granite is higher than most other Scottish, Caledonian granites (Gallagher et al., 1971). Table 61 shows the mean U content to be above that commonly encountered in world granites, whereas the mean Th content is more typical, resulting in unusually low, mean Th/U ratios. Other elements measured by Tweedie (1979; including Cu, Pb, Mo, Zn, Zr, F, P₂O₅ and K₂O) fall within the range of common world granites. Table 61 also shows that U tends to be higher in more altered granite, including both fine-grained and porphyritic-types, suggesting that U enrichment is a post-magmatic, rather than a magmatic process. Completely unaltered granite has not been found and even the freshest samples have a strong pink colouration.

Table 62 gives bulk U and Th analyses for the least-altered granite and granite showing various degrees and types of alteration. It is evident that high counts obtained during field radiometry do not necessarily indicate correspondingly high contents of U in the rock. This is partly because of complications during measurement of the gamma rays and partly because surface leaching may have selectively removed U, while leaving the gamma-emitting daughter products of the ²³⁸U decay sequence (see Appendix 3). U lies mainly in the range 6-20 ppm, with five anomalous values of 62-650 ppm corresponding to highly altered granite samples. Sample H414, recovered from a borehole in the fine-grained granite, shows low U and a high Th/U ratio, suggesting

that surface leaching of U has occurred to a depth of at least 9m. Th concentrations lie within, or close to, the range expected for granite, with most values restricted to the 20-30 ppm range but three samples from alteration zones and reddened granite are slightly enhanced in Th (up to 44 ppm), whereas two altered samples with very high U (510-650 ppm) are depleted in Th (8-17 ppm).

Localised, intense alteration is characterised, in a number of widely scattered localities in the fine-grained granite (Fig. 82), by an impersistent zone of greenish-yellow, disaggregated rock (Plate 122), typically 10-30 cm in width, although some zones in Caen Burn are several metres in width. For about 180 m along the track to Creag Thoraraidh (Location 36, Fig. 84), a large number of closely-spaced alteration zones are well exposed and strike roughly east-west, dipping steeply to the north. The alteration zones are developed along prominent joint sets in the granite but, elsewhere, fault planes may also be exploited by alteration and U enrichment (Plate 123). All zones of alteration occur within very reddened granite wall-rock (Plates 124 and 125).

Thin-section petrography shows the alteration to comprise extreme sericitisation of feldspar and biotite which may be bleached or Fe-stained or completely removed (Plate 126). Abundant, disseminated patches and veinlets of Fe-oxide were probably derived from the alteration of biotite and are accompanied by euhedral to subhedral grains of martite. TiO_2 is frequently present and includes anatase as scattered, subhedral grains or pseudomorphs after sphene, together with disseminated leucoxene. The wallrock contains very little or no sericitisation but Fe-oxide is much more abundant as staining of biotite and as veinlets and aggregates of haematite.

Counts from the inner alteration zones often greatly exceed the background (70-90 cps), while counts from the reddened wall-rock are lower, but still anomalous. This is reflected in high U contents (83-650 ppm) in some samples (e.g. 46B, 28E in Table 62), although others (e.g. 5A, 53A) contain much lower U (11-13 ppm), which may be vulnerable to leaching from the porous, disaggregated zones. Measurements by Tweedie (1979 and 1981) have shown that enriched U is accompanied by anomalously high Pb, Zn, F and K₂O in these alteration zones. The high K may be related to the F content and reflects the amount of sericitic alteration (Tweedie, op. cit.) but the mineralogical locations of the Pb and Zn in the zones have not been determined.

At Ord Burn, in the eastern part of the intrusion (grid ref. 055 177, Fig. 85), a 9 m high exposure of very reddened, quartz-veined granite is anomalously radioactive and contains a 10 cm wide, yellowish, disaggregated zone with 650 ppm U. High counts, peaking well over 1000 cps, are associated with the zone which contains a marginal, 15 mm wide vein of uraniferous hydrocarbon. The hydrocarbon is brittle and coal-like and is closely associated with a light-grey, plastic clay. The exposure corresponds, in location, to the "Cu-Mo mineralisation, cut by a multimetallic hydrocarbon vein" described by Tweedie (1979 and 1981) who measured 3 % U, 1 % Pb, 0.9% Bi, 0.4% Cu, 0.3 % Se, 0.1% Mo, 400 ppm Zn, 200 ppm Th and detected W in the hydrocarbon. Autoradiographs suggest the U is dispersed evenly throughout the hydrocarbon but is also present as sub-microscopic particles of a U mineral (Tweedie, op. cit.). Tweedie (op. cit.) also noted veins and joint coatings of pyrite, chalcopyrite, molybdenite, quartz, fluorite, autunite and torbernite.

In Caen Burn, 3.5 km north of Helmsdale (Location 7, Fig. 84), a dark-brown, clay-filled alteration zone, approximately 15 cm wide (Plate 127) contains 510 ppm U. Immediately on either side of the zone, which trends approximately east-west and dips 60° to the south, the granite is pale yellow and remains very friable up to about 50 cm away. Counts in this altered wall-rock are still high, although U is only 19 ppm. Tweedie (1979) described similar clay-filled structures from the fine-grained granite and attributed them to weathering of post-alteration shearing. These clay-filled shears may be equivalent to the "radioactive minor structures" of Gallagher *et al.* (1971) who measured high Th, Cu, Pb, Zn, As and Mo in addition to the high U which they believed to be adsorbed on to the clay-fractions from circulating groundwaters.

In the north of the intrusion, porphyritic granite, exposed along Allt Cille Pheadair and its tributaries (Fig. 83), is pervasively disaggregated and contains residual corestones and layers of more competent rock, which locally show minor faulting (Fig. 86). The disaggregated granite tends to give enhanced counts up to 130 cps, although these increase to 200 cps in areas of Fe-oxide staining. Often, the radioactivity in a stream-cutting of disaggregated granite increases from top to bottom, implying surface leaching of U. The residual corestones and layers contain average concentrations of U (Table 61) whereas the disaggregated granite contains enhanced concentrations of U (12-17 ppm) which are adsorbed on to clay minerals and limonite (Tweedie, 1979). 100-300 ppm U were measured in clay fractions, obtained during drilling, which showed the disaggregation to persist to a depth of 35 m at Allt na Muic (Gallagher *et al.*, 1971). Disaggregation is thought to have occurred during deep weathering of

the granite which may have been facilitated by hydrothermal alteration, prior to unroofing of the pluton in Lower Old Red Sandstone times (Gallagher et al., op. cit.). The weathering released U which has been leached by groundwater, giving rise to anomalous concentrations in stream-water, sediments and peat (Gallagher et al., op. cit.).

Enhanced counts (up to 160 cps) were frequently obtained away from granite exposures, where thick deposits of limonite-coated peat occur in stream beds, such as Gartymore Burn (Locations 29-34, Fig. 83). Tweedie (1979) measured 490 ppm U, 119 ppm Pb and 11 ppm Mo in dried peat from a spring in the Caen valley, while Plant (1971) believed such anomalous concentrations to represent adsorption on to carbonaceous material in the peat. Even away from streams, high counts need to be interpreted with caution, due to the presence of radioactive peat.

4. Ousdale arkose

a) Petrography

The arkose is, megascopically, very similar to the granite from which it is derived. It is composed of poorly sorted, angular to rounded clasts of granite (more than 10 mm in diameter) plus roughly equal proportions of disaggregated quartz, orthoclase and plagioclase. Fine-grained iron-oxide staining on the periphery of clasts suggests some weathering occurred prior to the formation of the arkose (Bowie et al., 1973). Virtually all of the biotite has been removed in the arkose and only small, rare flakes are preserved in quartz. Muscovite is quite common in some samples and comprises isolated flakes which may have been produced by the alteration of biotite although, unlike the granite, they contain no Fe-oxide staining.

Martite is absent or much less common than in the granite, while

Fe-oxide replaces or pseudomorphs pyrite in some borehole samples of arkose. Disseminated Fe-oxide is much less abundant in borehole samples of arkose than in surface samples of arkose and granite, while TiO_2 , in the form of subhedral anatase, pseudomorphs after sphene and disseminated leucoxene, is more abundant. Other minerals found in the arkose include fluorite (Plate 128), calcite (Plate 129), baryte (Plate 130) and various sulphides (e.g. pyrite, marcasite, chalcopyrite, covellite, galena) but these are rare or have not been identified in the granite. In a cutting along the A9, 8 km north east of Helmsdale (Location 21, Fig. 85), the arkose is locally replaced by veins of dark purple fluorite (Plate 131).

b) U mineralisation

Samples of fluorite-bearing arkose collected from the Ousdale and Glen Loth areas (grid refs. ND 066 201 and NC 937 127 respectively) contain normal amounts of U (Table 62). Five areas of anomalous radioactivity were described in the Ousdale area (Fig. 87) by Gallagher et al. (1971). At Anomaly 1, uraniferous hydrocarbon-rich, clay lenticles were found in a thin arkosic horizon within the Ousdale mudstones, 15 m above the contact with the arkose (Gallagher et al., op. cit.). The U is present as extremely fine-grained uraninite, dispersed through the hydrocarbon (Bowie et al., 1973).

Two boreholes were drilled over radiometric anomalies in the lower valley of Ousdale Burn, above a coastal waterfall (Plate 132; Anomaly 2, Fig. 87). The anomalies are lensoidal in shape, with the axis of elongation parallel to the burn and a corresponding north-west south-east trending fault. The mineralisation is tabular in form, dipping eastwards and truncated westwards by reverse faulting which

downthrows mudstones beneath arkose (Fig. 125). Disequilibrium between radiometric and chemical assays for U in the boreholes indicates surface leaching down to 2.5 - 3 m depth, although a surface sample collected from the site of Borehole 1 (Plate 132) contains 300 ppm U (Table 62). From 3 to 10.7 m depth in Borehole 1, the average U content of the split core was 200 ppm U and from 2.4 to 7.6 m in Borehole 2 the average was 300 ppm U (Fig. 88). Highest U concentrations in Borehole 2 (up to 900 ppm U) occur with shearing at 7.6 m and are associated with the introduction of disseminated pyrite, chalcopyrite, marcasite, covellite and hydrocarbon. Fission-track studies (Bowie et al., 1973) have shown that U is largely concentrated in the groundmass of the arkose and its distribution is controlled by sedimentary bedding in the siltstones and mudstones.

Anomalies 3 and 4 in Fig. 87 constituted large blocks of uraniferous arkose containing disseminations and joint coatings of torbernite (Gallagher et al., 1971) but the trenches have now been filled in. The trench at Anomaly 5 has been partially infilled, but the most radioactive part is still exposed (Plate 133, Fig. 89). A closely jointed and altered arkose horizon, interbedded with a basal conglomerate facies, gives counts up to 1700 cps, corresponding to a U content of 1400 ppm U (Table 62), while Gallagher et al. (1971) measured up to 1800 ppm U, together with high values for Cu, Pb, Mo, Be, As and W. Brightly coloured, secondary uranyl minerals, which occur as joint coatings (Plate 134) and dispersed grains, include torbernite and metatorbernite (Gallagher et al., 1971). Fission-track studies (Bowie et al., 1973) showed U to be concentrated in the groundmass and in kaolinite along post-consolidation cracks but not in the abundant, red staining associated with feldspar. Detrital crystals

of apatite are partially or completely altered to torbernite and metatorbernite.

In addition to the uraniferous hydrocarbon at Anomaly 1, minor deposits of uraniferous hydrocarbon have been found near the unconformity between the Lower Old Red Sandstone and the Helmsdale granite at Westgarty Burn and Allt Briste (grid refs. NC 988 125 and ND 050 171 respectively). The masses of hydrocarbon, up to 3 cm across and intergrown with pyrite, replace the sandstones (Parnell, 1985). Analyses revealed enrichments in U (up to 1000 ppm) which, in the Westgarty sample, was evenly distributed throughout the hydrocarbon and accompanied by enriched REE.

5. Genesis of U mineralisation

On the basis of geochemical and geophysical evidence, Watson and Plant (1979) divided the granites of northern Scotland into two groups:

1. Older granites and newer, forceful granites (Pre-Devonian).
2. Newer, permitted granites (Devonian).

The Helmsdale granite belongs to the first group in which intrusions are characterised by a lack of geochemical, aeromagnetic or gravity anomalies, high $^{87}\text{Sr}/^{86}\text{Sr}$ ratios and background U values (Simpson et al., 1979). These features suggest derivation by crustal ultrametamorphism and partial melting, with the newer, forceful granites, such as Helmsdale, rising further from the site of partial melting (Simpson et al., op. cit.). The Lower Devonian, permitted granites (e.g. Cairngorm) are characterised by distinct geophysical and geochemical anomalies (Plant et al., 1982) and high U and low $^{87}\text{Sr}/^{86}\text{Sr}$ ratios, suggesting a mantle origin (Simpson et al., op. cit.).

High U concentrations in many of the Devonian, permitted granites

resulted from an emplacement of U-enriched magmas from subcontinental lithosphere, underplated onto pre-existing, Precambrian basement. Enrichment of U and other incompatible elements resulted from scavenging during the ascent of F-rich volatiles after the breakdown of phlogopite (Simpson et al., op. cit.). Plant et al. (1982) emphasised the distinction between "metalliferous" granites, with high primary magmatic contents of U (e.g. Lower Devonian, permitted granites) and "mineralised" granites, in which U has been further concentrated into secondary mineral occurrences due to reaction of the magma with epizonal water (e.g. Helmsdale granite).

A number of studies at Helmsdale (e.g. Simpson et al., 1976; Watson and Plant, 1979; Tweedie, 1979; Bowie et al., 1973) have suggested that U mineralisation in the granite was post-magmatic and fault-controlled. Tweedie (1979 and 1981) envisaged a weak, pervasive, low- to medium-temperature (100-400°C) hydrothermal event which doubled the U content of the upper part of the intrusion. Meteoric water was transported down the plane of the Helmsdale fault until it reached a deep heat source (the fine granite interior or a later intrusion), which resulted in its upward migration, leaching and transporting metals and F on the way. On reaching the upper, cooler part of the fine granite, the K-, F- and U-bearing fluids were channelled along cooling joints where they gave rise to the intense zones of potassic alteration. Shearing in these alteration zones, related to normal movement on the Helmsdale fault, gave rise to the "clay-filled shears" which adsorbed further U from circulating ground-waters. More pervasive alteration occurred throughout the bulk of the granite, depositing U along grain boundaries and in secondary alteration products. Tweedie (1979) believes the lower U contents and degrees of

alteration in the porphyritic granite to reflect a decreasing intensity of hydrothermal alteration and U enrichment outwards from the fine-grained granite.

Similar models, involving deeply convecting meteoric water about cooling plutons, have been envisaged in order to explain the epigenetic mineralisation of U and other elements associated with granites from south-west England and Scotland (Simpson et al., 1979), the north of England (Brown et al., 1980) and New Hampshire, U.S.A. (Fehn et al., 1978). Continued hydrothermal convection requires an extensive system of channels for heating and circulating water. High concentrations of radioelements in the granite may produce enough heat to maintain the hydrothermal convective systems, giving rise to mineralisation, long after initial emplacement of the magma (e.g. Darnley et al., 1965).

The metalliferous hydrocarbon at Ord Burn is believed by Tweedie (1979) to have precipitated from brines, rich in metals and hydrocarbon, leached from Middle Devonian sediments. In Caithness, these sediments contain abundant carbonaceous material and the appropriate trace elements are enriched in various facies (Bowie et al., 1970; Michie, 1972). The highly fractured and faulted granite provided a pathway for compaction fluids expelled from the down-faulted sediments (Fig. 90). A similar origin may apply to other deposits of uraniferous hydrocarbon (e.g. Gallagher et al., 1971; Parnell, 1985) which occur in the Lower Old Red Sandstone, close to the Helmsdale fault.

In the Ousdale arkose, evidence for the sedimentary control of U suggests that it was at least partly introduced from the granite during deposition of the arkose (Bowie et al., 1973). No U mineralisation has been noted in the overlying, Middle Old Red Sandstone, Badbea breccia, despite its similar lithology to the arkose, according to

Gallagher et al., (1971) who envisaged the introduction of granite-derived U during pre-Middle Old Red Sandstone earth-movements. Tabular enrichments of U were subsequently modified by faulting, as demonstrated by the association of radiometric anomalies with the Helmsdale fault and its splays. A general association of U with fluorite suggests that F-complexing aided the transport of U in the mineralising fluids (see Chapter 2, Section 1.b.).

Chapter 7 Distribution of Uranium in the Helmsdale Granite
and Ousdale Arkose

1. Introduction

Fission-track radiography was used to locate U-bearing phases in polished sections of granite and arkose and these were examined using the mineralogical techniques described in Appendix 1. Although U standards were not irradiated along with the samples, the relative U levels of different minerals/features can be assessed from the fission-track densities, which are abbreviated in the text (see Key to Abbreviations, p. 30).

The locations of surface samples and sites of boreholes in the arkose and granite are shown in Figs. 83-85 and 87. Samples of Ousdale arkose are dealt with first, so that accessories common to both rock-types can be referred back to the arkose, in which they were more completely studied.

2. Ousdale arkose

a) Primary magmatic sites

i) Zircon

Zircon is common in most samples and ranges from 10-220 μm in diameter, although it typically averages 60 μm in diameter. Grains may be euhedral but usually have at least one irregular side which truncates the concentric, fine-scale zoning, indicating a detrital origin. Zoning, apparent in transmitted and reflected light, is complex and successive zones may have different crystal forms, resulting in a variation in thickness for individual zones around a crystal (Plate 135). Locally, more than one nucleus of zoning in a zircon indicates the merging of individual crystals during their growth

(Plate 136). Relatively large, outer, incomplete zones may be authigenic overgrowths (Plate 137).

Zircon occurs as individual grains or clusters of grains which may be interstitial or included in quartz, feldspar, TiO_2 , pyrite, iron-oxide or hydrocarbon (Plate 138). It shows no evidence of metamictisation. Zircon gives M to DFT, while ED spectra often show distinct peaks for U, accompanied by minor Hf, Ca and Fe but no Th (Figs. 94 and 95). Less commonly, U is significantly enriched in outer zones/overgrowths relative to the cores (Figs. 96 and 97; Plate 137) and, in one example, a continuous outer zone exhibits an interrupted pattern of U enrichment (Plates 139 and 140) which is reminiscent of the sector zoning in zircon described by Hoffman and Long (1984). Quantitative analyses (Table 63A) reveal 1-2 wt % HfO_2 , which is normal for zircon (Chapter 2, Section 2.b.i.) and which is uniformly distributed, although one grain (Plate 139) contains approximately 2.5 wt % HfO_2 in the core and 1.4 wt % HfO_2 in its outer zone. U and Th are typically below or close to the detection limit and average 0.3 wt % oxide, with either element dominating in a particular analysis. Other analyses reveal an enrichment of U, Th or Y in the outer zones of zircon (Table 63B, Fig. 93). Y is often below detection but ranges up to 0.6 wt % Y_2O_3 in one grain (Fig. 91) and 1 wt % Y_2O_3 in the outer zone of another one (Fig. 92). The latter analysis is very atypical for zircon in the arkose and also gave approximately 1 wt % ThO_2 , compared with approximately 0.1 to 0.2 wt% ThO_2 in the core.

ii) Sphene

Sphene is a rare accessory, only found included in quartz. Subhedral to euhedral, rhombic crystals range from 10 to 100 μm in length and are pale buff or colourless but may exhibit weak pleochroism

(Plates 141 and 142). Spene is associated with M-FFT but ED spectra do not reveal any U. Quantitative analyses of one grain (Table 64) show that U and Th are below or just above the detection limit, while Fe ranges from 6-7 wt % Fe_2O_3 , which is high, compared with analyses of spene by Deer et al. (1966). Low analytical totals (89-96 wt%) may be at least partly due to the presence of OH and/or F.

iii) Apatite

Apatite is a common accessory in the arkose, forming clusters of indistinct, lozenge-shaped crystals which are randomly scattered in the matrix or are isolated in quartz (Plate 128). The colourless, clear crystals range up to 100 μm long and rarely contain fluid inclusions which are oriented parallel to the crystal length and contain vapour bubbles (Plate 143). Larger apatites (up to 1 mm across) are less common and typically form euhedral, hexagonal crystals which show a progressive replacement by metatorbernite at Anomaly 5 (see Section b.iii.). NFT-FFT are associated with apatite (Plate 144) in which U and Th are below the detection limits of the probe and SEM (Table 67; Sample 491, Grain 1, Analysis 1).

b) U minerals

i) Coffinite

Coffinite (Chapter 2, Section 2.a.iii.) has only been identified at Anomaly 2, where it occurs in both surface and borehole arkose. In Borehole 2, the uranous silicate is found down to 5 m depth but is most abundant between 2.5 and 5.0 m, where bulk U contents range from 100-900 ppm. It is also present in more modest amounts throughout Borehole 1, but never attains the maximum amounts found in Borehole 2.

The mineral was first revealed in ED spectra (Fig. 102), since its

optical properties are quite indistinct and it can easily be mistaken for Fe-oxide. Identification has been confirmed by XRD (Table 65) and TEM, and the latter also indicates partial metamictisation of the coffinite lattice as a result of radiation damage (Plates 145 and 146; see Chapter 5, Section 3.a. on metamictisation). Coffinite varies from yellow through dark brown to opaque or can be weakly anisotropic but is normally isotropic. A reflectance of between 7 and 8% (measured in air at 546 nm and 589 nm) slightly exceeds that of quartz or feldspar but is less than hydrocarbon, while faint, brownish internal reflections are often present, especially under oil. Grains, which range from submicroscopic to 500 μm in length, are always anhedral and typically occur as interstitial fillings along grain boundaries and cleavages of feldspar etc. (Plates 147 and 148).

Coffinite is characteristically intergrown with other accessory minerals, particularly TiO_2 (Types 2 and 3 in Section c.ii.) and pyrite (Plates 149-151). BSEI of coffinite from 5.5m depth in Borehole 1 show it to be intimately intergrown with needles of TiO_2 which it locally appears to replace and pseudomorph (Plates 152-154). It is frequently impossible to resolve TiO_2 : coffinite admixtures in ED spectra from the SEM, which display peaks for U, Ti and Si together (Fig. 98). In some spectra, the peak for Si is unusually low or non-existent (Fig. 99), suggesting the presence of a uranotitanate (see Chapter 2, Section 2.a.v.). A similar phenomenon has been noted for coffinite without TiO_2 , in which the Si : U ratio is unusually low or Si is absent (Fig. 100), suggesting the presence of uraninite (Section b.ii.).

Admixtures which cannot be resolved under the SEM have also been noted between coffinite and pyrite, a Cu sulphide (possibly covellite), a LREE-phase and hydrocarbon (Fig. 101). Coffinite may also overgrow

the above phases, together with marcasite, galena, apatite, xenotime and zircon (Plate 155). In some cases, coffinite appears to replace pyrite and hydrocarbon (Plates 149, 150 and 156). At 7.7 m depth in Borehole 1, coffinite is associated with fluorite, together with calcite-marcasite veinlets (Plate 186).

Coffinite gives BFT-DFT, while ED spectra may show only U and Si with trace Ca (Fig. 102). Locally, it also contains significant P, Zr or Th with trace LREE (Figs. 103-106). A particularly P-rich, Th-coffinite is associated with an Fe-oxide alteration of pyrite in quartz, at 0.6 m depth in Borehole 2 (Fig. 104). EPMA is needed to definitely confirm the presence of P or Zr, since peaks for these elements lie very close together in an ED spectrum.

In a sample (802) from 5.5 m depth in Borehole 1, a 60 μm diameter, subhedral, squarish, dark brown ?coffinite (Plate 157) contains significant Zr (Fig. 105). The shape and composition suggest that it may be a pseudomorph after zircon, but the consistency of Zr : U : Si ratios for different analysis spots, together with the homogeneity of the grain in high magnification BSEI photographs (Plate 158) do not indicate the presence of residual zircon fragments. Similarly, analyses of a Zr-rich, coffinite-like phase from 1.9 m depth in Borehole 2 reveal a uniform composition (Fig. 106) and do not indicate the presence of admixed zircon (Plate 159). The 40 μm diameter phase is closely associated with a TiO_2 pseudomorph after sphene and contains approximately equal proportions of U and Zr along with Si and significant Th (Table 66; Sample 476A). Variable Fe in analyses of both Zr-rich grains suggest the presence of Fe-oxide staining.

Quantitative analyses of more typical coffinite from 0.4 m depth

in Borehole 2 (Plates 160 and 161, Table 66) reveal approximately 0.2-2.0 wt % CaO and 0.2-2.9 wt % PbO. Si is very variable and generally depleted in the formula, while analytical totals range from approximately 80 to 90 wt%. The hypothetical (OH) content of the coffinite was estimated from the analyses in Table 66, using the formula $U(SiO_4)_{1-x}(OH)_{4x}$, which implies that the sums of the cations should equal one (see Appendix 4). The results (Table 66; bottom row) indicate that the estimated wt % H₂O hypothetically present as (OH) is often far short of accounting for the poor analytical totals. Possible causes of poor analytical totals and stoichiometry of coffinite are discussed in Chapter 2 (Section 2.a.iii.) and Chapter 5 (Section 3.c.)

ii) ?Uraninite

No uraninite has been identified optically, but its presence is suspected from ED spectra which show high U with no or little Si (Fig. 100). These occurrences are usually associated with coffinite and locally correspond to grains/veinlets showing no internal reflections and a slightly higher reflectance than the coffinite. The presence of uraninite is also suggested by ED spectra for a LREE-phase (Plate 182; Section c.v.) which show widely varying U relative to constant LREE, Ca, Th and Si (Figs. 107-110). Alternatively, there has been preferential absorption of the lower energy Si K X-rays from coffinite by pits, cracks etc. This seems less likely, since many more coffinite grains with poorly polished surfaces give normal U:Si ratios. TEM studies of a coffinite with normal U:Si ratios did not reveal the presence of uraninite (Plate 145).

iii) Uranyl minerals

Metatorbernite (Chapter 2, Section 2.c.) has been identified in surface samples from Anomalies 3, 4 and 5 but the Anomaly 5 examples were studied in most detail. The hydrated copper uranyl phosphate is locally abundant as joint or fracture coatings and discrete grains which may be dispersed or present as trails, 10's mm long, sometimes along Fe-oxide-rich veinlets. The phase is optically distinctive as pale green, anhedral, 80-200 μm diameter grains with a perfect cleavage and vivid indigo to purple, anomalous interference colours (Plate 162).

Large, euhedral, apatite crystals show various degrees of replacement by metatorbernite (Plates 163-166) which often forms hexagonal or tabular, polycrystalline pseudomorphs up to 2 mm long (Plates 167-169). A characteristic ginger coloration is probably due to staining by Fe-oxide which is apparent in many analyses (Table 67 and Fig. 111) and which renders the mineral isotropic. Some pale green crystals show incipient Fe-oxide development along cleavages. The mineral is commonly associated with muscovite and cleavage planes in the two minerals may be coincident, while grain boundaries appear gradational, suggesting the replacement of one phase by the other (Plate 170). Metatorbernite is also associated with sericite in altered feldspar, and it may be overgrown by leucoxene.

BFT clearly reveal the presence of metatorbernite (Plate 169) which, with the exception of Fe, is compositionally pure and only gives U, P and Cu in ED spectra (Fig. 111). Quantitative analyses (Table 67) reveal up to 1% CaO, together with deficient Cu in the formula, while poor analytical totals indicate the presence of 4 to 18 wt % H_2O (by difference). Cu is often less than half the concentration measured in

published analyses, and this could be due to an unmeasured element(s) or, more likely, analytical error. XRD powder patterns for the grain in Plate 168 agree closely with the pattern for ideal metatorbernite, although the d-spacing for (002) is too small (8.52 Å; Table 65).

At Anomaly 5, hand specimens of the most radioactive samples show joint coatings, veinlets and dispersed specks of a dark green, flaky mineral which has been identified as torbernite by XRD. Table 65 shows the d-spacing for (002) to be too small (9.3 Å), perhaps implying a partial dehydration to metatorbernite. A paler, yellow-green mineral associated with the torbernite strongly fluoresces emerald green in ultra-violet light and is likely to be autunite, although this is yet to be confirmed. The autunite commonly forms dispersed specks which are enclosed by rims of non-fluorescing torbernite.

c) Other sites for U

i) Fe-oxide

Secondary Fe-oxide comprises a particularly important site for U in surface samples in which it is abundantly disseminated along grain boundaries and cracks as haematite and goethite. Less commonly, Fe-oxide is associated with the altered remains of biotite or occurs as martite. The Lexans of metatorbernite-bearing surface samples are often saturated with M-DFT associated with Fe-oxide which appears to contain variable amounts of U, since the density of tracks can vary locally between different patches of Fe-oxide. ED spectra reveal a minor U peak, usually as a shoulder to a K peak (Fig. 112). In these samples, thick lines of M-DFT often follow hairline cracks in quartz or feldspar in which there is very little Fe-oxide apparent. The secondary haematite dusting of K-feldspar is never associated with FT.

In the borehole samples of arkose, Fe-oxide is much less common and largely occurs as replacements of pyrite. The pyrite has NFT but the Fe-oxide gives DFT, while the ED spectrum for one analysis reveals a minor peak for U, along with minor Ca, Al, Cu and major Si, S and Fe (Fig. 113). Fe-oxide also occurs as veinlets, often in association with TiO_2 .

ii) TiO_2

TiO_2 is a ubiquitous, secondary accessory in surface and particularly borehole samples in which, spatially, it is often the dominant source of FT. Three morphological types have been recognised:

1. Subhedral, generally squarish TiO_2 has some irregular or "stepped" margins, possibly reflecting cleavage planes (Plate 171). Grains range from 40 to 500 μm across but are usually between 100 and 200 μm and typically occur as small clusters. Interference colours are usually masked by the blue-grey or reddy-brown colours of the mineral but interference figures show the birefringence to be extreme and the mineral to be uniaxial negative. This indicates anatase which is confirmed by XRD (Table 65) and TEM studies. The anatase has a reflectance of approximately 20 % and often contains abundant, white to yellow internal reflections, although these may be absent. Anatase usually occurs interstitially but small inclusions sometimes occur in muscovite, deforming the cleavage, indicating an authigenic origin. Anatase is associated with N-DFT, although U is below detection on the probe and SEM.

2. Leucoxene (finely divided TiO_2) is commonly disseminated along grain boundaries (Plate 172), cleavages in muscovite, in fractures and associated with the remains of altered biotite. It comprises

submicroscopic particles but randomly oriented needles are sometimes resolved under high power, in reflected light. Abundant, white internal reflections are diagnostic and may be stained yellow or brown due to admixed Fe-oxide. Leucoxene is associated with M-DFT but U has not been detected on the probe or SEM. Rare grains comprise TiO_2 as trellis patterns (Plate 173). These may have replaced ilmenite lamellae in magnetite, which has since been removed.

3. Euhedral, diamond-shaped aggregates of TiO_2 range from 50 to 1000 μm long and are common, though not as abundant as morphology types 1 and 2. They are presumed to be pseudomorphs after sphene, although no sphene of this size survives. The aggregates comprise fine crystals of TiO_2 , possibly anatase, along the margins which enclose irregular cores of leucoxene, quartz, feldspar and, rarely, calcite (Plate 174) or fluorite. Small zircons are sometimes included in the pseudomorphs (Plate 175) which are locally associated with the remains of altered biotite. The distinctive grains occur interstitially or are included in quartz or feldspar, often along hairline fractures. Clusters occur locally and, in one example, two pseudomorphs are intergrown. The pseudomorphs are invariably associated with M-DFT. U is usually below detection on the SEM but ED spectra sometimes give minor peaks for U as "shoulders" to peaks for K (Fig. 114).

iii) Hydrocarbon

Hydrocarbon is distinctive as opaque, globular masses up to 2 mm across (Plate 176) or as interstitial networks or veinlets up to 1.5 mm long. The reflectance is low but slightly exceeds that of coffinite and the colour varies from yellowish to greenish grey. Hydrocarbon is usually isotropic but sometimes exhibits a weak, undulose anisotropy.

An interstitial patch of hydrocarbon, 1 mm across, was found in

surface arkose at Glen Loth (grid ref. 937 127). Most hydrocarbon was found at Anomaly 2 in samples from both boreholes, but it is particularly common between 2.5 and 5 m depth in Borehole 2, where it is closely associated with coffinite. The coffinite is admixed with the hydrocarbon and forms overgrowths and replacements (Plate 156). Hydrocarbon is invariably associated with pyrite and marcasite which overgrow, cross-cut and replace it (Plate 176), while chalcopyrite forms numerous, small (<30 μm diameter), anhedral inclusions. TiO_2 commonly forms inclusions in hydrocarbon and, in one grain (Plate 177), it comprises abundant, irregular strands. In sample 771, hydrocarbon is associated with more limonite-stained areas of arkose and locally shows replacement by a limonite-leucoxene admixture. Other inclusions comprise detrital zircon (Plate 138) and authigenic xenotime (Plate 178).

Hydrocarbon is usually associated with D-BFT and ED spectra show significant, though variable U, S, K, Ca and minor Si, Fe, Ti and Pb (Figs. 115-116). It is likely that much of the U in hydrocarbon is present as admixed coffinite, since U varies directly with Si, and U alone is locally undetected. Other analyses show that the Si concentration is insufficient to account for all the U as admixed coffinite and U may also be adsorbed or form an organo-metallic complex (see Chapter 2, Section 2.e.iv.). Quantitative analyses revealed a uniform composition:

4.56 wt % UO_2 , 0.68 wt % SiO_2 , 1.30 wt % S, 4.30 wt % K_2O ,
1.82 wt % CaO, 0.62 wt % FeO.

The Ca and K probably originate from inorganic impurities, although Al and Si are too low for these to be clay minerals. Fe and S are probably present as pyrite, while excess S may be chemically bonded to the H and C.

iv) Xenotime

Xenotime is a very rare accessory which has only been identified in sample 771, where it forms anhedral, granular inclusions up to 160 μm long in hydrocarbon (Plate 178). It may be intergrown with coffinite or overgrown on zircon (Plate 179). Trace U has been detected in ED spectra, along with significant HREE (Figs. 117-118), but higher concentrations of U are correlated with high Si and probably represent contamination of analyses from coffinite.

v) LREE-phase(s)

Although fairly widespread, the LREE-phase(s) is easily overlooked and has so far only been identified using the SEM. The difficulty in observing the phase optically arises from its small size (usually approximately 20 μm in diameter) and poorly crystallised and polished nature and from the fact that it is often intimately associated with other phases, such as TiO_2 , coffinite (Fig. 120) and Fe-oxide. Under the SEM, it is apparent as bright, anhedral grains (Plates 180-182) which are usually associated with areas of DFT.

ED spectra (Figs. 107-110 and 119-121) reveal major peaks for Ce which exceed those for La, although La peaks were not observed in one grain. Ca is always present and, where it is high relative to the LREE (Fig. 121), the phase could be a fluorocarbonate of Ca and LREE, such as parisite or synchysite. Usually, the Ca peak is much lower, suggesting the phase is the LREE-fluorocarbonate, bastnaesite or the LREE-fluoride, fluocerite. Neither U nor Th have been detected in the Ca-LREE phase but quantitative analyses have revealed up to 1.13 wt % UO_2 and 6.6 wt % ThO_2 in the Ca-poor LREE phase.

vi) Unidentified sites

In many cases, FT cannot be correlated with definite mineralogical sites for U. This is particularly true in the mineralised, surface samples where extensive areas of DFT correspond to the matrix of fine-grained quartz, feldspar and unidentified material (Plates 183 and 184). ED analyses have revealed major Al, Si, Ti and Fe with minor K and Ca from quartz, feldspar, TiO_2 and Fe-oxide, with trace U occurring as a small shoulder to the peak for K (Fig. 122). The U could be held within the TiO_2 and/or Fe oxide. Uraniferous fractures, 10-20 μm wide and several mm long cut altered K-feldspar and appear to be filled with sericite, and possibly clay. ED spectra of fractures associated with DFT have revealed major Si, Fe, S and Ti along with minor Al, K, Ca and U shoulders to the K peak (Fig. 112).

In the vicinity of coffinite, hydrocarbon or metatorbernite, DFT may be associated with grain boundaries or fine cracks in quartz, in which there is no obvious site for the U (Plate 185). Similarly, M-DFT occur along thin veinlets of apparently pure quartz or calcite (Plate 186). FT are not usually associated with fluorite but, in rare cases, point sources of MFT occur in the dark purple centres of fluorite cubes. These could originate from tiny opaque inclusion, possibly of TiO_2 or Fe-oxide.

At 7.8 m depth in Borehole 2 (Sample 774), M-DFT are associated with anastomosing marcasite veins up to 3 mm thick (Plate 187) and probably related to shearing logged at this depth (Fig. 88). Close study shows that the FT do not come from the marcasite itself, but rather from point sources in the matrix between the marcasite polyhedra. Some of the DFT are associated with 30 μm zircons scattered in the matrix but most cannot be correlated with any specific phase.

3. Helmsdale granite

a) Primary magmatic sites

i) Zircon

Zircon is a widespread accessory of similar abundance and character to zircon in the arkose and is usually included in the altered remains of biotite, in martite or in TiO_2 aggregates. It ranges from 10-120 μm in diameter and, in common with grains in the arkose, irregular edges of subhedral zircons frequently truncate the fine, concentric zoning. It invariably gives M to very DFT.

ii) Sphene

As in the arkose, sphene forms rare, euhedral inclusions in quartz, 60-150 μm long and associated with F-MFT. One lozenge-shaped example gives DFT point sources at either end of the crystal (Plates 188 and 189).

iii) Apatite

Apatite is less common than in the arkose and forms isolated or clustered, lozenge-shaped crystals 40-160 μm long or euhedral, hexagonal grains up to 400 μm across. All apatites give FFT but U was not detected in the ED spectrum of a 70 μm diameter, hexagonal grain from Sample 46B.

b) Other sites

i) Fe-oxide

Fe-oxide is abundant and occurs as martite and disseminated patches or veinlets of haematite/goethite, usually associated with altered biotite. The martite grains are typically subhedral to euhedral, polygonal in shape and measure 80-700 μm across. Martite is

bluish-tinted, light grey with a reflectance of approximately 30 % and usually exhibits strong blood-red internal reflections which are confined to the grain edges or along lamellae. In distinctly anisotropic grains, a polycrystalline, lamellar structure is apparent. Grains are included in quartz, disseminated Fe or Ti oxide and altered biotite, which may also be partly enclosed by martite. The accessory mainly occurs in alteration zones or reddened wallrock but is also found in the borehole samples of least-altered granite. M to very DFT are uniformly distributed throughout martite or may be limited to the grain boundary (Plate 190).

In the reddened granite at Location 28, haematite progressively replaces or completely pseudomorphs pyrite cubes up to 2 mm across. DFT are associated with the haematite but none are associated with the pyrite (Plates 191 and 192). Most other DFT in this sample are associated with haematite-filled cracks and veinlets, some of them 10's mm long and 10's μm wide, although U has not been detected in ED spectra. As in the arkose, FT are not associated with the haematitic dusting of K-feldspar, although MFT are associated with particularly dense patches of Fe-oxide in feldspar from sample 13A. In the reddened wallrock of alteration zones, M-DFT are associated with Fe-oxide staining which is interstitial or occurs with altered biotite, and with haematite veinlets which locally show variations in the density of FT along their length. The alteration zones themselves tend to be bleached and contain less Fe-oxide than the wallrock, although U-enriched alteration zones (e.g. sample 39B) contain abundant Fe-oxide which gives DFT.

ii) TiO₂

Like the arkose, both surface and borehole samples of granite contain abundant TiO₂ as subhedral anatase, disseminated leucoxene and diamond-shaped pseudomorphs after sphene. Most TiO₂ is included or overgrown on biotite in which the cleavage is locally deformed by inclusions of TiO₂ pseudomorphs after sphene (Plate 193). TiO₂ generally gives rise to FT but these range from FFT to very DFT, with no obvious correlation between TiO₂ morphology and U content. In some TiO₂ pseudomorphs, however, the well-crystallised anatase contains less U than the finer-grained TiO₂ or leucoxene (Plates 194 and 195). ED spectra reveal trace Si, Nb and Fe but no U in anatase from sample 46B. Similarly, there is no consistent difference between the FT densities of associated TiO₂ or Fe-oxide and the U content can predominate in either phase. Intimate mixtures of TiO₂ and Fe-oxide are common as pseudomorphs after sphene and give DFT. In some alteration zones, the bulk of FT are associated with TiO₂ (Plates 196 and 197), due to the selective removal of Fe-oxide, which tends to be concentrated in the reddened wallrock.

iii) Phyllosilicates

There is a general association of FT with altered biotite in most samples of granite but it is the associated Fe-oxide staining and not the bleached or chloritised mica itself, that actually gives rise to the tracks. Alteration zones are composed largely of quartz and pale yellow sericite which has replaced the feldspar and biotite and is locally accompanied by coarse muscovite flakes, while wallrock samples often show an incipient development of sericite. The pale yellow coloration may be due to Fe-oxide staining, since an alteration zone at

Location 47 contains colourless sericite, whereas the altered wallrock contains pale yellow sericite. Both varieties of sericite are locally associated with uniformly distributed, very FFT, indicating very low concentrations of U (Plates 196, 197). Clay- and sericite-filled veinlets in the wallrock of an alteration zone at Location 53 are not associated with FT. The XRD trace of material from a uraniferous, clay-rich, alteration zone at Location 7 (Plate 127) revealed only quartz and illite.

iv) Hydrocarbon

In polished blocks, the uraniferous hydrocarbon at Location 28 appears yellowish-grey, with irregular areas of subtly varying reflectance and numerous voids. Inclusions of quartz, pyrite and marcasite are apparent in reflected light and have been confirmed in XRD traces (Table 65), while BSEI photographs and ED analyses have further revealed common, 20-40 μm diameter inclusions of galena. ED analyses of the hydrocarbon itself detected evenly distributed U, Fe, S, Cu, Si and Ca (Fig. 123) and quantitative analyses gave;

0.6-0.8 wt % U; 0.4 wt % Fe; 0.4-0.5 wt % S; 0.15-0.2 wt % Ca and 0.02 wt % P and K.

4. Summary of U distribution

In both the granite and arkose, high concentrations of U are associated with zoned, anhedral zircon, whereas apatite and rare sphene contain much lower U. In the granite, much of the U is associated with secondary Fe-oxide and TiO₂ in which U contents locally vary. The Fe-oxide occurs as martite, disseminated patches

and veinlets of haematite/goethite and, locally, as a replacement of pyrite. TiO_2 occurs as anatase, pseudomorphs after sphene and disseminated leucoxene which may be admixed with Fe-oxide. In U-enriched alteration zones and the reddened wallrock, Fe-oxide or clay minerals are the main site for U, while sericite contains negligible U. In alteration zones which have been bleached, the U content is much lower and is held dominantly in TiO_2 .

Fe-oxide and TiO_2 also account for the generally high "background" level of U in the arkose, but coffinite and metatorbernite are found in samples with the highest U contents at Anomalies 2 and 5 respectively. The coffinite has an interstitial, late-stage appearance and is generally found in "reduced" areas of arkose, in association with sulphides, hydrocarbon and TiO_2 . Locally, it contains high Th and P and appears to demonstrate substantial solid solution with $ZrSiO_4$, while qualitative analyses suggest the presence of trace amounts of uraninite. Rare xenotime is only found with hydrocarbon, while a small, poorly-crystallised LREE-phase(s) is widespread but of low abundance and contains variable amounts of Ca, Th and U.

Minor amounts of hydrocarbon are locally found in the vicinity of the Helmsdale fault, both in the granite and arkose and significant U contents are at least partly adsorbed or present as an organometallic complex. Distinctive metatorbernite in oxidised, surface arkose is late-stage and occurs as disseminated grains, veinlets and replacements of apatite. It is locally accompanied by joint-coatings and dispersed grains of torbernite and autunite. The location of disseminated U associated with the matrix, grain boundaries, cracks and veining in the mineralised arkose has not been determined but TiO_2 , Fe-oxide and phyllosilicates are likely hosts.

Chapter 8 Discussion and Conclusions on the Helmsdale Material

1. Introduction

The results in Chapter 7 confirm earlier FT studies which have shown that U in the granite is largely disseminated in secondary Fe-oxides and along grain boundaries (Tweedie, 1981; Bowie et al., 1973). FT point sources are associated with small zircon crystals, as noted by Bowie et al. (op. cit.), who also found an association with chloritised biotite and U-enriched apatite, although the last two observations were not confirmed in the samples studied here.

The results from the Ousdale arkose largely agree with those of Bowie et al. (1973) who found concentrations of U with marcasite veining in the borehole samples and in clay-filled, late-stage cracks in the mineralised, surface samples. They also noted concentrations in the fine-grained groundmass of both borehole and surface material but "disseminated fluorite and resistate minerals" are unlikely to contribute much to these. The occurrences of metatorbernite replacing apatite at Anomaly 5 and of uraniferous hydrocarbon near the Helmsdale fault (see Chapter 6) were reconfirmed.

Another secondary site for U, in both granite and arkose, is TiO_2 which is likely to be a dominant contributor to bulk U in unmineralised, Fe-oxide-poor samples e.g. from the borehole arkose or from the bleached alteration zones in the granite. Although Tweedie (1981) noted an association of high-density, FT point sources with altered sphene in the granite, previous studies have not assessed the role of TiO_2 , in general, as a site for U in the granite and arkose.

Coffinite is likely to be a major contributor to bulk U in the mineralised samples of arkose at Anomaly 2 but it has not previously

been noted at this locality. Other phases which have not been previously described from the arkose and which are present in only trace amounts, include the LREE-phase(s) and xenotime.

2. Crystallisation of the granite

The eroded appearance of zircon from the granite suggests that detrital grains were inherited from a precursor sedimentary rock which had previously been assimilated by the granite. This origin is indicated by the U-Pb ages of zircon xenocrysts which average approximately 2050 my (Pidgeon and Aftalion, 1978). The presence of euhedral zircon and possible overgrowths of zircon suggests that new zircon also formed during crystallisation of the granite.

The enrichment of $U \pm Th \pm Y$ in the outer zones of some zircons may reflect an accumulation of these incompatible elements in the melt during crystallisation of the host rock. U-enriched outer zones which are incomplete and asymmetrical, either represent late overgrowths, formed during the crystallisation of the Helmsdale granite or much older zone relicts which were partially removed during deposition of the precursor sedimentary rocks. The U contents of some zircons exceed the range of 600-800 ppm U measured by Pidgeon and Aftalion (1978), although the values in Table 63 should be treated with caution since U is close to the detection limit of the microprobe.

In both the granite and arkose, sphene is rarely preserved and only when enclosed in quartz, whereas TiO_2 pseudomorphs after sphene are common in both rocks and tend to be larger and interstitial or lie along hairline cracks in quartz or feldspar. The alteration of sphene to $TiO_2 \pm$ calcite is well documented in other granites (Chapter 2, Section 2.e.i) where it has been attributed to hydrothermal processes.

The post-magmatic fluids responsible for this alteration must have been pervasive but it is not clear whether they acted before or after the deposition of the arkose.

The low U contents of unaltered sphene, together with the variable contents of the pseudomorphs, suggest that U was adsorbed on to the TiO_2 from circulating fluids and was not inherited from the original sphene. However, it is possible that the interstitial sphenes, which are now replaced, crystallised later than those preserved in quartz and originally contained higher U, since later generations of sphene tend to be U-rich (Chapter 2, Section 2.b.vi.). The deformation of the cleavage in biotite around an inclusion of a large TiO_2 pseudomorph suggests that this later generation of sphene crystallised after the biotite (Plate 193).

Euhedral, hexagonal apatite is found in both the granite and arkose and is of primary magmatic origin, according to Tweedie (1981) who believed the smaller apatite "needles" to be of secondary origin. Modal estimates of Tweedie (1981), based on whole rock Zr and P_2O_5 , indicate that the maximum contribution from zircon and apatite to the whole rock U content of the granite is approximately 1 ppm. The contribution from sphene must be even lower, considering its rarity and low U content.

3. Alteration of the granite

The Ti in anatase and leucoxene may have been released from the alteration of primary biotite and ilmenite by pervasive, post-magmatic fluids. Ilmenite was not identified in the samples of granite and arkose examined but it was noted by Tweedie (1979) and it may originally have been associated with the magnetite which has now

largely been replaced by haematite. The remobilisation of Ti from biotite is suggested by a close, spatial association of altered biotite with anatase and leucoxene (along cleavages). Biotite, together with magnetite and ilmenite, are also likely sources for the large amounts of secondary Fe-oxide in the granite and surface samples of arkose. This remobilisation of Fe-oxide must have occurred on a scale of several metres or more, since the large amount of haematite and goethite in particularly reddened samples could not all have come from locally altered, primary accessories. TiO_2 is more abundant than Fe-oxide in the borehole samples of arkose, compared with the granite. This may be due to the removal of biotite, ilmenite and Fe-oxide and the accumulation of the less mobile TiO_2 break-down products during and/or after deposition of the arkose. The presence of admixtures of Fe and Ti oxides in the granite indicates the contemporaneous remobilisation of Fe and Ti.

FT in the granite and arkose are mainly associated with Fe- and Ti-oxides, although concentrations of U are below or close to the detection limit of the microprobe and SEM. These low concentrations of uniformly distributed U are unlikely to represent inclusions of a U mineral but are probably adsorbed on the Fe- and Ti-oxides which are efficient concentrators of U (Chapter 2, Sections 1.c., 2.e.i. and 2.e.ii.). The confinement of FT to the margins of some martite cubes (Plate 190) suggests that U was adsorbed after the replacement of magnetite by haematite. Elsewhere, FT are uniformly distributed throughout martite, other Fe-oxides and TiO_2 , suggesting that U was adsorbed during the deposition of these phases. Experimental studies (Chapter 2, Section 2.e.i) have shown that concentrations of U, reaching up to 100's ppm, are initially adsorbed on to colloidal

Ti(OH₄) and Fe-oxyhydroxides which eventually crystallise as uraniferous TiO₂ and Fe-oxide respectively. The local variations in U concentrations associated with Fe-oxide and TiO₂ may reflect differences in their sorptive capacity e.g. variable surface area to volume ratios or differences in their accessibility to the mineralising fluids via fractures, grain boundaries etc..

U concentrations attain 100's ppm in some zones of localised sericitic alteration at Helmsdale, while a similar association of U enrichment with sericitisation has been noted in other granites (Chapter 2, Section 2.e.iii.). Although sericite is able to adsorb low concentrations of U, most of the U in the alteration zones is held in Fe-oxide and TiO₂, with sericite itself contributing a very minor amount. Presumably, the U was introduced along with the K-rich fluids responsible for the sericitic alteration. Cathelineau (1983) studied clay-rich, hydrothermal U ore bodies in French leucogranitic rocks and concluded that K-rich fluids were favourable for the transport and deposition of U. The U was deposited as pitchblende whereas, at Helmsdale, there is no obvious U mineral associated with the uraniferous, clay-rich alteration zones. It is likely that the U is held in illite which has a high sorptive capacity for U or can incorporate it in the interlayer positions of the clay structure (Chapter 2, Section 2.e.iii.).

At Location 28 minor hydrocarbon, which appears to have been introduced during localised sericitisation, may be genetically related to other occurrences of hydrocarbon close to the Helmsdale fault in the Ousdale arkose. The high concentrations of uniformly distributed U are likely to be adsorbed or present as an organometallic complex, since no inclusions of a U mineral are evident.

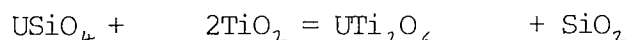
4. Mineralisation of the arkose

Since the abundance of coffinite, the only U mineral identified in the borehole samples at Anomaly 2, is roughly correlated with the bulk U content, it seems likely that this mineral accounts for much of the U in the arkose. A very approximate modal analysis was carried out on a sample of arkose containing relatively small amounts of coffinite, in order to facilitate grain counting and measurement. The results (Appendix 7) indicate that coffinite may account for most of the bulk U content (60 ppm) of Sample 471, with the remaining U presumably held in hydrocarbon, TiO_2 , Fe-oxide and zircon.

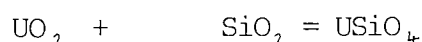
The coffinite mineralisation is clearly epigenetic and, from overgrowths and replacement textures, appears to have succeeded TiO_2 and hydrocarbon deposition. TiO_2 -coffinite intergrowths and replacements have been reported elsewhere (Chapter 2, Section 2.a.iii.) but no explanations of this association have been offered. One possibility is that migrating, U-bearing solutions were adsorbed and concentrated by colloidal $Ti(OH)_4$ or "titanogel" which subsequently crystallised as coffinite plus TiO_2 . The abundant TiO_2 -U associations in the arkose may represent the initial stages of this process, where the U activity was insufficient for the crystallisation of coffinite. The process differs from the "Pronto Reaction" of Ramdohr (1957) in which U-bearing solutions react with TiO_2 or Ti-bearing solutions with uraninite to give a "brannerite-type" mineral of variable composition. Examples of the Pronto Reaction have been widely documented in quartz pebble conglomerates, sandstones and altered granites (Chapter 2, Section 2.a.v.)

At Ousdale, brannerite has not been definitely identified,

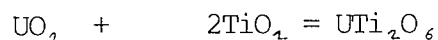
although some SEM spectra are open to interpretation as indicating a U-Ti phase (Fig. 99). The problem of why coffinite + TiO₂ formed in preference to brannerite or uranotitanates of variable composition can be addressed using the system UO₂-TiO₂-SiO₂ as a model for the more complex, natural geochemistry. Thermodynamically, at fixed pressure and temperature, in this 3-component system, the chemical-potential diagram of μ_{TiO_2} versus μ_{SiO_2} (or $\ln a_{\text{TiO}_2}$ versus $\ln a_{\text{SiO}_2}$) contains bivariant fields, each of which is defined by the stability of a single phase (Fig. 124). Chemical equations can be written among the idealised mineral compositions:



(Coffinite) (Brannerite)



(Uraninite)



The coefficients of TiO₂ and SiO₂ define the slopes of field boundaries in the diagram, but leave indeterminate the positions of their intersection (which, in principle, will change if pressure and temperature are changed).

At Ousdale, the occurrence of intergrown coffinite and anatase in quartz is interpreted as an equilibrium assemblage at saturated SiO₂ and TiO₂ (marked on Fig. 124a). Complications arise through the substitution of other components in the natural system e.g. U⁶⁺, H₂O, Th, Zr, P. For example, the assemblage quartz + uraninite + coffinite is stable if sufficient U⁶⁺ substitutes in uraninite (Chapter 2, Section 2.a.iii.). If coffinite is hydrated, it will be destabilised by low $a_{\text{H}_2\text{O}}$ or high temperatures. The restriction of most coffinite to low-temperature deposits e.g. Colorado Plateau-type, further suggests

that coffinite stability is favoured by low-temperatures which must therefore have prevailed in the mineralised arkose.

At higher temperatures, the point of SiO_2 and TiO_2 saturation in Fig. 124a will move into the fields of brannerite and uraninite which are stable at metamorphic and magmatic temperatures respectively (Figs. 124b and c). Brannerite or uranotitanates of variable composition may also form at low temperatures (e.g. in the Blind River-Elliot Lake or Witwatersand deposits). Fig. 124a suggests that brannerite may only form at low temperatures metastably, where the TiO_2 is oversaturated (i.e. the activity of TiO_2 exceeds that for anatase stability).

Metastably high a_{TiO_2} may occur in the vicinity of amorphous, Ti-rich gel or crystalline TiO_2 . Discussions of brannerite (Chapter 2, Section 2.a.v.) suggest that Ti-rich gel may be a precursor to the formation of brannerite, which is frequently associated with altered, detrital Fe-Ti oxides. Metastably high concentrations of TiO_2 are able to accumulate as a result of the low mobility of Ti, whereas the high solubility of uranyl complexes allows the migration of U to areas of high a_{TiO_2} , where brannerite can form.

The above argument suggests that brannerite did not form at low temperatures in the Ousdale arkose because localised overconcentrations of Ti were absent. The redistribution of Ti, preventing the accumulation of high a_{TiO_2} , is suggested by the replacement of TiO_2 by coffinite. Furthermore, the presence of F (indicated by fluorite in the arkose) can enhance the mobility of Ti (Alderton *et al.*, 1980).

In Borehole 2, coffinite mineralisation is greatest between 2.5 and 5 m depth where it is associated with sulphides and hydrocarbon. Bulk U contents are 100 ppm or greater from 2m depth down to the shear at 7.5m depth (Fig. 88). This spatial association of the mineralisation

with the shear may have a genetic significance. Organic-rich fluids, ascending the shear, could have permeated along the bedding of the porous arkose, depositing the hydrocarbon. This provided a suitable reducing environment for the precipitation of coffinite and sulphides from younger, oxidising solutions (Fig. 125). Alternatively, the U may have been transported in the reducing fluids with the organic matter, perhaps as uranous-organic complexes, which later precipitated as the coffinite-hydrocarbon admixtures. An association of FT with marcasite veining at the depth of the shearing (Plate 187) lends support to the introduction of U along this channelway.

At Borehole 1 (Fig. 88), the coffinite mineralisation attains a lower grade and is more uniformly dispersed. Sulphides and hydrocarbon are much less abundant, whereas fluorite and calcite are more common than in Borehole 2. In the absence of faulting to act as a channelway, the solutions gave rise to the more disseminated mineralisation, penetrated by Borehole 1. The presence of fluorite and calcite suggests that F and CO₂ were available for complexing with uranyl.

The coffinite is evidently younger than the Lower Devonian arkose but, in the absence of geochronological data, it is unclear when the mineralisation was introduced. Gallagher et al. (1971) believe the U was introduced before the deposition of the overlying Middle Old Red Sandstone Badbea breccia, which is unmineralised. Other evidence suggests that coffinite is much younger than this. Ramdohr (1961) found that Miocene-Recent coffinites were fresh and non-metamict, whereas Precambrian-Miocene coffinites were metamict or pseudomorphed by quartz and pitchblende. Diffraction patterns, obtained from the Ousdale coffinite by XRD and TEM (Plate 145), show that the crystal lattice is only partially metamict, suggesting that the coffinite is pre-Miocene but may be considerably younger than Lower Devonian in age.

Oldest coffinites are dusted by numerous inclusions of radiogenic galena (Speer, 1982) but no galena was observed in the Ousdale coffinite, although low amounts of unevenly distributed Pb were measured (up to 2.9 wt % PbO). It is possible that any radiogenic galena has since been leached from the coffinite.

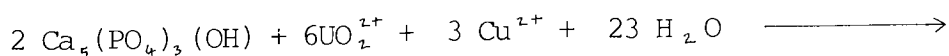
It appears that there was a limited mobilisation of Zr, P and Th, along with the U, judging from the high contents of these elements in some coffinite analyses and ED spectra (Table 66, Figs. 103-106). Zr was probably derived from zircon which is rarely overgrown and appears to be replaced by coffinite (Plate 155). The P could have come from apatite which is locally overgrown by coffinite. The source of Th is unknown, since no Th-rich, primary accessories have been identified in the arkose, although thorite and monazite have been reported from the granite. Zircon is an unlikely source for the Th, as its content of this element is very low (Table 63A) so that the Th was probably introduced, together with the U.

Trace amounts of Y and REE were also introduced during the mineralisation, giving rise to the xenotime and LREE-phase(s). The occurrence of xenotime as inclusions in the hydrocarbon is reminiscent of similar associations noted by Rahman (1979) and Parnell (1985) (see Chapter 2, Section 2.e.iv.). Its morphology, spatial restriction to secondary hydrocarbon and overgrowth on zircon suggest that xenotime is authigenic and not of primary magmatic origin. Although it is locally overgrown by coffinite, xenotime itself contains very low U and it may have been introduced before the U. The Ca-poor LREE-phase, on the other hand, contains significant U and Th and is locally intergrown with coffinite, suggesting that it crystallised during the U mineralisation and, thus, after the xenotime. The hydrocarbon is locally overgrown by leucoxene which is also included in it, suggesting that Ti

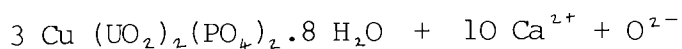
was mobile during the mineralisation of the arkose.

Like other U^{6+} minerals, the uranyl phosphates at Anomalies 3, 4 and 5 characteristically form under supergene, oxidising conditions, usually from the alteration of primary U^{4+} minerals (Chapter 2, Section 2.c.). In this respect, it is significant that the uranyl phosphates have only been identified in weathered, surface samples of arkose and Bowie *et al.* (1973) attribute their origin to weathering processes. If the uranyl phosphates are secondary, there is no evidence of the primary U mineralisation, which may lie some distance away. Transport of uranyl from the site of weathering is further suggested by veining of metatorbernite and by the restriction of the mineralisation to a closely jointed and altered arkose horizon (Gallagher *et al.*, 1971) which may have acted as a channelway to the mineralising solutions. It is possible, however, that the minor pyrite and hydrocarbon described from Anomaly 5 (Gallagher *et al.*, *op. cit.*) were associated with an earlier phase of reduced U mineralisation that was later oxidised.

The exclusive mineralisation of U as uranyl phosphates at Anomalies 3, 4 and 5 suggests that U was carried as uranyl-phosphate complexes, which predominate over other inorganic complexes of uranyl in waters of pH 4 - 7.5 at concentrations of CO_2 , U^{6+} and PO_4 found in typical, natural waters (Dongarra, 1984). Gieré (1986) described the transport of U^{4+} and other high valence cations as PO_4^{3-} complexes. The PO_4^{3-} may have come from primary magmatic apatite but the replacement of apatite by metatorbernite suggests that dissolved UO_2^{2+} and Cu^{2+} migrated to the PO_4^{-3} which did not go into solution:



(Apatite)



(Metatorbernite)

A similar association of torbernite in apatite has been described in mineralised, altered granite and arkose from Ireland (Ashworth, per. comm.)

Metatorbernite has a lower H₂O content than torbernite and can be obtained by boiling torbernite in water or by desiccating it at ordinary temperatures (Fronzel, 1958). At Ousdale, metatorbernite either formed by the alteration of torbernite or it crystallised directly from fluids which were hotter than those responsible for the torbernite. Crystallisation from hot fluids might imply a hydrothermal rather than a supergene origin to the metatorbernite.

Surface samples from Anomaly 2 (in the Ousdale valley) contain coffinite which shows no sign of oxidation to secondary uranyl minerals. Active erosion by Ousdale Burn may have prevented the accumulation of secondary uranyl minerals, as surface samples from the valley are much less weathered than those from Anomaly 5.

5. Paragenesis of U-sites in the granite and arkose

Fig. 126 relates the paragenesis of U-bearing phases to the crystallisation and hydrothermal alteration of the granite and to the mineralisation of the arkose. It is difficult to correlate the formation of different U-sites in the granite and arkose and a number of assumptions have been made in Fig. 126:

- a) Mineralisation of the arkose occurred after the hydrothermal alteration of the granite. The two events may have occurred concurrently but there was more likely to have been a time-gap between the release of U from the granite during its alteration and the mobilisation of this U along faults to the arkose. If this assumption is true, then the hydrocarbon associated with localised alteration of

the granite at Ord Burn (Location 28 on Fig. 85) must be older than the hydrocarbon associated with coffinite mineralisation in the arkose, although they may still share a common source (see Chapter 6, Section 5).

- b) The formation of secondary TiO_2 and Fe-oxide occurred after the deposition of the arkose, as well as during the alteration of the granite. Although much of the TiO_2 in the arkose was probably inherited from the granite, the presence of leucoxene overgrowing metatorbernite (Plate 168), hydrocarbon and other secondary accessories in the arkose suggests that Ti continued to be mobilised.
- c) U in secondary sites, such as Fe-oxide, TiO_2 , phyllosilicates and hydrocarbon, was incorporated shortly after or during the formation of these products. However, it is possible that U was adsorbed on to these sites from modern-day, circulating groundwater. Gallagher et al. (1971) believe U, from circulating groundwater, to have been adsorbed on to the clay alteration zones which do not, in their opinion, necessarily represent altered, uraniferous veins.
- d) The uranyl phosphates are presumed to be secondary, having been remobilised from a primary U mineral, such as coffinite, although there is no direct evidence of this (i.e. coffinite altering to uranyl phosphate).

Chapter 9 Summary and Discussion

1. Introduction

The Ririwai and Helmsdale granites have very different geological settings and share little in common, with respect to their mineralogical sites for U and Th. Despite the obvious differences, both Ririwai and Helmsdale are characterised by alteration processes associated with the remobilisation of radioelements. At Ririwai, these processes included albitisation, microclinisation and greisenisation which, according to fluid inclusion data (Kinnaird *et al.*, 1985b), were associated with temperatures in the range 260-460°C. At Helmsdale, the granite was subjected to haematitic and potassic alterations in the low to medium temperature range, 100-400°C (Tweedie, 1979). In the Ousdale arkose, low temperatures were probably associated with coffinite, hydrocarbon, and TiO₂-bearing mineralisation, while the secondary uranyl phosphates may have had a supergene origin.

Rather than attempt a direct comparison of the two granites, the data and interpretations from two areas of differing alteration and temperature regimes will be summarised as a contribution to an understanding of the mineralogy and geochemistry of U, Th and associated elements in general.

2. Ririwai

The Ririwai biotite granite is unusually enriched in both U and Th, which are held in primary thorite, zircon, monazite and pyrochlore. The compositions of zircon and its inclusions suggest that growth of this accessory was discontinuous and records localised changes in the precipitation of haematite, thorite, Hf and other trace elements from

the melt. During post-magmatic processes, the primary accessories were altered and dissolved, while new U- and/or Th-bearing accessories crystallised. Pervasive fluids affecting the biotite granite altered zircon to a metamict variety, enriched in Th, U, Y, P, Fe, Mn and Ca, along pre-existing zones and cracks. Locally, thorite compositions were modified, resulting in extreme enrichments of Zr, sometimes accompanied by high Y contents which tend to be concentrated towards grain margins. Monazite was altered to an unidentified LREE-phase, probably bastnaesite or fluocerite, with loss of much of the Th and fractionation of the LREE. Low temperature, late-stage fluids locally precipitated Zr-rich coffinite, along with sphalerite and molybdenite.

More intense, localised alteration and albitisation completely remobilised primary accessories and gave rise to a distinctive generation of haematite- and uranothorite-enriched zircon (Type 2) with clear, Hf-enriched rims (Type 1). In the albitised samples, Type 2 zircon overgrew or replaced a U-enriched, clear, metamict zircon variety (Type 3). Zircon was later replaced by feldspar, REE-rich fluorite and uranothorite which, together with xenotime, also overgrew the zircon. During albitisation, U was remobilised and concentrated in uranothorite and rare Ta-?pyrochlore, but it is not clear whether there was a nett enrichment in U.

U was also remobilised, but not necessarily enriched, during the later, more restricted process of microclinisation in the Ririwai lode, giving rise to Y-coffinite and uranothorite. Subsequent greisenisation locally remobilised or altered zircon and deposited Y-(± Zr-)rich thorite, which was overgrown by traces of xenotime and a LREE-phase(s) of complex and variable composition. Accessory mineral compositions and bulk geochemistry suggest that Th, Y and REE were introduced and U

depleted during greisenisation.

Compositions of coffinite, altered zircon and thorite indicate extensive solid solution among these minerals and xenotime. Comparisons with published analyses of synthetic and natural material suggest that these compositions may be metastable and formed at low temperatures. Rapid cooling after the post-magmatic alteration processes may have prevented the exsolution of zircon-thorite-coffinite-xenotime solid solutions to the stable end-member compositions. The complex and variable compositions of unidentified LREE- and Th-Pb-P-phases may also reflect solid solution among simple end-members. As with members of the zircon group, these metastable products may have been preserved during rapid cooling, following greisenisation.

Slower cooling of the granite allowed the coprecipitation or exsolution of relatively Y-, Zr-poor uranothorite in unaltered zircon containing low U, Th, Y etc., but these compositions have been locally modified by post-magmatic alteration. Cooling during albitisation may also have been sufficiently gradual to allow the exsolution of initially unstable zircon compositions to haematite-, thorite-bearing zircon. Unexsolved Type 3 zircon, containing up to 6 wt % UO_2 , persisted as a clear, metamict variety, however, and it is possible that haematite inclusions play a role in nucleating thorite during exsolution. Extensive thorite-coffinite solid solutions appear to be stable, since U attains 29 wt % UO_2 in some exsolved uranothorite inclusions.

The transport of U during alteration at Ririwai may have occurred in oxidising fluids, since U^{6+} is able to form soluble, uranyl complexes. The sub-solidus movement of Th, Zr, Hf, Y and REE is not so

easily explained, since these elements usually have a fixed valency state and are relatively immobile under normal conditions. The mobility of these and other HFS elements is increased by halide or carbonate complexing which have been invoked during various alteration processes in a number of world-wide examples (Chapter 5, Section 6). The widespread occurrence of yttrifluorite, containing LREE-phase inclusions and locally replacing zircon in the rocks at Ririwai, suggests that F was available for complexing with REE, Y, U, Th, Zr and Hf during late-magmatic to post-magmatic processes. During albitisation, element mobilities may have been further enhanced by alkali-fluoride complexing and carbonate-complexing which is suggested by the presence of interstitial calcite. Such complexing may explain the alteration and dissolution of accessories such as zircon and monazite, which are highly stable under normal circumstances.

3. Helmsdale

Unlike the Ririwai biotite granite, the Helmsdale granite crystallised from a magma containing normal concentrations of U and Th. U enrichment in the granite was associated with pervasive and localised, hydrothermal alteration, during which biotite and magnetite were altered to haematite, feldspar was altered to sericite and clay and sphene (and ilmenite?) were altered to TiO_2 . Adsorption of U on to these secondary alteration products probably accounts for much of the high rock U content, of which only a small proportion resides in zircon xenocrysts, primary sphene or apatite.

In the mineralised Ousdale arkose, much of the U occurs in coffinite which is commonly associated with and appears to replace hydrocarbon, sulphides and TiO_2 . The first two may have helped reduce

dissolved U^{4+} , leading to the precipitation of coffinite, but the significance of TiO_2 is less clear. Possibly, U was adsorbed and concentrated by colloidal $Ti(OH)_4$ or titanogel, which later crystallised as $TiO_2 +$ coffinite. Adsorption of U by TiO_2 is commonly demonstrated by an association of fission-tracks with anatase or leucoxene. The absence of brannerite, which often results from a reaction between U and Ti in other areas, may be due to insufficiently high temperatures and activity of TiO_2 , perhaps related to F-complexing of Ti. As at Ririwai, the complexing of Ti, U and other elements by F and CO_2 in the arkose is suggested by the presence of late fluorite and calcite respectively.

Quantitative analyses of some coffinite revealed traces of Ca and Pb, but it is otherwise pure, while ED spectra of other grains have shown significant quantities of P, Zr and Th, which may have been remobilised from apatite and zircon and introduced with the U, respectively. Substitution of these elements in coffinite is reminiscent of the solid solutions with xenotime, zircon and thorite end-members observed in coffinites from Ririwai. The Ousdale coffinite, together with the Th \pm U-rich LREE-phases, may also represent metastable compositions, formed during the rapid cooling after a low-temperature, hydrothermal event. The identification of impure coffinite and LREE-phases associated with granites from the diverse geological settings of Helmsdale and Ririwai could mean that such phenomena are more common than the literature suggests.

The coffinite, sulphides, hydrocarbon and associated trace xenotime and LREE-phases may have been introduced well after deposition of the Lower Devonian arkose, by mineralising solutions ascending channelways formed by splays of the Helmsdale fault. The U could have

been leached from the granite, during its alteration, by deeply convecting hydrothermal fluids. Where the arkose has escaped recent erosion, the U deposits have been weathered and remobilised to form secondary uranyl phosphates.

a) Comparison of Ousdale with other areas

Coffinite is frequently found in epigenetic U deposits in sandstones from other parts of the world; notably the Colorado Plateau and Wyoming deposits of the western United States. In these tabular-shaped "roll-front" deposits, the mineralised zone is located at or near oxidation-reduction interfaces caused by the introduction of oxidising, U-bearing groundwater. Within the aquifer, the expanding zone of oxidising groundwater destroys carbonaceous debris, oxidises pyrite and otherwise alters the sandstone. As the oxidising groundwater passes through the "redox" interface, a decrease in Eh and pH causes the precipitation of U and sometimes associated V, Mo and Se (De Voto, 1978).

On a much smaller scale, the Ousdale arkose superficially resembles these roll-front deposits in that the U mineralisation is tabular in shape (Gallagher et al., 1971) and it comprises coffinite, which was probably reduced by pre-existing or contemporaneous sulphides and hydrocarbon. The deposit at Ousdale may differ in origin from the roll-front deposits, in that the mineralisation was fault-controlled, rather than associated with a progressing zone of oxidising groundwater.

The Ousdale U deposit also shares a number of features with a much larger, unique type of strata-bound, sediment-hosted ore deposit in South Australia (Table 68). The Olympic Dam Cu-U-Au deposit at Roxby Downs was discovered in 1975 and has been described by Roberts and

Hudson (1983), although a detailed genetic model has yet to be developed. Like Ousdale, the Olympic Dam deposit has coffinite, accompanied by sulphides, LREE-phases, TiO_2 , haematite, baryte and fluorite, but it additionally contains uraninite, restricted brannerite and native Au, Ag and Cu. Despite the presence of fluorite, suggesting that F^- was available for complexing with Ti, it appears that overconcentrations of TiO_2 were able to accumulate, leading to the precipitation of brannerite at Olympic Dam.

4. Suggestions for future work

a) Techniques

The mineralogical and petrographic techniques employed in this study have proved invaluable for the characterisation of U- and Th-bearing phases. The use of fission-track radiography enables the location of poorly-crystallised, U-bearing phases that may otherwise have been overlooked; notably coffinite. The technique is sensitive to disseminated, low concentrations of U that are well below the detection limit of the electron microprobe. The semi-quantitative measurement of low concentrations of adsorbed U could be achieved if Lexans, attached to standards containing a range of U contents, were irradiated along with the samples. A comparison of fission-track densities from the samples with those from the standards would provide an estimate of U contents. At very low concentrations of U, more quantitative measurements could be made by counting fission-tracks.

Fission-track studies have yet to be carried out on the borehole and surface samples of biotite and albitised granite at Ririwai, and could reveal a further mineralogical site(s) for U. In the Helmsdale granite, the fission-track radiography of hydrocarbon from Ord Burn

should confirm whether the U is dispersed evenly or concentrated as inclusions of a U mineral.

The SEM, with ED microanalysis, has revealed the complex chemical compositions and textural relations of U- and Th-bearing phases, while the electron microprobe has enabled the quantification of solid solution ranges among members of the zircon group. In order to fully characterise some minerals (e.g. the LREE-phases), further micro-analytical techniques are required. The TEM has proved useful in confirming the identity of coffinite, even when the mineral lattice has suffered partial metamictisation, although use of this technique, together with XRD, requires meticulous sample preparation which is very difficult, when dealing with fine-grained, poorly crystallised phases. TEM studies of the very fine-grained, U-Ti-bearing inclusions in conglomerates from the Witwatersrand Basin (Chapter 2, Section 2.a.v.) could be undertaken in order to characterise these obscure phases more fully.

Use of an ion microprobe would enable the dating of U- and Th-bearing accessories, such as zircon or monazite although, at Ririwai, isotopic ratios may have been disturbed by subsolidus alteration. Dating of coffinite and thorite should, in theory, give approximate ages for the various processes of alteration and mineralisation but these accessories are susceptible to radiogenic Pb loss (Chapter 2, Section 2.a.iii.). If the coffinite at Ousdale proves to be much younger than the granite and arkose, this would suggest that hydrothermal convection cells were maintained well after cooling of the intrusion.

b) Bulk geochemistry

Detailed mineralogical work should be accompanied by bulk geochemical data for the same samples, enabling at least approximate mass balance calculations. Ideally, these would help determine the remainder rock U and Th contents, after accounting for known radioelement-bearing accessories, but complications are likely to arise through the variable compositions of U- and Th-bearing accessories (e.g. the thorite at Ririwai).

In the Ousdale arkose, further modal analyses of coffinite are required to more accurately assess the contribution of this mineral to the bulk U content. Results from several sections per sample need to be averaged, in order to compensate for the heterogeneous distribution of coffinite at the millimetre scale (as shown by the calculations in Appendix 7, where the estimated U contribution from coffinite exceeds the measured bulk U content). Measurement is very difficult in the more mineralised samples, where coffinite is intimately intergrown with sulphides, TiO_2 and hydrocarbon, so that results would probably represent minimum contributions from coffinite.

Adequate whole-rock data are also required to determine the spatial scale at which elements are remobilised. For example, further U and Th analyses of the biotite granite and albitised granite at Ririwai should confirm whether albitisation is accompanied by a nett enrichment of these elements in the rock or whether it is associated with their remobilisation on a much smaller scale. Mineralogical studies at Ririwai suggest there is significant post-magmatic remobilisation of elements such as Th, Zr, Hf, Y and REE, which are normally regarded as relatively immobile after crystallisation of a rock. There could be important consequences for the use of these elements to monitor magmatic processes, if their remobilisation exceeds the scale of a hand-specimen.

c) Sample selection

Both borehole and surface samples need to be studied, in order to discriminate between the effects of supergene processes and those of hydrothermal processes. At Ririwai, geochemical data suggest that there has been surface leaching of U from the granite, but it is not clear which phase(s) has been affected. A comparison of U sites in the borehole and surface samples using fission-track radiography should prove useful in this respect.

At Helmsdale, there has probably been surface leaching of U to a depth of at least 9 m, locally, and many of the radioactive alteration zones in surface exposures contain unexpectedly low U contents. Conversely, it is uncertain whether the high U contents of a few alteration zones are related to the hydrothermal alteration itself, or whether they were adsorbed on to the zones at a much later time, during supergene processes. In the Ousdale arkose, hydrothermal processes associated with coffinite mineralisation are apparent in borehole samples, whereas the supergene remobilisation of U to form secondary uranyl phosphates is seen in surface samples.

Preliminary fission-track studies of ignimbrites from volcanic centres in the Air massif, Niger, suggest that U is associated with secondary haematite and TiO_2 , together with zircon (Chapter 3, Section 6.). Further detailed study is required to fully understand the effects of supergene processes on the distribution of U and Th in these volcanic rocks. Comparisons could be made with the Helmsdale granite, where U is also associated with secondary haematite and TiO_2 .

Samples for mineralogical and geochemical study need to be chosen with care. For example, in the wallrock of the Ririwai lode, geochemical measurements of some samples indicate a loss of U

associated with microclinisation whereas mineralogical studies of other samples seem to indicate U enrichments. Both mineralogical and geochemical investigations of more samples from precisely determined locations in the Ririwai lode wallrock should help clarify the pattern of U mobilisation during microclinisation.

In the borehole granite at Ririwai, the examination of samples immediately above and below 125 m depth should reveal the extent of greisenisation at this depth. A study of samples above 100 m may reveal further coffinite mineralisation, while any mineralogical changes associated with a decrease in Th and U content at 10 m, could be observed.

Peralkaline facies in the Ririwai complex, particularly the arfvedsonite albite granites, warrant a detailed examination of their accessory minerals, since Kinnaird *et al.* (1985b) measured enriched concentrations of trace-elements, including Th (up to 318 ppm), Zr (up to 5552 ppm) and Hf (up to 258 ppm). F-complexing may have played a significant rôle in these rocks which contain up to 0.94 % F.

d) Solid solution

Solid solution among members of the zircon group deserves more study in the light of analytical data from Ririwai and Ousdale. Much more experimental work is required in the system U-Th-Zr-Si-Y-P, in order to clarify the conditions under which metastable solid solutions can persist. Correlations of unit cell sizes with solid solution and hydration among members of the zircon group, using XRD or TEM, would be interesting. There may be implications for solid solution among members of other mineral groups, e.g. the bastnaesite group, which contains variable concentrations of U, Th, Ca, Y and Pb (assuming that the unidentified LREE-phases are fluorocarbonates).

Chapter 10 Synthesis and Final Remarks

1. Ririwai area

Fig. 127 represents an attempt to put the mineralogical results of this study of the Ririwai samples into a geological and geochemical context, which is necessarily speculative in part. The Figure includes the principal discoveries resulting from this study, which are summarised as follows:

- a) An extensive solid-solution range is found in thorite and coffinite, along with a broad correlation between the type of host-rock and the composition range of these minerals. These compositions are probably metastable, resulting from rapid cooling after metasomatism of the granite. Mineral chemistry has also helped distinguish different generations of thorite and suggested trace-element compositions of the various altering fluids (see below). Qualitative analyses have revealed different generations of a LREE-phase(s), which appears to accommodate significant, but variable concentrations of U, Th, Y, Pb and Ca.
- b) Alteration of zircon can produce irregular patches, enriched in Th, U and other minor elements, along pre-existing zoning and cracks. These patches are now metamict and apparent by their low reflectance. A combination of probe analysis and interpretation of back-scattered electron images confirms that the metamict zircon contains both chemically bound water and submicroscopic voids.
- c) In the albitised rocks, complex zoning of zircon includes a distinct, oscillatory banding of Hf and zircon domains, rich in inclusions, interpreted as exsolved uranothorite.

Fluid movements are shown schematically in Fig. 127. It is plausible to suggest that the K-bearing fluids producing the

microcline (Fig. 127, Stage 6) are derived from the earlier albitising fluids (Stages 2-5), since albitisation is mainly an exchange of Na for K and should produce K-rich fluids. The origin of the albitising fluids themselves (marked "e.g. from an alkali granite" in Stage 2 of Fig. 127) remains a matter of speculation. Alkali granites are a possibility because some of them were intruded at a late stage at Ririwai, although there is no definite evidence that any of them are actually later than the biotite granite itself (Martin and Bowden, 1981). It must also be remembered that these late intrusions were emplaced into a volcanic pile (indicated schematically in Fig. 127, Stage 1) so that circulation of fluids would involve the lavas and possibly involve surface waters. The various stages in Fig. 127 will now be annotated.

Bulk geochemistry shows that the Ririwai biotite granite crystallised from a melt containing lower MgO, CaO, TiO₂ and P₂O₅ but higher K₂O and Na₂O compared to I-type granitoids of similar SiO₂ content (Kinnaird et al., 1985a). Presumably, the absence of apatite reflects both low P₂O₅ and low CaO concentrations in the melt. Analyses of the host biotites should confirm whether the melt was F-rich, although bulk analyses for F do not show exceptionally high values (see Table 58).

Bulk geochemical analyses indicate that the melt had exceptionally high concentrations of U and Th (Table 57), which occur largely in uranothorite, with lesser contributions from monazite, pyrochlore and zircon. Another important site for U may exist, in order to account for the Th:U ratios of one in borehole samples. Higher Th:U ratios in surface samples of granite probably reflect a loss of U during weathering and also suggest that the "missing" site for U is leachable.

Primary geochemical patterns in the biotite granite have been overprinted by metasomatism, which has introduced Al, Fe and Si but depleted Ca (Kinnaird *et al.*, 1985b). It is not clear where these fluids originated, but one possibility is that Al and Si were expelled from the peralkaline granites (Fig. 127). The peralkaline granites owe their character to a deficiency in Al rather than to particularly high alkalis and the albite granites have undergone desilication (Kinnaird *et al.*, *op. cit.*). These fluids may also have introduced Th, U, Y, Zr, P etc. during the subsolidus alteration of primary thorite, zircon and monazite (Fig. 127, Stage 2).

If the borehole truly penetrates the roof zone of an underlying, albitised granite (Fig. 127, Stages 3-5), one might expect a more abrupt change in mineralogy than is observed. Possibly, the albitising fluids from the roof have permeated into and altered the overlying granite. Another possibility is that albitising fluids were derived from a source outside the biotite granite, such as the peralkaline granites.

Albitised rocks have a distinctive zircon population of fewer grains, which tend to be larger than those of the biotite granite. This, together with the interstitial, authigenic appearance of some grains, suggest that zircon re-crystallised during albitisation, although bulk geochemical data do not suggest that Zr was introduced with the fluids (Table 58).

The increased abundance of thorite inclusions in zircon and the increased U contents of some zircon and uranothorite suggest that Th and U were remobilised during albitisation although, like the Zr, bulk geochemical data do not indicate an enrichment of these radioelements (Table 57). This is unexpected, since albitisation in other areas

(Chapter 5, Section 6) is frequently associated with significant enrichments of U, Th, Zr and other incompatible elements. The U is typically carried as carbonate-complexes, while the other elements may form halide-complexes. At Ririwai, the presence of interstitial calcite in the albitite suggests that CO₂ was available for complexing in the fluids, but temperatures may have been too high for the formation of uranyl-carbonate complexes, which give way to uranyl-hydroxide and uranyl-fluoride complexes at temperatures above 200°C (see Figs. 1 and 2). Fluid inclusion data from albitised rocks (Kinnaird *et al.*, 1985b) confirm the presence of CO₂ but show that temperatures reached 260-460°C. Thus, temperatures may even have been too high for significant uranyl-fluoride complexing, although the presence of interstitial fluorite suggests that F was available. The embayment of zircon by yttrifluorite, which contains inclusions of a Th-bearing LREE-phase (Plate 81) further suggests that F was available for complexing with Zr, Hf, Th, Y and REE. However, the high concentration of F which might be expected in the volatile-rich, residual melt of a roof-zone is not confirmed by bulk values of F in the albitised rocks (see Table 58). Thus, although some F-complexing of U, Th, Zr, Hf, Y and REE may have occurred, insufficiently high F levels and excessive temperatures may have inhibited complexing as a mechanism for trace-element enrichment during albitisation of the Ririwai biotite granite.

Bulk geochemical data for the microcline show increased concentrations of K₂O and a depletion of Na₂O, together with Zr, Hf, Th, U, Y and REE relative to the biotite granite. It is possible that the K₂O originated from fluids expelled after albitisation of the granite (Fig. 127, Stage 6). A depletion in REE has been attributed by Kinnaird *et al.* (1985b) to the destabilisation of host accessories, although

direct mineralogical evidence of this is lacking. Similarly, there is no direct evidence that depleted Zr concentrations were due to the dissolution of zircon; rather a decrease in size and abundance of this accessory may have been due to primary magmatic variations. It is possible that chloritisation of biotite was accompanied by the dissolution of thorite, which has only been found interstitially and included in Li-mica in the microcline. Contrary to the geochemical evidence, the presence of late Y-rich coffinite, Y-rich thorite, LREE-phases and ?microlite suggest that U, Th, Y and LREE were partitioned to the rock.

Geochemically, greisenisation is characterised by a marked decrease in K_2O and Al_2O_3 , due to feldspar breakdown, with a complementary increase in Li content due to the development of Li-rich micas (Kinnaird et al., 1985b). Norm calculations show this as a decrease in orthoclase and albite with concomitant increase in quartz (Fig. 18). Bulk geochemical data are not available for the incipiently greisenised granite at 125 m, but a sample 10 m above has enhanced Li (Table 58). The greisenising fluids responsible for alteration at 125 m may have been channelled from the nearby Ririwai lode, along cooling joints in the granite (Fig. 127, Stage 7a), but the earlier microclinising fluids appear not to have migrated as far. Zircon relicts at 125 m suggest that, in places, F activity was sufficiently high to corrode zircon, although grains in the main lode were altered, rather than corroded. The available bulk data for the lode greisen do not show Zr enrichment, so that locally high Zr concentrations in thorite were probably remobilised from altered zircon, rather than introduced with the greisenising fluids (Fig. 127, Stage 7b).

A bulk analysis of greisen from the Ririwai lode (Table 57) shows

a substantial enrichment in Th, which corresponds to an abundance of thorite in this sample, although U is not significantly enriched. In other samples of greisen, monazite is relatively common (Table 44) and it is possible that enhancements of LREE, relative to the microclinised wallrock, reflect the crystallisation of new monazite, together with other, minor LREE-phases. Similarly, enhancements in Y and HREE may be related to new xenotime, Y-rich thorite and yttrifluorite in the greisen.

2. Helmsdale area

In the Helmsdale area, the principle discovery is that coffinite is the main carrier of U in the subsurface mineralisation of the Ousdale arkose. Although other minerals have been found (e.g. xenotime, LREE-phases), the relatively simple mineralogy here does not lead to a complex model as at Ririwai. Also, the mineralisation is relatively localised and related to faulting (Fig. 125). However, a feature in common with Ririwai is the occurrence of late fluorite and calcite, which suggests that F and CO₂ were available for complexing. In the weathered, surface arkose, the mineralisation of uranyl phosphates suggests that phosphate complexing was important.

Apart from U, attention is focussed on Ti as an element mobilised by complexing in the subsurface arkose. It is argued that mobility of Ti is the key to understanding the occurrence of the coffinite-TiO₂ association, rather than uranotitanates.

Appendix 1 Petrographic and Mineralogical Techniques

1. Light microscopy

Rock samples were prepared as uncovered thin-sections, measuring 25 mm square (for SEM and fission-track work) or 48 by 28 mm in size (for EPMA) or were mounted in 30 mm diameter araldite blocks. After grinding with 400, 800 and 1200 mesh carborundum, the sections and blocks were polished using, successively, 6 μm and 1 μm grade polishing paste.

A Vickers transmitted and reflected light petrographic microscope was used for routine observation of the polished sections and blocks at x50, x100 and x400 magnification, but a Zeiss microscope was available for high magnification, oil-immersion studies and for the taking of photomicrographs. Reflectance measurements were made using a Reichert reflex spectral microphotometer.

2. Alpha-particle autoradiography

Details of alpha-particle autoradiography are given by Bowie (1977). Photographic nuclear emulsions have been used in the past for recording the alpha particle emission from the natural decay of ^{232}Th or ^{238}U and their daughters in geological materials in order to locate and identify U- and Th-bearing phases. Although suitable for showing the distribution of point sources of U or Th in ore grade material, nuclear emulsion plates are expensive and light sensitive.

The availability of relatively inexpensive, convenient plastic detectors, such as CR-39 and cellulose nitrate, has now made autoradiography more of an attractive method (Basham *et al.*, 1982a). CR-39 plastic was used by Mackenzie *et al.* (1984) to define the distribution of alpha emitting species in a 0.5 mm thick slab of mineralised granite from the Ririwai lode in Nigeria. A smooth surface of the block was held in close contact with the plastic for a period of 60 days with a set of axes marked on the plastic being exactly aligned with those on the rock. After exposure, the plastic was removed and etched with NaOH solution and the resulting clusters of faint grey/white alpha tracks on the transparent plastic were emphasised with black ink. CR-39 was similarly used on polished thin-sections of samples from the Ririwai lode which are described in Chapter 4.

Cellulose nitrate, which was also used on some of the Nigerian and Scottish samples, was described by Basham and Easterbrooke (1977) who compared its merits with emulsion autoradiography. Apart from the convenience of use, cellulose nitrate detectors have a superior track contrast and require a shorter exposure, since the tracks can be enlarged by the extension of etching times. As the detector is biased towards the lower energy-level of the alpha spectrum it is more sensitive to U and, due also to the shorter tracks and exclusion of beta-particle tracks, it shows better definition than emulsion autoradiographs. Film LR115 Type II was tightly bound to polished thin sections of rock (Plate 198) and left for 6 months (in the case of the Nigerian samples) and 9 months (for the Helmsdale granite samples), prior to etching in 2.5 M KOH at 25°C for 24 hours.

3. Fission-track radiography

Accounts of fission-track radiography are given by Bowie (1977) and Kleeman and Lovering (1967). The technique is based on the fission of ^{235}U , which is induced by thermal neutron irradiation. If the fission fragments so produced are allowed to bombard an overlay of mica (Price and Walker, 1963) or Lexan polycarbonate film (Bowie *et al.*, 1973), the tracks can subsequently be rendered visible by etching. The Lexan and sample can be directly compared with a matching precision of between 10 and 50 μm (Bowie *et al.*, *op. cit.*). The mica overlay resolves track densities of up to 9×10^8 tracks per cm^2 , whereas the Lexan has a lower resolution of 5×10^7 tracks per cm^2 (Thiel *et al.*, 1972), although all mica exhibits a background of "fossil" tracks, mainly resulting from the spontaneous decay of ^{238}U . Quantitative results can be obtained if glass standards, with known amounts of U, are irradiated in the neutron flux along with the sample and the numbers of tracks per unit area counted in each case and compared (e.g. Bajo *et al.*, 1983). In this study, fission-track radiography was used qualitatively and a broad classification of the different track densities referred to in the text is listed in the Key to Abbreviations (page 30).

Polished and cleaned thin sections measuring 2.5 x 3 cm in size were overlain with Lexan film cut to the dimensions of the slide and fixed with adhesive tape. Forty sections were loaded into a pure aluminium cylindrical container with a screw top, such that the Lexan overlays were in direct contact back to back for each pair of sections (Plate 199). The samples were irradiated for a length of time inversely proportional to their suspected U contents (6 hours for a content greater than 1000 ppm U, up to 60 hours for a content less than 10 ppm U) in a neutron flux of 10^{16} neutrons (n) per cm^2 . After irradiation and a period of cooling (several months), the Lexans were etched in a solution of 6 N NaOH at 90°C for a few minutes.

Basham *et al.* (1982a) comment that the use of a high irradiation dose (5×10^{15} n/ cm^2) tends to overemphasise visually the importance of abundant minerals with relatively low U contents, as track saturation densities may be obtained at only 20 ppm. Plate 184 shows the high density of tracks obtained from arkose carrying low concentrations of redistributed U associated with iron-oxide alteration products.

In over-irradiated Lexans, it is very difficult to correlate areas of high track density with specific petrographic features. Individual phases containing high U exceed the recording capacity of the Lexan, giving rise to areas of brown discoloration, with no fission tracks apparent (Plate 169). In order to bring out features such as microcracks and minerals with low concentrations of U (<0.1 ppm), as well as to estimate the contents of phases containing higher contents of U (>50 ppm), Caruso and Simmons (1985) used two irradiation doses of 1.1×10^{17} n/ cm^2 (for U contents of 70 ppb to 30 ppm) and 6.1×10^{15} n/ cm^2 (for minerals containing up to 500 ppm U) for the same samples.

Compared with autoradiography, the fission track technique is more sensitive (with detection limits down to the order of 1 ppb U) and is specific to U, since ^{232}Th only undergoes fission when irradiated by fast neutrons of energies greater than 0.9 MeV. It is therefore suited to samples containing disseminated, low-grade U mineralization, as

found in the Ousdale arkose and Helmsdale granite, for example (Plates 183 and 184).

By differential exposure to thermal neutrons, followed by exposure to fast neutrons, two fission-track patterns can be produced; one reflecting U and the other U together with Th. Mackenzie *et al.* (1984) used a combination of alpha autoradiography and fission track radiography, in order to determine the differential distributions of U and Th in a sample of mineralised granite from the Ririwai lode, Nigeria.

Kleeman and Lovering (1967) found that the irradiated Lexan developed a detailed print of the rock surface as a result of variations in the density of small, shallow pits present on the plastic surface after etching. These pits arise from a lower order of damage caused by the passage of charged particles with masses lower than those of fission fragments. These are recoil ions (such as OH^-), ejected from the mineral surfaces due to the fast neutron component of a largely thermal neutron flux. Features, such as grain boundaries and cracks, are faithfully reproduced on the plastic, enabling accurate matching of the fission tracks with minerals in the sample. Unfortunately, this copying effect was not apparent in the Lexans used in this study, and so other methods of matching the fission and alpha tracks with the samples were tried.

For preliminary observations, it was satisfactory to carefully place the transparent Lexan over the section, so that the two were almost in register and fission tracks associated with an adjacent grain could be viewed after re-focussing (e.g. Plate 190). A more convenient and precise method involved the making of a 250 x 200 mm sized negative print of the whole section, by placing the slide directly into the negative carrier of a photographic enlarger. A transparent overlay of the Lexan, in register with the photographic print, was made by substituting the section in the enlarger with the corresponding Lexan plate (while maintaining the same degree of enlargement) and tracing the image of the Lexan onto tracing paper. The tracing paper was then taped in the matching position onto the negative print. Grains on the print, which coincided with fission track clusters on the overlay, could then be observed in detail under the microscope or SEM.

4. Electron probe microanalysis (EPMA)

a) Introduction

The electron microprobe is used for the non-destructive, chemical micro-analysis of mineral grains down to 5 μm in diameter. It is of particular use in U and Th mineralogy, where grains are frequently less than 50 μm in size, are poorly crystalline and very difficult to characterise optically, and may be metamict, rendering XRD useless, unless heating is employed. A particular advantage of the electron microprobe is its ability to measure small-scale chemical variations, which enables the study of compositional zoning and solid solution ranges within mineral grains. Elements from Na to U can be routinely analysed and detection limits can reach 100 ppm (Table 69) with an accuracy down to 1%, depending on the element being measured. Compared with wet chemical analysis, EPMA is far easier and quicker to use and has been directly responsible for the discovery of many new minerals, including those of U.

The following is a brief description of the theory and practice of EPMA (dealt with in more detail by Long, 1977) and a discussion of the problems and limitations of the technique, as applied to this study.

b) Principles of EPMA

A characteristic X-ray spectrum is generated when a finely focussed beam of electrons hits the surface of a solid material. From the wavelengths and intensities of the peaks in the spectrum, the elements present may be identified and their concentrations measured by comparing them with intensities from materials of known composition.

The source of the electron beam is an electron gun consisting of a tungsten filament which, when heated, gives off electrons by thermionic emission. A negative potential of 5 to 50 kV accelerates the electrons through an earthed aperture. Two magnetic lenses are used to focus the beam to a fine "probe" incident on the specimen surface. Different probe currents and diameters are obtained by varying the current in the lenses. The beam can be scanned, to provide a back-scattered image of the specimen surface, or focussed to a fine point (1 μm diameter) for analysis. The electron column and stage are under vacuum but the specimen can be isolated from the rest of the machine and quickly changed, using the specimen chamber.

In wavelength-dispersive spectrometry (WDS), the X-rays emitted from the specimen are diffracted by an analysing crystal and their intensities measured by counters which can be moved to various angles of 2θ , depending on the element being analysed. This contrasts with energy-dispersive spectrometry (EDS), which is described in Section 5.

c) Instrumentation

The instrument used was a Cambridge Microscan V electron microprobe (Plate 200), with a beam take-off angle of 75° from the sample. Two spectrometers are available, enabling the simultaneous measurement of a pair of elements using a choice of crystals from Ba Stearate, RAP (both for very light elements), PET and LiF. Each spectrometer has both a sealed and a gas-flow proportional counter. Rapid location of standards and analysis spots is possible using a servo drive.

d) Sample preparation

Polished thin sections, measuring 48 x 28 mm or smaller, were thoroughly cleaned in Inhibisol, prior to carbon coating under vacuum to a thickness of approximately 250 Å. If necessary, silver dag was painted along the slide edges to increase conductivity of the sample. Araldite blocks were similarly prepared but had to be inserted into an improvised clamp in the specimen holder.

e) Standards

The quality and preparation of standards is a very important factor affecting the accuracy of the analysis results so that standards should satisfy the following conditions:

- (i) An accurately known chemical composition.
- (ii) Homogeneous, physically and chemically on a sub-micron scale.
- (iii) Takes a good polish.
- (iv) Stable under electron bombardment in a vacuum and also stable in air.
- (v) Any differences which exist in the valency or bonding of the specimen and standard do not give rise to errors in the measurement of the intensity ratios.

Typically, standards used are pure metals, synthetic compounds or simple minerals (Table 70). Standards were polished and coated like the samples. Problems associated with particular standards are discussed in Section h.iv..

f) Analysis procedure

Photomicrographs were used to aid the location of grains under the electron beam, in conjunction with a light microscope built into the microprobe, or a scanning electron image produced on a cathode ray oscilloscope. The latter method was found particularly useful, since many of the minerals analysed (e.g. thorite) are of high average atomic number, thus giving high contrast in a back-scattered electron image (BSEI). X-ray scanning images, showing the distribution of different elements, were sometimes used to help locate small grains of a known mineral.

A beam current of 50 mA at either 15 or 20 kV, depending on the nature of the sample (see Section h.v. below), was used. The sample was focussed under high magnification using the reflected light microscope attachment and the beam was focussed with the final condenser lens, while viewing the BSEI.

In many cases, it was found advantageous to acquire a spectral scan of the mineral, prior to its analysis, so that suitable peak and background positions could be chosen (Fig. 128). After "peaking-up" on standards and measuring them, the samples were analysed using two counting intervals of ten seconds each for background positions, and five or more such counting intervals for peak positions. X-ray scanning images and line concentration profiles were found particularly useful for demonstrating compositional zoning in mineral grains.

g) Processing of results

Raw counts were corrected and converted to weight % oxides using the program "MACZAF", supplied by Micro-analysis Consultants Ltd. The program applies initial corrections for probe current drift, and counter deadtime, prior to calculating the apparent weight % of elements. Atomic number, absorption and fluorescence corrections (ZAF) are applied to give a true weight %, which can be optionally expressed as weight % oxide and recalculated to give the chemical formula. Some indication of the quality of analyses is shown by the closeness of the chemical formulae to the expected mineral stoichiometry and by the closeness of the oxide total to 100% (bearing in mind the problems, discussed below, which may lead to low totals). The program also calculates detection limits (Table 69) and precisions for each element analysed.

h) Problems encountered with EPMA of accessory minerals

Difficulties which have arisen during the EPMA of accessory minerals include those specific to the measurement of U, Th and REE and those related to the unsuitable nature of standards and mineral grains for analysis:

i) Suitable X-ray emission lines for U and Th

The higher intensity M X-ray emission lines of U and Th are measured, in preference to the L lines, which have too high an energy to be diffracted by the commonly available crystals as first-order reflections and which also require a high operating voltage and probe current. However, the ZAF correction procedure for the L lines is more completely understood and involves lower corrections for absorption and fluorescence (Bowles, 1978).

Unfortunately, there are problems with using $U M_{\alpha}$ for measurement, due to the greater efficiency of the Ar-filled detector for $U M_{\beta}$ radiation. In the gas-flow proportional counter used, the absorption edge for Ar (3.203 KeV) is just exceeded by the characteristic energy of $U M_{\beta}$ (3.337 KeV) whereas the $U M_{\alpha}$ line (3.171 KeV) lies on the low energy side of the ArK edge. Hence $U M_{\alpha}$ is much less efficiently

detected than $U M_{\beta}$ by Ar, resulting in a greater width and recorded intensity of the latter. Fig. 130 shows the effect of using two different mixtures of gas (97.5% Ar with 2.5% CO_2 and 90% Ar with 10% CH_4) in the flow counters, on the intensity of counts for $U M_{\alpha}$ relative to $U M_{\beta}$. The dilution of Ar with methane further reduces the α/β intensity ratio, implying that the differing absorption of the $U M_{\alpha}$ and $U M_{\beta}$ lines by Ar is probably a complex effect, involving the quenching gas.

The absorption edge of Ar also gives rise to an increased level of continuum radiation on the high energy side of $U M_{\alpha}$. The result of using $U M_{\alpha}$, especially when measuring very low concentrations of U, is that erroneously low figures for weight % U are obtained. One solution is to use the background value on the low energy side of $U M_{\alpha}$ only. Alternatively, if the Xe-filled sealed detector is used, the peak to background ratio of $U M_{\alpha}$ is enhanced although the intensities of both $U M_{\alpha}$ and $U M_{\beta}$ are decreased. A third option is to use the higher intensity $U M_{\beta}$ peak, although the correction for M_{β} is less well understood than that for M_{α} (Bowles, 1978). Cameron-Schimann (1978) used $U M_{\beta}$ with a correction factor to subtract the minor contribution of $Th M_{\gamma}$ from this peak, when K (the $K K_{\alpha}$ peak interferes with $U M_{\beta}$) was absent.

Since many of the thorites analysed in the Nigerian samples contain significant levels of U, it was thought that the $U M_{\alpha}$ peak (at $53^{\circ}07'20$) might suffer from interference with $Th M_{\beta}$ (at $53^{\circ}32'20$). Fig. 130 shows the effect of increasing Th content on the peak height of $U M_{\alpha}$ relative to $U M_{\beta}$, (which suffers less interference from $Th M_{\gamma}$) for the two different gas mixtures used in the flow counter. The right hand side of the plot corresponds to a maximum contribution of about 20% to the height of the $U M_{\alpha}$ peak relative to the $U M_{\beta}$ peak for thorite containing 70 wt % ThO_2 . This could lead to an overestimation of UO_2 by up to 2 wt % for thorite containing about 10 wt % UO_2 . Thus, when measuring U in thorites, the $U M_{\beta}$ peak should be used or a correction factor should be applied to results obtained using the $U M_{\alpha}$ peak. The interference of $K K_{\alpha}$ with $U M_{\beta}$ presented no problems, since none of the U-bearing minerals measured contain detectable concentrations of K.

ii) ZAF correction factors for U and Th

Cameron-Schimann (1978) outlined the special considerations which need to be made when ZAF matrix correction factors are applied to measurements of U and Th minerals. The corrections for atomic number become particularly important for such minerals due to their high average atomic number. Additionally, an accurate estimate of the water content is ideally needed for hydrous minerals, such as coffinite, since the oxygen in the water significantly affects the corrections. The ZAF correction program used here accounts for the presence of unmeasured oxygen by subtracting the total measured elements from 100%. This method assumes that low totals result wholly from the presence of water rather than void space. Although void space may occur in metamict minerals, H_2O is frequently reported in the literature in coffinite and other orthosilicates of the same group (Speer, 1982). This method is thus preferred over estimating oxygen by stoichiometry from the

measured cations only, which would overestimate the amount of void space and under-correct the measured elements for X-ray absorption by oxygen.

Accurate correction for absorption effects is currently not possible due to the uncertainty surrounding the values of mass absorption coefficients for the M lines of U and Th. Cameron-Schimann (op. cit.) discussed the effect of absorption on light elements caused by the presence of high U and/or Th. Elements such as Mg or Na are underestimated but no problem was found with Si, despite the theoretical effect of the absorption edges of U and Th on the fluorescence of Si radiation. Although fluorescence corrections for the M lines of U and Th are generally small because of the low fluorescence yields, the commonly neglected continuum fluorescence correction takes on unusually significant proportions in high atomic number minerals.

iii) Measurement of REE

It is helpful to acquire a spectral scan of REE-rich minerals, prior to their analysis, in order to identify interfering elements and locate the optimum wavelengths for background measurements. Fig. 128 of a typical monazite scan illustrates the difficulty in picking a suitable background position in a crowded spectrum. The most intense L_{α} lines of some elements (eg. Nd L_{α}) are unsuitable for measurement as they cannot be resolved from other peaks (Ce L_{β_1}) and so alternative lines have to be used (Nd L_{β_1}). Since the β_1 lines of some elements were used in preference to the α lines, the energies of the emission lines stored in the correction program were suitably amended. In fact, results obtained from processing the same results using the amended and unamended programs varied only within analytical error. Exley (1980) used count times of 60 seconds for La, Ce and Nd and 100 seconds for Y and other REE. Although REE-rich minerals, such as monazite, give higher counts for REE, the backgrounds are higher, giving lower peak to background ratios and poorer detection limits (Exley, op. cit.).

High totals for monazite (Table 34) may have been due to an increase in the heights of the REE peaks measured, as a result of interference from unidentified peaks. Roeder (1985) was able to calculate % overlap for interfering REE peaks and so produce overlap corrections which, when applied, would give the actual number of counts due to a measured element. However, rather than measure overlapping peaks and apply corrections, alternative lines with no obvious interfering peaks were used in this study.

Table 70 shows, for the different REE measured, the corresponding lines used. In xenotime, monazite and the other REE-phases, some of the very minor REE present may not have been measured, due to severe peak interferences or lack of suitable standards. In Y-rich thorite and coffinite, the trace amounts of HREE present were not normally measured, but it was found that their concentrations varied directly with the concentration of Y (which was measured).

iv) Problems with standards

Bowles (1978) pointed out the disadvantages of using pure U metal as a standard. Despite being produced to a high degree of purity (99.8%) so that its composition is accurately known, U metal oxidises very rapidly in air, although this process can be retarded by carbon coating. The use of U metal as a standard when measuring very low concentrations of U requires the application of large ZAF correction factors and any inherent errors in these factors may become significant. A solution to these problems is to use synthetic UO_2 for the measurement of U-rich minerals and an artificial glass containing an accurately measured amount of UO_2 for the measurement of trace amounts of U. The glass standard used in this case was prepared by Smellie *et al.* (1978) and contains 4.78 wt% U_3O_8 . Probe analyses of the glass are compared to those published by Smellie *et al.* (*op. cit.*) in Table 71. Slightly low values were obtained for CaO, Al_2O_3 , and SiO_2 but U_3O_8 was almost 18% too high. This was due either to low counts obtained on the U metal standard used, to an error in the analysing and/or ZAF matrix correction procedure or the published value of 4.78 wt% U_3O_8 is incorrect.

In order to test the first hypothesis, it was decided to test the standards for U against each other. Table 72 shows the results of analysing identical spots in coffinite and uraninite grains in the same session, using the three different standards for U. Comparisons are made between analyses using a freshly polished and carbon-coated U metal standard and analyses made using the standard a month after polishing, when a surface oxide layer had formed. The measured concentration of U in coffinite, using the metal standard, is virtually identical for both sets of analyses. For uraninite, however, the second analysis gave a lower result for U, rather than a higher result, which would be expected, had oxidation reduced counts from the metal standard. Thus, although the metal standard consistently gives a higher result for U relative to the oxide standard, this cannot be due to oxidation of the metal. The glass standard gives concentrations which vary inconsistently with those of the metal and oxide. This variation probably reflects poor counting statistics as well as amplification of analytical errors due to extrapolation of the low U concentration glass to the high U concentration specimens. The use of artificial glasses as standards for EPMA is regarded as suspect by some workers. Cameron-Schimann (1978) prepared four glass standards containing approximately 8 and 18% UO_2 and ThO_2 but found that they did not make good analytical standards due to their unpredictable homogeneity and stability under the electron beam.

High oxide totals were obtained for zircon when a pure Zr metal standard was used. Acceptable totals were obtained when Zr was measured using a zircon standard and Figs. 129A and 129B show plots of wt% ZrO_2 obtained using the metal against wt% ZrO_2 obtained using the zircon standards for a range of Zr concentrations in zircon and thorite respectively. Possible causes of such anomalously high values for Zr include; errors in the ZAF correction factors for the pure Zr standard; differences in the valency or bonding of Zr in the metal and zircon; impurities of another element in the metal. The latter possibility was not confirmed by a spectral scan of the metal standard.

v) Problems with samples

A number of factors may contribute to low oxide totals and poor stoichiometry in mineral analyses. Some of the minerals analysed contain elements which cannot be detected or measured quantitatively on the microprobe i.e. H, O, F, C. In the case of the unidentified REE-phase, an estimate of the wt % F must be made if the mineral is assumed to be a fluorocarbonate, in order to avoid over-estimating the O content. Also, the matrix effects of the unmeasured F on the results for other elements should, ideally, be taken into account. Low totals may also be due to the presence of elements in concentrations near or below the detection limit e.g. REE in thorite or coffinite.

Water and other volatiles may be vapourised under the beam, where the temperature rise at 20 kV and 100 nA reaches almost 200°K. This is the case with hydrous minerals such as coffinite or metatorbernite, which often exhibit a dark spot where the beam has intercepted the mineral surface. The effect of this is to artificially increase the wt % of remaining elements in the mineral. The problem can be alleviated by using a lower operating voltage and/or beam current or by scanning or defocussing the beam during the analysis of a reasonably large, chemically homogeneous phase. Table 46 shows that analyses of a thorite, at 15 kV and at 20 kV, do not give significantly different results.

Analyses for U are given as UO_2 for minerals containing U^{4+} (e.g. coffinite, thorite, zircon). Natural uraninites are always partially oxidised and show a composition range from $UO_{2.07}$ to $UO_{2.25}$ (Chapter 2, Section 2.a.i.). Basham *et al.* (1982a) warn that low probe totals for uraninite may indicate that some oxidation of U^{4+} to U^{6+} has occurred or, alternatively, that adsorbed water is present. It is likely that, for other U^{4+} minerals, there has been varying amounts of oxidation also. Since the extent of oxidation for different U^{4+} minerals is not known, all U analyses are presented as UO_2 to facilitate comparisons between them. It is realised that oxidation of U may mean that oxide totals presented for coffinite, for example, are up to 1 wt % too low (assuming that all the U should be reported as $UO_{2.25}$).

Since many of the minerals analysed contain significant amounts of U and/or Th, their crystal structures have received various degrees of radiation damage and resultant metamictisation. The effect of metamictisation on zircon, for example, is to decrease its density but increase its volume as submicroscopic voids and defects are produced (Chapter 2, Section 2.b.i). This void content results in the missing weight % observed in analyses of metamict zircon, thorite, coffinite etc.. Barritt (1983) attributed low totals in thorite and U/Th-rich zircon, to decay fragment damage. Alteration and incipient breakdown associated with metamictisation may prevent the structural balance of analyses (Deer *et al.*, 1981). For example, the formulae calculated from the analyses of metamict thorite, coffinite and zircon invariably show depleted Si but excessive Th, U, Zr etc..

Another effect of the radioactive decay of U and Th is to produce an unstable series of intermediate daughter products which do not necessarily remain in the crystal lattice. The final decay product, Pb, may remain dispersed throughout the structure or may gather into discrete areas rich in Pb, or form galena if S is present, producing a highly inhomogeneous material (Bowles, 1978). Cameron-Schimann

(op. cit.) found the radiogenic Pb in uraninite to migrate away from the point of analysis, but this movement could be kept to a minimum by keeping to a low operating voltage and beam current.

In practice, most of the radioactive minerals analysed contain radiogenic Pb below or near the limit of detection of the probe, since the host granites etc. from Scotland and Nigeria are comparatively young. The distributions of Pb in thorite, pyrochlore and an unidentified Th-Pb-P-phase were found to be relatively homogeneous.

Other adverse affects on analyses include small grain-size and the presence of inclusions and of holes or scratches caused by the poor polish taken by some grains. These problems can be overcome, to some extent, by using a lower operating voltage (15 kV), which gives a smaller excited volume under the grain surface and hence reduces electron scattering and fluorescence of adjacent areas. For the measurement of zircon containing abundant inclusions of thorite measuring less than 10 μm across, it was found helpful to direct analyses using high magnification, BSEI photographs.

5. Scanning electron microscopy (SEM) with energy dispersive (ED) microanalysis

An account of SEM with microanalysis is given by Southworth (1975), while details of processing data from ED spectrometry (EDS) are outlined in Long (1977). The SEM enables the high magnification (x200 to x100k), high-resolution (about 10 nm) observation and photography of small, poorly crystallised phases which are difficult to identify under the light microscope.

A beam of electrons, which is focussed to a spot 100 to 300 Å in diameter, is dynamically scanned across a quadrant of the 25 mm square, polished section. Coating of the section with carbon under a vacuum, or with conductive spray prevents the build-up of a charge, while silver dag is painted on to ensure electrical contact between the sample and mount. In emissive mode, the SEM has a positively biased electron collector, which captures the low energy, secondary electrons generated within 50 Å of the specimen surface, so that the resulting image is, to a large extent, dependent on variations in surface flatness.

Reflected-light photomicrographs facilitate grain location and the positioning of spots for microanalysis. In cases where the SEM image contrast was extremely low, use was made of a co-ordinate system of location. A small-scale, negative photograph of a thin section is made by placing it in the negative carrier of a photographic enlarger. Fine wire is then wound around the section to form a grid (Plate 201). The section is then replaced in the enlarger (while maintaining the same degree of enlargement) and the projected grid marked on tracing paper. The paper is accurately aligned over the photograph of the section (using the image from the enlarger), thus forming a grid overlay, which exactly corresponds to the wire grid on the section. Grains of interest can be marked on the overlay in relation to the wire grid, which is clearly visible under the SEM. The grains can then be re-located, using the photograph, during light microscopy (with the grid removed).

A small component of the SEM image results from primary, high-energy electrons which are scattered back from a few micrometres below the specimen surface, giving rise to a slight contrast arising from differing average atomic number between minerals. This effect was enhanced by using an SEM in reflective mode, in which a slightly negatively charged collector captures mainly the primary, high energy electrons, producing a true back-scattered electron image (BSEI). The principle is outlined by Hall and Lloyd (1981). The backscattering coefficient increases with increasing atomic number, so minerals with relatively high average atomic number appear brighter in the BSEI. Although, in this mode, the resolution is poorer (about 50 nm) due to the greater depth of penetration of the electrons, contrast is enhanced, allowing the qualitative discrimination of phases with relatively small differences in average atomic number, by manipulation of the contrast scale in the image.

In the X-ray mode, the image is formed from the X-rays generated by the incident beam of electrons interacting with the sample just below the surface. The X-rays are characteristic of the elements present and so show clearly their distributions across the area of the specimen scanned. Alternatively, qualitative analyses may be carried out on separate points in the specimen by simply stopping the scan.

The X-rays are sampled on the basis of their photon energies in an ED system which is suited to the SEM, due to the low beam energies used and the decreased X-ray intensities obtained. The superior performance of the Li-doped, Si crystal detector allows the simultaneous gathering of X-rays of all energies at sufficient counts in about one minute. Spectra of X-ray energy versus intensity are presented in Volume II for various accessory minerals described in Chapters 4 and 7.

For semi-quantitative analyses, the nett X-ray intensities are obtained by spectral deconvolution before ZAF corrections are applied to give the concentrations of elements present. Since the efficiency of detection of the solid-state detector remains constant for long periods, it is possible to measure the characteristic intensities from all relevant standards and to store these as ratios to the intensity from one easily reproducible standard (eg. Co). In the course of routine analysis, only the single standard is then measured in order to give the individual standard intensities from the stored ratios. The principle is the same as that used for fully quantitative analysis in ED electron probes (Long, 1977), but is regarded as only semi-quantitative in the present combination of an analytical attachment (supplied by Link Systems) with a machine designed specifically as an SEM (Cambridge S150; see Plate 202).

Although it is much quicker to use and has a greater resolution of the beam, SEM with EDS suffers from a number of inherent disadvantages compared to EPMA with WDS (Section 4). The crowded ED spectrum results in inferior element discrimination and there are interferences of the following peaks;

U M :Th M , U M :K K , U M :Ca K , P K :Y L :Zr L , LREE L

which are measured for many of the accessory minerals described in Chapters 4 and 7, although spectral stripping corrects for this up to a certain point, during semi-quantitative measurements. Compared with WDS, EDS has a lower precision and accuracy, a poorer detection limit (0.2 wt%) and can only measure elements down to Na in atomic number.

6. Transmission electron microscopy (TEM)

Only limited use was made of TEM in this study, but a comprehensive introduction to the technique is provided by Loretto (1975). Part of a doubly-polished, demountable section containing the grain of interest was attached to a 3 mm diameter, Ti grid by epoxy resin. After ion-beam thinning to a thickness of approximately 0.5 μm , the sample was placed in the holder of a JEOL 4000FX TEM, operating at an accelerating voltage of 400 kV. Electron diffraction patterns and micrographs were obtained from coffinite (Plates 145 and 146), haematite, anatase and phyllosilicates.

7. X-ray diffraction (XRD)

Where determination of chemical composition leads to equivocal identification of a mineral, XRD provides an independent, alternative technique, which is described by Zussman (1977). A Philips X-ray

powder diffractometer with Co tube-target and Fe filter was sufficient for relatively large amounts of mineral separate.

In most cases, however, mineral grains ranging from 60 to 300 μm in diameter were extracted from a polished thin-section or block, using a spring-loaded, diamond-tipped tool fitted to the objective socket of a microscope. A small ball of gum was rolled over the section beneath a blank slide, so that the powdered mineral grains adhered to it. The specimen-gum mixture was picked up by a fine glass capillary, which had been dipped in more gum, and placed in a 57.3 mm radius Debye-Scherrer powder camera. Exposure times, using a fine, circular collimator, ranged from 3 to 5 hours.

Appendix 2 Instrumental Neutron Activation Analysis (INAA)
for the Measurement of U and Th

1. Introduction

Detailed accounts of the use of INAA in the geosciences are given by Muecke (1980) and Goles (1977). INAA provides a relatively rapid, multi-element analysis of high quality without the need of chemical separation and with minimal sample preparation and standardisation. Plant *et al.* (1976) gave the limits of detection for Th and U as 0.5 ppm and 1 ppm respectively. The analytical precision for Th was 25% and for other elements 5 to 15% at the 95% confidence limit.

The only other technique comparable with INAA in terms of quality, speed and convenience is X-ray fluorescence (XRF), but only a few trace elements can be rapidly determined by XRF with good precision. Other techniques (e.g. spark source mass spectrometry, atomic absorption spectrometry and emission spectrometry) either have a lower precision, are slow or require substantial sample preparation. The main drawback of INAA is its relatively high cost (£10 per sample), which has limited the number of samples analysed in this study (at the London University Reactor Centre).

2. Sample preparation

Large hand-specimen samples were cleaned of weathered surfaces as far as possible, before crushing in a jaw crusher to 1 cm sized fragments. Many of the samples were so altered, they could be pulverised with a hammer. A Tema mill was used to reduce the gravel to rock flour after 3 minutes, with tungsten rings. At every stage, contamination between samples was minimized by air-brushing or washing in water or acetone.

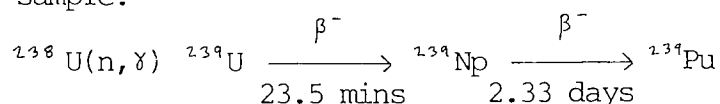
Rock gravel was halved or quartered before milling to ensure unbiased sampling. This was also ensured, prior to weighing, by mixing each rock powder thoroughly for 5 minutes and, during weighing, by collecting powder from random positions with a spatula for each sample. Accurate weighing is crucial to the quality of the results, and amounts of around 0.2 g and 1 g were measured to the nearest 0.0001 g for each sample and sealed into polyethylene vials, suitable for the irradiation.

3. Irradiation

The vials were suspended in the core of a 100 kw Consort reactor, where they were bathed in a flux of low energy (thermal) neutrons of $1 \times 10^{12} \text{ n/cm}^{-2}/\text{sec}^{-1}$. An irradiation time of 1 day and cooling time of 2.5 days (approximately the half life of ^{239}Np) were chosen to maximise the activity of the radioisotopes of interest and minimise the activity of other radioisotopes, especially ones that are potentially interfering. Use of a Cd filter gives a narrower range of thermal neutrons, resulting in a much enhanced peak to background ratio of the gamma peaks subsequently measured.

During the irradiation, a fraction of the ^{239}U present in each sample undergoes neutron capture, a process involving the absorption of

a low-energy neutron by a nucleus and the prompt emission of gamma rays. The resulting mass increase of 1 produces a new isotope which, in the case of ^{238}U , is unstable and decays, through the emission of beta particles and gamma rays (of energy 74.7 KeV) to ^{239}Np . ^{239}Np itself is converted to ^{239}Pu , through beta decay, emitting gamma rays of energy 106.14 KeV, which are measured to determine the concentration of U in the sample:-



The sensitivity of INAA for a particular element depends on several factors during irradiation and counting. Rather than measure these factors independently, a standard with known concentrations of the element(s) of interest is included with the sample so that all the conditions of irradiation and detection cancel. A solution of a mixture of known amounts of pure chemicals, evaporated on to filter paper, is routinely included with each batch of samples irradiated. However, the standard material is of very different physical and chemical composition compared with the unknowns, resulting in different spectra for the two types of material and the introduction of serious systematic errors during peak area determinations. To overcome this problem, a powdered rock of known composition is used as a reference standard for each batch of 10 samples. SY-2, produced by CANMET was used in this case because it contains U and Th in roughly similar amounts to many of the samples analysed (290 ppm U and 380 ppm Th) and its major and trace element contents do not seriously differ from those of the unknowns. In order to ensure activation of standards and unknowns by identical fluxes of neutrons, the standards and unknowns are placed in the reactor in close proximity to each other.

4. Counting

Counting of the gamma rays was carried out on a planar pure Ge detector, which is the most efficient for energies up to 200 KeV. Each sample was counted for 17 elements (including U and Th) simultaneously for 1 hour, using a Nuclear Data 6620 multichannel analyser with on-line computing facilities for immediate trace element concentration measurements. This provides 4000 channels for analysis of an energy spectrum spanning 1 MeV. The samples are adjusted for optimum distance from the counters to ensure maximum counts but a minimum counter deadtime (below 15%).

5. Interferences

Problems frequently encountered with INAA are interfering nuclear reactions, which occur during activation and cooling, and spectral interferences, which appear during the detection of radioactivity. Of the former type of interference, primary reactions are the most important in the analysis of U-rich samples, in which the fission of U enhances the LREE and other elements (Plant *et al.*, 1976). Spectral interferences result from radioisotopes with peak energies similar to those being measured for the analysis of U and Th.

6. Short irradiation for the analysis of U

In order to form a useful comparison with the long irradiation method and to analyse a larger, more representative sample of rock powder, 1 g amounts of the same samples were subjected to much shorter periods of irradiation (15 minutes), cooling (5 minutes) and counting (5 minutes) for the analysis of U only. Shorter times are necessary because of the much greater matrix interferences of the larger samples and because the radioisotope being measured (^{234}U at 74.7 KeV) has a half-life of only 23.5 minutes.

For the standards, a solution of 100 ppm U was evaporated on to pieces of filter paper which were packed tightly into the 1 g capsules in order to simulate, as closely as possible, the matrix properties of the samples. The 3 standards were evenly interspersed with the samples and the capsules sequentially irradiated, allowed to cool and counted automatically, using a fast, pneumatic transfer system. The concentration of U (in ppm) was calculated, using the following equation:-

$$\text{U ppm} = \frac{\text{cps U} \cdot 100}{\text{c} \cdot \text{wt}}$$

Where:-

cps U = Counts per second for uranium.

wt = Weight of the rock sample analysed.

c = Constant derived from the mean average of the cps U obtained from three standards containing 100 ppm U.

7. Assessment of the results

The results of U analyses using the long and short irradiation methods are compared in Table 73. With a few exceptions, there is a close correlation between results for the two methods, although the short irradiation method tends to give higher results, especially at lower concentrations. Since the two methods rely on measuring the peaks originating from the decay of two different radioisotopes (^{234}Np for long and ^{234}U for short irradiation), they provide, to some extent, an independent check on the counting technique.

A limited estimate of precision of the technique is given by the duplicate measurements of the SY2 standard for the two batches of samples analysed. At the 95% confidence limit, Th has a precision of $\pm 1.0\%$ and U has a precision of $\pm 2.7\%$ and $\pm 5.2\%$ for the long and short irradiation methods respectively.

Accuracy is assessed by the mean value for Th obtained from SY2 (417ppm) which differs from the published Th content (380ppm) by approximately 10%. The accuracy for U is better and values of 295 and 272.5 for SY2 differ from the published U content (290ppm) by 1.7% and 6% for the long and short irradiation methods respectively.

Appendix 3 Field Radiometry

A portable gamma scintillometer giving a direct digital reading of the activity in counts per second (developed at Harwell) was used to select the more radioactive samples in the field. Measurements were treated as qualitative, but the principles underlying quantitative gamma-ray spectrometry in the field are relevant. Regarding source parameters, Cassidy (1981) recognised three important prerequisites for quantitative spectrometry:

1. Secular equilibrium in the sample between the parent radioelements (U and Th) and their daughter decay products.
2. Chemical homogeneity of the source.
3. Constant source-detector geometry.

Samples from exposures giving high counts were sometimes found to contain unexpectedly low U contents (Table 62). One possibility is that there has been a net loss of ^{238}U relative to its radioactive decay products. The ^{232}Th series, on the other hand, may be considered to be in equilibrium in most geological environments (Adams and Gasparini, 1970). Another possibility is that the U is heterogeneously distributed, on a small scale, within the outcrop measured. Løvborg *et al.* (1971) calculated that an isotropic detector (i.e. without a collimator) with a centre elevation of 5 cm measures a bowl-shaped effective sample of thickness ~15 cm, surface diameter ~80 cm and mass ~50 kg (i.e. an order of magnitude larger than a conventional hand sample). Lastly, anomalously high counts may result if the solid angle of detection does not remain constant at 180° . Killeen and Carmichael (1972) recommend that a constant geometry is obtained if the outcrop is relatively flat for a distance of about 2 m from the counter, which is at an elevation of about 10 cm. Unfortunately, it was impossible to achieve this geometry for many small outcrops with surface irregularities in the Helmsdale area.

Appendix 4 Calculation of Hypothetical wt. % H₂O in Coffinite, Thorite and Zircon

Coffinite e.g. Sample 100, Grain 4, Analysis spot 1.

Oxide wt. %		Recalculated to 4 oxygens		Recalculated to U + Th + etc. = 1
ThO ₂	1.94	Th	0.027	
UO ₂	69.2	U	0.938	
Y ₂ O ₃	0.30	Y	0.010	
CaO	0.81	Ca	0.053	
ZrO ₂	4.01	Zr	0.119	
HfO ₂	0.37	Hf	0.006	
FeO	0.01	Fe	0	
SiO ₂	14.23		Si	0.864
P ₂ O ₅	0.12		P	0.006
As ₂ O ₃	0.24		As	0.009
Total	91.23		1.153	0.879
				0.762

Assuming the formula for coffinite is (U, Th, etc.) (SiO₄)_{1-x} (OH)_{4x}:
Hypothetical (OH) content = 1 - (Si + P + As) on the assumption that
U + Th + etc. = 1.

$$\text{For Grain 4: } 4(1 - 0.762) = 0.952 \text{ (OH)-groups} \\ = 0.952/2 = 0.476 \text{ H}_2\text{O "molecules"}$$

A factor F to convert the molecule no. to wt. % can be derived from U:
0.938/1.153 = 0.814 U atoms (normalising to U + Th + etc. = 1)

$$F = \frac{\text{wt. \% UO}_2}{\text{mol. wt. UO}_2 \times \text{No. of U atoms}} = \frac{69.2}{270 \times 0.814} = 0.315$$

$$\text{Wt. \% H}_2\text{O} = (\text{No. of H}_2\text{O "molecules"}) (\text{mol. wt. H}_2\text{O}) F \\ = 0.476 \times 18 \times 0.315 \\ = 2.7$$

Similarly for thorite and zircon, assuming that the formulae are:
(Th, U, etc.) (SiO₄)_{1-x} (OH)_{4x} and
(Zr, Hf, etc.) (SiO₄)_{1-x} (OH)_{4x} respectively.

Appendix 5 Calculation of Hypothetical Initial Composition of Type 2 Zircon from the Albitised Granite (411 m Depth)

Assumptions

1. All the thorite inclusions in the intermediate zone of Type 2 zircon formed by exsolution from this zone only.
2. The quadrant of thorite inclusions measured (Plate 72) contains a thorite : zircon ratio which is representative of the overall zone, in its original 3 dimensional form.
3. The composition of the thorite inclusion measured is representative of the compositions of all the thorite inclusions in the zone.
4. The Zr content of the thorite inclusion, which was not measured, is low enough not to significantly affect the results of the calculation. This is likely, since the oxide total is near to 100 %.
5. The composition of zircon measured is close to the mean composition of zircon in the zone.
6. The haematite inclusions do not significantly affect the results.

The area proportion of thorite : zircon was measured from a BSEI photograph (Plate 72) using a microcomputer with a Hewlett Packard 9874A digitiser.

Area proportion thorite : zircon = 2231 : 51485 = 4.33 \equiv volume proportion

Unit-cell volume of thorite 312.7 Å³
 " zircon 260.8 Å³
 (from data in ASTM index)

Therefore, estimated molar proportion thorite : zircon is

$$\frac{4.33}{312.7} : \frac{95.67}{260.8} = 0.01385 : 0.36683$$

molar proportion of thorite is $\frac{0.01385}{0.01385 + 0.36683} = 0.0364$

Hypothetical recalculation prior to exsolution (omitting Fe):

	from zircon	from thorite	total
Zr (0.952/1.044)	0.9636		0.879
Hf (0.055/1.044)	0.9636		0.051
U (0.003/1.044)	0.9636	(0.354/1.111) 0.0364	0.014
Th (0.003/1.044)	0.9636	(0.668/1.111) 0.0364	0.025
Y (0.002/1.044)	0.9636	(0.023/1.111) 0.0364	0.003
Ca		(0.066/1.111) 0.0364	0.002
			<u>0.974</u>
Si (0.965/1.044)	0.9636	(0.928/1.111) 0.0364	0.921
P (0.005/1.044)	0.9636		0.005
			<u>0.926</u>

Hypothetical initial composition of zircon:

Mol. % (Zr + Hf) = 100(0.879 + 0.051)/0.974 = 95.48
 Mol. % (Th + U) = 100(0.014 + 0.025)/0.974 = 4.00
 Mol. % Y = 100 x 0.003/0.974 = 0.31

Appendix 6 Samples Collected in the Helmsdale Area, Northern Scotland
(see Figs. 82-85 for sample locations)

Sample No.	Sample description	Locality	*Grid Ref.	c.p.s.
5A	Green-yellow, limonite-stained, friable alteration zone.	Caen Burn, gorge section	015 188	140
5B	Pinkish granite with green flecks.	"	"	200
7A	Dark-coloured, clay-rich alteration zone.	Caen Burn	018 191	700
7B	Altered granite wallrock (on right).	"	"	780
7C	Fractured granite wallrock.	"	"	
7D	Altered granite wallrock (on left).	"	"	300
7E	Fractured granite wallrock.	"	"	220
7F	Least altered granite.	"	"	140
7G	" " "	"	"	150
10	Reddened, porphyritic granite.	Allt Staoine	027 213	
11	The same, in a fault zone.	"	027 217	
12	Very fractured, reddened granite.	Allt na Muic	000 213	200
13A	" " "	"	999 215	180
13B	Pale pink granite.	"	"	120
18A-L	Ousdale arkose with secondary uranyl mineralisation.	BGS, Surface Anomaly 5, Ousdale.	067 181	<1700
20A-E	Ousdale arkose with fluorite.	Bridge over tributary, Glen Loth.	937 127	70
21A-E	Ousdale arkose with fluorite.	A9 road cutting, Ousdale.	066 200	80-130
22A-E	Ousdale arkose. Well-bedded, with minor fluorite. Coffinite.	Coastal waterfall, Ousdale Burn. (Anom. 2)	075 185	200-1200
23A and B	Ousdale mudstone.	Cliffs at Ceann Ousdale.	076 186	70
24	Well bedded Ousdale arkose.	10 m above Loc. 22.	075 185	500
27	Grey-white granite with minor pyrite.	Ord Burn.	055 176	80
28A	Reddened granite.	"	055 177	400
28B	Reddened, fractured granite.	"	"	170
28C	Reddened wallrock of alteration zone.	"	"	900
28D	" " "	"	"	"
28E	Disaggregated alteration zone.	"	"	5700
28F	Hydrocarbon in alteration zone.	"	"	"
28G	Red granite with quartz veining and altered pyrite.	"	"	200
28H	Close to quartz vein.	"	"	
29	Fine, pink granite.	Gartymore Burn	987 162	110
30	" with radioactive peat.	"	988 160	130

31	Altered granite.	Gartymore Burn	986	156	110
32	Red fine granite.	"	988	158	100
33	Pink granite with haematite veins.	"	989	158	90
34	Slightly reddened granite.	"	990	158	100
35	Fractured granite with limonite.	Track to Creag	033	170	115
36A	Yellow, friable alteration zone.	Thoraraidh	029	177	135
36B	Altered granite wallrock.	"	"	"	180
36C	Least altered wallrock of zone.	"	"	"	120
37	Pinkish, fine granite.	Caen Burn.	027	192	120
38A	Red granite wallrock.	"	026	193	100
38B	Greenish alteration zone.	"	"	"	120
39A	Fault plane surface.	"	024	193	140
39B	Crush zone in fault.	"	"	"	190
39C	" " "	"	"	"	160
40	Red, fine granite.	"	"	"	150
41	Pink, fine granite.	"	022	193	110
42	Fractured, red granite.	"	020	193	260
43	Altered, porphyritic granite	Culgower Burn.	972	125	120
44A	Granite wallrock.	"	971	128	120
44B	Greenish, Fe-stained alteration.	"	"	"	160
45	Pink, fine granite.	Allt an Dir.	012	192	110
46A	Fractured, red granite.	"	009	195	350
46B	Disaggregated granite in zone.	"	"	"	400
46C	Wallrock of zone.	"	"	"	400
46D	Red, fractured wallrock.	"	"	"	280-
					450
46E	Thin, white clay band along edge of alteration zone.	"	"	"	
46F	Disaggregated granite in zone.	"	"	"	500
47A	Pink, fine granite.	Caen Burn.	017	190	110
47B	Altered wallrock.	"	"	"	
47C	Disaggregated green and orange granite in alteration zone.	"	"	"	280
48	Altered granite in fault crush zone.	Allt Cille Pheadair.	991	194	130
49	Fractured, haematised porphyritic granite.	"	993	208	150
50A	Fe-oxide crust in disaggregated, porphyritic granite.	"	993	211	160
50B	Residual granite layer in disaggregated porphyritic granite.	"	"	"	130
51	Fe-stained, porphyritic granite.	Allt na Maoile	008	220	150
52	Pale, disagg. porphyritic granite, with reddened granite corestones.	Allt na Muic	999	216	130
52A		"	998	216	
53A	Yellow-green, Fe-stained, disaggregated alteration zone.	Lothmore valley	965	119	230
53B	Pale green altered wallrock.	"	"	"	180
53C	Bleached, porphyritic granite.	"	"	"	170
54	Well-bedded arkose with clasts of ?Moine quartzite.	Glen Loth	938	164	60

* OS map, 1:50 000 scale, Sheet 17.
 c.p.s. Counts per second at outcrop, using portable gamma scintillometer.

Appendix 7 Approximate Modal Analysis of Coffinite in the
Ousdale Arkose

Coffinite grains in Section 471 were measured from high magnification SEM photographs and the contribution of coffinite to the rock U content was calculated:

Grain No.	Area of grain (μm^2)
1	12089
10	5100
12	800
4	25000

Total area of coffinite = 42989 \approx $4.3 \times 10^4 \mu\text{m}^2$
Total area of section = $4.6 \times 10^8 \mu\text{m}^2$

$$V = \frac{U \text{ ppm}}{Z \times D}$$

where: U ppm = U content of rock contributed by coffinite
 V = Volume proportion of coffinite
 = $\frac{4.3 \times 10^4}{4.6 \times 10^8}$
 D = Density of coffinite relative to host rock
 = 2
 Z = U content of coffinite (ppm)
 = 6×10^5

Thus: $\frac{4.3 \times 10^4}{4.6 \times 10^8} = \frac{U \text{ ppm}}{12 \times 10^5}$

$$U \text{ ppm} = 112 \text{ ppm}$$

Measurements of many more sections from this sample are required to give a more representative value of the contribution of coffinite to the rock U content. The contribution exceeds the measured bulk U content (60 ppm) because coffinite distribution is likely to be very heterogeneous on the scale of one thin section. Even allowing for this, it seems likely that the volume of coffinite accounts for most of the rock U content of Sample 471.

References

- Abdel-Gawad, A. M. and Kerr, P. F. (1961): Urano-organic mineral association: *Am. Mineral.* 46, p. 402-419.
- Adamek, P. M. and Wilson, M. R. (1979): The evolution of a uranium province in north Sweden: *Phil. Trans. R. Soc. Lond. A* 291, p. 355-368.
- Adams, J. A. S. and Gasparini, P. (1970): Gamma-ray spectrometry of rocks. *Methods in geochemistry and geophysics* 10: Elsevier.
- Adams, J. A. S. and Richardson, K. A. (1960): Thorium, uranium and zirconium concentrations in bauxite: *Econ. Geol.* 55, p. 1653
- Ahrens, L. H. (1965): Some observations on the uranium and thorium distributions in accessory zircon from granitic rocks: *Geochim. Cosmochim. Acta.* 29, p. 711-716.
- Ahrens, L. H., Cherry, R. D., and Erlank, A. J. (1967): Observations on the Th-U relationship in zircons from granitic rocks and from kimberlites: *Geochim. Cosmochim. Acta.* 31, p. 2379-2387.
- Ahrens, L. H. and Erlank, A. J. (1969): Hafnium: In: *Handbook of Geochemistry*, II-5, Chapt. 72B-0, (Wedepohl, K. E., ed.) Springer, Berlin etc., 1978.
- Alderton, D. H. M., Pearce, J. A. and Potts P. J. (1980): Rare earth element mobility during granite alteration : evidence from southwest England: *Earth Planet. Sci. Lett.* 49, p. 149-165.
- Allman-Ward, P. (1985): Distribution of uranium and thorium in the western lobe of the St. Austell granite and the effects of alteration processes: In: *High heat production (HHP) granites, hydrothermal circulation and ore genesis*, I.M.M., London, p. 437-458.
- Altschuler, Z. S., Clarke, R. S., and Young, E. J. (1954): Uranium in apatite: *Bull. Geol. Soc. Am.* 65, p. 1225-6.
- Anderson, I. (1987): Palaeontologists probe for Earth's biggest beast: *New Scientist*, No. 1557, 23 April, p. 24.
- Andersen, T. and Neumann, H. (1985): Identity of "freyalite", an alleged rare-earth-rich variety of thorite and its pre-metamict composition: *Am. Min.*, 70, No.10, p. 1059-1064.
- Andreoli, M. A. G., Robb, L. J., Meyer, M., Ainslie, L. C. and Hart, R. J. (1985): Granitoids of the pre-Witwatersrand basement: clues to the source of uranium placer mineralization: Report presented at I.A.E.A. Technical Committee Meeting on Recognition of Uranium Provinces, Sept. 18-20, 1985, London, 15 p.
- Arribas, A. (1966): New mineralogical and metallogenic data on coffinite: *Estud. Geol., Inst. Invest. Geol. "Lucas Mallada"* 22, p. 47-59. (Chem. Abst. 68:51943.)
- Ashley, P. M. (1984): Sodic granitoids and felsic gneisses associated with uranium-thorium mineralisation, Crocker's Well, South Australia: *Mineral. Deposita* 19, p. 7-18.
- Bagnall, K. W. (1972): *The actinide elements*: Elsevier, Amsterdam, 272 p.
- Bajo, C., Rybach, L. and Weibel, M. (1983): Extraction of uranium and thorium from Swiss granites and their microdistribution. 2. Microdistribution of uranium and thorium: *Chem. Geol.*, 39, p. 299-318.
- Baker, J. H. (1985): Rare earth and other trace element mobility accompanying albitization in a Proterozoic granite, W. Bergslagen, Sweden: *Min. Mag.* 49, p. 107-15.
- Ball, T. K. and Basham, I. R. (1979): Radioactive accessory minerals in granites from south-west England: *Proc. Ussher Soc.*, 4, Pt.3, p. 437-448.
- Ball, T. K., Basham, I. R. and Michie, U. McL. (1982): Uraniferous vein occurrences of south-west England - paragenesis and genesis: In: *Vein-type and similar uranium deposits in rocks younger than Proterozoic*: Proc. Tech. Comm. Meeting, Lisbon, I.A.E.A., Vienna, p. 113-158.

- Ballantyne, S. B. and Littlejohn, A. L. (1982): Uranium mineralization and lithogeochemistry of the Surprise Lake batholith, Atlin, British Columbia: In: Uranium in Granites, (Maurice, Y. T., ed.): Geol. Surv. Canada, Paper 81-23, p. 145-155.
- Baranov, V. I. and Lieh-T'ien, Tu (1961): The relation of the uranium concentrations in zircon, monazite and sphene from granites to the alterability of these minerals: *Geochemistry* 11, p. 1148-1150.
- Baranov, V. I., Lieh-T'ien, Tu and Korobkov, V. I. (1962): Geochemistry of uranium and thorium in the granitic rocks of the Kyzyltau Massif (central Kazakhstan). Part 2. Modes of occurrence of radioactive elements in granitic rocks: *Geochemistry* 5, p. 469-483.
- Barretto, P. M. C. (1985): Identification of uranium province in Brazil: Report presented at I.A.E.A. Technical Committee Meeting on Recognition of Uranium Provinces, Sept. 18-20, 1985, London, 23 p.
- Barretto, P. M. C. and Fujimori, K. (1986): Natural analogue studies: geology and mineralogy of Morro do Ferro, Brazil: *Chem. Geol.*, 55, p. 297-312.
- Barritt, S. D. (1983): The controls of radioelement distribution in the Etive and Cairngorm granites: implications for heat production: Ph.D. thesis, Open University.
- Barthel, F. H. (1974): Review of uranium occurrences in Permian sediments in Europe, with special reference to uranium mineralizations in Permian sandstone: In: Formation of Uranium Ore Deposits, I.A.E.A. Proc., Vienna, p. 277-288.
- Basham, I. R., Ball, T. K., Beddoe-Stephens, B. and Michie, U. M. (1982a): Uranium-bearing accessory minerals and granite fertility: I. Methods of identification and evaluation: In: Uranium Exploration Methods, Proc. Symp., I.A.E.A./N.E.A., Paris, June, 1982, p. 385-398.
- Basham, I. R., Ball T. K., Beddoe-Stephens, B. and Michie U. M. (1982b): Uranium-bearing accessory minerals and granite fertility: II. Studies of granites from the British Isles: In: Uranium Exploration Methods, Proc. Symp., I.A.E.A./N.E.A., Paris, June, 1982, p. 399-414.
- Basham, I. R., Bowles, J. F. W., Atkin, D. and Bland, D. J. (1982c): Mineralogy of uranium distribution in samples of unaltered and sericitised granite from Urgeirica, Portugal, in relation to mineralization processes: In: Vein-type and similar uranium deposits in rocks younger than Proterozoic: Proc. Tech. Comm. Meeting, Lisbon, I.A.E.A., Vienna. p. 299-309.
- Basham, I. R., Vairinho, M. M. B. and Bowles, J. F. W. (1982d): Uranium-bearing accessory minerals in the São Pedro Do Sul granite, Portugal: In: Vein-type and similar uranium deposits in rocks younger than Proterozoic: Proc. Tech. Comm. Meeting, Lisbon. I.A.E.A., Vienna, p. 279-298.
- Basham, I. R. and Easterbrook, G. D. (1977): Alpha-particle autoradiography of geological specimens by use of cellulose nitrate detectors: *Trans. Inst. Mining Metall. B* 86, p. 96-98.
- Basham, I. R. and Rice, C. M. (1974): Uranium mineralization in Siwalik sandstones from Pakistan: In: Formation of Uranium Ore Deposits, I.A.E.A. Proc., Vienna, p. 405-418.
- Bayushkin, I. M. (1970): Uraninite-coffinite mineralization in a uranium-molybdenum deposit: *Mestorozhd. Urana. Zon. Paragenezisy*, p. 73-92.
- Bayushkin, I. M. and Dikov, Yu. P. (1974): Uranium silicates in hydrothermal uranium mineralization: *Geochem. Internat.*, 11, Pt.2, p. 1162-1170.
- Bayushkin, I. M., Vlasov, B. P., Volovikova, I. M. and Tyutin, V. N. (1968): Uranium-molybdenum mineralization in a buried extrusive dome of felsites: *Geol. Vop. Genezisa Endogennykh Uranovykh Mestorozhd.*, p. 207-34.

- Belova, L. N., Tananaeva, G. A. and Frolova, K. E. (1969): Coffinite: *At. Energ.*, 27(i), p. 61-63.
- Berzina, I. G., Yeliseyeva, O. P. and Popenko, D. P. (1974): Distribution relationships of uranium in intrusive rocks of northern Kazakhstan: *Int. Geol. Rev.*, 16, No.11, p. 1191-1204. (Chem. Absts. 80:5691).
- Bohse, H., Rose-Hansen, J., Sørensen, H., Steenfelt, A., Løvborg, L. and Kunzendorf, H. (1974): On the behaviour of uranium during crystallization of magmas - with special emphasis on alkaline magmas: In: *Formation of Uranium Ore Deposits*, I.A.E.A. Proc., Vienna, p. 49-60.
- Bomber, B. J., Ledger, E. B. and Tieh, T. T. (1986): Ore petrography of a sedimentary uranium deposit, Live Oak County, Texas: *Economic Geology*, 81, p. 131-142.
- Borovec, Z., Kribek, B. and Tolar, V. (1979): Sorption of uranyl by humic acids: *Chem. Geol.*, 27, p. 39-46.
- Boulton, J. (Editor) (1978): *Management of radioactive fuel wastes: The Canadian disposal program*: Atomic Energy of Canada Ltd., Rep., AECL-6314, 135 p.
- Bowden, P. (1966): Zirconium in younger granites of northern Nigeria: *Geochim. Cosmochim. Acta*, 30, p. 985-93.
- Bowden, P. (1982): Magmatic evolution and mineralization in the Nigerian younger granite province: In: *Metallization Associated with Acid Magmatism*, (Evans A. M., ed.), John Wiley and Sons Ltd., London, p. 51.
- Bowden, P., Van Breemen, O., Hutchison, J. and Turner, D. C. (1976): Palaeozoic and Mesozoic age trends for some ring complexes in Niger and Nigeria: *Nature*, London, 259, p. 297-299.
- Bowden, P., Bennett, J. N., Kinnaird, J. A., Whitley, J. E., Abaa, S. I. and Hadzigeorgiou-Stavrakis, P. K. (1981): Uranium in the Niger-Nigeria younger granite province: *Mineralogical Magazine*, 44, p. 379-89.
- Bowden, P. and Kinnaird, J. A. (1984a): The petrology and geochemistry of alkaline granites from Nigeria: *Physics of the Earth and Planetary Interiors*, 35, p. 199-211.
- Bowden, P. and Kinnaird, J. A. (1984b): Geology and mineralization of the Nigerian anorogenic ring complexes: *Geologisches Jahrbuch*, B 56, p. 3-65.
- Bowie, S. H. U. (1955): Thucolite and hisingerite-pitchblende complexes from Nicholson Mine, Saskatchewan, Canada: *Bull. Geol. Surv. Gt. Br.* 10, p. 45-57.
- Bowie, S. H. U. (1977): Radiographic techniques: In: *Physical Methods in Determinative Mineralogy*, (Zussman, J., ed.), 2nd edition, Academic Press, p. 677-687.
- Bowie, S. H. U. and Atkin, D. (1956): An unusually radioactive fossil fish from Thurso, Scotland: *Nature*, 177, p. 487-8.
- Bowie, S. H. U., Ostle, D. and Gallagher, M. J. (1970): Uranium reconnaissance in northern Scotland: *Trans. Inst. Min. Met.* B 79, p. 180.
- Bowie, S. H. U., Simpson, P. R. and Rice, C. M. (1973): Application of fission-track and neutron activation methods to geochemical exploration: In: *Geochemical Exploration 1972*, (Jones, M. J., ed.), *Trans. Inst. Min. Met.*, London, p. 359-372.
- Bowles, J. F. W. (1978): Quantitative microprobe analysis of uranium minerals: *Microscope*, 26 p. 55-67.
- Breger, I. A. (1974): The role of organic matter in the accumulation of uranium: In: *Formation of Uranium Ore Deposits*, I.A.E.A. Proc., Vienna, p. 99-123.

- Brodin, B. V., Mel'nikova, A. M., Osipov, B. S. and Pavlov, E. G. (1976): Apatite-brannerite-pitchblende association of hydrothermal quartz veins: *Izv. Akad. Nauk SSSR, Ser. Geol.* 11, p. 67-79 (Russ.).
- Brookins, D. G. (1975): Coffinite-uraninite stability relations in Grants Mineral Belt, New Mexico: *Am. Assoc. Petroleum Geologists Bull.* 59, p. 905 (Abstract only).
- Brown, G. C., Cassidy, J., Oxburgh, E. R., Plant, J., Sabine, P. A. and Watson J.V.(1980): Basement heat flow and metalliferous mineralization in England and Wales: *Nature*, 288, p. 657-659.
- Brynard, H. J. (1984): A review of the regional setting of some South African granites and their potential as uranium provinces: Report to the I.A.E.A. / N.E.A. Meeting on the Recognition of Uranium Provinces, Keyworth, 23-25 May, 1984, 9 p.
- Bursill, L. A. and McLaren, A. C. (1966): Transmission electron microscope study of natural radiation damage in zircon ($ZrSiO_4$): *Phys. Stat. Sol.*, 13, p. 331-343.
- Cameron, J. (1982): Mineralogical aspects and origin of the uranium in the vein deposits of Portugal: In: Vein-type and similar uranium deposits in rocks younger than Proterozoic: Proc. Tech. Comm. Meeting, Lisbon, I.A.E.A., Vienna, p.349-370.
- Cameron-Schimann, M. (1978): Electron microprobe study of uranium minerals and its application to some Canadian deposits: Unpublished Ph.D. thesis, University of Alberta.
- Caruba, R., Baumer, A., Ganteaume, M. and Iacconi, P. (1985): An experimental study of hydroxyl groups and water in synthetic and natural zircons: A model of the metamict state: *Am. Min.* 70, p. 1224-1231.
- Caruso, L., Swinden, T. and Simmons, G. (1982): Uranium migration through microcracks, Geevor Tin Mine, Cornwall, England: *Trans. Am. Geophys. Union*, 63, No.45, p. 1128.
- Caruso, L. and Simmons, G. (1985): Uranium and microcracks in a 1000-meter core, Redstone, New Hampshire: *Contrib. Mineral. Petrol.* 90, p. 1-17
- Cassidy, J. (1981): Techniques of field gamma-ray spectrometry: *Min. Mag.* 44, p. 391-8.
- Cathelineau, M. and Leroy, J. (1981): Reactions between uranium veins and their host rocks in Vendée and Limousin (France): *Min. Mag.* 44, p. 417-23.
- Cathelineau, M. (1983): Potassic alteration in French hydrothermal uranium deposits: *Mineral. Deposita* 18, p. 89-97.
- Cathelineau, M. (1987): U-Th-REE mobility during albitization and quartz dissolution in granitoids: Evidence from south-east French Massif Central: *Bull. Mineralogie*, 2, 19 p. (in press).
- Chatterjee, A. K. and Strong, D. F. (1984): Rare-earth and other element variations in greisens and granites associated with East Kemptville Tin Deposit, Nova Scotia, Canada: *Trans. Instn. Min. Metall.* B 93, p. 59-70.
- Chatterjee, A. K. and Strong, D. F. (1985): Review of some chemical and mineralogical characteristics of granitoid rocks hosting Sn, W, U, Mo deposits in Newfoundland and Nova Scotia: In: High heat production (HHP) granites, hydrothermal circulation and ore genesis, I.M.M., London, p.489-516.
- Chovan, M. and Kral, J. (1979): Uranium in accessory minerals of granite rocks in Veporides: *Geologicky Zbornik - Geologica Carpatica*, 30, 2, Bratislava, p. 227-234.
- Chyi, L. L. (1986): Characteristics and genesis of zirconium and hafnium deposits: In: *Mineral Parageneses, 1986*, Athens. (Craig, J.R., Hagni, R.D., Kiesel, W., Lange, I.M., Petrovskaya, N.V., Shadlun, T.N., Udubasa, G., Augustithis, S.S., eds.).

- Clark, G. J., Gulson, B. L. and Cookson, J. A. (1979): Pb, U, Tl, Hf and Zr distributions in zircons determined by proton microprobe and fission track techniques: *Geochim. Cosmochim. Acta*, 43, p. 905-918.
- Clark, S. P. Jr., Peterman, Z. E. and Heier, K. S. (1966): Abundances of uranium, thorium and potassium: In: *Handbook of Physical Constants*, (Clark, S. P., Jr., ed.), *Geol. Soc. Am. Mem.* 97, p. 521-541.
- Clarke, R. S., and Altschuler, Z. S. (1958): Determination of the oxidation state of uranium in apatite and phosphorite deposits: *Geochim. Cosmochim. Acta*, 13, p. 127-142.
- Clemmey, H. (1981): Some aspects of the genesis of heavy mineral assemblages in Lower Proterozoic uranium-gold conglomerates: *Min. Mag.* 44, p. 399-408.
- Correia Neves, J. M., Lopes Nunes, J. E. and Sahama, Th. G. (1974): High hafnium members of the zircon-hafnion series from the granite pegmatites of Zambézia, Mozambique: *Contrib. Mineral. Petrol.*, 48, p. 73-80.
- Cuney, M. (1978): Geologic environment, mineralogy and fluid inclusions of the Bois Noirs-Limouzat uranium vein, Forez, France: *Econ. Geol.*, 73, p. 1567-1610.
- Dall'aglio, M., Gragnani, R. and Locardi, E. (1974): Geochemical factors controlling the formation of the secondary minerals of uranium: In: *Formation of Uranium Ore Deposits*, I.A.E.A. Proc., Vienna, p. 33-48.
- Darnley, A. G., English, T. H., Sprake, O., Preece, E. R. and Avery D. (1965): Ages of uraninite and coffinite from south-west England: *Min. Mag.* 34, p. 159-176.
- Davies, R. V., Kennedy, J., McIlroy, R. W., Spence, R. and Hill, K. M. (1964): Extraction of uranium from sea-water: *Nature*, 203, p. 1110-1115.
- Davis, G. L. (1976): The ages and uranium contents of zircons from kimberlites and associated rocks: *Carnegie Inst. Wash. Year Book*, 62, p. 223-227.
- Davis, G. L. (1977): Zircons from the mantle: *Carnegie Inst. Wash. Year Book*, 77, p. 895-897.
- Deer, W. A., Howie, R. A. and Zussman, J. (1962): *Rock forming minerals. Volume 5, Non-silicates: 1st Ed.*, Longman.
- Deer, W. A., Howie, R. A. and Zussman, J. (1966): *An introduction to the rock-forming minerals: Longman*, 528 p.
- Deer, W. A., Howie, R. A. and Zussman, J. (1981): Zircon: In: *Rock forming minerals. Volume 1A, Orthosilicates: 2nd Ed.*, Longman, p. 418.
- DeVoto, R. H. (1978): Uranium in Phanerozoic sandstone and volcanic rocks: In: *Short Course in Uranium Deposits: Their Mineralogy and Origin*, (Kimberley, M. M., ed.): *Mineral. Assoc. of Canada*, p.293-306.
- Dmitriev, L. V. and Leonova, L. L. (1962): Uranium and thorium in granites of the Kaib Massif (Central Kazakhstan): *Geokhimiya*, p. 665-72.
- Dongarra, G. (1984): Geochemical behaviour of uranium in the supergene environment: In: *Uranium geochemistry, mineralogy, geology, exploration and resources*. (de Vivo, B.; Ippolito, F.; Capaldi, G.; Simpson, P. R., eds.), I.M.M., London, p. 18-22.
- Dubinchuk, V. T., Pen'kov, V. F., Uspenskiy, V. A., Avdonin, A. S. and Shevchenko, V. N. (1977): Replacement of uraninite by kerrite and coffinite: *Geochemistry International*, 14, p. 182-187 (Translated from *Geokhimiya*, 2, p. 283-288).
- Effimoff, I. (1972): The chemical and morphological variations of zircons from the Boulder Batholith, Montana: Ph.D. dissertation, Univ. of Cincinnati.
- Ehmann, W. D., Chyi, L. L., Garg, A. N. and Ali, M. Z. (1979) The distribution of zirconium and hafnium in terrestrial rocks, meteorites and the moon: In: *Origin and distribution of the elements* (Ahrens, L. H., ed.). Pergamon Press, New York, p. 247-259.

- Ellsworth, H. V. (1928): Thucolite, a remarkable primary carbon mineral from the vicinity of Parry Sound, Ontario: *Amer. Mineral.* 13, p. 419-441.
- El Shazly, E. M., El Hazek, N. M. T. and Abdel Monem, A. A. *et al.* (1974): Origin of uranium in Oligocene Qatrani sediments, Western Desert, Arab Republic of Egypt: In: Formation of Uranium Ore Deposits, I.A.E.A. Proc., Vienna, p. 467-478.
- Exley, R. A. (1980): Microprobe studies of REE-rich accessory minerals: implications for Skye granite petrogenesis and REE mobility in hydrothermal systems: *Earth and Planetary Science Letters*, 48, p. 97-110.
- Feather, C. E. (1981): Some aspects of Witwatersand mineralization, with special reference to uranium minerals: In: Genesis of uranium and gold-bearing Precambrian quartz-pebble conglomerates, (Armstrong, F. C. ed.), Prof. Pap. U. S. Geol. Surv. 1161-A-BB, p. Q1-Q23.
- Fehn, U., Cathles, L. M. and Holland, H. D. (1978): Hydrothermal convection and uranium deposits in abnormally radioactive plutons. *Econ. Geol.* 73, p. 1556-1566.
- Ferris, C. S. and Ruud, C. O. (1971): Brannerite: its occurrences and recognition by microprobe: *Colorado School Mines Quarterly*, 66, No.4, p. 1-35.
- Finch, C. B., Harris, L. A. and Clark, G. W. (1964): The thorite - huttonite phase transformation as determined by growth of synthetic thorite and huttonite single crystals: *Am. Min.* 49, p. 782-785.
- Flynn, R. T. and Burnham, C. W. (1978): An experimental determination of rare earth partition coefficients between a chloride containing vapour phase and silicate melts: *Geochim. Cosmochim. Acta*, 42, p. 685-701.
- Fontan, F., Monchoux, P. and Autefage, F. (1980): Présence de zircons hafnifères dans des pegmatites granitiques des Pyrénées Ariégeoises: leur relation avec les niobo-tantalates: *Bull. Minéral.* 103, p. 88-91.
- Foord, E. E., Cobban, R. R. and Brownfield, I. K. (1985): Uranoan thorite in lithophysal rhyolite - Topaz Mountain, Utah, USA: *Min. Mag.* 49, p. 729-31.
- Ford, K. L. and O'Reilly, G. A. (1985): Airborne gamma-ray spectrometric surveys as an indicator of granophile element specialization and associated mineral deposits in the granitic rocks of the Meguma Zone of Nova Scotia, Canada: In: High heat production (HHP) granites, hydrothermal circulation and ore genesis, I.M.M., London, p. 113-133.
- Fournier, R. O. (1976): Exchange of Na⁺ and K⁺ between water vapour and feldspar phases at high temperature and low vapour pressure: *Geochim. et Cosmochim. Acta* 40, p. 1553-1561.
- Fowler, M. B. (1981): Uranium content, distribution and migration in the Glendessarry syenite, Inverness-shire: *Min. Mag.*, 44, p. 443-8.
- Fron del, C. (1953): Hydroxyl substitution in thorite and zircon: *Am. Mineral.* 38, p. 1007-1018.
- Fron del, C. (1956): Mineral composition of gummite: *Amer. Mineral.* 41, p. 539-568.
- Fron del, C. (1958): Systematic mineralogy of uranium and thorium: *United States Geological Survey Bulletin*, No. 1064, 400 p.
- Fron del, J. W. (1964): Variation of some rare earth elements in allanite: *Amer. Mineral.* 49, p. 1159-1177.
- Fron del, C. and Collette, R. L. (1957): Hydrothermal synthesis of zircon, thorite and huttonite: *Am. Min.* 42, p. 759-765.
- Fryer, B. J. and Edgar A. D. (1977): Significance of rare earth distributions in coexisting minerals of peralkaline undersaturated rocks: *Contrib. Mineral. Petrol.* 61, p. 35-48.

- Fuchs, L. H. and Gebert, E. (1958): X-ray studies of synthetic coffinite, thorite and uranothorites: *Am. Min.* 43, p. 243-248.
- Fuchs, L. H. and Hoekstra, H. R. (1959): The preparation and properties of uranium (IV) silicate: *Am. Mineral.* 44, p. 1057-1063.
- Gallagher, M. J., Michie, U. McL., Smith, R. T. and Haynes, L. (1971): New evidence of uranium and other mineralization in Scotland: *Trans. Instn. Min. Metall.* B 80, p. 150-173.
- Gandhi, S. S. (1983): Age and origin of pitchblende from the Gunnar deposit, Saskatchewan: Current research, Part B, *Geol. Surv. Canada, Paper 83-1B*, p. 291-297.
- George, D. R. (1951): Thorite from California: a new occurrence and variety: *Am. Min.* 36, p. 129-132.
- Giere, R. (1986): Zirconolite, allanite and hoegbomite in a marble skarn from the Bergell contact aureole: implications for mobility of Ti, Zr and REE: *Contrib. Mineral. Petrol.* 93, No. 4, p. 459-470.
- Gocht, W. and Pluhar, E. (1981): Type and origin of uranium mineralization in the Khorat Plateau, Thailand: *Econ. Geol.* 76, p. 1232-1244.
- Goldhaber, M. B., Reynolds, R. L. and Rye, R. O. (1983): Role of fluid mixing and fault-related sulfide in the origin of the Ray Point uranium district, South Texas: *Econ. Geol.* 78, No. 6, p. 1043-1063.
- Goles, G. G. (1977): Instrumental methods of neutron activation analysis: In: *Physical Methods in Determinative Mineralogy*. (Zussman, J., ed.), Academic Press. 2nd edition, p. 343-369
- Goni, J. (1957): Sur un phénomène d'altération du sphène et les produits qui en résultent: *Bull. Soc. franc. Min. Crist.*, 80, p. 199.
- Gorz, H. (1974): Microprobe studies of inclusions and compilation of minor and trace elements in zircons from the literature: *Chemie der Erde*, 33, p. 326-357.
- Gramaccioli, C. M. and Segalstad, T. V. (1978): A uranium- and thorium-rich monazite from a south-Alpine pegmatite at Piona, Italy: *Am. Min.* 63, p. 757-761.
- Grauert, B. and Seitz, M. G. (1973): Uranium gain of detrital zircons studied by isotopic analyses and fission track mapping: *EOS (Am. Geophys. Union, Trans.)* 54, No.4, p. 495 (Abstr.).
- Grauert, B., Seitz, M. G. and Soptrajanova, G. (1974): Uranium and lead gain of detrital zircon studied by isotopic analyses and fission track mapping: *Earth Planet. Sci. Lett.*, 21, p. 389-399.
- Guthrie, V. A. and Kleeman, J. D. (1986): Changing uranium distributions during weathering of granite: *Chem. Geol.* 54, p. 113-126.
- Haji-Vassiliou, A. (1980): The form of occurrence of uranium in deposits associated with organic matter: *Econ. Geol.* 75 (4), p. 609-17.
- Haji-Vassiliou, A. and Kerr, P. (1972): Uranium-organic matter association at La Bajada, New Mexico: *Econ. Geol.* 67, p. 41-54.
- Halenius, U. and Smellie, J. A. T. (1983): Mineralisations of the Arjeplog-Arvidsjaur-Sorsele uranium province: Mineralogical studies of selected uranium occurrences: *Neues. Jahrbuch Miner. Abh.* 147, 3, p. 229-252.
- Halenius, U., Smellie, J. A. T. and Wilson, M. R. (1986): Uranium genesis within the Arjeplog-Arvidsjaur-Sorsele uranium province, northern Sweden: In: *Vein type uranium deposits*, (Fuchs, H. D., ed.), Rep. No. IAEA-TECDOC-361, p. 21-42.
- Hall, A. (1971): Greisenisation in the granite of Cligga Head, Cornwall: *Proc. Geol. Assoc.* 82, p. 209-230.
- Hall, M. G. and Lloyd, G. E. (1981): The SEM examination of geological samples with a semiconductor back-scattered electron detector: *Am. Min.*, 66, p. 362-368.

- Harrison, R. K. (1975): Concretionary concentrations of the rarer elements in Permo-Triassic red beds of south-west England: *Bull. Geol. Surv. G. B.*, 52, p. 1-26.
- Harrison, R. K., Old, R. A., Styles, M. T. and Young, B. R. (1983): Coffinite in nodules from the Mercia mudstone group (Triassic) of the I.G.S. Knowle borehole, West Midlands: *Rep. Inst. Geol. Sci.*, No. 83/10, p. 12-16.
- Headley, T. J., Ewing, R. C. and Haaker, R. F. (1981): High resolution study of the metamict state in zircon: 39th Annual Proceeding of the Electron Microscopy Society of America (Bailey, G. W., ed.), p. 112-113.
- Heinrich, E. W. (1963): Xenotime and thorite from Nigeria: *Am. Min.* 48, p. 206-207.
- Heinrich, E. Wm. (1981): Hydrothermal alterations of conglomeratic uranium ores, Pronto Mine, Ontario, Canada: In: *Ore Genesis the State of the Art*. Springer-Verlag, Berlin, Heidelberg, New York, 1982, p. 16-24.
- Henderson, P. (1984) (Ed.): *Rare Earth Element Geochemistry*. Developments in Geochemistry 2: Elsevier, Amsterdam and Oxford.
- Henry, C. D. and Duex, T. W. (1981): Uranium in diagenesis of Pruett, Duff and Tascotal formations, Trans-Pecos, Texas: *Am. Assoc. Petroleum Geologists, Studies in Geology* 13, p. 167-180.
- Hoffman, J. F. and Long, J. V. P. (1984): Unusual sector zoning in Lewisian zircons: *Min. Mag.* 48, p. 513-17.
- Hogarth, D. D. (1977): Classification and nomenclature of the pyrochlore group: *Am. Min.*, 62, p. 403-410.
- Hostetler, P. B. and Garrels, R. M. (1962): Transportation and precipitation of uranium and vanadium at low temperatures, with special reference to sandstone-type uranium deposits: *Econ. Geol.* 57, No. 2, p. 137-167.
- Hutton, C. O. (1950): Heavy detrital minerals: *Bull. Geol. Soc. Am.* 61 (7), p. 635-716.
- Ishak, A. K. and Dunlop, A. C. (1985): Drainage sampling for uranium in the Torrington district, New South Wales, Australia: *J. Geochem. Explor.*, 24, p. 103-119.
- Ixer, R. A., Ashworth, J. R. and Pointer, C. M. (1987): Accessory mineralogy of the Ririwai biotite granite, Nigeria and its albitised and greisenised facies: *Symposium of the Thirteenth Colloquium of African Geology*, St. Andrews University, Scotland, 10-13 Sept., 1985.
- Jackson, N. J., Drysdall, A. R. and Stoesser, D. B. (1985): Alkali granite-related Nb-Zr-REE-U-Th mineralization in the Arabian Shield: In: *High heat production (HHP) granites, hydrothermal circulation and ore genesis*, I.M.M. London, p. 479-487.
- Jacobson, R. R. E. and Macleod, W. N. (1977): Geology of the Liruei, Banke and adjacent younger granite ring-complexes: *Geol. Surv. Nigeria Bull.*, 33, 117 p.
- Jefferies, N. L. (1985a): The distribution of the rare earth elements within the Carnmenellis Pluton, Cornwall: *Min. Mag.*, 49, p. 495-504.
- Jefferies, N. L. (1985b): Uraninite within the Carnmenellis Pluton, Cornwall: In: *High heat production (HHP) granites, hydrothermal circulation and ore genesis*, I.M.M., p.163-168.
- Jefford, G. (1962): Xenotime from Rayfield, Northern Nigeria: *Am. Min.* 47, p. 1467-1472.
- Jenkins, D. A. B. (1974): A mineralogical investigation of uraniferous hydrocarbons and titanates: Unpublished Ph.D. thesis, University College, Cardiff.
- Jennings, J. K. and Leventhal J. S. (1977): A new structural model for humic material which shows sites for attachment of oxidised uranium species: *Short papers of U. S. Geol. Surv. U-Th Symposium, Circular* 753, (Campbell, J. A. ed.), p. 10-11.

- Kamineneni, D. C. (1986): Distribution of uranium, thorium and rare-earth elements in the Eye-Dashwa Lakes Pluton - a study of some analogue elements: *Chem. Geol.*, 55, p. 361-373.
- Kamineneni, D. C. and Bonardi, M. (1983): Bastnaesite in fractures of the Eye-Dashwa Lakes Pluton, Atikokan, northwestern Ontario: *Canadian Mineralogist*, 21, p. 115-119.
- Kamineneni, D. C., Chung, C. F., Dugal, J. J. B. and Ejeckam, R. B. (1986): Distribution of uranium and thorium in core samples from the Underground Research Laboratory Lease Area, southeastern Manitoba, Canada: *Chem. Geol.*, 54, p. 97-111.
- Kasanskij, V. I., Laverov, N. P. and Tugarinov, A. I. (1976): Sources of the ore material of endogenous uranium deposits: *Z. Agnew. Geol.* 22, p. 448-455.
- Katayama, N., Kubo, K. and Hirono, S. (1974): Genesis of uranium deposits of the Tono Mine, Japan: In: *Formation of Uranium Ore Deposits*, I.A.E.A. Proc., p. 437-452.
- Kerrich, R. and Fryer, B. J. (1979): Archaean precious-metal hydrothermal systems, Dome Mine, Abitibi greenstone belt; II, REE and oxygen isotope relations: *Can. J. Earth Sci.*, 16, No. 3, Part 1, p. 440-458.
- Khvostova, V. A. (1969): Rare element distribution in the Ural metamorphosed conglomerates: *Geokhimiya* (3), p. 328-34.
- Killeen, P. G. and Carmichael, C. M. (1972): Experimental survey with a portable gamma-ray spectrometer, Blind River area, Ontario: a case history: In: *Uranium prospecting handbook*, (Bowie, S. H. U., Davis, M., Ostle, D., eds.), I.M.M., London, p.306-312.
- Kim, Soo Jin (1978): Chemical composition of the coffinite from the Woodrow Mine, New Mexico: *U.S.A. Mining Geol. (Korea)* 11, 183-186.
- Kimberley, M. M. (1978): High-temperature uranium geochemistry: In: *Short Course in Uranium Deposits: Their Mineralogy and Origin*, (Kimberley M. M., ed.). Mineralogical Association of Canada, p. 101-104.
- Kinnaird, J. A. (1985): Hydrothermal alteration and mineralization of the alkaline anorogenic ring complexes of Nigeria: *J. Afr. Earth Sci.*, 3, No. 1/2, p. 229-251.
- Kinnaird, J. A., Batchelor, R. A., Whitley, J. E. and Mackenzie, A. B. (1985a): Geochemistry, mineralization and hydrothermal alteration of the Nigerian high heat producing granites: In: *High heat production (HHP) granites, hydrothermal circulation and ore genesis*. I.M.M., p. 169-195.
- Kinnaird, J. A., Bowden, P., Ixer, R. A. and Odling, N. W. A. (1985b): Mineralogy, geochemistry and mineralization of the Ririwai complex, northern Nigeria: *Journ. Afr. Earth Sci.*, 3, No. 1/2, p. 185-222
- Kish, L. and Cuney, M. (1981): Uraninite-albite veins from the Mistamisk Valley of the Labrador Trough, Quebec: *Min. Mag.*, 44, p. 471-83.
- Kleeman, J. D. and Lovering, J. F. (1967): Uranium distribution in rocks by fission-track registration in Lexan plastic: *Science*, 156, p. 512.
- Kochenov, A. V. *et al.* (1981): Forms of separation and conditions of uranium precipitation in exogenous epigenetic ore deposits: *Geokhimiya*, 5, p. 769-78.
- Kohler, H. (1970): Die Änderung der zirkon morphologie mit dem differentiation grad eines granit: *Neues Jahrb. Mineral.*, *Monatsh* 9, p. 405-420.
- Koppel, V. and Sommerauer, J. (1974): Trace elements and the behaviour of the U-Pb system in inherited and newly formed zircons: *Contrib. Mineral. and Petrol.* 43, p. 71-82.
- Kornichuk, I. and Burtik, T. (1974): Lithological features and facies of uranium ore deposits in formations in the Socialist Republic of Romania: In: *Formation of Uranium Ore Deposits*, I.A.E.A. Proc., p. 343-357.

- Korolev, K. G. and Rumyantseva, G. V. (1976): Conditions of formation of collomorphic uranotitanates and brannerite: *Internat. Geol. Rev.*, 18, p. 167-171.
- Krasnobayev, A. A. (1979): Mineralogical-geochemical features of zircons from kimberlites and problems of their origin: *Internat. Geology Rev.*, 22, No. 10, 1980, p. 1199-1209.
- Krasnobayev, A. A., Znamenskiy, N. D., Starkov, V. D. and Loginova, L. G. (1976): Rare earths in the zircons of the Urals: *Geochem. Int.*, 13, No.2, p. 40-50.
- Krauskopf, K. B. (1967): *Introduction to Geochemistry*: McGraw-Hill, New York, 721 p.
- Krauskopf, K. B. (1986): Thorium and rare-earth metals as analogs for actinide elements: *Chem. Geol.*, 55, p. 323-335.
- Kresten, P. (1974): Uranium in kimberlites and associated rocks, with special reference to Lesotho occurrences: *Lithos* 7, p. 171-180.
- Kresten, P., Fels, P. and Berggren, G. (1975): Kimberlitic zircons - a possible aid in prospecting for kimberlites: *Mineral. Dep.*, 10, p. 47-56.
- Krishna Rao, N. and Rao, G. V. U. (1983): Uranium mineralization in Singhbhum shear zone, Bihar: III Nature of occurrence of uranium in apatite-magnetite rocks: *Journal Geological Society of India*, 24 (11), p. 555-561.
- Krogh, T. E. and Davis, G. L. (1973): Additions of uranium to zircon and migration of strontium and rubidium during regional metamorphism in the Grenville Province in Ontario: *E.O.S. (Am. Geophys. Union, Trans.)* 54, No. 4, p. 494, (Abstr.).
- Langmuir, D. (1978): Uranium solution-mineral equilibria at low temperatures with applications to sedimentary ore deposits: *Geochim. Cosm. Acta*, 42, p. 547-569.
- Langmuir, D. and Herman, J. S. (1980): The mobility of thorium in natural waters at low temperatures: *Geochim. Cosm. Acta*, 44, p. 1753-1766.
- Lemoine, A. (1975): Contribution a l'étude du comportement de UO_2 en milieu aqueux a haute température et haute pression: Ph.D. thesis, Nancy, 111 p.
- Leroy, J. (1978): The Margnac and Fanay uranium deposits of the La Crouzille district (Western Massif Central, France): geologic and fluid inclusion studies: *Econ. Geol.* 73, p. 1611-1634.
- Letian, D. (1986): Granite-type uranium deposits of China: In: *Vein type uranium deposits*. (Fuchs, H. D., ed.). A technical document issued by the International Atomic Energy Agency, Vienna. I.A.E.A.-TECDOC-361. p. 377-393.
- Lindroos, H. and Smellie, J. A. T. (1979): A stratabound uranium occurrence within Middle Precambrian ignimbrites at Duobblon, northern Sweden: *Econ. Geol.*, 74, p. 1118-1130.
- Littlejohn, A. L. (1981): Alteration products of accessory allanite in radioactive granites from the Canadian shield: reply: *Current Research, Part C; Geol. Surv. Can.*, Paper 81-1C, p. 93-94.
- Loiselle, M. C. and Wones, D. R. (1979): Characteristics and origin of anorogenic granites: *Geol. Soc. Am. Abstr.* 11, p. 468.
- Long, J. V. P. (1977): Electron probe microanalysis: In: *Physical Methods in Determinative Mineralogy*, (Zussman, J., ed.), 2nd Ed., Academic Press, p. 273-341.
- Loretto, M. H. (1975): Electron microscopy: In: *Physicochemical Methods of Mineral Analysis* (Nicol, A. W., ed.), Plenum Press, New York and London, p. 321-355.
- Løvborg, L., Wollenberg, G. H., Sorensen, P. and Hansen, J. (1971): Field determination of uranium and thorium by gamma-ray spectrometry, exemplified by measurements in the Ilimaussaq alkaline intrusion, South Greenland: *Econ. Geol.*, 66, p. 368-84.
- Lovering, T. G. (1955): Progress in radioactive iron oxides investigations: *Econ. Geol.* 50, p. 186-95.

- Ludwig, K. R. and Grauch, R. I. (1980): Coexisting coffinite and uraninite in some sandstone-host uranium ores of Wyoming: *Econ. Geol.* 75, p. 296-302.
- Ludwig, K. R., Nash, J. T. and Naeser, C. W. (1981): U-Pb isotope systematics and age of uranium mineralization, Midnite Mine, Washington: *Econ. Geol.*, 76, p. 89-110.
- Lyakhovich, V. V. (1962): Rare earth elements in the accessory minerals of granitoids: *Geochem.*, 1, p. 39-51.
- Mackenzie, A. B., Bowden, P. and Kinnaird, J. A. (1984): Combined neutron activation and particle track analysis of element distributions in a rock slice of mineralized granite: *Journal Radioanalytical and Nuclear Chemistry, Articles*, 82/2, p. 341-352.
- Mackevett, E. M. (1963): Geology and ore deposits of the Bokan Mountain uranium-thorium area, Southeastern Alaska: *U.S. Geol. Surv., Bull.*, 1154, 125 p.
- McLennan, S. M. and Taylor, S. R. (1979): Rare earth element mobility associated with uranium mineralization: *Nature*, 282, p. 247-250.
- Manning, D. A. C. and Pichevant, M. (1984): Experimental studies of the role of fluorine and boron in the formation of late-stage granite rocks and associated mineralisation: *Proc. 27 Int. Geol. Congress Moscow 9*, VNU Science Press, Utrecht, The Netherlands, p. 353-372.
- Mannucci, G., Diella, V., Gramaccioli, C. M. and Pilati, T. (1986): A comparative study of some pegmatitic and fissure monazite from the Alps: *Can. Min.* 24, p. 469-474.
- Marlow, A. G. (1981): Remobilization and primary uranium genesis in the Damaran orogenic belt, Namibia: Ph.D. thesis, Leeds University.
- Martin, R. F. and Bowden, P. (1981): Peraluminous granites produced by rock-fluid interaction in the Ririwai nonorogenic ring-complex, Nigeria: mineralogical evidence: *Can. Min.*, 19, p. 65-82.
- Martin Calvo, M. (1974): The role of humic natural organic matter in uranium concentration: In: *Formation of Uranium Ore Deposits*, I.A.E.A. Proc., p. 125-137.
- Maurice, Y. T. (1982): Uraniferous granites and associated mineralization in the Fury and Hecla Strait area, Baffin Island, N. W. T.: In: *Uranium in granites*. (Maurice, Y. T., ed.), *Geol. Surv. Canada, Paper 81-23*, p. 101-113.
- Medenbach, O. (1976): *Geochemie der elemente in zirkon und ihre raumliche verteilung-eine untersuchung mit der electronenstrahlmikrosonde*: M.S. Thesis, Ruprecht Karl Universitat, Heidelberg.
- Michie, U. McL. (1972): Further evidence of uranium mineralization in Orkney: *Trans. Instn. Min. Metall.*, B 81, p. 53-4.
- Mihalik, P. (1968): The geochemistry of some uranium minerals in the Dominion Reef and Witwatersrand systems: *National Institute for Metallurgy, Res. Rep.*, 414.
- Miller, A. R. (1983): A progress report: uranium-phosphorus association in the Helikian Thelon Formation and Sub-Thelon saprolite, Central District of Keewatin: *Current Research, Part A*, *Geol. Surv. Canada, Paper 83-1A*, p. 449-456.
- Mineyev, D. A. (1963): Geochemical differentiation of the rare-earths: *Geochem. Int.* 12, p. 1129-1149.
- Moench, R. H. (1962): Properties and paragenesis of coffinite from the Woodrow Mine, New Mexico: *Am. Min.*, 47, p. 26-33.
- Morton, R. D. (1974): Sandstone-type uranium deposits in the Proterozoic strata of N. W. Canada: In: *Formation of Uranium Ore Deposits*, I.A.E.A. Proc., p. 255-273.
- Morton, R. D. (1978): The identification of uranium minerals: In: *Short course in uranium deposits: their mineralogy and origin*, (Kimberley, M. M., Ed.), *Mineral. Assoc. of Canada*, p. 141-183.
- Muecke, G. K. (Ed.) (1980): *Short course in neutron activation analysis in the geosciences: Mineral. Assoc. Canada, Short Course Handb.*, 5, 279 p.

- Mueller, A. and Halbach, P. (1983): The Anderson Mine (Arizona) - an early diagenetic uranium deposit in Miocene Lake sediments: *Econ. Geol.* 78, p. 275-292.
- Muench, O. B. (1931): The analysis of cyrtolite for lead and uranium: *Am. J. Sci.*, 21, 350-357.
- Mumpton, F. A. and Roy, R. (1959): Low-temperature equilibria among ZrO_2 , ThO_2 and UO_2 : *Journal of The American Ceramic Society*, 43, No. 5, p. 234-240.
- Mumpton, F. A. and Roy, R. (1961): Hydrothermal stability studies of the zircon-thorite group: *Geochim. Cosmochim. Acta*, 21, p. 217-238.
- Nagasawa, H. (1970): Rare earth concentrations in zircons and apatites and their host dacites and granites: *Earth Planet. Sci. Lett.*, 9, p. 359-364.
- Nakashima, S., Disnar, J. R., Perruchot, A. and Trichet, J. (1984): Experimental study of mechanisms of fixation and reduction of uranium by sedimentary organic matter under diagenetic or hydrothermal conditions: *Geochim. Cosmochim. Acta* 48, p. 2321-2329.
- Nash, J. T. (1977): Speculation on three possible modes of emplacement of uranium into deposits of the Midnight Mine, Stevens County, Washington: Short papers of U.S. Geol. Surv., U-Th symposium, Circular 753, (Campbell, J. A., ed.), p. 33.
- Nash, J. T., Granger, H. C. and Adams, S. S. (1981): Geology and concepts of genesis of important types of uranium deposits: *Econ. Geol.* 75th Anniv. Vol., p. 63-116.
- Nord, G. L. (1977): Characterization of fine-grained black uranium ores by transmission electron microscopy: Short papers of U.S. Geol. Surv., U-Th Symposium, Circular 753, (Campbell, J. A., ed.), p.29-31.
- Oesterlen, M. and Vetter, U. (1986): Petrographic-geochemical characteristics and genesis of an albitized uraniferous granite in northern Cameroon, Africa: In: Vein type uranium deposits, (Fuchs, H. D., ed.). A technical document issued by the International Atomic Energy Agency, Vienna, I.A.E.A.-TECDOC-361, p. 113-142.
- Ono, A. (1975): Chemistry and zoning of zircons from some Japanese granitic rocks: *J. Japan Assoc. Min. Pet. Econ. Geol.*, 71, p. 6-17.
- Openshaw, R. (1979): Etude du système ThO_2 - UO_2 - SiO_2 : *Rapport Annuel du Cent. Rech. Petrogr. Geochim.*, Nancy, p. 88-89.
- Orajaka, I. P. (1986): Geochemistry of Kaffo Valley albite-riebeckite granite, Liruei granite ring-complex, Northern Nigeria: *Chemical Geology*, 56, No 1/2, p. 85-92
- Overstreet, W. C. (1967): The geologic occurrence of monazite: U.S. Geol. Surv. Prof. Paper, 530, 327 p.
- Pagel, M. (1982): The mineralogy and geochemistry of uranium, thorium and rare-earth elements in two radioactive granites of the Vosges, France: *Min. Mag.* 46, No. 339, p. 149-161.
- Parnell, J. (1984): The distribution of uranium in kolm: evidence from backscattered electron imagery: *Geologiska Foreningens i Stockholm Forhandlingar*, 106, Pt. 3, p. 231-234.
- Parnell, J. (1985): Uranium/rare earth-enriched hydrocarbons in Devonian sandstones, northern Scotland: *N. Jb. Miner. Mh.*, H.3, p. 132-144.
- Pavlenko, A. S., Orlova, L. P., Akhmanova, M. V. and Tobelko, K. I. (1965): Thorbastnaesite, a thorium fluorcarbonate: *Zap. Vses. Mineralog. Obschestva* 94(1), p. 105-13 (Russian). (Chem. Absts. 62-12910).
- Pavlenko, A. S., Vainshtein, E. E. and Shevaleefskii, I. D. (1957): On the hafnium-zirconium ratio in zircons of igneous and metasomatic rocks: *Geochem.*, p. 411-430.
- Peking Institute of Uranium Geology and X-ray Laboratory, Wuhan Geological College (1978): Orthobrannerite - a new mineral of the brannerite group: *Acta Geol. Sin.*, p. 241-51 (Chinese text; English abstract).

- Pen'kov, V. F. (1976): Mechanism of the formation of metasomatic manifestations of uranium containing bitumens in sandstone: Dokl. Akad. Nauk SSSR, 230(1), p. 198-201. (Russian)
- Perez, J. B. (1985): Nouvelles données sur le complexe granitique anorogénique de Taghouaji (République du Niger) influence des fluides au cours de la cristallisation: Ph.D. Thesis, Nancy University (France) and Niamey University (Niger).
- Phair, G. and Shimamoto, K. O. (1952): Hydrothermal uranorthorite in fluorite breccias from the Blue Jay Mine, Jamestown, Boulder County, Colorado: Am. Min., 37, p. 659-666.
- Pidgeon, R. T. and Aftalion, M. (1978): Cogenetic and inherited zircon U-Pb systems in granites: Palaeozoic granites of Scotland and England: In: Crustal Evoln. in N.W. Britain and adjacent regions, (Bowes, D. R. and Leake, B. E., eds.), Geol. J. Spec. Issue No. 10, p. 183-220.
- Pidgeon, R. T., O'Neil, J. R. and Silver, L. T. (1973): Observations on the crystallinity and the U-Pb isotopic system of a metamict Ceylon zircon under experimental hydrothermal conditions (abstract): Fortschr. Mineral. 50, p. 118.
- Plant, J. (1971): Orientation studies on stream-sediment sampling for a regional geochemical survey in northern Scotland: Trans. Inst. Min. Metall., B 80, p. 324-45.
- Plant, J., Brown, G. C. and Simpson, P. R. (1982): Signatures of metalliferous granites in the British Isles: In: Uranium in granites, (Maurice, Y. T., ed.), Geol. Surv. Canada, Paper 81-23, p. 169-170.
- Plant, J., Goode, G. C. and Herrington, J. (1976): An instrumental neutron activation method for multi element geochemical mapping: J. Geochem. Exp. 6, p. 299-319.
- Pliler, R. and Adams, J. A. S. (1962): The distribution of uranium and thorium in a Pennsylvanian weathering profile: Geochim. Cosmochim. Acta., 26, p. 1137-1146.
- Poty, B. P., Leroy, J. and Cuney, M. (1974): Fluid inclusions in uranium ores from intragranitic deposits in Limousin and Forez (Massif Central, France): In: Formation of Uranium Ore Deposits, I.A.E.A. Proc., p. 569-582.
- Premoli, C. (1982): The Madadzang uranium prospect in the Mayo Kebbi region of Chad: In: Vein-type and similar uranium deposits in rocks younger than Proterozoic. Proc. Tech. Comm. Meeting, Lisbon, I.A.E.A., Vienna, p. 195-209.
- Price, P. B. and Walker, R. M. (1963): A simple method of measuring low uranium concentrations in natural crystals: Applied Physics Letters, 2, No. 2, p. 23.
- Price, V., Cook, J. R., Fay, W. M. and Karfunkel, B. S. (1982): Chemical variations in monazite from the southeastern United States: In: Uranium Exploration Methods, Proc. Symp., I.A.E.A./N.E.A., Paris, June 1982, p. 431-444.
- Pupin, J. P. (1980): Zircon and granite petrology: Contrib. Mineral. Petrol. 73, p. 207-220.
- Pupin, J. P. and Turco, G. (1975): Typologie du zircon accessoire dans les roches plutoniques dioritiques, granitiques et syénitiques: facteurs essentiels déterminant les variations typologiques: Pétrologie, T. I, 2, p. 139-156.
- Ragland, J. N., Billings, G. K. and Adams, J. A. S. (1967): Chemical fractionation and its relationship to the distribution of thorium and uranium in a zoned granite batholith: Geochim. Cosmochim. Acta. 31, p. 17-34.

- Rahaman, M. A., Van Breeman, O., Bowden, P. and Bennett, J. N. (1984): Age migrations of anorogenic ring complexes in northern Nigeria: *Journal of Geology*, 92, p. 173-184.
- Rahman, M. A. (1979): *Geology, mineralogy and genesis of uranium mineralization in Mauji-Reshian area, Azad Kashmir, Pakistan: M.Sc. Thesis, University of Aberdeen.*
- Ramakrishnan, S. S., Gokhale, K. V. G. K. and Stubbarao, E. C. (1969): Solid solubility in the system zircon-hafnon: *Mat. Res. Bull.*, 4, p. 323-328.
- Ramdohr, P. (1957): Die "Pronto-Reaktion": *Neues Jahrb. Min., Monatsh.*, p. 217-222.
- Ramdohr, P. (1961): Das vorkommen von coffinit in hydrothermalen uranerzgangen, besonders vom Co-Ni-Bi-typ: *N. Jb. Miner., Abh.* 95, 3, p.313-324.
- Ranchin, G. (1971): La géochimie de l'uranium et la différenciation granitique dans la province uranifère du nord-Limousin: *Sci. de la Terre, Mém.* 19, 394 p.
- Rankin, A. H., Alderton, D. H. M., Thompson, M. and Goulter, J. E. (1982): Determination of uranium: carbon ratios in fluid inclusions decrepitated by inductively coupled plasma emission spectroscopy: *Min. Mag.* 46, p. 179-86.
- Read, H. H. (1931): The geology of central Sutherland (explanation of sheets 108 and 109): *Mem. Geol. Surv. Scotland*, p. 193-6.
- Read, H. H. (1961): Aspects of Caledonian magmatism in Britain: *L'pool Manchr. geol. J.*, 2, p. 653-83.
- Read, H. H., Ross, G. and Phemister, J. (1925): The geology of the country around Golspie, Sutherlandshire (Strath Fleet, Strath Brora, Glen Loth): *Geol. Surv. Scotland*, p. 41-45.
- Reynolds, R. L. and Goldhaber, M. B. (1978): Origin of a south Texas roll-type uranium deposit: I. Alteration of iron-titanium oxide minerals: *Economic Geology* 73, p. 1677-1689.
- Reynolds, R. L., Goldhaber, M. B. and Grauch, R. I. (1977): Uranium associated with iron-titanium oxide minerals and their alteration products in a south Texas roll-type deposit: *Short papers of U.S. Geol. Surv. U-Th Symp., Circular* 753, (Campbell, J. A., ed.), p. 37-39.
- Rich, R. A., Holland, H. D. and Petersen, U. (1977): Hydrothermal uranium deposits (Developments in economic geology 6): Amsterdam, Elsevier Scientific Pub. Co., 264 p.
- Rimsaite, J. (1977): Mineral assemblages at the Rabbit Lake uranium deposit, Saskatchewan: a preliminary report: Report of activities, Part B; *Geol. Surv. Can., Paper* 77-1B, p. 235-246.
- Rimsaite, J. (1978): Layer silicates and clays in the Rabbit Lake uranium deposit, Saskatchewan: Current research, Part A; *Geol. Surv. Can., Paper* 78-1A, p. 303-315.
- Rimsaite, J. (1980): Mineralogy of radioactive occurrences in the Grenville structural province, Bancroft area, Ontario: a progress report: Current research, Part A; *Geol. Surv. Can., Paper* 80-1A, p. 253-264.
- Rimsaite, J. (1981a): Isotope, scanning electron microscope, and energy dispersive spectrometer studies of heterogeneous zircons from radioactive granites in the Grenville structural province, Quebec and Ontario: Current research, Part B; *Geol. Surv. Can., Paper* 81-1B, p. 25-35.
- Rimsaite, J. (1981b): Alteration products of accessory allanite in radioactive granites from the Canadian shield: discussion: Current research, Part C; *Geol. Surv. Can., Paper* 81-1C, p. 89-92.

- Rimsaite, J. (1982a): The leaching of radionuclides and other ions during alteration and replacement of accessory minerals in radioactive rocks: Current research, Part B; Geol. Surv. Can., Paper 82-1B, p. 253-266.
- Rimsaite, J. (1982b): Mineralogical and petrochemical properties of heterogenous granitoid rocks from radioactive occurrences in the Grenville structural province, Ontario and Quebec: In: Uranium in granites, (Maurice, Y. T., ed.), Geol. Surv. Can., Paper, 81-23, p. 19-30.
- Rimsaite, J. (1983): Selected mineral associations in radioactive occurrences in the Grenville structural province: a progress report: Current research, Part B, Geol. Surv. Can., Paper 83-1B, p. 23-37.
- Rimsaite, J. (1984): Selected mineral associations in radioactive and REE occurrences in the Baie-Johan-Beetz area, Quebec: a progress report: Current research, Part A, Geol. Surv. Can., Paper 84-1A, p. 129-145.
- Rimsaite, J. (1986): Mobilization and preservation of radioactive and rare-earth elements in some Canadian vein-type and granite-hosted uranium deposits of Precambrian age: In: Mineral Parageneses, Athens, 1986, (Craig, J. R. et al., eds.), p. 346-385.
- Robb, L. J. and Schoch, A. E. (1985): Deuteric alteration and uranium mineralization processes in leucogranite intrusions from the Namaqualand metamorphic complex, South Africa: In: High heat production (HHP) granites, hydrothermal circulation and ore genesis, I.M.M., London, p. 301-314.
- Roberts, D. E. and Hudson, G. R. T. (1983): The Olympic Dam copper-uranium-gold deposit, Roxby Downs, South Australia: Econ. Geol. 78, No. 5. p. 799-822.
- Robinson, A. and Spooner, E. T. C. (1984): Postdepositional modification of uraninite-bearing quartz-pebble conglomerates from the Quirke Ore Zone, Elliot Lake, Ontario: Econ. Geol. 79, p. 297-321.
- Robinson, G. W. (1978): The occurrence of rare earth elements in zircon: Ph.D. Dissertation, Queens University, Kingston, Ontario, Canada.
- Robinson, S. C. (1950): Mineralogy of the Goldfields District, Saskatchewan (Interim account): Geol. Surv. Can., Paper 50-16.
- Robinson, S. C. and Abbey, S. (1957): Uranothorite from eastern Ontario: Can. Mineral. 6, p. 1-14.
- Roedder, E. and Coombs, D. S. (1967): Immiscibility in granitic melts, indicated by fluid inclusions in ejected granitic blocks from Ascension Island: J. Petrol. 8, p. 417-451.
- Roeder, P. L. (1985): Electron-microprobe analysis of minerals for rare-earth elements: use of calculated peak-overlap corrections: Can. Min. 23, p. 263-271.
- Rogers, J. J. W. and Adams, J. A. S. (1969): Uranium: In: Handbook of Geochemistry, II-2, Chapt. 92B-O, (Wedepohl, K. E. ed.), Berlin etc: Springer, 1978, 52 p.
- Romans, P. A., Brown, L. L. and White, J. C. (1975): An electron microprobe study of yttrium, rare earth and phosphorus distribution in zoned and ordinary zircon: Am. Min., 60 p. 475-480.
- Romberger, S. B. (1984): Transport and deposition of uranium in hydrothermal systems at temperatures up to 300°C: geological implications: In: Uranium geochemistry, mineralogy, geology, exploration and resources, (de Vivo, B.; Ippolito, F.; Capaldi, G.; Simpson, P. R., eds.), I.M.M., London, p. 12-17.

- Rose, W. I. Jr. and Bornhorst, T. J. (1981): Uranium and thorium in selected Quaternary volcanic rocks of Guatemala and Sumatra; evidence for uranium redistribution: In: Uranium in volcanic and volcanoclastic rocks, (Goodell, P. C., ed.), A.A.P.G. Studies in Geology, 13, p. 13-21.
- Rose, A. W. and Burt, D. M. (1979): Hydrothermal alteration: In: Hydrothermal ore deposits (Barnes, H. L., Ed.). John Wiley and Sons, p. 173-235.
- Ruh, R. and Wadsley, A. D. (1966): The crystal structure of ThTi_2O_6 (brannerite): Acta crystallogr., 21, p. 974-8.
- Ruhlmann, F. (1980): Some examples of uranium-titanium associations: (in French) Bull. Mineral., 103, p. 240-244.
- Ruzicka, V. and Le Cheminant, G. M. (1984): Uranium deposit research, 1983: Current research, Part A, Geol. Surv. Can., Paper 84-1A, p. 39-51.
- Ruzicka, V. and Littlejohn, A. L. (1982): Notes on mineralogy of various types of uranium deposits and genetic implications: Current Research, Part A, Geol. Surv. of Can., Paper 82-1A, p. 341-349.
- Saager, R. and Stupp, H. D. (1983): U-Ti phases from Precambrian quartz-pebble conglomerates of the Elliot Lake area, Canada and the Pongola Basin, South Africa: Tscherma's Mineralogische und Petrographische Mitteilungen 32(2-3), p. 83-102.
- Saager, R., Thiel, K., Hennig, G. J. and Bangert, U. (1981): Uranium redistribution in weathered conglomerates of the early Precambrian Pongola supergroup, S. Africa - inferences from a study by alpha spectrometry and fission track micromapping: Journ. Geochem. Exp., 15, p. 233-249.
- Sahama, T. G. (1981): Growth structure in Ceylon zircon: Bull. Mineral., 104, p. 89-94.
- Sarcia, J. A. (1983): L'uranium des albitites: Notes et Mémoires Compagnie Française des Pétroles, 18, p. 57-60.
- Sassano, G. P., Fritz, P. and Morton, R. D. (1972): Paragenesis and isotopic composition of some gangue minerals from the uranium deposits of Eldorado, Saskatchewan: Canadian Jour. Earth Sci., 9, p. 141-157.
- Sawka, W. N. and Chappell, B. W. (1985): Geothermal implications for the Sierra Nevada batholith from vertical and horizontal compositional zoning studies in contrasting pluton types: In: High heat production (HHP) granites, hydrothermal circulation and ore genesis. I.M.M., London, p. 329-343.
- Schidrowski, M. (1981): Uraniferous constituents of the Witwatersrand conglomerates: ore-microscopic observations and implications for the Witwatersrand metallogeny: In: Genesis of uranium- and gold-bearing Precambrian quartz-pebble conglomerates, (Armstrong, F. C., ed.), Prof. Pap. U. S. Geol. Surv., 1161-A-BB, p. N1-N29.
- Schindlmayr, W. E. and Beerbaum, B. (1986): Structure related uranium mineralisation in the Westmoreland district, Queensland, Australia: In: Vein type uranium deposits, (Fuchs, H. D., ed.). A technical document issued by the International Atomic Energy Agency, Vienna. I.A.E.A.-TECDOC-361, p. 85-100.
- Semenov, E. I. and Kazakova, M. E. (1961): Hydrothorite in pegmatites of the Lovozero alkaline Massif: Trudy Inst. Mineral., Geokhim. i. Kristallokhim. Redkikh Elementov 7, p. 123-9.
(Chem. Absts., 56:5658)
- Shannon, R. D. (1976): Revised effective ionic radii and systematic studies of interatomic distances in halides and chalcogenides: Acta Crystallogr., A32, p. 751-767.
- Shirvington, P. J. (1983): Fixation of radionuclides in the ^{238}U decay series in the vicinity of mineralized zones: 1. The Austatom Uranium Prospect, Northern Territory, Australia: Geochim. Cosmochim. Acta, 47, p. 403-412.

- Sillén, L. G. and Martell, A. E. (1964): Stability constants of metal-ion complexes: Chem. Soc. London, Spec. Publ. 17, 754 p.
- Silver, L. T. and Deutsch, S. (1963): Uranium-lead isotopic variations in zircons: a case study: Jour. Geology, 71, No. 6, p. 721-758.
- Silver, L. T., Williams, I. S. and Woodhead, J. A. (1980): Uranium in granites from the southwestern United States: actinide parent-daughter systems, sites and mobilization: First year report for the Dept. of Energy, DOE-GJBX-45(81), California Inst. of Technology, 379 p.
- Silver, L. T., Woodhead, J. A., Williams, I. S. and Chappell, B. W. (1984): Uranium in granites from the southwestern United States: actinide parent-daughter systems, sites and mobilization: Second year report for the Dept. of Energy, DOE-GJBX-7(84), California Inst. of Technology, 431 p.
- Simpson, P. R., Plant, J. and Cope, M. J. (1976): Uranium abundance and distribution in some granites from northern Scotland and southwest England as indicators of uranium provinces: In: Geology, mining and extractive processing of uranium. (Jones, M. J., ed.), I.M.M., London, p. 126-139.
- Simpson, P. R. and Bowles, J. F. W. (1977): Uranium mineralization of the Witwatersrand and Dominion Reef systems: Phil. Trans. R. Soc. Lond. A. 286, p. 527-548.
- Simpson, P. R., Brown, G. C., Plant, J. and Ostle, D. (1979): Uranium mineralization and granite magmatism in the British Isles: Phil. Trans. R. Soc. Lond. A. 291, p. 385-412.
- Smellie, J. A. T. (1982a): The mineralogy and genesis of uranium in rhyolitic ignimbrites of Precambrian age from Duobblon, Sweden: Min. Mag. 46, p. 187-199.
- Smellie, J. A. T. (1982b): Radioactive mineral phases from Precambrian granites within the Olden Window, Jamtland, N. Sweden: In: Uranium Exploration Methods, Proc. Symp., I.A.E.A./N.E.A., Paris, June 1982, p. 415-429.
- Smellie, J. A. T., Cogger, N. and Herrington, J. (1978): Standards for quantitative microprobe determination of uranium and thorium with additional information on the chemical formulae of davidite and euxenite-polycrase: Chem. Geology, 22, p. 1-10.
- Smellie, J. A. T. and Laurikko, J. (1984): Skuppesavon, northern Sweden: a uranium mineralization associated with alkali metasomatism: Mineral. Deposita 19, p. 183-192.
- Smith Jr., D. K. (1984): Uranium mineralogy: In: Uranium geochemistry, mineralogy, geology, exploration and resources. (de Vivo, B.; Ippolito, F.; Capaldi, G.; Simpson, P. R., eds.): I.M.M., London, p. 43-88.
- Smith, W. L., Franck, M. L. and Sherwood, A. N. (1957): Uranium and thorium in the accessory allanite of igneous rocks: Amer. Min., 42, p. 367.
- Sommerauer, J. (1977): Die chemisch-physikalische stabilität natürlicher zirkone: Schweiz. Min. Petr. Mitt. 57, p. 484 (Abstract).
- Southworth, H. N. (1975): Scanning electron microscopy and microanalysis: In: Physicochemical Methods of Mineral Analysis, (Nicol, A. W., ed.), Plenum, p. 421-450.
- Speer, J. A. (1982a): Zircon: In: Reviews in Mineralogy Volume 5: Orthosilicates, (Ribbe, P. H., ed.), Mineralogical Society of America, 2nd Ed., p. 67-112.
- Speer, J. A. (1982b): The actinide orthosilicates: In: Reviews in Mineralogy Volume 5: Orthosilicates, (Ribbe, P. H., ed.), Mineralogical Society of America, 2nd Ed., p. 113-135.
- Speer, J. A., Solberg, T. N. and Becker, S. W. (1981): Petrography of the uranium-bearing minerals of the Liberty Hill Pluton, South Carolina: phase assemblages and migration of uranium in granitoid rocks: Econ. Geol. 76: p. 2162-2175.
- Staatz, M. H., (1978): I and L uranium and thorium vein system, Bokan Mountain, southeastern Alaska: Econ. Geol., 73, p. 512-523.

- Staatz, M. H., Adams, J. W. and Wahlberg, J. S. (1976): Brown, yellow, orange and greenish-black thorites from the Seerie pegmatite, Colorado: *J. Res. U. S. Geol. Surv.* 4(5), p. 575-82.
- Staatz, M. H. and Brownfield, I. K. (1986): Trace- and minor-element mineralogy of the microgranite at Ghurayyah Kingdom of Saudi Arabia: *U. S. Geol. Surv., Open File Report No. OF 86-0105*, 12 p.
- Stacey, H. R. and Kaiman, S. (1978): Uranium minerals in Canada: their description, identification and field guides: In: *Short Course in Uranium Deposits: Their Mineralogy and Origin*, (Kimberley, M. M., ed.), Mineral. Assoc. of Canada, p. 107-140.
- Steenfelt, A. and Armour-Brown, A. (1985): Characteristics of the South Greenland uranium province: Report to I.A.E.A. Technical Committee Meeting on Recognition of Uranium Provinces, Sep. 18-20, 1985, Geol. Museum, London, England, 29 p.
- Steiger, R. H. and Wasserburg, G. J. (1966): Systematics in the Pb^{208} - Th^{232} , Pb^{207} - U^{235} , and Pb^{206} - U^{238} systems: *J. Geophys. Res.*, 71, No. 24, p. 6065-6090.
- Stieff, L. R., Stern, T. W. and Sherwood, A. M. (1956): Coffinite, a uranous silicate with hydroxyl substitution: a new mineral: *Am. Min.* 41, p. 675-688.
- Stuart, E. J., Bornhorst, T. J., Rose, W. I. and Noble, D. C. (1983): Distribution and mobility of uranium and thorium in the peralkaline Soldier Meadow tuff, northwestern Nevada: *Econ. Geol.* 78, p. 353-358.
- Stuckless, J. S. and VanTrump, G. (1982): An evaluation of uranium content in zircons from igneous rocks of the contiguous United States as an aid to exploration and resource assessment: In: *Uranium Exploration Methods, Proc. Symp., I.A.E.A./N.E.A. Paris, June 1982*, p. 369-384.
- Szymanski, J. T. and Scott, J. D. (1982): A crystal-structure refinement of synthetic brannerite, UTi_2O_6 , and its bearing on rate of alkaline-carbonate leaching of brannerite in ore: *Can. Min.* 20, p. 271-279.
- Taylor, R. P. and Fryer, B. J. (1982): Rare earth element geochemistry as an aid to interpreting hydrothermal ore deposits: In: *Metallization Associated with Acid Magmatism*, (Evans, A. M., ed.), John Wiley and Sons Ltd., p. 357-364.
- Thiel, K., Herr, W. and Becker, J. (1972): Uranium distribution in basalt fragments of five lunar samples: *Earth and Plan. Sci. Letts.*, 16, p. 31-44.
- Thiel, K., Saager, R. and Muff, R. (1979): Uranium distribution in early Precambrian gold-bearing conglomerates of the Kaapvaal Craton, South Africa: a case study for the application of uranium-fission track micromapping: Univ. Witwatersrand, Economic Geology Research Unit, Info. Circular no. 134.
- Tiangang, L. and Zhizhang, H. (1986): Vein uranium deposits in granites of Xiaozhuang ore field: In: *Vein Type Uranium Deposits*, (Fuchs, H. D., ed.). A technical document issued by the I.A.E.A., Vienna. *TECDOC-361*, p. 359-376.
- Tieh, T. T. and Ledger, E. B. (1981): Fission track study of uranium in two granites of central Texas: *Contrib. Mineral. Petrol.* 76, p. 12-16.
- Tole, M. P. (1985): The kinetics of dissolution of zircon ($ZrSiO_4$): *Geochim. Cosmochim. Acta* 49, p. 453-458.
- Troëng, B. (1982): Uranium-rich granites in the Olden Window, Sweden: *Min. Mag.* 46, p. 217-226.
- Tugarinov, A. I. (1975): Origin of uranium deposits: In: *Recent Contributions to Geochemistry and Analytical Chemistry*, (Tugarinov, A. I., ed.), Halsted Press, p. 293.

- Tweedie, J. R. (1979): Origin of uranium and other metal enrichments in the Helmsdale granite, eastern Sutherland, Scotland: *Trans. Inst. Min. Met.*, vol. B 88, p. 145-153.
- Tweedie, J. R. (1981): The origin of uranium and other metal concentrations in the Helmsdale granite and the Devonian sediments of the north-east of Scotland: Ph.D. thesis, Aberdeen University.
- Udas, G. R. and Mahadevan, T. M. (1974): Controls and genesis of uranium mineralisation in some geological environments in India: In: *Formation of Uranium Ore Deposits*, I.A.E.A. Procs., p. 425-436.
- Veniale, F., Pirgorini, B. and Sogetti, F. (1968): Petrological significance of the accessory zircon in the granites from Baveno, Orfano and Alzo (north Italy): *Int. Geol. Congr. Report*, 23rd Session, Czechosl., 13, p. 243-268.
- Vlasov, K. A. (1966a) (ed.): *Geochemistry and mineralogy of rare elements and genetic types of their deposits. Vol. I. Geochemistry of rare elements: Israel Program for Scientific Translations, Jerusalem.*
- Vlasov, K. A. (1966b) (ed.): *Geochemistry and mineralogy of rare elements and genetic types of their deposits. Vol. II. Mineralogy of rare elements: Israel Program for Scientific Translations, Jerusalem, 945 p.*
- Vochten, R., Huybrechts, W., Remaut, G. and Deliens, M. (1979): Formation of meta-torbernite starting from curite: crystallographic data and electrokinetic properties: *Phys. Chem. Minerals.* 4, p. 281-290.
- Von Knorring, O. and Hornung, G. (1961): Hafnian zircons: *Nature* 190, No. 4781, p. 1098-1099.
- Von Pechmann, E. and Bianconi, F. (1982): Synmetamorphic uranium mineralisation from Tiraun, Graubunden, Switzerland: *Min. Mag.* 46, p. 173-178.
- Voultsidis, V. and Classen, D. (1978): Probleme und Grenzbereiche der Uranmineralogie: *Erzmetall.* 31, p. 8-13.
- Wallis, R. H., Saracoglu, N., Brummer, J. J. and Golightly, J. P. (1984): The geology of the McClean uranium deposits, northern Saskatchewan: *Canadian Mining and Metallurgical Bulletin*, 77(864), p.69-96.
- Watson, E. B. (1980): Some experimentally determined zircon/liquid partition coefficients for the rare earth elements: *Geochim. Cosmochim. Acta* 44, p. 895-897.
- Watson, J. V. and Plant, J. (1979): Regional geochemistry of uranium as a guide to deposit formation: *Phil. Trans. R. Soc. Lond. A* 291, p. 321-338.
- Webb, P. C. and Brown, G. C. (1984a): The eastern Highlands granites: heat production and related geochemistry: Report written for the B.G.S.-Imperial College-Open University collaborative investigation into the potential for hot dry rock geothermal development in selected Caledonian granites.
- Webb, P. C. and Brown, G. C. (1984b): Lake District granites: heat production and related geochemistry: See Webb and Brown (1984a).
- Webb, P. C., Tindle, A. G., Barritt, S. D., Brown, G. C. and Miller, J. F. (1985): Radiothermal granites of the United Kingdom: comparison of fractionation patterns and variation of heat production for selected granites: In: *High heat production (HHP) granites, hydrothermal circulation and ore genesis*, I.M.M., London, p. 409-424.
- White, M. V. W. and Martin, R. F. (1980): The metasomatic changes that accompany uranium mineralisation in the nonorogenic rhyolites of the Upper Aillik Group, Labrador: *Can. Min.*, 18, p. 459-479.
- Williams-Jones, A. E. and Sawiuk, M. J. (1985): The Karpinka Lake Uranium Prospect, Saskatchewan: a possible metamorphosed Middle Precambrian sandstone-type uranium deposit: *Econ. Geol.* 80, p. 1927-1941.

- Yada, K., Tanji, T. and Sunagawa, I. (1981): Application of lattice imagery to radiation damage investigation in natural zircon: *Physics and Chemistry of Minerals*, 7, p. 47-52.
- Yang, M. and Li, Y. (1980): Uranothorite of the Oh-Po deposit, Pai-Yung, Inner Mongolia, China: *K' o Hsueh T' ung Pao*, 25(12), p. 558-560. (Chem. Absts. 93:153270)
- Yeliseyeva, O. P. (1977): Content and distribution of uranium, thorium, yttrium and the rare earth elements in accessory minerals in granitoids: *Geochem. Int.* 14, Pt. 5, p. 37-49.
- Yeliseyeva, O. P., Ryabchikov, I. D. and Bogatyreva, N. A. (1975): On the types of distribution of uranium in accessory zircon: *Geochem. Int.* 11, Pt. 5, p. 960-968.
- Zagruzina, I. A. and Smyslov, A. A. (1978): Uranium and thorium in rocks of the Soviet northeast: *Int. Geol. Review* 20, Pt. 10, p. 1230-1238.
- Zharkova, O. V. and Tananaeva, G. A. (1968): Fluorite-pitchblende mineralization in greisens: *Geol. Vop. Genezisa Endogennykh Uranovyykh Mestorozhd.*, p.292-301.
- Zielinski, R. A. (1982): The mobility of uranium and other elements during alteration of rhyolite ash to montmorillonite: a case study in the Troublesome Formation, Colorado, U.S.A.: *Chem. Geol.* 35, p. 185-204.
- Zimmer, P. (1983): Etude experimentale du système ternaire UO_2 - ThO_2 - SiO_2 à haute température et haute pression en présence d'une phase aqueuse. Comparaison avec les systèmes UO_2 - ZrO_2 - SiO_2 et ThO_2 - ZrO_2 - SiO_2 . Implications géologiques. Thèse troisième cycle, Univ. Nancy.
- Zussman, J. (1977): X-ray diffraction: In: *Physical Methods in Determinative Mineralogy* (Zussman, J., ed.), 2nd Ed., Academic Press